A METHODOLOGY FOR PREDICTING AND MITIGATING LOSS OF CONTROL INCIDENTS FOR GENERAL AVIATION AIRCRAFT

A Thesis
Presented to
The Academic Faculty

by

Evan D. Harrison

In Partial Fulfillment
of the Requirements for the Degree
Doctor of Philosophy in the
School of Aerospace Engineering

Georgia Institute of Technology
December 2018

A METHODOLOGY FOR PREDICTING AND MITIGATING LOSS OF CONTROL INCIDENTS FOR GENERAL AVIATION AIRCRAFT

Approved by:

Prof. Dimitri Mavris, Advisor
School of Aerospace Engineering
Georgia Institute of Technology

Prof. Daniel Schrage
School of Aerospace Engineering
Georgia Institute of Technology

Dr. Simon Briceno
School of Aerospace Engineering
Georgia Institute of Technology

Prof. Imon Chakraborty
Department of Aerospace Engineering
Auburn University

Charles "Cliff" Johnson
Aviation Research Division
Federal Aviation Administration

Date Approved: November 1, 2018(?)

To Caitlin.

ACKNOWLEDGEMENTS

I have come now to the end of my journey through graduate school and find myself deeply humbled by the number of people to whom I owe great appreciation in aiding me on this journey. I first would like to express my deep gratitude for my adviser, Prof. Dimitri Mavris. He not only provided me with immense opportunity to engage in meaningful research but provided an environment within with my pursuit of knowledge could flourish. I would like to thank Prof. Mavris for his invaluable insights and guidance, and for inspiring me to carry the torch on to the next generation. I also extend my thanks to the other members of my thesis committee: Prof. Daniel Schrage, Dr. Simon Briceno, Prof. Imon Chakraborty, and Cliff Johnson. Thank you each for taking the time to review my work and for providing your insights and feedback.

During my time in graduate school I had the pleasure of working and studying alongside so many incredibly talented people, many of whom I am honored to count now as my friends. To all those in my lab, ASDL, I thank you for being an amazing network of colleagues and for your collective willingness to lend a helping hand. To the late Hernando Jimenez whose example and mentorship inspired me to continually push myself as a researcher and to lead others to do the same. Tejas Puranik and Sanggyu Min, my co-researchers in our saga of small aircraft safety. Mayank Bendarkar and Dushyanth Rajaram, my co-TAs and the sounding board for many of my wildest ideas. To Etienne Demers-Bouchard for his infectious scientific curiosity and friendship. Thank you to Gokcin Cinar, whose example and advice as she completed her own thesis helped to guide me through this final stage of my journey. And to Tanya Ard-Smith, Adrienne Durham, and Ruth Pimentel for their faithful administration of our lab and for their patient assistance towards me as I navigated

the bureaucracy of graduate school.

Outside of my graduate studies I have found myself surrounded by a number of close friends whose support over the years has been quite dear. Michael Ellis who first inspired me to pursue graduate school and helped to mentor me as I found my footing there. Alex and Liz Freemon who have been dear, dear friends to my wife and I for the past decade. John and Laurie O'Brien who joined Caitlin and I on numerous adventurous and helped to remind me of the life beyond graduate school. To Jonathan Ludwikowski and Kyle Buck, who helped me create a place of wonder amidst our busy lives with our D&D campaigns. The new friends I have found at Mount Vernon Baptist Church, for their caring friendship in this last year.

Ultimately this journey would not be possible without the love and support of my family. To my parents Ann and Jimmy "Bud" Harrison who have supported me tirelessly throughout my life. I am here today because of your love and continual support over my academic journey, and I doubt that I can ever adequately express how appreciative I am to you. To my sister Lauren Harrison who has always inspired me with her courage to follow her own path through life. To my grandparents Herbert and Selina Hopkins and the late Donald and Mary-Ellen Harrison, to whom I am delighted bring one last "report card" and who demonstrated to me the value of hard work and calm determination. To my parents-in-law Ken and Denise Collins for their encouragement and love, and to Caleb, Kristi, Aaron, and Casey Collins who lovingly welcomed me as a brother. And to my wife, Caitlin Harrison, who has walked with me on this journey and shared in all of its joys and sorrows. Thank you for your love, patience, and gentleness towards me through it all.

Lastly I thank my Lord and Savior, Jesus Christ. All glory or honor that I may have earned I give to you.

TABLE OF CONTENTS

LIST OF TABLES

LIST OF FIGURES

SUMMARY

In comparison with other modes of transportation, aviation has earned a clear distinction as the safest mode of travel. In recent years aviation has also achieved steady improvement in the accident rates, further distinguishing the safety of aviation with respect to other transportation modes. When aviation accidents do occur, however, it has been found that the most likely cause of these accidents is loss of control (LOC). Annual analysis of accident data indicates that LOC is consistently the most common cause of aviation accidents and fatalities for commercial aircraft worldwide and the Federal Aviation Administration (FAA) identifies LOC as the most important safety concern for general aviation (GA) as well.

Recent work to identify and mitigate LOC events has been largely successful in identifying the sequence of events that typically precedes a LOC incident. Using this knowledge, several proposals have been made to break this sequence through application of advanced techniques and methods to detect, mitigate, or recover from events that may lead to LOC. These methods often assume the presence of advanced vehicle systems, such as advanced avionic systems and automated aircraft control, which imply intended application to future aircraft systems. Many existing aircraft are not equipped with such systems, leaving a gap between existing aircraft capability and the proposed solutions to address LOC. This is particularly true for GA, where the average age of an active vehicle in the GA fleet is estimated by the FAA to be 40 years old, suggesting that the typical GA aircraft lack such advanced on-board systems.

The objective of this dissertation is to develop a methodology which enables the

identification and mitigation of LOC for a typical GA fixed wing aircraft. The methodology which is developed within this work seeks to satisfy this objective through a combination of three key components. First, as LOC is understood within the existing literature as a deviation of the aircraft from normal operation, an appropriately defined LOC envelope will enable the prediction of LOC onset. Then to monitor this envelope during flight all necessary states of the vehicle must also be either observed or estimated. As it is assumed that only data collected by personal electronic devices is available, unobserved aircraft states and control actions of the pilot must be estimated within the methodology using existing or developed techniques. Finally, the methodology will aid in recovery of the aircraft in the event of LOC through synthesis of LOC recovery strategies which would be communicated to a human pilot through aural cues. This proposed methodology is summarized as a method of Mitigation by Envelope Restriction for Loss-of-control INcidents (MERLIN).

The dissertation presents tools for implementing each of these components and includes a set of methods for synthesizing a dynamic vehicle model for use alongside the method. The various aspects of this methodology are also tested through a series of experiments. First the primary sources of uncertainty which affect the LOC envelope estimation process are identified and studied, yielding quantification of the effects of this uncertainty on the envelopes and a strategy for compensation. Secondly the expected error of the estimation of flight states is analyzed and the impact that this error has within the mitigation effort is accounted for through quantification of this error and the implementation of a strategy for mitigating the likelihood that this error causes erroneous evaluations of the vehicle's condition. Finally a full demonstration of the MERLIN method is presented within a simulation framework which includes the simulation of vehicle dynamics, pilot behavior, LOC envelope definition and real-time monitoring, and the communication of simplified recovery actions.

CHAPTER I

MOTIVATION

Among multiple modes of transportation, aviation has earned the distinction as the safest mode of travel. The focused coordination among governmental agencies, manufacturers, and operators has produced an operating environment that is safer than all others in terms of nearly every pertinent metric. Surveys of the historical safety trends additionally attest that aviation has continually improved in terms of safety as a mode of transportation. At odds with this continual improvement, however, is the loss-of-control (LOC) phenomena.

In some ways the improvements to overall aviation safety accentuate aircraft LOC. Represented in Figure 1 is a brief summary of worldwide accident statistics for commercial aircraft [28], with descriptions of the abbreviations used in this data provided in Table 1. These data suggest that LOC is both the most common cause of accidents in general and the most common cause of fatal aircraft accidents. Further, it is observed that for the period between 2007 and 2016, LOC was the case of over twice as many on-board fatalities as the next most common category, controlled flight into terrain (CFIT), and that LOC accounts for nearly half (47.5%) of the total number of on-board fatalities in this time period.

This prevalence is not limited to just commercial aviation. Rather, LOC is identified as the most common cause of general aviation (GA) aircraft incidents by the Federal Aviation Administration, followed by CFIT and SCF-PP [57]. In addition, the National Transportation Safety Board reports that in 2015 only 30 total accidents, with zero fatal accidents, occurred during Part 121 operations (i.e. commercial aircraft). During this same time 1282 accidents occurred in GA operations, of which 238

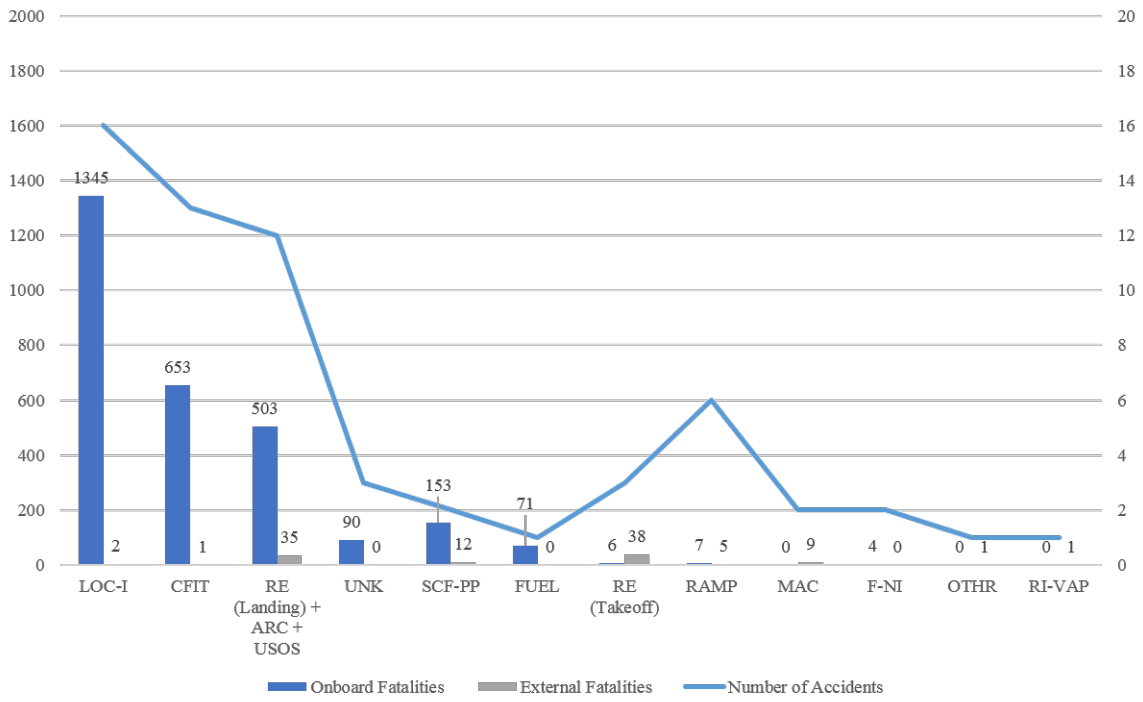

Figure 1: Number of accidents and associated fatalities by occurrence category for global commercial fleet, 2007 through 2016 [28].

Table 1: Description of CICTT abbreviations used in Figure 1.

ARC	Abnormal Runway Contact
CFIT	Controlled Flight Into or Toward Terrain
F-NI	Fire/Smoke (Non-Impact)
FUEL	Fuel
LOC-I	Loss of Control In-Flight
MAC	Midair/Near Midair Collision
OTHR	Other
RAMP	Ground Handling
RE	Runway Excursion (Takeoff or Landing)
RI-VAP	Runway Incursion - Vehicle Aircraft, or Person
SCF-PP	System/Component Failure or malfunction (Powerplant)
UNK	Unknown or Undetermined
USOS	Undershoot/Overshoot

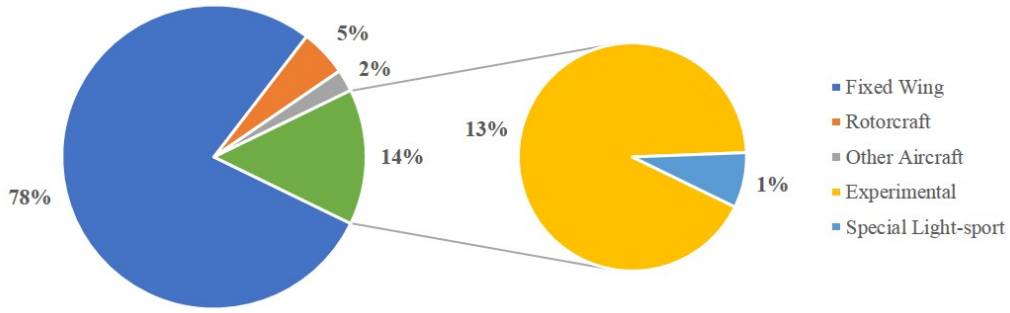

Figure 2: Makeup of active general aviation vehicles by category, CY 2015 [52].

were fatal. This amounts to an accident rate of only 0.33 accidents per 100,000 departures or 0.17 accidents per 100,000 flight hours for Part 121 operations compared to a rate of 1.10 accidents per 100,000 departures or 5.85 accidents per 100,000 flight hours for GA [123]. Together these data suggest that accidents are more common for GA than for commercial aviation, which further implies that LOC events most commonly involve GA vehicles.

In addressing the prevalence of LOC in GA operations, it is helpful to first consider the demographics of this particular portion of the wider aviation system. The GA fleet is also characterized by a wide variety of vehicles that fall under this classification. In Figure 2 an overview of the categories of vehicles which made up the GA fleet in 2015 are provided along with their respective percentage of the fleet. The large majority of vehicles that make up the GA fleet are fixed wing aircraft, followed by a combination of experimental and special light-sport category aircraft. It is worth noting that the many aircraft in the experimental and light-sport categories can also be considered as fixed wing aircraft, however the available data does not delineate these categories in this manner. However, given the dominance of fixed wing aircraft in the GA fleet further exploration into this sub-class of the GA fleet is warranted.

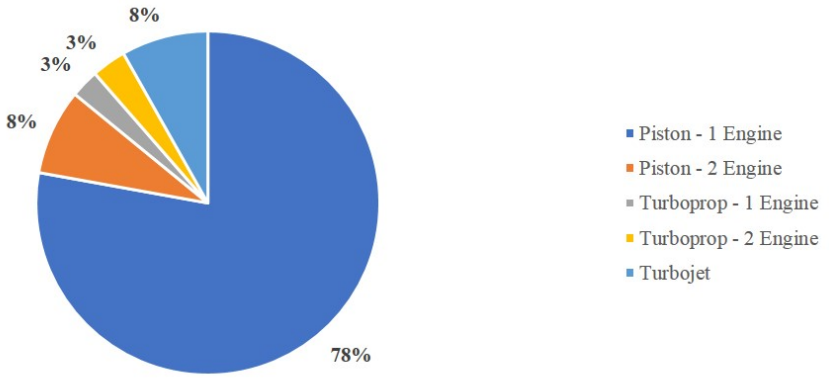

Figure 3: Makeup of general aviation fixed wing aircraft fleet, CY 2015 [52].

Viewed separately from the GA fleet as a whole, the classification "fixed wing aircraft" is used to describe a general class of aircraft that may be further separated by propulsive type. This categorization is provided in Figure 3 which provides a breakdown of the types of vehicles considered as fixed wing aircraft within the GA fleet. As with the GA fleet in general, the fixed wing aircraft category is primarily dominated by a single sub-category: single-engine piston aircraft. The data of Figure 2 and Figure 3 taken together indicate that nearly 61% of the entire GA fleet is made up of fixed wing, single-engine piston aircraft. [52]

Alongside the variety in aircraft types considered as GA, typical GA operations are also widely varied. In general, however, the data collected by the FAA indicate that the 69% of vehicles in the GA category are used for personal use. The next most common uses for GA vehicles are for business with a paid flight crew and for instructional use, with 7.9% and 7.8% of all GA vehicles respectively. Eight other specific primary uses for GA vehicles are identified by the FAA, apart from the "other" categorization, each containing less than 10% of the total GA fleet with five uses containing less than 1% each [52].

An additional characteristic of the GA fleet to consider is the age of the fleet. Vehicles which fall into the GA categorization include vehicles that were produced 60

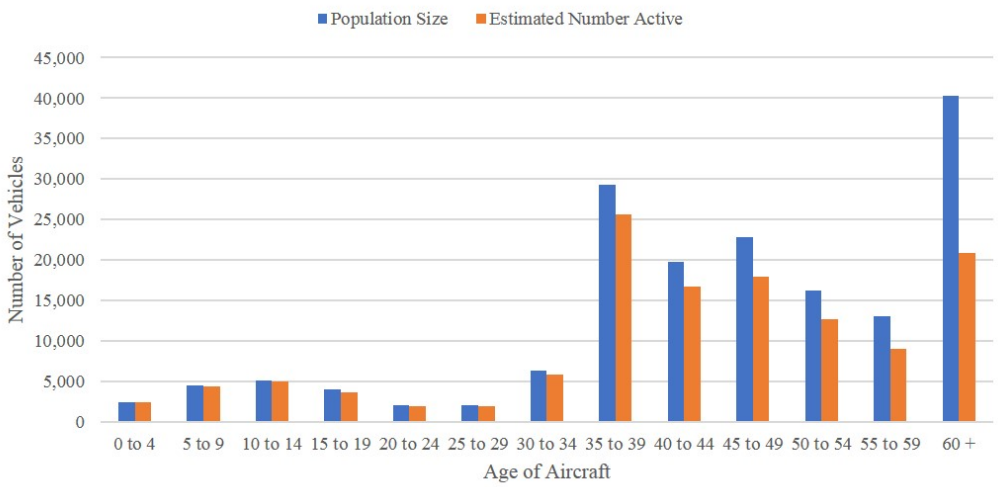

Figure 4: Age of general aviation fixed wing aircraft fleet, CY 2015 [52].

or more years ago, many of which are considered to be in active use. This can be noted in particular for fixed wing GA aircraft through the data presented in Figure 4. From these data somewhat surprising trends are observed. One may note that the majority of fixed wing aircraft that make up the GA fleet are 35 years old or older, which means they were built before 1980. In addition, it is observed that a large majority of aircraft age 35 or older are considered active as of 2015, though the percentage of active aircraft with respect to total aircraft per age range in general increases as the age of the aircraft decreases. The trends in aircraft age less than 35 additionally suggest that this prevalence is likely not to change soon, as the number of aircraft per age group decreases with decreasing age for aircraft less than 15 years old. From these data the average age of a fixed wing aircraft is found to be at least 42.9 for the total population and 40.2 for active aircraft. This statistic is corroborated by similar values provided by the General Aviation Manufacturers Association (GAMA), who additionally provide that the average age of a fixed wing, single-engine piston aircraft in the U.S. is 45.4 years old [66].

Taken together these data provide a picture of the vehicles that are statistically most susceptible to LOC events. While LOC is a key area of concern for all aircraft

categories, the data suggests that GA aircraft are most at risk in terms of LOC event occurrence. The demographics available for GA vehicles suggest that the most common vehicle present within the GA fleet as a whole are fixed wing, single-engine piston aircraft with an average age of at least 40 years. Further, it is likely that these vehicles are for personal use, which implies that the pilots are likely not part of some business which regularly trains and assesses their proficiency. It is concluded then that this class of vehicles is most likely to be involved in LOC events, and as such this work will endeavor to provide a methodology which addresses this risk.

This work is not the first which seeks to address the problem of LOC for aircraft. Indeed, many key contributions are present within the literature such as the recent work by Belcastro et al. [19] to generate a holistic approach to LOC intervention. In review of this work and the work by other researchers in the field, it is found that the methodologies therein for LOC mitigation or intervention are tailored for application to commercial aircraft systems, and are in large part ill-suited for application to GA fixed wing aircraft. Given this absence of appropriate strategies, and driven by the need to address LOC for GA fixed-wing aircraft identified from the accident and fleet statistics, this present work intends to develop a methodology which enables mitigation of LOC events for fixed-wing GA aircraft. This goal is encapsulated in the research objective for this proposed work:

Research Objective:

Develop a methodology for the prediction and mitigation of LOC incidents for fixed-wing GA aircraft within the typical GA operation limitations.

The remainder of this thesis will consist of the following sections:

- Chapter 2 presents a review of relevant background material collected from literature review

- Chapter 3 presents the formulation of the problem in terms of the research objective, questions, and experiments
- Chapter 4 presents a set of methods for developing a dynamic fixed-wing general aviation aircraft model
- Chapter 5 presents the development and testing of the loss-of-control envelope capability
- Chapter 6 presents the development and testing of the state and pilot action estimation capability
- Chapter 7 presents the development and testing of the loss-of-control mitigation capability
- Chapter 8 presents a summary of the work alongside some conclusions, contributions, and recommendations for future work

CHAPTER II

BACKGROUND AND LITERATURE REVIEW

From the outset of aircraft design, gaining and maintaining control over the vehicle has been of principal importance. While working towards creating their seminal flying machine, the Wright brothers spent considerable time testing various aspects of flight on a glider they created in 1902. In particular, it was with this glider which the Wright brothers implemented a new system - three-axis control of an air vehicle. This system gave the brothers the capability of maintaining control of their glider in both calm and turbulent conditions, laying the groundwork for a revolution in transportation the following year. In reference to their accomplishment in 1903, Wilbur Wright noted that they had successfully developed an aircraft with "sufficient power to fly, sufficient strength to withstand the shocks of landings, and sufficient capacity of control to make flight safe in boisterous winds, as well as in calm air" [127].

Many aspects of flight control have changed since the pioneering achievement of the Wright brothers, but one core aim remains largely the same: design a vehicle with sufficient stability and controllability. Yet this aim of ensuring "sufficient capacity of control" [127] in all conditions has proven to be difficult. Since the early days of flight, accidents linked to an inability to maintain control of the vehicle have been a key concern for both aircraft designers and operators. In recent years LOC has continued to be a major factor in aviation accidents, even as our collective understanding of this phenomena has grown with time.

Indeed, in its yearly report on worldwide aviation commercial jet aircraft accidents, Boeing identifies loss of control in-flight (LOC-I; defined by the CAST/ICAO Common Taxonomy Team [32]) as the both the most common and most fatal cause

of jet aircraft accidents from 2007 to 2016 [28]. Over this period of time, LOC-I was the cause of 25% of fatal jet aircraft accidents, out of a total of 62 fatal accidents, accounting for 47% of the 2832 on-board fatalities. The next highest accident category for this same time period was controlled flight into terrain, which was the cause of 21% of fatal accidents and 23% of on-board fatalities [28]. These data present a stark message: LOC remains as pressing a concern for the modern aircraft designer as it was for Orville and Wilbur Wright.

The pervasive nature and associated high risk of fatal accidents has led to a sizable body of literature describing LOC from various perspectives. This diversity of perspectives is reflected in a diversity of definitions and characterizations of the LOC phenomena. In seeking to describe and ultimately mitigate LOC, it must be appropriately characterized. Rather than generating an entirely new working definition, a satisfactory definition will be sought from within the existing literature.

2.1 Loss of Control Characterization

Many authors within the literature, particularly those presenting statistical surveys and analysis of accident statistics, rely upon classification of LOC laid out by various regulatory agencies. These definitions or classifications are typically qualitative, providing insights into the nature and tangible events of the LOC phenomena. While somewhat incomplete for the task at hand, they nevertheless provide some key insight into the LOC phenomena upon which later development rests, and as such are an appropriate starting point for the current investigation.

In recent years a partnership between the Commercial Aviation Safety Team (CAST) and the International Civil Aviation Organization (ICAO) known as the CAST/ICAO Common Taxonomy Team (CICTT) has developed a set taxonomies for aviation accident and incidents. This taxonomy has allowed for increased clarity

across the global aviation community by providing an industry standard with regards to aviation incident definitions. From the CICTT's taxonomy, the occurrence definition for loss-of-control in-flight is [32]:

> Loss of aircraft control while, or deviation from intended flightpath, in flight.
>
> Loss of control in-flight is an extreme manifestation of a deviation from intended flight-path. The phrase "loss of control" may cover only some of the cases during which an unintended deviation occurred.

In addition the CICTT taxonomy provides additional guidance for the usage of this occurrence category. This guidance clarifies situations which may precede or even instigate an LOC event. In some instances the aircraft may be degraded in some way, such as the case of component or system failures or icing of the lifting surfaces. Unimpaired aircraft are still at risk of LOC through various situations which lead to "deviation from intended flightpath," such as stalls, spins, stall/spins, or pilot-induced oscillations [32].

A similar definition of LOC provided by FAA describes LOC as "an unintended departure of an aircraft from controlled flight" [58]. Their perspective closely resembles the CICTT's specification of LOC while also providing some additional insight. In particular, the FAA comments that LOC may occur as a result of departure from the "normal flight envelope," while providing additional contributing factors which include several human factors considerations such as "poor judgment or aeronautical decision making" [58].

The LOC categorizations provided by the CICTT and FAA accentuate many important facets of this phenomena. Additionally, the numerous factors and considerations provided by these organizations suggest that the LOC is a rather complex phenomenon that can arise during a range of situations. Unfortunately however, while the qualitative classifications employed by the CICTT and FAA provide meaningful

descriptions of LOC, they do not describe the boundary or threshold between normal flight and LOC. In order to enable inclusion within the design process, a more precise characterization of the boundary is needed, namely a characterization that provides an indication of the onset of LOC quantitatively.

Given the known complexity of the LOC phenomena, it is surmised that this transition from normal flight to LOC is similarly complex. Within the literature, several researchers have investigated the factors and causes that play a role in LOC events, concluding that the sequence of events that precede LOC are, in fact, quite varied. Further, these data do exhibit some noteworthy patterns that aid in the quantification of a LOC boundary.

It may be observed that the basic notion of "deviation from an intended flight path" may occur at any point within a given flight. Statistical analysis of the timing LOC events however suggests that some LOC more commonly occurs within some phases of operation. A summary of data which includes the number of LOC events and resulting onboard fatalities for a set of LOC events collected by Belcastro et al. [18] is provided in Figure 5. The statistics represented in Figure 5 reflects LOC incidents and accidents involving commercial fixed-wing aircraft between 1996 and 2010 occurring primarily in North America and Europe. These data suggest that the most common phase of flight within which LOC occurs is takeoff and initial climb, such that 31% of LOC events occurred during this phase. This is followed by three phases of similar occurrence rates: 17% of events occurred during approach, 16% during climb, and 15% during cruise. In terms of on-board fatalities these four phases once more appear as the highest ranking, though the ordering is shifted. Namely LOC events which occurred in cruise are most fatal, accounting for 28% of the total onboard fatalities. This is followed by climb at 24%, takeoff and initial climb at 21%, and then approach at 11%. This mismatch is noteworthy as it suggests that the most common phase in which LOC events occur is not necessarily the most fatal, whereas the relatively

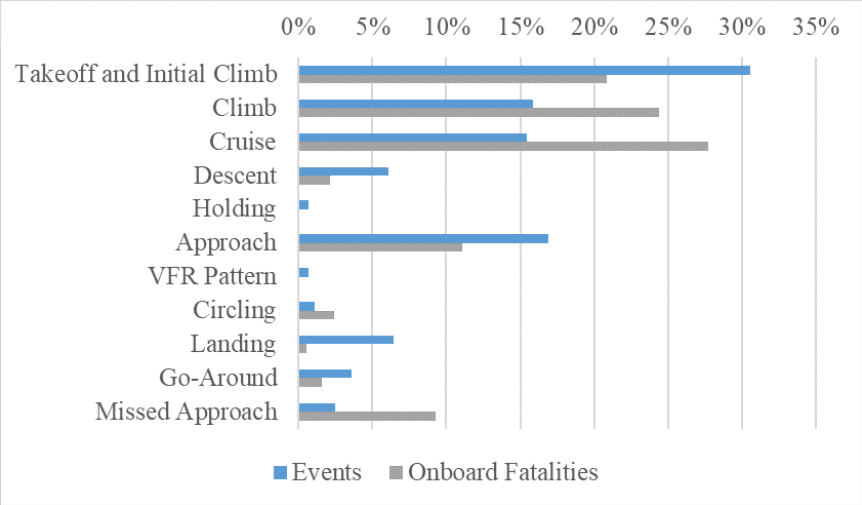

Figure 5: Number of LOC events and resulting on-board fatalities per phase of flight, adapted from Belcastro et al. [18].

less likely phase is the most fatal. While additional study would be required to fully understand this phenomena, it is possible that this higher level of fatality is related to the difference in the initial energy state of the vehicle. That is, during initial takeoff and during approach the aircraft will have a relatively lower total energy than during cruise, and to a lesser degree than during climb phase, such that though LOC events are more common during takeoff or approach their relatively lower total energy may contribute to a lower occurrence of on-board fatalities.

A notable examination of the various causal factors the precede LOC events was carried by Belcastro and Fostor [17]. This study examined data collected from aircraft operated mostly by air carriers under Part 121 that were involved in LOC events between the years of 1979 and 2009 and identified three broad categories of contributing factors to LOC. A summary of these categories is provided in Figure 6. The first was labeled as "adverse on-board conditions," which included various vehicle factors like damage or impairment and crew-related factors like mode confusion (i.e. confusion on behalf of a human with regards to the current operating mode of an automated system). The second category was a grouping of "external hazards and disturbances"

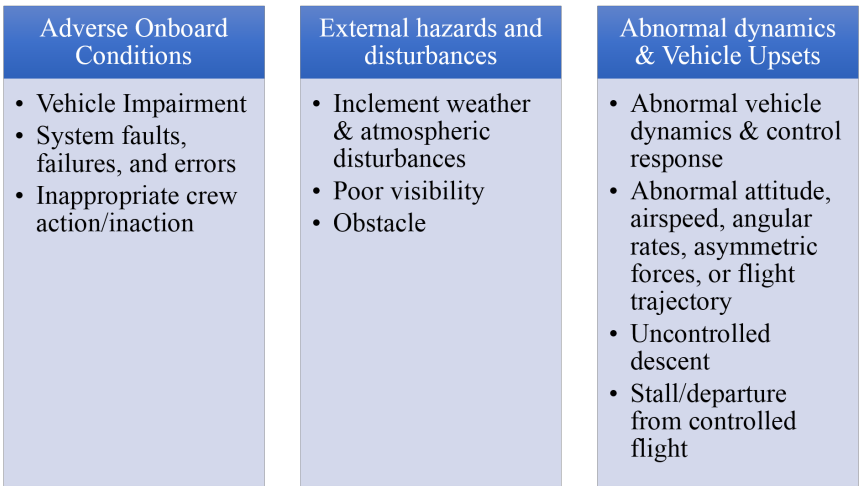

Figure 6: Categories of LOC causal factors, adapted from Belcastro et al. [20].

that consisted of environmental conditions that often contributed to LOC events. Belcastro and Foster's final category was "vehicle upsets," a category populated by various vehicle performance conditions like "abnormal attitude" or "abnormal flight trajectory." These categories were not posed as exclusive or independent, as a single LOC event often had contributing factors that fell into more than one of the given categories. Indeed, the authors studied the events that preceded the LOC events within the data and identified the sequences of causal factors that took place for each case.

Within each category of LOC causal factors shown in Figure 6 the most common members of each category are provided. While each member has been observed to have occurred in previous LOC incidents, some members are noted by Belcastro and Foster as more prevalent than others. Among adverse onboard conditions the most common events were "System faults, failures, and errors" and "Inappropriate crew action/inaction", occurring in 45.2% and 42.8% of the collected LOC data, respectively [17]. The most common external hazards were weather related, with snow or icing contributing to 22.2% of events and wind-related events like gusts, wind-shear, or thunderstorms contributing to 14.3% of LOC events within the data

set [17]. In addition, a separate study by Belcastro et al. [18]"Poor visibility" was observed to contribute to many LOC events, due primarily to limited visibility due to night-time operation, fog, or haze. Among LOC events which involve some abnormal dynamics or vehicle upsets it is most common that this event is a stall departure, which was noted to occur in 38.9% of all studied LOC events [17]. Other common vehicle upset conditions included "Abnormal vehicle attitude, airspeed, angular rates, asymmetric forces, or flight trajectory" which together contributed to 27.5% of LOC events, followed by "Uncontrolled descent" in 11.9% of events [17].

The analysis of Belcastro et al. [17] additionally revealed some notable trends, particularly with respect to the most commonly observed sequences of causal events. The authors identified a generalized set containing seven causal sequences, finding that these sequences represented, or were present in, 88.9% of the data set [17]. Inspection of these generalized sequences reveals some notable trends with respect to the typical event chain observed immediately preceding an LOC event. Most commonly it was observed that the initial factor in these causal sequences was some problem with the vehicle or an external disturbance. In addition, the final event within most of these sequences was a vehicle upset and the authors additionally note that "vehicle upsets are rarely the precipitating factor in the LOC sequence" [17]. An inappropriate crew response was also a common factor in the generalized causal sequences, albeit with a degree of variance as to their relative timing within the causal sequence, typically observed as a linkage between a disturbance to the vehicle and the upset of the vehicle. This common sequencing is represented in Figure 7, demonstrating the most general progression of causal events between normal flight and an LOC event.

In a subsequent similar study using a larger data set, Belcastro et al. [20] continued this identification of LOC causal factors. However, the later study focused more heavily on the identification of the worst-case combination of causal factors in terms

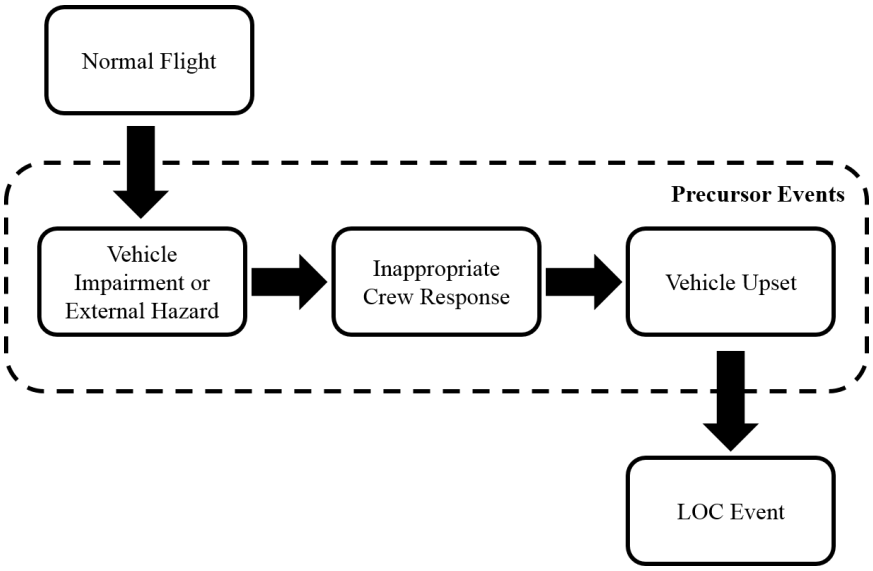

Figure 7: General causal sequence from normal flight to LOC event, adapted from Belcastro and Jacobson [21].

of both the number of accidents attributed to a given combination and the number of fatalities involved in ensuing accident. Their study observed that the general LOC sequence identified by Belcastro and Foster [17], and depicted in Figure 7, further demonstrates the general form of the worst-case scenario. More specifically, the worst-case combination was found to be " System & Component Failures /Malfunctions, Inappropriate Crew Action / Inaction, and Vehicle Upset Conditions" [21].

The analysis of casual events preceding a LOC event yields a more complete characterization of the progression from normal, safe flight to LOC. Qualitatively speaking, these results suggest that the boundary between normal flight and LOC should be characterized by an interaction of adverse system or environmental factors, the actions of the pilot, and the behavior of the aircraft in off-nominal or upset conditions. These observations are in agreement with the regulatory classifications employed by the CICTT and FAA, and also align with other work found within the literature. In particular, a similar, and popular, description of LOC is provided by Wilborn and Foster, stating that LOC is:

> outside the normal operating flight envelopes; not predictably altered by pilot control inputs; characterized by nonlinear effects, such as kinematic/inertial coupling, disproportionately large responses to small state variable changes, or oscillatory/divergent behavior; likely to result in high angular rates and displacements; characterized by the inability to maintain heading, altitude, and wings-level flight [174].

Taken together, these qualitative characterizations of LOC indicate a set of conditions from which a LOC threshold could be defined quantitatively. In particular, the most relevant causes of LOC are identified as [19]

1. Excursion from nominal flight envelope or entry into upset condition
2. Highly nonlinear flight dynamics
3. Degradation of pilot control efficacy

These causes will be leveraged in Section 2.2 as possible aspects from which a quantitative description of LOC will be gleaned.

2.2 Loss of Control Quantification

Within the literature, three prominent perspectives on LOC quantification. First, building upon the notion of LOC as some excursion from a nominal flight condition several authors define envelopes which separate nominal flight from LOC conditions. Second, as the final event in the causal sequence identified by Belcastro and Jacobson [21] is vehicle upset it follows that the detection of vehicle upset would similarly provide a quantitative assessment of LOC onset. Third, the highly nonlinear flight dynamics common to LOC provide another means of quantifying LOC through analysis and better understanding of dynamics of the vehicle near LOC conditions. These three perspectives and the relevant literature they include will be further within this section.

2.2.1 Flight Envelopes

In general a flight envelope is understood to be some subset of the state space within which the vehicle may operate safely. These envelopes can be viewed as constraints upon various aspects of the aircraft, including the vehicle's performance or representations of its physical limitations. From the perspective of LOC definition and analysis, a more nuanced view of flight envelopes will be considered. In addition to the condition that the interior of a given flight envelope indicates a domain of safe operation, the exterior of the set should also correspond to the LOC region. With this view, then, the flight envelope itself satisfies the desire for a quantifiable boundary between normal flight and LOC.

This approach is corroborated by the work done by Wilborn and Foster [174]. Using various data collected from aircraft accidents involving LOC, Wilborn and Foster developed a criterion for detecting the presence of LOC within flight data named the "Quantitative Loss-of-Control Criteria (QLC)" [174]. This QLC is a union of five envelopes, each consisting of pre-defined constraints placed on two key aircraft states. For each state considered within the envelopes some minimum and maximum accepted value is used to define a set boundary that defines the envelope. A summary of these envelopes and the states each constrains is shown in Table 2. In addition, Wilborn and Foster studied the onset of LOC predicted with the QLC using a set of flight data within which LOC was known to have occurred. This study indicated that "borderline LOC" is indicated whenever two of the five envelopes is exceeded simultaneously, while the excursion from three or more envelopes indicates the onset of LOC. Additionally, the authors noted that during normal operation "maneuvers, even if aggressive, usually do not exceed more than one envelope" [174].

The application of the QLC is an intuitive and straightforward approach that has proven to be both effective and somewhat popular within the literature. Many authors have implemented the QLC as a means of readily identifying LOC using either

Table 2: Summary of QLC envelopes developed by Wilborn and Foster [174]

Name of Envelope	**First State**	**Second State**
Adverse Aerodynamics	Angle of Attack, α	Sideslip Angle, β
Unusual Attitude	Bank Angle, ϕ	Pitch Angle, θ
Structural Integrity	Velocity, V	Load Factor n
Dynamic Pitch Control	Dynamic Pitch Angle, $\theta' = \theta + \dot{\theta}$	Percent Pitch Control
Dynamic Roll Control	Dynamic Roll Angle, $\phi' = \phi + \dot{\phi}$	Percent Roll Control

real or simulated flight data, such as Ref. [14, 99, 178]. However the means by which the envelopes are defined are not entirely precise, being tied to commonly accepted standards for "good" values of various state minima and maxima. This means of envelope definition results in envelopes that are divorced from the actual dynamics or capabilities of the vehicle. Should a more rigorous and vehicle-specific determination of flight envelopes be desired, and some results within the literature have suggested methods by which these envelopes could generated in such a fashion. For instance, Keller et al. [93] and Tang et al. [166] have demonstrated the methods for dynamic and adaptive flight envelope determination based upon various changes or faults in the vehicle.

In pursuit of other rigorous definitions of flight envelopes, it is helpful to consider the general intent or goal of the flight envelopes themselves. These envelopes answer the question: within what region or set of conditions can the aircraft be assured to operate and maneuver safely? This perspective aligns quite closely with the notion of safe sets or the safe maneuvering envelope, which can be defined as "the set of all initial conditions such that the ensuing trajectories of the system do not violate imposed constraints" [112]. Based upon this definition of the safe set, the region of the state space within which LOC occurs will lie outside the safe set so long as appropriate constraints are specified, making safe sets an attractive option for the definition of an LOC boundary characterization.

To study these sets mathematically, we first consider the state vector as $x \in \mathbb{R}^n$

and let $\mathcal{C}$ be a subset of the state space $\mathbb{R}^n$. In particular, this subset $\mathcal{C}$ is defined as

$$\mathcal{C} = \{x \in \mathbb{R}^n | l(x) > 0\} \tag{1}$$

where $l : \mathbb{R}^n \to \mathbb{R}$ is a continuous function. The function $l(x)$ may be thought of distance measure of the state x from a set of boundaries such that $l(x) = 0$ if the state is on some boundary and $l(x) > 0$ if it is within the boundaries [106]. The safe set, $\mathcal{S}$, is then defined as "the largest positively control-invariant set contained in $\mathcal{C}$" [98].

The determination of the safe set has been performed for several vehicles within the literature, producing regions of the state-space within which the vehicle can be safely maneuvered (see Ref. [5,40,89,97,98,105,112,171]). Computation of the safe set itself is closely related to reachability analysis, through which a subset of the state space can be identified such that some valid control action exists that ensures that the vehicle remains within the safe set for all time. Within efforts to assess LOC, reachability analysis has been carried out by several authors, such as Refs. [6, 7, 12, 98, 130, 171].

Performing the computation necessary to identify the safe set is often accomplished numerically. While many methods for performing this computation are present within the literature, only one of the more common methods will be presented. This method was proposed by Lygeros, who demonstrated the computation of the safe set by solving the Hamilton-Jacobi equations [106]. For some terminal time, T, and control set, U, then the relevant equations to be solved are then

$$H(p, x) = \min \left\{ 0, \sup_{u \in U} p^T f(x, u) \right\} \tag{2}$$

$$\frac{\partial V}{\partial t} + H(\frac{\partial V}{\partial x}, x) = 0, V(x, T) = l(x) \tag{3}$$

The function $V(x, t)$ is a weak solution of the terminal value problem above. From the function, the safe set is then defined as

$$\mathcal{S}(t, \mathcal{C}) = \{x \in \mathbb{R}^n | V(x, t) > 0\} \tag{4}$$

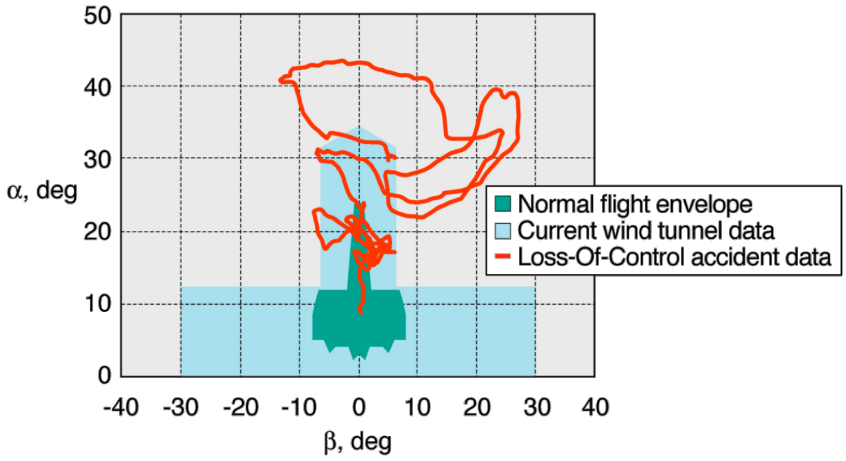

Figure 8: Depiction of difference between aerodynamic testing envelope and sample LOC conditions, from Foster [61]

2.2.2 Vehicle Upset Detection

With respect to LOC events, vehicle upsets typically refer to either stalls or spins, however can also refer to divergent flight phenomena such as unstable phugoid or spiral modes. The dynamics of these conditions is often quite complex, requiring high-fidelity analysis and testing to measure and assess in many cases. In fact, a comparison of flight data recorded during an LOC event and the range of conditions typically tested within a wind-tunnel, as shown in Figure 8, suggests that even extensive testing will often not provide data relevant to upset conditions. Indeed, existing studies and modeling efforts of the aerodynamics of these regions relies upon extensive wind-tunnel testing performed using a scale model of existing vehicle designs [121, 124].

Given this challenge, a more tractable approach is to pursue methods which identify the onset of vehicle upset conditions. This task closely aligns with the definition of flight envelopes that were formerly discussed. Onset of a vehicle upset can be considered as a departure from safe, normal flight, therefore becoming some portion of the flight envelope boundary that should be identified. Indeed, traditional aircraft performance analysis can provide pertinent estimates of the onset of some vehicle upset

conditions, such the calculation of velocities at which stall is predicted to occur.

Within recent literature there has been some development of criteria for detecting stalls and spins in aircraft flight data [30, 131]. These criteria have been developed for use with flight data, lending some promise to similar uses for different vehicles. In addition to the flight data itself, the work by Bunge et. al. [30] additionally suggests the detection of stalls or spins are, at least in part, reliant upon the monitoring of various state constraints. These constraints should therefore also be incorporated into the determination of flight envelopes.

2.2.3 Nonlinear Fixed Wing Flight Dynamics

As a specific case of a controlled dynamical system, aircraft are most accurately described as nonlinear systems. However the dynamics of many aircraft have been observed to be nearly linear within some nominal flight regimes, such as during nominal cruising conditions. As such much of the dynamic analysis of nominal flight conditions has historically been performed using linear systems theory, particularly a linearized version of the nonlinear equations of motion about some operating condition. While the simplification to linear dynamics is often a reasonable approximation, many flight regimes are highly nonlinear in nature, such as in flight conditions very close to vehicle upset conditions (e.g. pre-stall). Indeed, it was noted by Wilborn and Foster that the LOC condition is "characterized by nonlinear effects, [174]" which implies that between normal flight conditions and LOC there is a corresponding transition from linear or quasi-linear dynamics to nonlinear dynamics and behavior.

A first approach in describing this transitive nature can be considered to be assessment of the degree of non-linearity of a given flight condition. One available measure of this degree of nonlinearity is the nonlinearity index developed by Omran and Newman [125]. The non-linearity index includes a set of non-negative scalar values evaluated for a given condition that indicate the "amount" of non-linearity as

increasing positive values and a value of zero indicating completely linear dynamics. An evaluation of the degree of nonlinearity of longitudinal aircraft dynamics over a flight envelope of altitudes and velocities was performed along with the discussion of the nonlinearity index by Omran and Newman [125]. More recent work by Abdallah et al. [2] demonstrates a more general application of the non-linearity index to a 6-DOF aircraft model over an $\alpha - \beta$ flight envelope.

While certainly useful, knowledge of the degree of non-linearity of a system in a certain condition does provide a complete picture. In many cases a quantification of the aircraft's stability is also required. Consider a general nonlinear dynamical system expressed as

$$\dot{x}(t) = f(x(t)), \quad x(0) = x_0, \quad t \in \mathcal{I}_{x_0} \tag{5}$$

with state $x(t) \in \mathcal{D} \in \mathbb{R}^n$, open domain $\mathcal{D}$, and continuous function $f : \mathcal{D} \to \mathbb{R}^n$. Stability of this general system is defined by Haddad and Chellaboina as the following: [77]

Definition 1. [i]

1. The zero solution $x(t) \equiv 0$ to Equation (5) is Lyapunov stable if, for all $\epsilon > 0$, there exists $\delta = \delta(\epsilon) > 0$ such that if $||x(0)|| < \delta$, then $||x(t)|| < \epsilon, t \geq 0$.

2. The zero solution $x(t) \equiv 0$ to Equation (5) is (locally) asymptotically stable if it is Lyapunov stable and there exists $\delta > 0$ such that if $||x(0)|| < \delta$, then $\lim_{t\to\infty} x(t) = 0$.

3. The zero solution $x(t) \equiv 0$ to Equation (5) is globally asymptotically stable if it is Lyapunov stable and for all $x(0) \in \mathbb{R}^n$, $\lim_{t\to\infty} x(t) = 0$.

Within the literature descriptions or analysis of local asymptotic stability is most common, particularly for work describing actual systems such as aircraft. In addition,

the analysis of the stability of equilibrium conditions has been found to be of particular importance for LOC. Statistical surveys of LOC accident data, such as the studies of Belcastro [17,20,21], have revealed that most LOC events involve a vehicle upset. This prevalence, as noted by Kwatny et al. [99], would suggest that an important facet of nonlinear flight dynamics to consider for LOC is the behavior near bifurcation points.

Within the past twenty years several authors have noted the relationship between undesirable behavior of aircraft and bifurcation, beginning with Carroll and Mehra's development of the bifurcation analysis and catastrophe theory methodology (BACTM) [31, 114]. Since their work many authors performing bifurcation analysis using the continuation method, a mathematical method for constructing equilibrium curves by varying some parameter. Notable work of this variety includes the stability analysis performed by Ananthkrishnan and Sinha [10], Goman et al.'s application to upset conditions like stall and spin [75], and Thomas et al.'s application for determining F-16 maneuver envelopes [169], with similar analysis shown within Refs. [13, 69, 72–74, 132, 133, 173]. A succinct overview of some history and theory of continuation methods, particularly when applied to aircraft dynamics, is given by Cummings [37].

While bifurcation points are of interest from a stability perspective, other properties of these points are also of interest for LOC analysis. Kwatny et al. define a bifurcation point of a system as an equilibrium point of the system that satisfies at least one of the following conditions [96]:

1. there is a transmission zero at the origin,

2. there is an uncontrollable mode with zero eigenvalue

3. there is an unobservable mode with zero eigenvalue

4. it has insufficient independent control

5. it has redundant outputs

The definition above poses bifurcation points not only as points of unstable dynamics, but also of points where the ability to control or regulate a system may be lost or degraded severely [99]. At the bifurcation point itself it has been shown that regulation of the system with linear feedback control is impossible, though it may still be controllable with some non-linear controller [95]. Indeed, this fundamental change in the dynamics of the nonlinear system at bifurcation points has been tied directly to LOC by Goman et al. [75].

This loss of control effectiveness relates very directly with measures of system controllability and observability. While for linear systems these properties can be tested with rather straightforward tests, these same tests are not as readily available for nonlinear systems. Studies of controllability and observability have been studied within the literature, such as the work by Hepner and Geering [81], Haynes and Hermes [80], Sussman et al. [165], and more recently by Wu [177]. The investigation of these properties, however, often become redundant, being implied by the investigation of other system properties, as can be noted by the definition of bifurcation points by Kwatny et al. [96].

2.3 Ongoing Loss of Control Abatement

Loss of control has come to be understood as a complex phenomenon requiring a focused and comprehensive strategy in order to effectively abate its effects. During their study of LOC causal events in flight data Belcastro and Foster examined flight data collected over a 15 year period. While new technologies were introduced over this time period, their analysis "showed little effect" in terms of improvement in LOC events [17]. This suggests that if improvements with regards to LOC are to be made that they will require more focused and coordinated efforts.

In 2000, the final report of the Joint Safety Analysis Team (JSAT), which was

commissioned by CAST, provided an extensive set of recommendations for LOC intervention [167]. These 576 recommendations included a wide range of suggested steps and represented a strategies that required close cooperation between manufacturers, operators, and regulatory body. The groupings used by JSAT for these recommendations speak to the scope of effort that the team anticipated would need to be accomplished [167]:

1. Design Issues
2. Training
3. Practices, Policies, and Procedures
4. Data Collection and Analysis
5. The Regulatory Role

Plainly it is ill-advised to pursue any singular implementation as the complete solution for LOC, for "there is no 'silver bullet' that will solve all such accidents" [101]. Rather what will likely be required is a portfolio of solutions, each carefully harmonized with the others. This view is echoed and expanded upon by the work of both Jacobson [88] and Belcastro et al. [19], and is in agreement with the diversity of recommendations for LOC intervention provided by the JSAT [167].

Considering the numerous causal factors identified for LOC, a natural framework for organizing technological strategies for LOC mitigation has been recommended by Belcastro [16,21] and is represented in Figure 9. This framework can be viewed as the foil of the general causal sequence depicted in Figure 7, aiming to 'break the chain' at each opportunity.

2.3.1 Avoidance and Detection of Hazards

The first potential method of intervention envisioned by Belcastro is a combination of avoidance and detection. The intention described by Belcastro for avoidance is

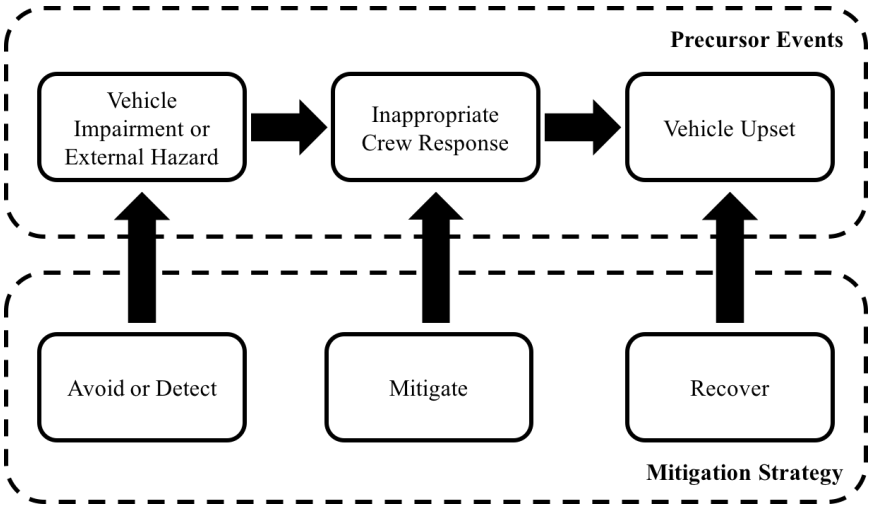

Figure 9: Framework for LOC mitigation strategies, adapted from Belcastro [16]

not merely to refrain from entering unsafe flight regimes, but also to anticipate using sensors, models, and training to anticipate external hazards and subsequently avoid them. This aspect of the strategy additionally considers improvements to system reliability as a means of avoiding potential vehicle impairments. Detection is a similar and closely related activity within the framework. Through an effective set of techniques and technologies, it is envisioned that external and internal hazards (i.e. atmospheric anomalies, vehicle health management) can be quickly detected and appropriately managed.

The process of avoidance and detection relies upon some capability of identifying an imminent LOC incident, typically through some quantitative assessment of LOC onset. These quantitative metrics can be used to monitor the vehicle state in real-time and present some indication of LOC proximity to the pilot. Some work has additionally tested the efficacy of providing visualization of the vehicle state to the pilot as a means of avoiding LOC situations, such as the work by Glaab and Takallu [70]. Quantitative prediction of LOC onset has also been utilized for predicting control limitations. For instance, Barlow et al. [14] present an algorithm that predicts the minimum control input that lead to some envelope excursion.

Alongside the detection of unsafe flight conditions is the detection of faults in the vehicle itself. The general problem of the detection of faults, including some component failure or other damage, is a well-studied problem in the literature. A thorough survey of fault detection, isolation, and reconfiguration (FDIR) methods as applied in a number of fields, including aviation, is provided by Hwang et al. [82]. A depiction of the general strategy employed by FDIR methods is also shown in Figure 10. In general, faults may be detected through some combination of hardware (i.e. sensors) and algorithms that compare measured system performance with expected system performance predicted with models.

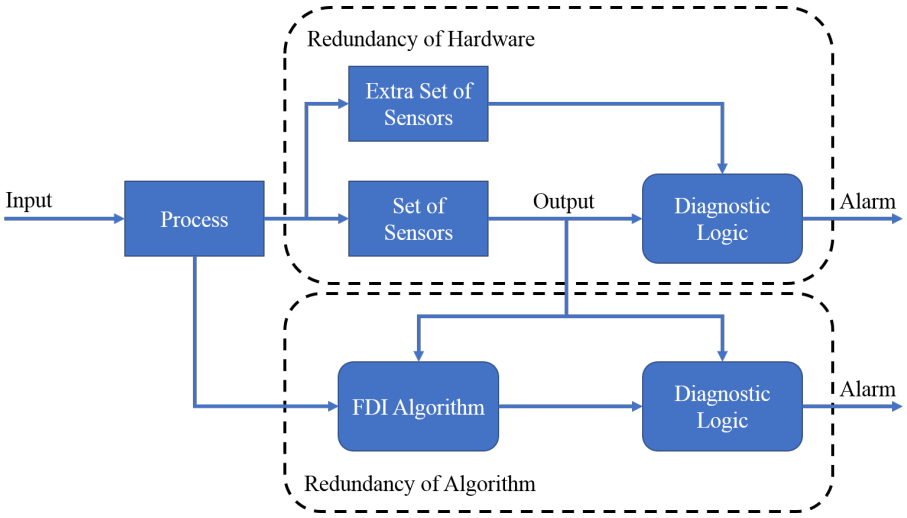

Figure 10: General process of fault detection through hardware and software observation, adapted from [82].

2.3.2 Mitigation of Inappropriate Response

In the event that a hazardous condition is unavoidable, then the second means of intervention is the mitigation of inappropriate responses. Given that some hazardous condition is encountered, such as a vehicle failure or unsafe operating condition, the intent of mitigation is to ensure that appropriate action is taken such that the vehicle does not enter into a vehicle upset condition and ultimately a LOC incident. From a technological perspective, mitigation may be achieved through "failsafe guidance and

control systems" that ensure safe vehicle operation in the event of some failure of the aircraft system [16]. Such control strategies have been explored within the literature, particularly for cases of vehicle faults. Similar effect can also be envisioned without automated flight control itself through systems that provide detailed information to the pilot in the event of a hazardous situation.

Within the literature numerous methodologies and algorithms have been presented which are either directly intended for mitigation of LOC or can be easily adapted for this purpose. Some noteworthy and representative examples of these algorithms will be presented briefly. Much work in the literature is concerned with the development of algorithms which are capable of providing assurances of safe operation in the presence of system faults. These methods are often present in manufacturing fields, where plant controllers must adapt to faults or failures in machinery, but the basic principles and often the algorithms themselves can be adapted for aircraft. In this area of research Blanke et al. [27] present a survey of some core concepts related to the general methods of fault-tolerant control, and a more comprehensive survey of fault-tolerant methods applied to a variety of fields is given by Hwang et al. [82]. For aircraft, many fault-tolerant algorithms are generated with specific categories of failures in mind. For instance, Chang et al. [34] presented results for a re-configurable control algorithm intended for LOC prevention in the event of elevator jams, though the authors additionally propose that such an algorithm could be extended to other system faults including actuator failures and structural damage. More recent work includes the methods of Donato et al. [39] for LOC prevention in the case of rudder jams.

Other approaches in the literature for LOC mitigation do not assume that some vehicle failure has occurred but address concerns related to mitigation of vehicle upset conditions. These approaches often fall into the category of flight envelope protection or protection of some pre-defined safe set. Some algorithms that provide a

representative sample include the work by Dogmo [40], McDonough [112] and Falkena et al. [49]. A more recent effort of note is that of Stepanyan et al. [163] who present a method for identifying imminent LOC conditions and provide auditory, visual, and tactile cues to a pilot in order to help mitigate the event from manifesting.

2.3.3 Recovery from Upset

The third and final segment of the intervention strategy framework proposed by Belcastro is the recovery of the vehicle from an upset condition. In aircraft with advanced control systems, recovery from upset conditions can be achieved through application of well-designed algorithms. Such algorithms can face some challenges, as they must often account for adverse conditions such as vehicle faults which may have been a causal factor in the onset of the upset condition in addition to the normal constraints of the vehicle.

There are a large number of proposed algorithms that can be identified for this portion of the LOC mitigation framework. Indeed, a general aim of many control algorithms is to provide some assurance of convergence to safe operating condition, particularly in the wake of some upset condition. Two general classes of algorithms will be presented, in accordance with the designation provided by Richards et al. [151]: offline and online algorithms.

The methods which are considered as "offline" typically exhibit approaches to LOC recovery that require extensive computation. In general these approaches seek to find a recovery strategy for a given set of LOC conditions that is then stored for future application on a real system. These methods are often attractive since a wide variety of conditions can be considered can potentially be explored and the relaxed constraint on computational expense present an opportunity to apply algorithms that require significant information or time to generate solutions.

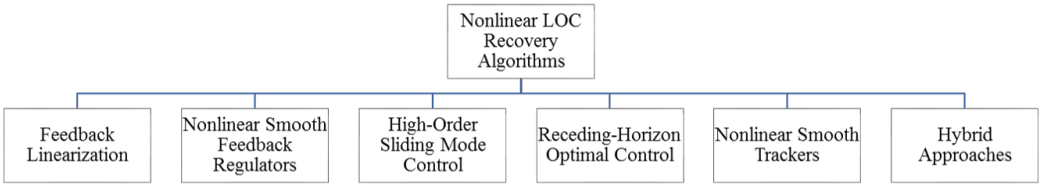

Figure 11: Overview of common LOC recovery algorithms.

Offline methods for recovery strategy generation can often be considered as optimization algorithms. That is to say, many offline algorithms pose the recovery problem as a constrained minimization problem where some optimal control strategy is sought from among the set of all possible control actions [151]. Others utilize various training or reinforcement learning techniques, such as training neural networks [44, 151] or some other machine learning methods like differential dynamic programming (DDP).

The set of "online" methods include algorithms which are intended to be applied in-situ. For aircraft, such algorithms are often intended for use in advanced avionics suites which include autonomous piloting capabilities. In theory, nearly any algorithm could be applied to the LOC recovery problem, though the performance of many algorithms may be found to be unsatisfactory. To attain more satisfactory performance the dynamic considerations of LOC conditions must be taken into account, in particular the highly nonlinear dynamics aircraft behavior of aircraft in LOC conditions (see §2.2.3). An overview of some popular methods found within the literature is given in Figure 11 and a short description of each method will be given below.

Feedback Linearization

A common technique in the analysis of nonlinear systems is the linearization of the system about some reference condition, such as a desired equilibrium point. This approach is often quite reliable, however use of the linearized system is restricted to some small neighborhood. Within the small neighborhood around the reference

condition, a feedback controller can be used to provide stability of the equilibrium condition [95]. At the edges of the LOC envelope, however, this process of linearization may become quite difficult due to proximity to bifurcation points. One approach is to utilize a method of linearization which can account for the presence of shifting model parameters, such as the linear parametric varying (LPV) model, and use this as the basis for feedback control [40, 42].

Nonlinear Smooth Feedback Regulators

While the use of feedback linearization has been suggested as an effective approach for LOC recovery, some improvement has been suggested through relaxation of the model linearization. By generating an "extended" linear model which includes some additional nonlinear terms a nonlinear smooth feedback regulator may be generated. Through the addition of nonlinear terms, the control allows for more accurate prediction and control of nonlinear behavior. However the inclusion of higher-order terms increases the complexity of the controller design, presenting a tradeoff that must tailored to each individual application, but has been shown to nevertheless be potentially effective in providing LOC recovery [42, 44].

High-Order Sliding Mode Control

A popular method for LOC recovery is the application of sliding mode control, particularly high-order sliding mode control [40, 42, 157, 178]. This method is attractive at least in part due to its *a priori* assurance of time to converge [100], which is to say that alongside generation of the control strategy one has a assured finite time in which the target condition will be reached. While the setup of this algorithm is somewhat more complex than other algorithms, it has been noted as providing solutions which are realizable in practical applications.

Receding Horizon Optimal Control

For control of linear systems, it can be shown that the optimal full-state feedback control gain is the linear quadratic regulator (LQR). In addition LQR is an attractive

solution for linear systems due to the assurances of robustness in the form of infinite gain margin and phase margin of 60°. Though restricted to application to linear systems, LQR design may be extended to nonlinear systems as receding horizon optimal (RHO) control. This approach retains some attractive features of LQR, namely the assurances of robustness [151], but the requirement to generate the solution to an optimization problem for each time-step presents some challenge for online implementation. It has been noted, however, that modern techniques are able to overcome this burden [108] and has seen application in recent literature for LOC recovery [64, 151].

Nonlinear Smooth Trackers

For many approaches, the restoration of the aircraft from an upset condition is done such that the vehicle is restored to either to the previous safe condition or some general known safe set. Alternative approaches however more specifically select the target safe condition and design an algorithm which tracks this chosen target [43, 45]. Often the target point is selected as the "nearest" point within the safe set to the current vehicle condition or some other "optimal" point [178]. In practice, these algorithms may closely mirror other algorithms, but with the method of target point selection providing the degree of separation.

Hybrid Approaches

Throughout the literature for LOC recovery techniques a common observation is that some additional improvement can often be found through application of more than one algorithm simultaneously. For instance, Donmgo et al. address the LOC recovery problem through application of feedback linearization coupled with high-order sliding mode control [40, 42]. In addition to some "overlapping" of control algorithms, Zhao et al. [180, 181] present a methodology which splits the LOC recovery problem into different stages, with a unique control application for each stage. In this approach, for instance, a certain algorithm may first be applied to arrest or "pre-condition" the LOC event from which a second algorithm generates a recovery strategy.

One common aspect of these LOC recovery algorithms is their overall complexity, both in their creation and in the sequence of control actions dictated by the algorithm. In general, the LOC recovery algorithms present within the literature assume the presence of some automated flight control system that is capable of quickly responding to an identified LOC event. Through survey of the GA fleet it was found that the average age of an active GA fixed wing aircraft is at least 40 years old, with 80% of active GA fixed wing aircraft being at least 35 years old [52]. Aircraft of this age likely were not built an autopilot system capable of full aircraft control. Some degree of automation is present within the GA fleet, as one-axis and two-axis autopilot systems are common for new aircraft and it is quite possible that older aircraft may be retrofit with such an autopilot device.

If a one-axis or two-axis autopilot system is onboard, though, it is likely intended for relieving pilot workload by maintaining some constant aircraft setting, such altitude or velocity, for long periods of time [53]. Such systems are ill-suited for adaptation to LOC recovery situations, which are dominated by high-frequency, nonlinear behavior. In addition, the LOC recovery algorithms present within the literature often are online strategies, suggesting integration into an advanced avionics system which includes extensive instrumentation of the aircraft. The retrofit of such systems to older aircraft is likely infeasible for many pilots due to the high cost of the system itself and the time and cost incurred to re-certify the vehicle once the new equipment has been installed. Given these constraints it is highly likely that the typical GA aircraft is not equipped with fully automated flight control systems, directly precluding the use of most of these algorithms that rely upon machine implementation. It could be argued that a human pilot may be able to execute some of these algorithms in some sense, as the control actions they may employ could align with those called for by a given algorithm. In practice, this would require the communication of the control commands called upon by the algorithm to the pilot in some fashion.

Table 3: General strategy for stall recovery, adapted from [54]

Sequence	Control Action	Intended Condition and/or Duration
1	Wing Leveler or Autopilot	Disconnect
2	Pitch	Nose Down until Stall Conditions Subside
3	Bank	Wings Level
4	Thrust	As Needed
5	Speed Brakes or Spoilers	Retract
6	Return to desired path	–

Table 4: General strategy for spin recovery, adapted from [54]

Sequence	Control Action	Intended Condition and/or Duration
1	Power	Idle
2	Ailerons	Neutral
3	Rudder	Full opposite to rotation
4	Elevator	Stick forward from neutral
5	Rudder	Neutralize once spin rotation stops
6	Elevator	Return to level flight

Guidance for upset recovery is provided to pilots, including pilots of GA aircraft, by the FAA through the *Airplane Flying Handbook* [54]. This guidance includes general strategies for recovery from both stalls and spins. The general strategy for stall in provided in Table 3 and the general strategy for spin recovery is provided in Table 4. This type of guidance for pilots provides a practical strategy for LOC recovery that is intended to be applicable in a wide range of conditions. In spirit, the recommendations of the FAA mirror some early development in the field of upset recovery, such as the spin recovery methods developed by Martin and Hill [107] and spiral recovery strategies of Lee and Nagati [102].

2.4 Observations from Literature

From the body of research identified from the literature, some key observations can be drawn which will more fully motivate later work. At the start it is to be noted that the LOC problem has been extensively studied. Among the collected results here, perhaps the most significant contribution is due to Belcastro and her various colleagues,

particularly in the development, avocation, and application of a unified framework for LOC research and eventual mitigation [19]. Much of the research present across the literature has come about in the last few decades, aided no doubt by the proliferation of flight data recording and more powerful computing capability. It can be seen that the wider availability of captured flight data in recent decades has enabled the quantitative analysis and identification of LOC conditions, as exemplified in the popular work in quantitative LOC envelope definition by Wilborn and Foster [174]. Alongside these quantitative measures, the ability to accurately simulate aircraft near to and even beyond upset conditions has enabled an accumulation of research on LOC mitigation that is bolstered by quantitative analysis. This is particularly true for the work performed on LOC recovery strategies, as nearly all proposed algorithms are tested on the high-fidelity simulation of a generic transport vehicle known as the Generic Transport Model (GTM) [61].

In review of the various approaches for LOC quantification, it is important to note that in many cases these different approaches do not each describe some unique event but rather offer different perspectives pertaining to the same event. This is to say that for a given LOC control event, one may consider that not only has some safe-operation flight envelope been violated, but that in doing so the vehicle has entered into an upset condition which is characterized most often by highly nonlinear vehicle behavior. The use, then, of any singular means of identifying or quantifying LOC either directly or indirectly implies the application of some or all other means of quantifying LOC. In this sense then, it is asserted that the proper application of the the various methods of LOC quantification requires some trade-off to be performed by the analyst.

An additional observation seen through the study of the causal chain of LOC events, depicted in Figure 7, there exist two implied skews which must be considered. First is the case for which some incident or failure has occurred which impairs the

vehicle and degrades its performance. In this case then a successful strategy should be capable of both correctly detecting the fault that has occurred and providing a strategy that avoids or recovers from the ensuing LOC event. The second case is for which an unimpaired vehicle enters some vehicle upset condition, which is either actively avoided or mitigated. The distinction between these two cases is somewhat subtle, but is significant in terms of the implications on the final LOC mitigation strategy such that some early consideration must be made which allows for one or both cases.

Finally, given the intent of the this work is to address LOC concerns for GA aircraft, it is appropriate to address how the background presented above applies to this specific subset of aviation. In general, most of the methods or techniques present within the literature were developed with transport aircraft in mind, or in other cases have only been applied to transport category aircraft. While this does not preclude their use for GA, it does imply that many of the constraints present for GA that are not present for other vehicles are likely to not have been considered in these methods. The dynamics of GA vehicles are qualitatively similar to transport aircraft, though it is known that in general transport aircraft tend to be more stable than GA aircraft. This decreased overall stability implies some increased tendency to enter into LOC situations, which may be captured through application of the quantitative methods presented before.

Other practical constraints of GA operation are more pressing when considering the reviewed LOC mitigation strategies. An implicit or explicit underlying assumption for many strategies or approaches for LOC mitigation or recovery is the availability of some advanced avionics capability which may include availability of full-state observation or the presence of autonomous aircraft control. For a typical GA vehicle, these capabilities are most often not present and inclusion of such capability is beyond

reach of many GA operators in terms of high acquisition cost and high cost of re-certification of the vehicle. Rather, a typical GA vehicle likely only has steam-gauges for representation of vehicle parameters to the pilot. The collection of fight data is sometimes only possible through the use of modern personal electronic devices which observe and collect data without interfacing with the aircraft systems or instruments. In addition, the pilot of the GA aircraft is the sole entity capable of controlling the aircraft, and any strategies or techniques used for LOC mitigation must be generated by the pilot. While it is possible to provide some level of recommendation to the pilot, perhaps through physical artifacts such as checklists or some other cue, the use of automated flight control is impractical.

CHAPTER III

PROBLEM FORMULATION

In Chapter 1, the prevalence of LOC events was noted within aviation. While aviation safety has improved over time, LOC remains a pressing concern for the aviation community. This concern is particularly acute for GA, which sees a high number of LOC incidents every year. The survey of the current understanding of LOC presented within Chapter 2 suggests that the efforts of the aerospace community to understand LOC phenomena have been fruitful. This research has precipitated ongoing efforts to enact LOC mitigation strategies within the aviation domain. Applying these present strategies to GA, however, presents unique challenges that have not yet been accounted for. If these or other LOC intervention strategies are to be effective in reducing the rate of LOC incidents within GA, then careful consideration of GA-specific constraints should be made.

This section of the dissertation is organized as follows. The overall objective of this dissertation, as formulated from these observations, will be presented in §3.1. In pursuit of this objective, several research questions have been identified, and are presented in §3.2.

3.1 Research Objective

In order to address the need for LOC mitigation for GA, the objective of this dissertation is:

Research Objective:
Develop a methodology for the prediction and mitigation of LOC incidents for fixed-wing GA aircraft within the typical GA operation limitations.

Pursuant to this objective, a series of research questions will be posed in the remainder of this section. Prior to these questions, some pertinent assumptions for this work are provided.

1. The definition of what constitutes a "general aviation" vehicle can be somewhat vague at times, and may encompass a wide variety of vehicle types. This work in particular will focus upon small, fixed-wing general aviation aircraft which fall into the normal category as defined in Part 23 of the FAR [55].

2. It is known that many LOC incidents are preceded by some fault or failure of the vehicle. However, this work will assume that the aircraft in question is fully functional, with no system failures that could degrade the operation of the vehicle.

3. The available data for the methodology is that which can be collected by personal electronic devices. Examples of such devices and their common use in GA aircraft are readily available. For the purposes of this work, it will be assumed that these devices, including some GPS capable devices and an altitude and heading reference system (AHRS) are in use on-board the aircraft and can actively provide real-time flight data.

4. Throughout this work, it is assumed that a sufficient flight simulation capability is available for use. This capability allows for the simulation of GA aircraft in realistic scenarios and the testing of various algorithms and methods. As part of this simulation capability, it is additionally assumed that calibrated performance models and models of rigid aircraft dynamics for a representative GA aircraft are available for use in the methodology. For reference, the general equations of motion that are used for vehicle simulation are given in Appendix C.

With this research objective in mind, the overarching hypothesis of this work may be stated as follows.

Overarching Hypothesis:

A model-based method with real-time evaluation of proximity to LOC boundaries and generation of situation-appropriate instructions for LOC avoidance or recovery will enable LOC prediction and avoidance for fixed-wing GA vehicles.

This overarching hypothesis is associated with the methodology that will be developed herein which identifies LOC envelopes, provides real-time estimation and assessment of flight conditions, and provides recovery strategy recommendations when appropriate. An overview of the methodology is given in Figure 12, where it can be observed that the methodology will consist of three major components. First a set of techniques and tools will be developed which allow for the estimation of LOC envelopes. Then the flight data available during the flight of a typical fixed wing GA aircraft will be used to estimate the required aircraft states. Finally a set of LOC recovery strategies will be generated that will enable the mitigation of or recovery from an LOC event. In short this methodology seeks mitigate LOC incidents by providing a framework which enables the restriction of the aircraft to a safe operating envelope. Thus this proposed methodology is a means of **M**itigation by **E**nvelope **R**estriction for **L**oss-of-Control **IN**cidents, or MERLIN. To test this this overarching an series of research questions are posed which will examine the capability of a methodology such as is described in the overarching hypothesis.

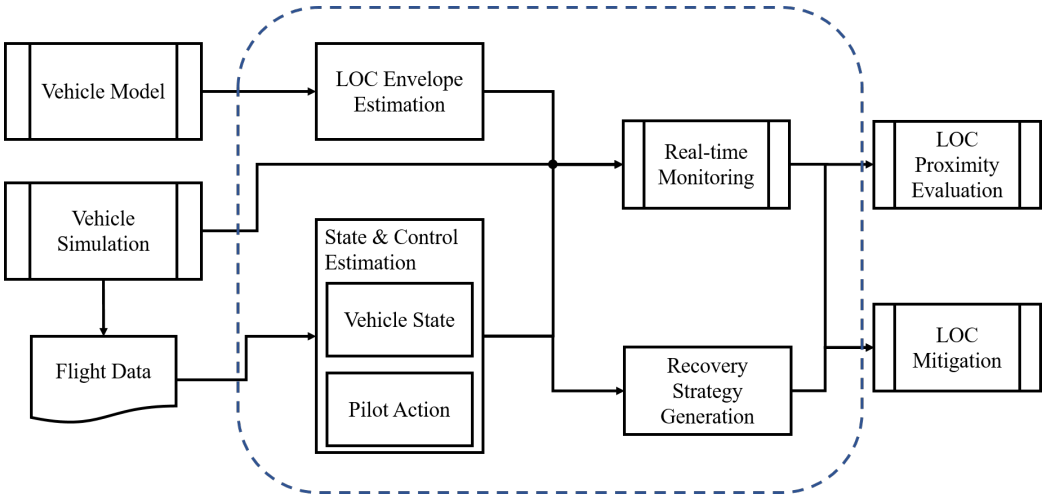

Figure 12: Overview of the MERLIN methodology.

3.2 Research Questions

Pursuant to the overall research of this work a series of research questions are developed. The first set of questions examines the proposed LOC envelopes of the methodology. Then a subsequent set of questions will be posed which relate to the evaluation of the aircraft's proximity to LOC onset in real-time. The final set of research questions then probes the generation of LOC recovery strategies and the efficacy of communicating the strategies to a human pilot.

3.2.1 Assessing Level of Confidence for LOC Envelopes

Within §2.2, various methods of quantifying LOC and its onset for aircraft were discussed. From these techniques, the generation of a LOC envelope can be constructed, and is discussed in more detail in the Chapter 5. In general the generation of an LOC envelope requires some assumptions to be made regarding the conditions for which LOC onset occurs. With a model of the flight dynamic performance of the aircraft in question, these onset conditions can then be used to define a set of LOC boundaries, collectively referred to as a LOC envelope. Inherent within this process are multiple sources of uncertainty, each affecting the implicit level of confidence associated with the prediction made by the LOC envelope. Given this, the first research question

posed by this work is:

Research Question 1:

What is the level of confidence afforded by a LOC envelope and how sensitive is this confidence to variability or uncertainty in the envelope generation process?

In answering this research question, two primary sources of epistemic uncertainty will be addressed. At the onset of envelope generation one selects certain threshold values which correspond to the onset of LOC conditions. These thresholds may arise from common practice or intuition, as demonstrated by Wilborn and Foster [174], or from more analytic processes. In either case, these thresholds are themselves uncertain, as the exact value for which LOC is said to occur is difficult to ascertain for a given vehicle. This uncertainty leads to some error in the prediction of the LOC threshold value and therefore to the LOC envelope which utilizes it. Consideration of this leads to the first sub-question:

Research Question 1.1:

How sensitive are the LOC boundaries of a given LOC envelope to variability of assumptions in the envelope generation process?

Within the literature, it has been demonstrated repeatedly that LOC envelopes built from assumed thresholds or conditions accurately represent LOC onset conditions [61, 174]. As these envelopes included some error, though not explicitly addressed, their observed accuracy suggests that this effect of this error is not an undue hindrance. Given this, the following hypothesis is formed:

Hypothesis 1.1: *The sensitivity of a LOC envelope with respect to uncertainty in assumptions is within reasonable limits and is correlated with the magnitude of assumption uncertainty.*

Alongside the uncertainty in threshold estimation, the second source of epistemic uncertainty considered at this stage of the proposal is that present within the modeling of the aircraft. It is well established that no model is truly perfect, and as such there is some level of error associated with the flight dynamic model of a given aircraft. When this imperfect model is used to generate estimates of LOC envelopes there is then a resultant error in the final product. Therefore the second sub-question considered is then:

Research Question 1.2:

How sensitive is the LOC envelope to uncertainty in the aircraft dynamical model?

While a dynamic model is known to have some error, this error in general is known to be small such that the model provides a sufficient approximation of the underlying system. Additionally, Haddad and Chellaboina [77] note that if a dynamic model is reasonably accurate then the resultant trajectories predicted by this model will be similar to the true trajectory for small, finite time horizons. Consider two dynamical systems,

$$\dot{x}(t) = f(x(t)), \quad x(t_0) = x_0, \quad t \in [t_0, t_1] \tag{6}$$

$$\dot{y}(t) = g(y(t)), \quad y(t_0) = y_0, \quad t \in [t_0, t_1] \tag{7}$$

with $f : \mathcal{D} \to \mathbb{R}^n$ and $g : \mathcal{D} \to \mathbb{R}^n$ and both f and g are Lipschitz continuous on $\mathcal{D}$. In particular, we restrict the system f to be uniformly Lipschitz continuous on $\mathcal{D}$ with Lipschitz constant L. Then suppose that the difference between the systems f and g can be expressed as

$$||f(x) - g(x)|| \leq \epsilon, \quad x \in \mathcal{D} \tag{8}$$

Equation (8) relates the systems f and g through their evaluations at all points on some domain $\mathcal{D}$. If one considers the system g as the "true" dynamical system

and the system f as an approximation of system g, then Equation (8) ensures that the error between these systems is bounded over the full domain by some constant ϵ. Of additional concern is then the way in which the error between the systems propagates through to the trajectories $x(t)$ and $y(t)$. That is, given some initial conditions and systems f and g with difference bounded as Equation (8), how "close" are the solutions $x(t)$ and $y(t)$ at some given future time?

Assuming that the initial conditions x_0 and y_0 are close to one another. More precisely, let

$$||x_0 - y_0|| \leq \gamma \tag{9}$$

Then the difference between the solutions $x(t)$ and $y(t)$ is

$$||x(t) - y(t)|| \leq \gamma e^{L|t-t_0|} + \frac{\epsilon}{L}\left(e^{L|t-t_0|} - 1\right) \tag{10}$$

The proof of Equation (10) is shown by Haddad and Chellaboina [77] and is provided in Appendix D for completeness.

This result yields some key insight into the theoretical impact that dynamical model error has upon the LOC envelope. First, Equation (10) provides assurance that if the error of the dynamical model is within some small bound then the outcome predictions made with this erroneous model will likewise be bounded. The bounds on the output solution error is seen to grow exponentially with time, implying that the accuracy of predictions with an inexact model can be quite trustworthy over small time intervals but rapidly degrades over time.

The LOC envelopes developed through the present methodology are likely to rely upon the dynamical model for the generation of the safe set. In the work by Lygeros [106], a numerical example based upon aircraft dynamics is provided. For this sample problem, it is noted that a time horizon of only 2.5 seconds is needed to ascertain the appropriate safe set. Separate work presented by McDonough and Kolmanovsky [111] also studied safe set generation through trajectory simulations that lasted 15 seconds

each. These result suggests that the exponentially growing error of Equation (10) as it relates to the LOC envelopes will have moderate effect, given the small time horizon for which the LOC envelopes can be expected to require.

The exponential growth of the error is also affected by two constants: the difference between initial conditions, γ, and the Lipschitz constant, L. By assuming that the analysis of dynamical model uncertainty effect on LOC envelopes is performed at identical initial conditions, then the value of γ can be assumed to be zero. Estimation of the growth in error for trajectories is then dependent on estimation of the Lipschitz constant, which provides an upper bound on the rate-of-change of a system. For the dynamical systems which will be studied, i.e. GA fixed-wing aircraft, it is reasoned that this limit is sufficiently low, as a high threshold would imply a system which is highly sensitive to any state perturbation. Therefore the following hypothesis is made:

Hypothesis 1.2: *The sensitivity of a LOC envelope with respect to uncertainty in the dynamic model over some finite time is within reasonable limits and is correlated with the magnitude of the dynamic model uncertainty.*

To address these questions and their respective hypotheses, three experiments will be performed. Experiment 1.1 and 1.2 are designed to test Hypothesis 1.1 and 1.2, respectively, and are designed to test the sensitivity of the LOC envelope to each source of epistemic uncertainty in isolation. In addition, Experiment 1.3 will test the level of confidence that can be expected from an LOC envelope under both sources of uncertainty simultaneously. These experiments will be described here briefly, with a more in depth discussion included in Chapter 5. The relationships between the first set of research questions and experiments is also depicted in Figure 13 for convenient reference.

Experiment 1.1: LOC Envelope Sensitivity to Assumption Uncertainty

During the generation of LOC envelopes, various performance thresholds will be defined. This definition will involve some level of uncertainty which will propagate to the final LOC envelope. Within this experiment, the threshold uncertainty will be modeled quantitatively and then propagated through the LOC generation procedure. This process can then be repeated while varying the assumed degree of uncertainty, resulting in a series of LOC envelopes which reflect various assumed threshold uncertainties. Then the sensitivity of the LOC envelope to this source of uncertainty will be assessed and used for later development.

Experiment 1.2: LOC Envelope Sensitivity to Model Uncertainty Along with the uncertainty in envelope threshold assumptions, an additional source of uncertainty in the LOC envelope generation procedure is error in the dynamical model of the aircraft. Using theories developed within the literature, the effect of this error can be related directly to error in predicted trajectories. Using this result, this experiment will perform a numerical propagation of the modeling error to the LOC envelope. As with the threshold uncertainty, these data will be utilized to quantify the sensitivity of the LOC envelope to modeling error and allow for assessment of reasonable limits to be imposed on the dynamical modeling error.

Experiment 1.3: LOC Envelope Level of Confidence Under Uncertainty Following the individual testing of the threshold assumption uncertainty and the uncertainty from modeling error, an additional experiment will be performed which tests the combined effect of the uncertainty on the LOC envelopes. Beginning from uncertainty bounds generated with Experiment 1.1 and 1.2 for each source of uncertainty, a set of tests will be performed within which various LOC envelopes will be produced with varying levels of uncertainty. From these tests a more realistic depiction of the effect of uncertainty on the LOC envelopes will be quantified. It is envisioned that from this experiment a set of uncertainty targets can be defined for a desired level of confidence, which will be of use for later experimentation and use of the full

methodology.

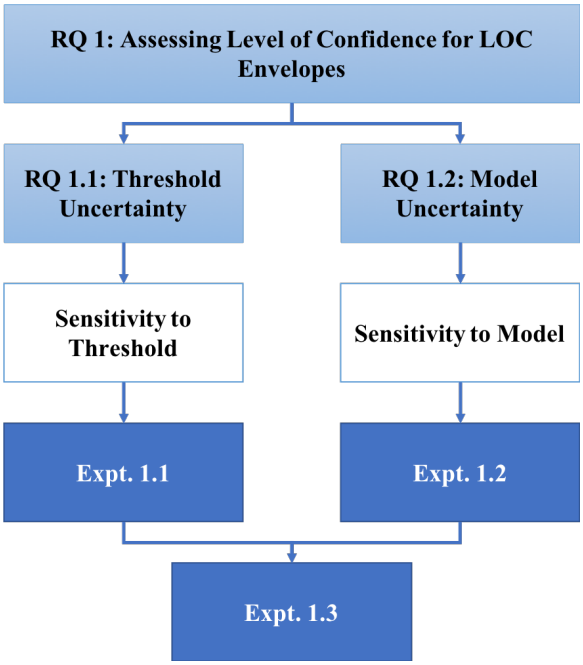

Figure 13: Overview of Research Question 1.

3.2.2 Real-time Evaluation of LOC Proximity

With an established LOC envelope, the methodology proposed within this work will address the prediction and mitigation of LOC using real-time evaluation of LOC proximity. This evaluation will rely upon real-time observation and assessment of the aircraft state and pilot controls. Yet, it is assumed that for the typical GA aircraft, information pertaining to the full aircraft state will be unavailable. Rather, a subset of the state vector is assumed to be available for use in this methodology. This constraint upon the data available during the flight of a typical GA aircraft leads then to the following research question:

Research Question 2:

How can the proximity of a GA vehicle to a LOC situation be assessed in real-time while considering the constraints on available flight data for typical GA aircraft?

Two issues require further consideration pertaining to this research question. As the data afforded through direct collection during flight is limited, some means of estimating the remaining states of the aircraft and the control actions of the pilot is required. This concern is addressed with the following sub-question:

Research Question 2.1:

How can missing data pertaining to the vehicle state and pilot control be accurately estimated?

Based upon the assumed data available to be collected through external measurement on-board a typical GA aircraft, the methodology should provide estimation of the un-observed portions of the aircraft state and all control actions of the pilot. These requirements are similar to those observed within the literature, albeit with no one resource which fully estimates all required aspects. From this, then, the following hypothesis is formulated:

Hypothesis 2.1:*All necessary states of the aircraft and the control actions of the pilot can be accurately estimated through a combination of state-estimation techniques, energy-based metrics, and an expectation-maximization algorithm.*

Using some combination of observed and estimated vehicle state with a generated LOC envelope, the proposed methodology evaluates the proximity of the aircraft to LOC in real-time. In addition to the error introduced through the estimation process, the collected states will be subject to some degree of noise arising. The following sub-question examines the accuracy of the resulting prediction of LOC onset:

Research Question 2.2:

What is the attainable accuracy or reliability of predicted LOC onset using a combination of collected and estimated flight data with *a priori* LOC envelopes?

As the true state of the aircraft and the pilot actions are unknown, there will be some error inherent in the estimation process. While the extent of the impact of this error will be ascertained as part of Experiment 2.2, it is first hypothesized that this analysis will yield a quantified relationship between the estimation error and the accuracy of LOC onset predictions. This assertion is expressed as Hypothesis 2.2:

Hypothesis 2.2: *The relationship between state and control estimation error and the accuracy of LOC onset can be quantified and will yield an attainable level of error needed for a given LOC onset confidence.*

The hypotheses for Research Question 2 will be tested with two experiments. Hypothesis 2.1 will be tested through Experiment 2.1, which will examine the accuracy of the state and control estimations using simulated flight data. Then Experiment 2.2 will test Hypothesis 2.2 through probabilistic analysis. A short description of these experiments is provided here, with more detail given in Chapter 6, and an overview of the relationships between the second set of research questions and the experiments is given in Figure 14.

Experiment 2.1: State and Control Estimation Accuracy In Chapter 6 a set of algorithms and methods will be described which enable the estimation of the full state of the aircraft along with the set of pilot control actions. This experiment will test the accuracy of these estimation techniques through application of flight simulation. Using an available flight simulation capability, a fixed wing GA aircraft will be simulated in nominal flight conditions while the full set of flight states and controls will be captured. From this full set of data a restricted set of data may be synthesized which reflects the data which may be assumed to be available during actual implementation of the methodology. The various estimation algorithms will then be deployed and the resulting estimations compared to the truth model collected as the full data set in order to yield an assessment of the accuracy of the methods.

Experiment 2.2: LOC Onset Prediction Accuracy This experiment will utilize both the estimation algorithms and the generated LOC envelopes to assess the accuracy of the LOC onset prediction capability. During this experiment the flight simulation capability will be used to simulate the flight of a fixed wing GA aircraft in both nominal and LOC conditions. The full data record of this simulated flight will then be used to construct a restricted data set. Then this restricted data set will be used to perform estimation of the "missing" aircraft states and controls and subsequent prediction of LOC onset using the generated LOC envelopes. Comparison of the predictions made by these portions of the methodology and the simulated aircraft data will then yield an assessment of the efficacy of the methodology to predict these conditions.

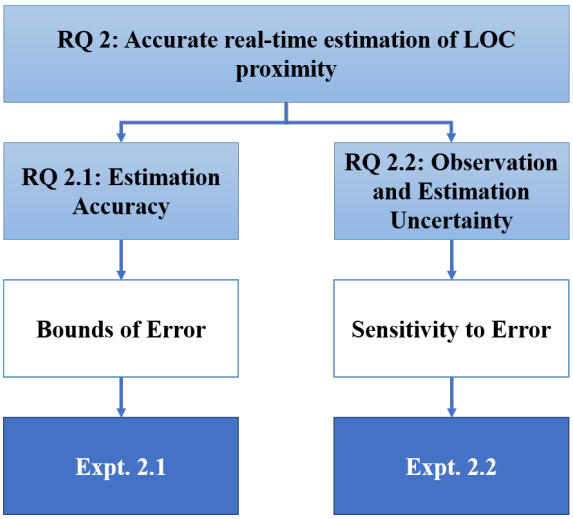

Figure 14: Overview of Research Question 2.

3.2.3 Generation and Recommendation of LOC Recovery Strategy

The first two research questions that have been presented largely pertain to the predictive capability of the methodology. Largely unaddressed thus far has been the capability of the methodology to mitigate a LOC event in the event that it occurs. This capability is the subject of the third and final research question, which is stated

below:

Research Question 3:

What is an appropriate strategy for LOC avoidance or recovery and how can this strategy be leveraged to synthesize real-time recommendations for a GA pilot?

From the literature survey provided in Chapter 2, several potential means of generating avoidance and recovery strategies were identified. In practice, many of the reviewed recovery strategies assume the presence of some on-board system for implementation of the generated recovery trajectory. For a the typical GA aircraft assumed by this work such a system is not available, with the pilot bearing sole responsibility for all avoidance and recovery actions. Therefore the LOC mitigation strategy generated by this methodology must meet these dual constraints, which is to generate a recommended mitigation strategy that is simultaneously accurate and sufficiently simple for communication with a human pilot. These two aspects are addressed in the following sub-questions:

Research Question 3.1:

What is an appropriate set of control actions for avoiding or recovering from LOC conditions?

Observation of the recommendations for upset recovery provided by the FAA [54] reveals a set of simple instructions for recovery from upset conditions. It is surmised from these recommendations that this type of instruction is an effective means of constructing recovery control actions when considering the pilots of GA aircraft. In, general, however the control strategies generated by methods found within the literature exhibit complex and sometimes non-intuitive control actions. Therefore it is desirable to generate a control strategy that not only allows for the avoidance or

recovery of the aircraft from LOC conditions but that is of a form that is appropriate for potential communication to and implementation by a typical GA pilot. From this point of view the following hypothesis is formulated:

Hypothesis 3.1: *A set of simplified control actions or archetypes can be generated such that an effective control strategy may be synthesized for a given LOC scenario.*

Once a strategy for avoidance or recovery from LOC has been created, it is assumed that this strategy must be communicated to the human pilot for implementation. During an imminent LOC situation, the pilot is quite likely to experience a heightened level of stress - a situation which is well known to inhibit cognitive function. Stress is known to cause individuals to focus their attention on some particular action or source at the exclusion of all others while simultaneously causing a reduction in one's working memory [162]. These considerations lead to the final sub-question of this work:

Research Question 3.2:

How can a specific set of control actions be efficiently communicated to a pilot during LOC conditions?

Given the general constraints of operating a GA aircraft with the additional situational demands of a stressful LOC condition, it is reasoned that the communication of LOC recovery recommendations should be accurate, concise, and timely. In other words, the methodology should clearly communicate the correct recommendation when it is needed in a clear and straightforward manner. Based on this reasoning, Hypothesis 3.2 is formulated.

Hypothesis 3.2: *A segmented control strategy consisting of properly arranged control archetypes can be recommended in stages with auditory prompts to the pilot at the appropriate time through real-time evaluation of aircraft state.*

The hypotheses for Research Question 3 will be tested through Experiments 3, which is briefly described below and more fully in Chapter 7. Finally, an overview of this research question is depicted in Figure 15.

Experiment 3: Efficacy of Simplified Recovery Strategy Methods From the literature review in Chapter 2 a set of LOC recovery algorithms was identified. Though these methods are not well-suited for direct implementation in the direct effort, they will serve as a basis for the generation of archetype sequences. This experiment will test the accuracy of these simplified sequences through simulation of the performance of the generated sequences of control commands in simulated recovery scenarios. By repeated simulation of a fixed-wing GA aircraft in LOC conditions and subsequent recovery using the developed recovery strategy, the efficacy of the method may be practically assessed. This final experiment will also test the efficacy of the communicated strategy. As it assumed that no automation capability is present on the typical fixed wing GA aircraft, then all LOC recovery strategies must be implemented by a human pilot. To test this communication a simulated pilot model will be employed which simulates the actions of a human pilot in response to a set of cues provided by the proposed methodology. This testing will be performed within the flight simulation, where the control commands of the simulation are provided by a pilot model which allows for varying response times and control aggressiveness.

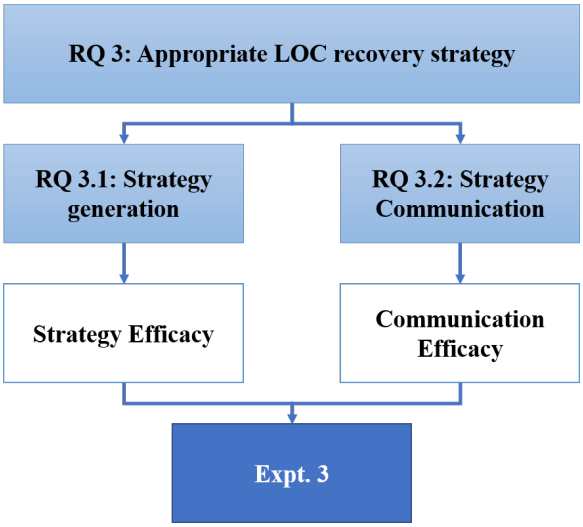

Figure 15: Overview of Research Question 3.

CHAPTER IV

DYNAMIC VEHICLE MODELING

In this section the development and application of a dynamic vehicle model will be discussed from two separate but related perspectives. First the application of the vehicle model within the LOC mitigation methodology will be considered, including a description of the envisioned applications of the vehicle model within the methodology and requirements imposed on the vehicle model but this usage. Then a discussion of notional model synthesis techniques will be presented which includes the development of a dynamic vehicle for use in demonstration and testing of the MERLIN methodology.

4.1 Methodology Vehicle Model Requirements

Within the methodology developed within this work it is assumed that a dynamic model of the GA aircraft of interest is available. In the deployment of the method the model's primary purpose is to aid in the construction of the LOC envelope and safe set, discussed in Chapter 5, and as such provides the most direct requirements for the vehicle model. Within the LOC envelope generation process the usage of a vehicle model is required for the construction of the safe set for a given normal operating envelope, as the definition of the normal operating envelopes is state-dependent. The estimation of the safe set may be performed with either nonlinear system dynamics, as demonstrated in the method proposed by Lygeros [106], or with linearized system dynamics as shown by McDonough and Kolmanovsky [111]. Selection of either of these options, then, will determine the type of vehicle model, nonlinear or linear, which is required. In this usage of linear models however it is to be noted that the underlying dynamics of the vehicle are known to be nonlinear, particularly as upset

conditions are approached, and care must be taken to carefully restrict the usage of linearized models to neighborhoods about the linearized conditions within which the assumptions of linearity remain valid.

In either case it is expected that the supplied vehicle model represents an accurate representation of the aircraft in question. This in general requires that the model provide an estimate of the vehicle's response in terms of forces and moments to the studied flight conditions, leading to a standard decomposition of the model to include methods for estimating the aerodynamic, propulsive, and inertial forces and moments of a given vehicle. As many methods for predicting these forces and moments are present within the literature it is instructive to additionally consider factors which allow for down-selection to a smaller set of applicable techniques.

For the GA aircraft considered within this research it may be assumed that the aircraft operates within the subsonic regime, allowing for the consideration of aerodynamic models which neglect Mach number effects. While operation in nominal flight conditions may often be well approximated with linear aerodynamic models these models are known to be less accurate near upset conditions such as stall and therefore the aerodynamic model must in general be nonlinear. Data which examines the characteristics of the GA fleet [52] suggest that the most common GA aircraft propulsive systems are single engine, piston-driven propellers, a trend which the propulsive model for the proposed methodology should reflect. In development of the propeller model the subsonic assumption present for the aerodynamic model no longer holds. In Figure 16 a contour plot is provided which demonstrates that the velocity due to both translational and rotational motion of the propeller may be well into the transonic regime at the propeller tip, thus Mach number effects should be included in determination of propeller performance. This propulsive system additionally provides guidance on the inertial modeling portion of the vehicle model, as the rotation of the engine-propeller system creates a gyroscopic effects which should be incorporated into

Table 5: Summary of vehicle model component requirements

Aerodynamic	Subsonic Nonlinear
Propulsive	Engine and Propeller Performance Includes Mach effects
Inertial	Body with $x-z$ symmetry Propeller inertia

the vehicle model. The remaining inertial properties may be assumed to apply to a rigid body having a plane of symmetry about the $x-z$ plane. A summary of these high-level model requirements is provided in Table 5.

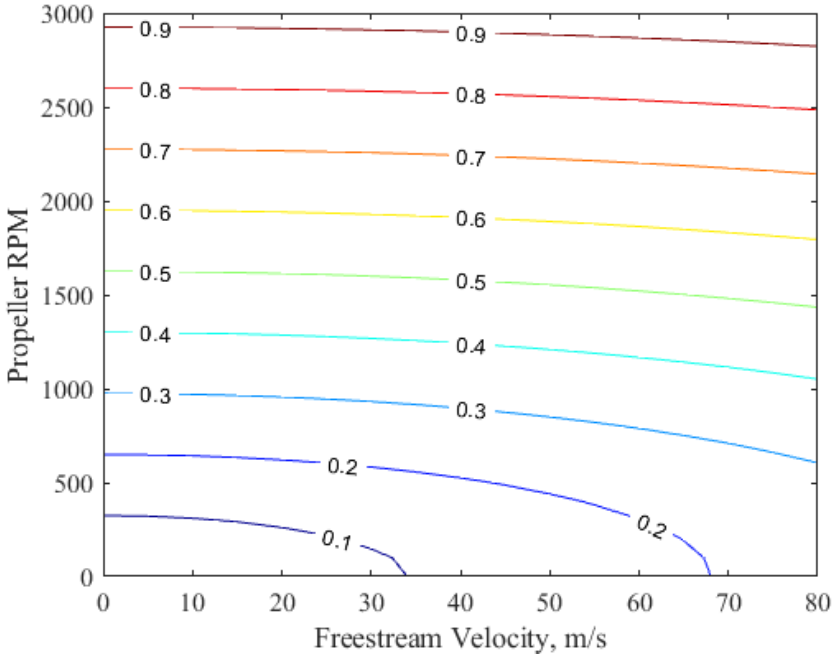

Figure 16: Propeller tip Mach number for propeller with $1m$ radius.

In the remainder of this section nominal methods of constructing a nonlinear dynamic aircraft model will be presented which satisfies these requirements. As a linear vehicle model may be gathered from linearization of the nonlinear model about a reference condition, the application of these methods may be used in constructing a vehicle model which satisfies either the nonlinear or linear method of safe-set determination. Alongside the presentation of these methods the definition of a particular

vehicle model will be provided which will serve as the test-bed for demonstration and experimentation of the LOC mitigation methodology.

4.2 Vehicle Model Synthesis

For testing and demonstration of the MERLIN framework a representative GA vehicle model will be required. While the modeling methods presented in this section may be generally applied, a particular model will also be provided which demonstrates these modeling techniques and provides a means of testing the LOC mitigation methodology.

The most popular variants of fixed-wing GA aircraft are high-wing and low-wing configurations, exemplified by the popularity of the high-winged Cessna 172 and low-winged Piper PA-28 commercial aircraft. While some anecdotal evidence may suggest the superiority of either high-wing or low-wing aircraft, related most often to secondary factors such as pilot comfort and accessibility, there is no clear performance distinction between the two categories.

Between each of the two primary GA categories, then, the selected aircraft model will reflect GA aircraft similar to the PA-28, a low-wing, single-engine aircraft produced by Piper Aircraft [139]. The PA-28 was first introduced in 1961 [22], seeing several revisions and modifications throughout its production history. Many of these revisions were minor such that the overall configuration and performance of PA-28 variants was similar. In producing a representative low-wing GA aircraft (LWGA) model, geometric and performance data will be drawn from publicly available information regarding the PA-28, and used in later validation to verify the reasonableness of the model.

4.2.1 Geometry Definition

In estimation of the aerodynamic, propulsive, and inertial properties of a given vehicle it is prudent to first define the geometric layout of the vehicle. Within the LOC mitigation methodology this geometric definition entails the outer mold line description of the vehicle along with specific exterior dimensions of the vehicle components. For a given vehicle these geometric parameters may often be gathered through information provided by the airframe manufacturer or may be measured directly.

For the specific model generated herein, an outer mold line of the aircraft model is first generated from three-views available within the PA-28-180 Owner's Handbook [137] and Service Manual [140], supplemented with data collected from three-views provided by McCormick [109]. These data were collected and used to define a complete vehicle geometry using the OpenVSP software, an open-source parametric geometry definition tool developed by NASA [110]. A representation of the final LWGA aircraft model geometry generated from this data is shown in Figure 17. In the remainder of this sub-section various geometric parameters commonly required during geometric definition will be briefly described.

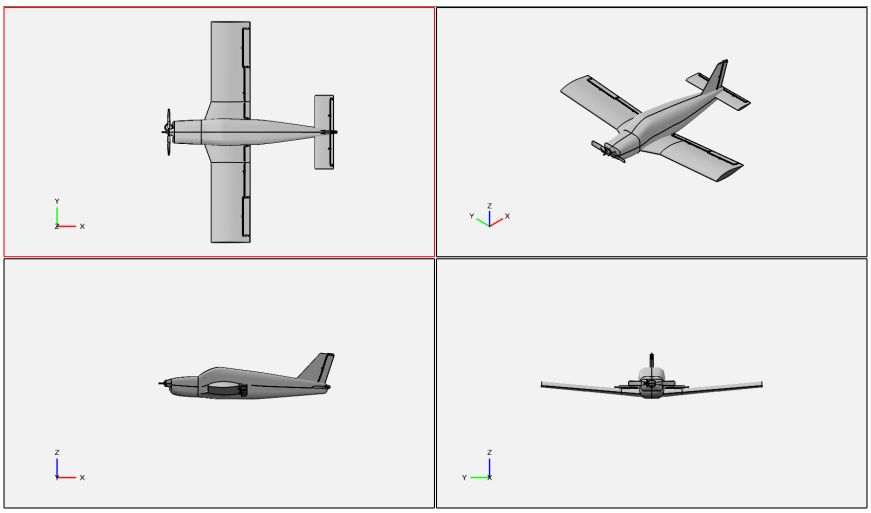

Figure 17: Three-view of the LWGA aircraft model geometry.

Geometric definition of the lifting surfaces, which traditionally includes the wing,

horizontal tail, and vertical tail, often focuses on determination of geometric factors which will affect the aerodynamic properties of the vehicle. These parameters include the overall wing span, area, and aspect ratio as well as more detailed information regarding the chord length along the span of these surfaces. For analysis which includes determination of the stability and control properties then the location and relative sizing of control surfaces is additionally required.

The wing geometry of the LWGA, shown in Figure 18, most closely resembles the wings present on the Piper Cherokee PA-28-180 variant of the PA-28 line of aircraft. This wing planform primarily consists of a rectangular wing shape, with a section of constant taper which spans from the root of the wing to one third of the wing span. In addition to the overall planform shape, the wing of the LWGA also shares most of its' dimensions with the PA-28-180 [109, 140]. The geometry of the LWGA wing additionally contains two control surfaces: outboard ailerons and inboard flaps. The dimensions of these control surfaces are provided along with a summary of the wing's geometric parameters in Table 6.

For the airfoil of the LWGA wing, the Piper PA-28 was again used as a reference. Early variants like the PA-28-180 and more recent variants such as the PA-28-181 are cited by McCormick [109] and Jackson et al. [87] as utilized the NACA $65_2{-}415$ airfoil. Abbott and von Doenhoff describe the NACA 6-series of airfoil as an attempted improvement over earlier airfoil designs "with the objective of obtaining desirable drag, critical Mach number, and maximum-lift characteristics" [1] and additionally provide experimental data for the NACA $65_2 - 415$.

The empennage of the LWGA model consists of a horizontal and vertical tail section. Each surface is depicted in Figure 19. The horizontal tail is a simple rectangular lifting surface whereas the vertical tail consists of a constantly tapered surface. Each surface of the empennage utilizes a symmetric airfoil section, namely the NACA 0012

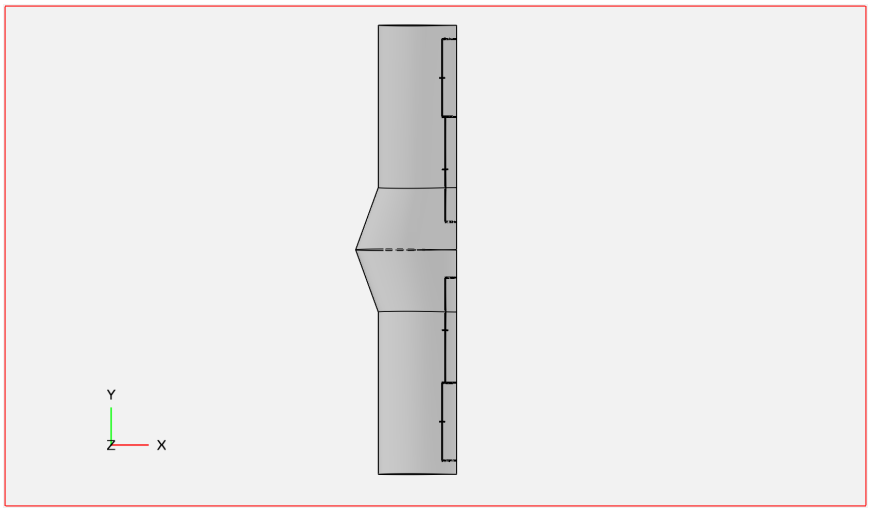

Figure 18: Top-view of the LWGA aircraft model wing planform geometry.

Table 6: Summary of wing geometry parameters.

Dimension	**Value**
Wing Span	9.144 m
Tapered Section Span	1.265 m
Root Chord	2.123 m
Tip Chord	1.600 m
Aileron Span	1.620 m
Aileron Width	0.3096 m
Flap Span	2.172 m
Flap Width	0.2540 m

for the horizontal tail and the NACA 0010 for the vertical tail. Rather than a sub-surface elevator located on the horizontal tail, the LWGA reflects the longitudinal control surface design of the PA-28-180 in its use of a stabilator, or full-surface elevator. For directional control, the LWGA rudder surface will comprise the aft 40 % of the vertical tail chord along the full span of the surface. Similar to the wing surface a summary of the geometric characteristics of the LWGA empennage are provided in Table 7.

While the fuselage geometries found on many commercial transport or business aircraft may be well approximated as bodies of revolution, this simplification is less applicable for common GA fuselages. Rather common GA aircraft such as the Cessna

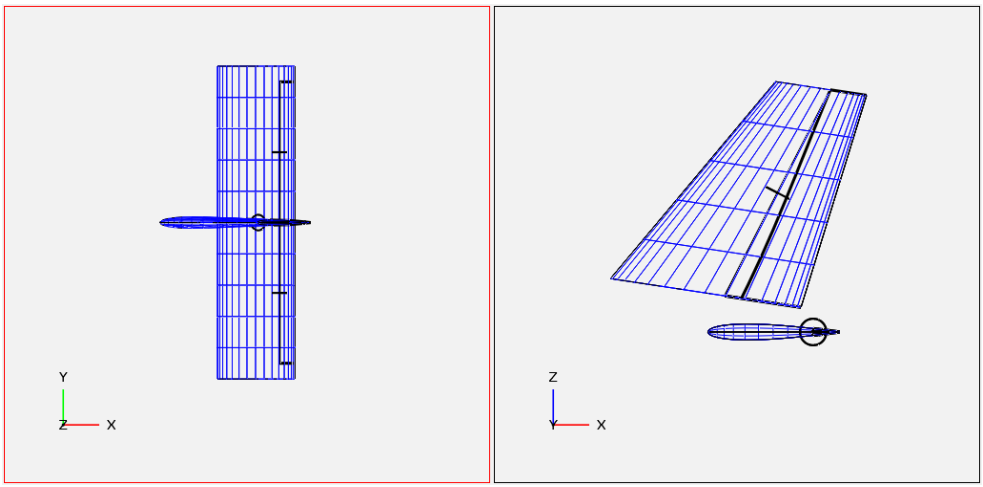

Figure 19: Top and side view of LWGA empennage surfaces.

Table 7: Summary of empennage geometry parameters.

Dimension	**Value**
Horizontal Tail Span	3.048 m
Vertical Tail Span	1.257 m
Horizontal Tail Chord	0.762 m
Vertical Tail Root Chord	1.109 m
Vertical Tail Tip Chord	0.530 m
Horizontal Tail Area	2.323 m^2
Vertical Tail Area	1.030 m^2
Rudder Root Width	0.135 m
Rudder Tip Width	0.0646 m

172 or Piper PA-28 typically feature a rounded rectangular cross sections which accommodate the engine and passenger compartments. Additionally the dimensions of these sections may vary non-uniformly over the length of the fuselage. As such it is generally found that while the overall length of the fuselage is commonly reported the particular dimensions (i.e. height and width) of the fuselage as a function of its length is more difficult to determine.

The fuselage geometry for the LWGA model was designed to reflect this commonly observed style of fuselage. Dimensionally the fuselage of the LWGA most closely reflects the fuselage on the PA-28-180 [140], while sharing some close similarity to the fuselage studied in various NASA wind tunnel tests [24, 26]. A representation

Table 8: Summary of fuselage geometric parameters.

Dimension	Value
Fuselage length	6.475 m
Fuselage maximum cross-section area	1.315 m^2
Fuselage volume	4.945 m^3

of the LWGA fuselage can be seen in Figure 20, and a summary of key geometric parameters is given in Table 8.

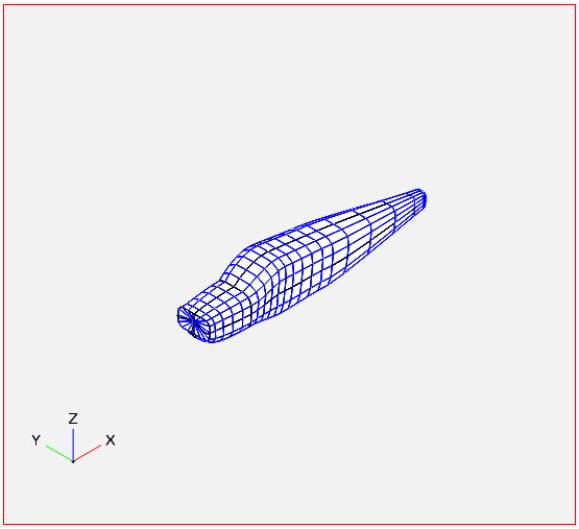

Figure 20: Isometric view of the LWGA fuselage.

In generating this fuselage particular care was taken in the selection of the cross-sectional shape. Wind tunnel testing conducted by Bihrle and Bowman [25] suggest that due to the difference in the moment arms between the fore and aft of the fuselage, the selection of cross-sectional shape of the aft sections has more influence that than of the forward sections. Later work to study fuselage aerodynamics by Pamadi and Taylor [128, 129] built upon this observation, implementing an "idealized" cross-sectional which most closely reflects aft cross-sections. This assumption of a single 'idealized' cross-sectional shape is similarly applied in this work, culminating in the rounded rectangular cross-section with a corner radius of $\frac{r}{b_0} = 0.245$. A sample representation of the "idealized" fuselage cross-section is shown in Figure 21.

With this fuselage cross-sectional shape defined and the general dimensions of the

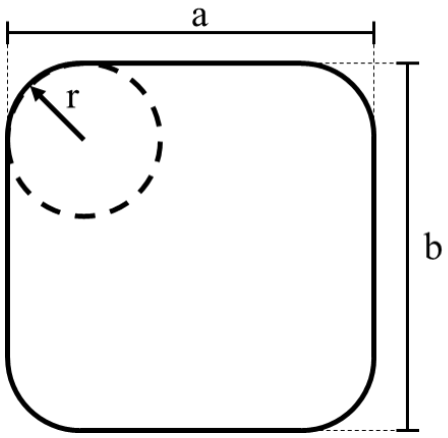

Figure 21: Depiction of rounded-rectangle fuselage cross-section.

fuselage collected from PA-28 data, the cross-sectional area of the fuselage along its length may then be calculated. In particular for a rounded rectangle cross-sectional area may computed as

$$A = ab - r^2 (4 - \pi) \tag{11}$$

The distribution of the fuselage geometry along the length of the LWGA is displayed in Figure 22, which shows a maximum cross-sectional fuselage area of approximately 1.315 m^2. Integration of the area along the length of the fuselage additionally allows for calculation of the fuselage volume of 4.945 m^3.

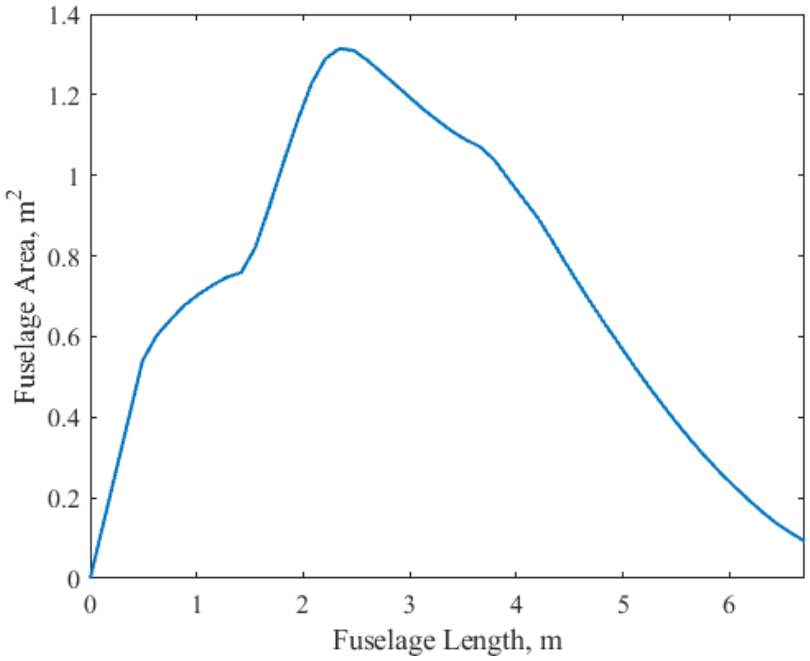

Figure 22: Cross-sectional area of the LWGA fuselage as a function of length.

4.2.2 Aerodynamic Modeling

In modeling of aerodynamic performance, a balance between fidelity and computational efficiency must be struck. The dynamic model of the LWGA is intended to serve as a realistic representation of the performance of a typical fixed-wing GA vehicle, particularly throughout the normal operating regime and approaching regions of loss-of-control. This application to both pre-stall and post-stall conditions requires an increased modeling fidelity which precludes some low-order modeling methods. At the same time, however, the desire for dynamic simulation of the vehicle model makes high-fidelity options like CFD undesirable due to the high computation time requirements. A compromise, then, will be struck through the construction of an aerodynamic model which captures the theoretical physics of the predominant phenomena and is augmented by observations and findings from empirical work. Two distinct aerodynamic models are developed herein, one for the system of lifting surfaces and a second for the aerodynamics of the fuselage. These models will be described in the

remainder of this section.

The general approach for development of an aerodynamic model of lifting surfaces was surveyed by Min et al. [116], which described the process of aerodynamic modeling for use in performance analysis as a "build-up" from 2-D, sectional characteristics to 3-D surface characteristics. This approach is common throughout classic performance analysis literature [11,149] and is present in recent work which models the full envelope performance of aircraft [9, 147, 153, 154].

Through much of the pre-stall region, both thin-airfoil theory and experimental results suggest that lift generated by an airfoil is predominately linear with angle-of-attack [1]. As stall is approached the linear behavior is degraded, behaving nearly quadratic with angle-of-attack. From these observations, then, the pre-stall and initial stall behavior of an airfoil may be modeled using the form supplied by Spera [161] and based upon work by Viterna and Janetzke [172] as

$$C_l = C_{l,\alpha}\left(\alpha - \alpha_0\right) - R_{Cl}\left(\frac{\alpha - \alpha_0}{\alpha_{Cl,max} - \alpha_0}\right)^N \tag{12}$$

with

$$R_{Cl} = C_{l,\alpha}\left(\alpha_{Cl,max} - \alpha_0\right) - C_{l,max} \tag{13}$$

$$N = 1 + \frac{C_{l,max}}{R_{Cl}} \tag{14}$$

The pre-stall lift curve model given in Equation (12) assumes that the lift curve is symmetric about the zero-lift angle-of-attack. This assumption is often reasonable for symmetric airfoils, which are the focus of the model developed by Spera [161], but less often observed for cambered airfoils. Given this consideration, Equation (12)

may be expanded as

$$\begin{cases} C_l = C_{l,\alpha}\left(\alpha - \alpha_0\right) - R_{Cl,max}\left(\frac{\alpha-\alpha_0}{\alpha_{Cl,max}-\alpha_0}\right)^{N_{max}} & \alpha \geq \alpha_0 \\ C_l = C_{l,\alpha}\left(\alpha - \alpha_0\right) - R_{Cl,min}\left(\frac{\alpha-\alpha_0}{\alpha_{Cl,max}-\alpha_0}\right)^{N_{min}} & \alpha < \alpha_0 \end{cases} \tag{15}$$

with

$$R_{Cl,max} = C_{l,\alpha}\left(\alpha_{Cl,max} - \alpha_0\right) - C_{l,max} \tag{16}$$

$$R_{Cl,min} = C_{l,\alpha}\left(\alpha_{Cl,min} - \alpha_0\right) - C_{l,min} \tag{17}$$

$$N_{max} = 1 + \frac{C_{l,max}}{R_{Cl,max}} \tag{18}$$

$$N_{min} = 1 + \frac{C_{l,min}}{R_{Cl,min}} \tag{19}$$

The corresponding pre-stall drag relationship developed by Spera [161] and generalized to allow for asymmetry about the zero-lift angle of attack is

$$\begin{cases} C_d = C_{d,0} + \left(C_{d,max,u} - C_{d,0}\right)\left(\frac{\alpha-\alpha_0}{\alpha_{Cd,max,u}-\alpha_0}\right)^{M} & \alpha \geq \alpha_0 \\ C_d = C_{d,0} + \left(C_{d,max,l} - C_{d,0}\right)\left(\frac{\alpha-\alpha_0}{\alpha_{Cd,max,l}-\alpha_0}\right)^{M} & \alpha < \alpha_0 \end{cases} \tag{20}$$

In the post-stall region up to approximately 90 degrees angle-of-attack, experimental results provided by Seidahl and Klimas [156] and Snyder et al. [160] suggest that the aerodynamic behavior of airfoil resemble the properties of flat plates. A comparison of the airfoil data presented by Seidahl and Klimas [156] and Snyder et al. [160] to the sectional lift of a flat plate is given in Figure 23, and the corresponding sectional drag in Figure 24. From Figure 23 and Figure 24 it is observed that in the post-stall region, between approximately 15 and 90 degrees angle of attack, the trends in both sectional lift and drag are quite similar to that observed for a flat plate.

In modeling this observed post-stall behavior, Spera [161] suggests a model similar

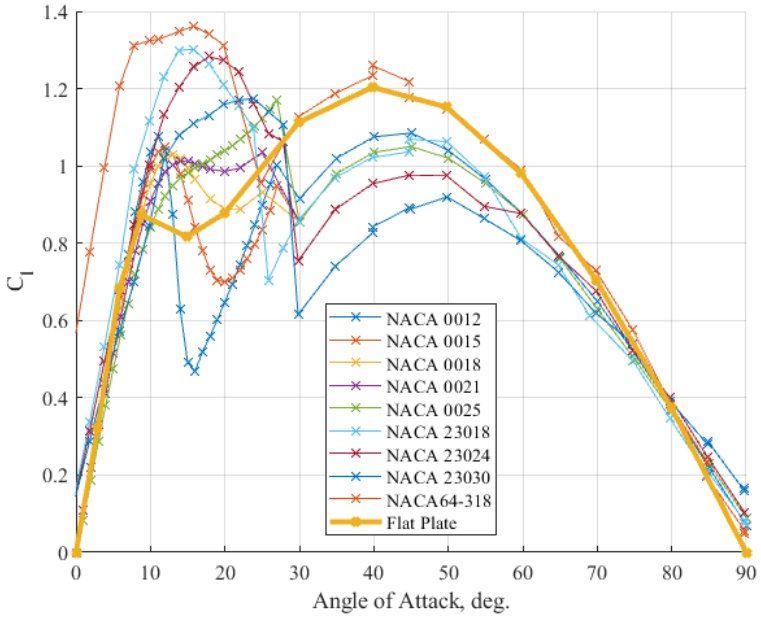

Figure 23: Comparison of various airfoils and flat plate sectional lift characteristics [156, 160].

to Equation (12):

$$\begin{cases} C_l = -0.032(\alpha - 92) - R_{Cl,2}\left(\frac{92-\alpha}{51}\right)^{N_2} & \alpha_{Cl,max} \leq \alpha \leq 92 \\ C_l = -0.032(\alpha - 92) + R_{Cl,2}\left(\frac{\alpha-92}{51}\right)^{N_2} & \alpha > 92 \end{cases} \tag{21}$$

As with the pre-stall equations, the assumption of symmetry about the origin may be relaxed to yield the following equations for the post stall region:

$$\begin{cases} C_l = -0.032(\alpha - 92) - R_{Cl2,max}\left(\frac{92-\alpha}{51}\right)^{N_{2,max}} & \alpha_{Cl,max} \leq \alpha \leq 92 \\ C_l = -0.032(\alpha - 92) + R_{Cl2,max}\left(\frac{\alpha-92}{51}\right)^{N_{2,max}} & \alpha > 92 \\ C_l = -0.032(\alpha - 92) - R_{Cl2,min}\left(\frac{92+\alpha}{51}\right)^{N_{2,max}} & \alpha_{Cl,max} \leq \alpha \leq 92 \\ C_l = -0.032(\alpha + 92) + R_{Cl2,min}\left(\frac{\alpha-92}{-51}\right)^{N_{2,min}} & \alpha < -92 \end{cases} \tag{22}$$

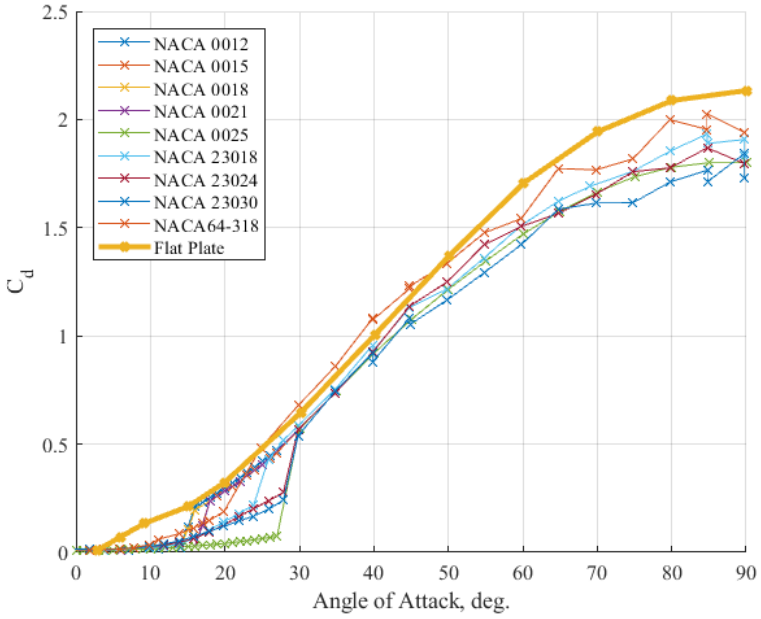

Figure 24: Comparison of various airfoils and flat plate sectional drag characteristics [156, 160].

where

$$R_{Cl2,max} = 1.632 - C_{l2,max} \tag{23}$$

$$R_{Cl2,min} = -1.632 - Cl2, min \tag{24}$$

$$N_{2,max} = 1 + \frac{C_{l2,max}}{R_{Cl2,max}} \tag{25}$$

$$N_{2,min} = 1 + \frac{C_{l2,max}}{R_{Cl2,max}} \tag{26}$$

$$C_{l2,max} = F_1 \times F_2 \tag{27}$$

$$F_1 = 1.190\left(1 - (t/c)^2\right) \tag{28}$$

$$F_2 = 0.65 + 0.35\exp\left[-\left(\frac{9}{AR}\right)^{2.3}\right] \tag{29}$$

$$C_{l2,min} = C_{l2,max} \tag{30}$$

The post-stall sectional drag, with the same considerations as above, is seen to be

$$\begin{cases} C_d = C_{d,max,u} + (C_{d2,max} - C_{d,max,u}) \sin \frac{\left(\alpha - \alpha_{Cd,max,u}\right)}{\left(90 - \alpha_{Cd,max,r}\right).*90)} & \alpha \geq \alpha_{Cd,max,r} \\ C_d = C_{d,max,l} + (C_{d2,max} - C_{d,max,l}) \sin \frac{\left(\alpha - \alpha_{Cd,max,l}\right)}{\left(-90 - \alpha_{Cd,max,l}\right).*90)} & \alpha \leq \alpha_{Cd,max,l} \end{cases} \tag{31}$$

with

$$C_{d2,max,u} = G_1 \times G_2 \tag{32}$$

$$G_1 = 2.3 \exp\left[-\left(0.65(t/c)\right)\right]^{0.9} \tag{33}$$

$$G_2 = 0.52 + 0.48 \exp\left[-\left(\frac{6.5}{AR}\right)^{1.1}\right] \tag{34}$$

In order to apply the pre-stall and post-stall sectional model described above, one must first generate a set of basic aerodynamic characteristics pertaining to the modeled airfoil. These parameters are:

- α_0
- $C_{l,\alpha}$
- $C_{l,max}$
- $C_{l,min}$
- $\alpha_{Cl,max}$
- $\alpha_{Cl,min}$
- $C_{d,0}$
- $C_{d,max,u}$
- $C_{d,max,l}$
- t/c
- AR ($AR = \infty$ for airfoil)
- M

This set of twelve parameters may be estimated from available existing pre-stall data. In the present method, the required sectional parameters are estimated from pre-stall airfoil data that is generated using the open-source panel method developed by Drela named XFOIL [46]. In addition to the nominal pre-stall data, the sectional characteristic of airfoils with deflected control surfaces was also generated using XFOIL, enabling the airfoil aerodynamic parameters to be functions of control surface deflection.

In addition to sectional lift and drag estimates of the sectional moment properties for the lifting surfaces will be required. The sectional moment at the airfoil quarter-chord consists of both the lift-independent sectional moment and additional moment induced by the accumulated lift and drag forces acting at the aerodynamic center. For small angles of attack thin-airfoil theory suggests that the aerodynamic center of an airfoil in subsonic flow is approximately at the quarter-chord point. This result is observed from experimental airfoil data, such as that provided by Abbott and von Doenhoff [1], that there is very little variation in sectional moment about the quarter-chord for pre-stall angles of attack. As the angle of attack increases, however, this assumed location of aerodynamic center no longer holds. Indeed Montgomerie [119] observes that as the angle of attack approaches 90 degrees the aerodynamic center shifts to the half-chord location, reflective of the aerodynamic similarity of airfoils to flat-plates in the post-stall region. Further, when the angle of attack is increased such that the flow is inverted, i.e 180 degrees angle of attack, it is to anticipated that the aerodynamic center would shift to the three-quarter-chord location. These observations presented by Montgomerie [119] are further supported by experimental airfoil, which demonstrate the aft-ward shift of the aerodynamic center from the approximate quarter-chord location to the approximate three-quarter-chord location as the angle of attack is increased from 0 degrees to 180 degrees.

Based upon the data presented by Montgomerie [119] an empirical model for the location of the aerodynamic center is developed and included in the sectional aerodynamic model. The model of aerodynamic center is anchored by the three observed phenomena noted above, namely (1) aerodynamic center near the quarter-chord in pre-stall, (2) aerodynamic center near half-chord at 90 degrees angle of attack, and (3) aerodynamic center near the three-quarter-chord at 180 degrees angle of attack. From the experimental data presented by Montgomerie [119] it is observed that the variation of the aerodynamic center location in the post-stall region varies linearly

with angle of attack. Thus in the post-stall region, a linear model is constructed which is anchored by the two post-stall aerodynamic center observations.

In order to ensure smoothness at the transition constant pre-stall region and linear post-stall region and at the transition between the linear post-stall region and constant aerodynamic center region at 180 degrees angle of attack a smoothing function is utilized. The selected smoothing function is of the form

$$s(x) = 0.5 + 0.5 \tanh\left(\frac{(x - A)}{B}\right) \tag{35}$$

and facilitates the smooth transition between any two functions $f(x)$ and $g(x)$ as

$$h(x) = s(x)f(x) + (1 - s(x))g(x) \tag{36}$$

The parameter A in Equation (35) represents the transition point between the functions $f(x)$ and $g(x)$ and the parameter B is determines the smoothness of the transition. For the transition between pre-stall and post-stall the parameter A is set to $\alpha_{Cl,max}$ or $\alpha_{Cl,min}$, whereas for the transition near 180 degrees angle of attack A is chosen to allow for a window of constant aerodynamic center that is approximately 10 degrees wide centered on 180 degrees. At all transitions the parameter B is selected as 0.1. Given these decisions, a sample representation of the aerodynamic center location model is given in Figure 25.

This approach for section aerodynamic force estimation was applied to the three lifting surfaces of the LWGA, visualizations for which are collected within Appendix F. The sectional lift, drag, and moment coefficients are given in Figure 96. In each of these figures three curves are shown which correspond to the deflection of a control surface which constitutes the aft 15% of the airfoil. In later use this control surface may be utilized to model the local effect of either aileron or flap deflection. Similar sectional aerodynamic data for the horizontal and vertical tail surfaces are shown in Figure 97 and Figure 98. For the horizontal tail it will be assumed that a full-surface control surface will be utilized (i.e. a "stabilator"), whereas for the vertical

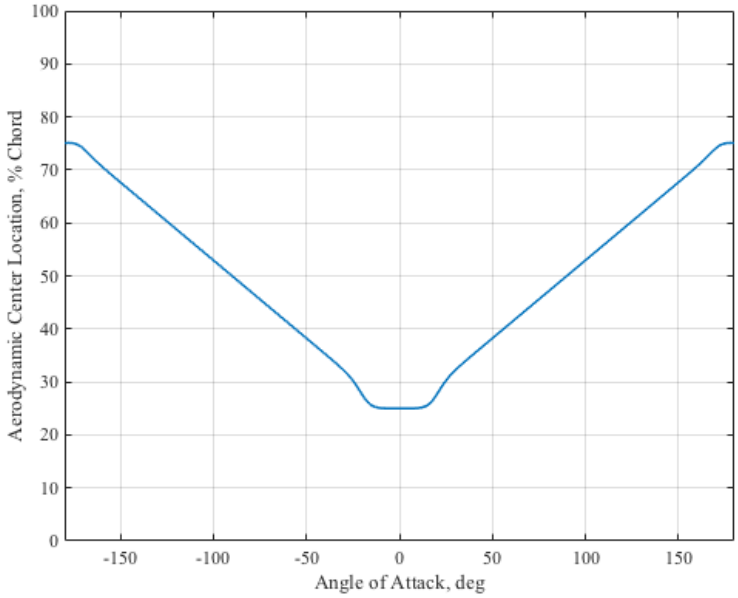

Figure 25: Sample representation of aerodynamic center location model.

tail control surface deflections for at 30% of the airfoil is provided.

Once the two-dimensional airfoil aerodynamic properties are available the aerodynamic forces of a three-dimensional surface can then be estimated. The survey of Min et al. [116] provide an overview of semi-empirical approaches [11, 149] for accounting for various three-dimensional effects in order to estimate the desired aerodynamic properties. While these methods allow for rapid estimation of three-dimensional effects, their semi-empirical nature present obstacles in terms of accuracy. As an alternative to this approach, the aerodynamic model of the LWGA estimates the three-dimensional aerodynamic properties of the lifting surfaces using an adaptation of Prandtl's lifting-line theory [11].

This adaptation is based upon the generalization of the classic lifting-line method developed by Phillips and Snyder [135]. The "modern" lifting-line method estimates the influence of bound vortex segments, in addition to the trailing horseshoe vortices included in Prandtl's classic lifting-line theory. With this additional consideration, the lifting-line theory presented by Phillips and Snyder [135] enables analysis of a

general lifting surfaces, including those with wing sweep and dihedral. While the full theory of the generalized lifting-line presented by Phillips and Snyder [135] is beyond the scope of this work, an overview of the algorithm used within the model is provided in Appendix B.

The lifting line algorithm described in Appendix B was used to model the three-dimensional aerodynamic properties of the LWGA lifting surfaces. In Figure 26 the total three-dimensional lifting properties of the lifting surface system is provided. Within Appendix F a summary of the aerodynamic forces and moments are provided for each lifting surface, and more extensive results are provided in Appendix A. Within Figure 99, Figure 100, and Figure 101 the individual three-dimensional lifting properties of the wing, horizontal tail, and vertical tail surfaces are provided.

Due in part to the greater variety in fuselage shapes, particularly among GA fixed-wing aircraft, there are fewer consistent and well-validated methods of fuselage aerodynamics present within the literature. Early work by Munk [120] which modeled airship hulls using potential flow theory has been observed in literature to be well suited for adaptation to similar body shapes, namely other bodies of revolution. In particular, the method provided by Munk [120] was later extended by Allen [4] to include additional terms for viscous forces with the intention of improving the accuracy of the model for bodies of revolution at general angles of attack. This extension was subsequently modified by Jorgensen [90–92] in attempt to generalize the theory for non-circular cross-sections at general angles of attack, and was more recently extended by Pamadi and Taylor [128, 129] for use in sideslip and spin conditions. This model of fuselage aerodynamics presented by Pamadi and Taylor [128] is summarized

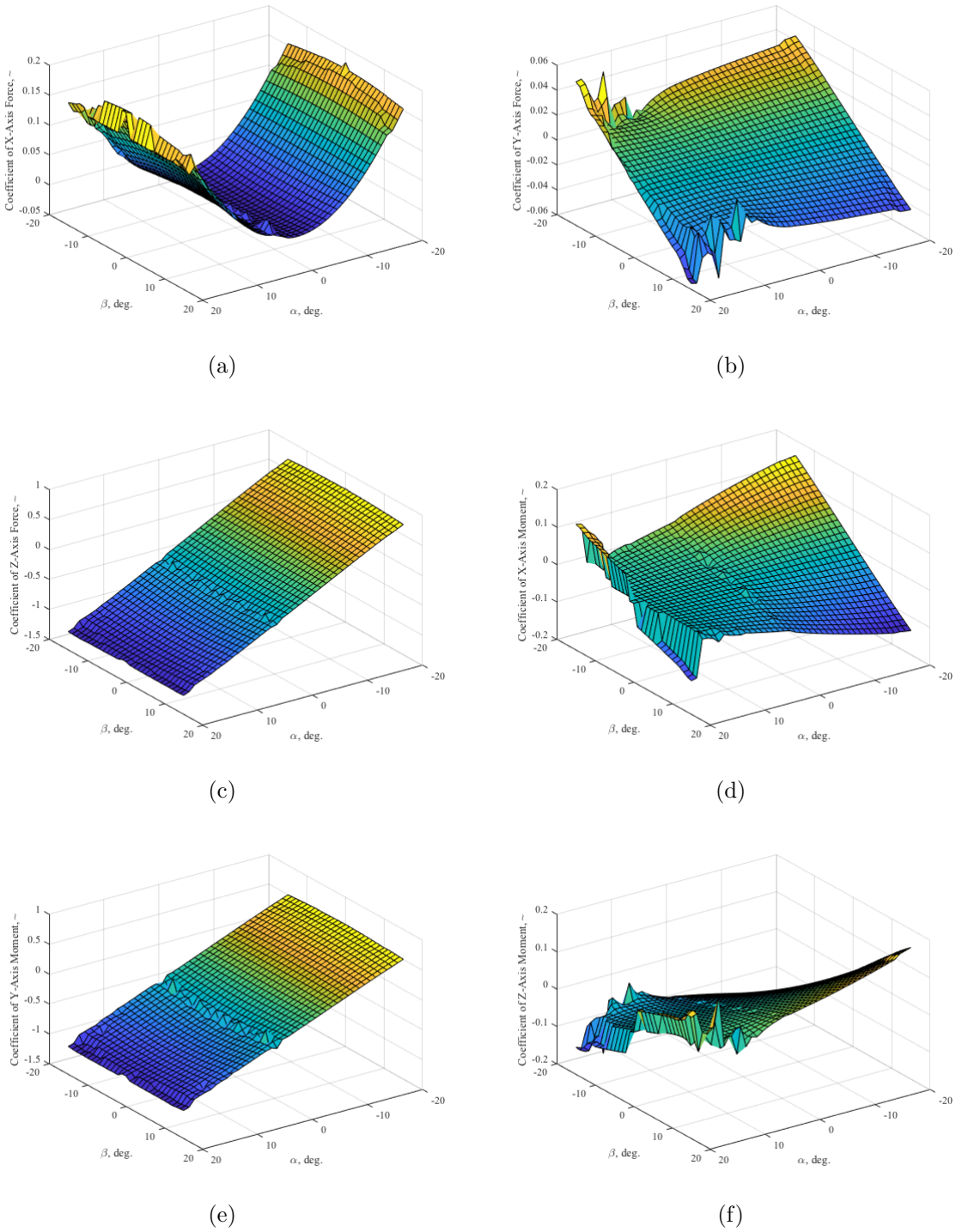

Figure 26: Force and moment coefficients for LWGA lifting surface system.

with the following set of equations:

$$C_{N,B} = C_{L,B}\cos\alpha + C_{D,B}\sin\alpha \tag{37}$$

$$C_{A,B} = -C_{L,B}\sin\alpha + C_{D,B}\cos\alpha \tag{38}$$

$$C_{L,B} = \frac{C_1(k_2-k_1)\sin 2\alpha\cos\frac{\alpha}{2}}{S_{B,max}}\int_0^l \frac{\mathrm{d}S_B}{\mathrm{d}x}\mathrm{d}x + \frac{\sin^2\alpha\cos\alpha}{S_{B,max}}\int_0^l \epsilon b C_{X,c}\mathrm{d}x \tag{39}$$

$$C_{D,B} = \frac{C_1(k_2-k_1)\sin 2\alpha\sin\frac{\alpha}{2}}{S_{B,max}}\int_0^l \frac{\mathrm{d}S_B}{\mathrm{d}x}\mathrm{d}x + \frac{\sin^3\alpha}{S_{B,max}}\int_0^l \epsilon b C_{X,c}\mathrm{d}x \tag{40}$$

$$C_{m,B} = \frac{C_1(k_2-k_1)\sin 2\alpha\cos\frac{\alpha}{2}}{V_B}\int_0^l \frac{\mathrm{d}S_B}{\mathrm{d}x}(x_{cg}-x)\mathrm{d}x + \frac{\sin^2\alpha}{V_B}\int_0^l \epsilon b C_{X,c}(x_{cg}-x)\mathrm{d}x \tag{41}$$

$$C_{Y,B} = -\frac{C_1(k_2-k_1)\sin 2\beta\cos\frac{\beta}{2}}{S_{B,max}}\int_0^l \frac{\mathrm{d}S_B}{\mathrm{d}x}\mathrm{d}x + \frac{\sin^2\beta}{S_{B,max}}\int_0^l \epsilon b C_{Y,c}\mathrm{d}x \tag{42}$$

$$C_{n,B} = -\frac{C_1(k_2-k_1)\sin 2\beta\cos\frac{\beta}{2}}{V_B}\int_0^l \frac{\mathrm{d}S_B}{\mathrm{d}x}(x_{cg}-x)\mathrm{d}x + \frac{\sin^2\beta}{V_B}\int_0^l \epsilon b C_{Y,c}(x_{cg}-x)\mathrm{d}x \tag{43}$$

In order to apply this model one must estimate the aerodynamic properties of the fuselage cross-sections, namely values of C_X and C_Y as functions of the local flow angle, ϕ_b, given by

$$\phi_b = \tan^{-1}\left(\frac{\tan\beta}{\sin\alpha}\right) \tag{44}$$

Various non-circular cross-section aerodynamic data shapes were collected by Polhamus et al. [141,142], which are notable in the present method due to their similarity to fuselage cross-sections commonly observed for GA aircraft. A sample of the data presented by Polhamus is provided in Figure 27 for a cross-section like the one shown in Figure 21.

Upon application of the above method of estimating fuselage aerodynamic forces and moments to the LWGA it was found that the predicted forces and moments were in disagreement with expected magnitudes and trends observed from wind tunnel data. A comparison of the estimated forces and moments as functions of the aerodynamic angles is presented in Figure 28 and Figure 29 alongside wind tunnel data

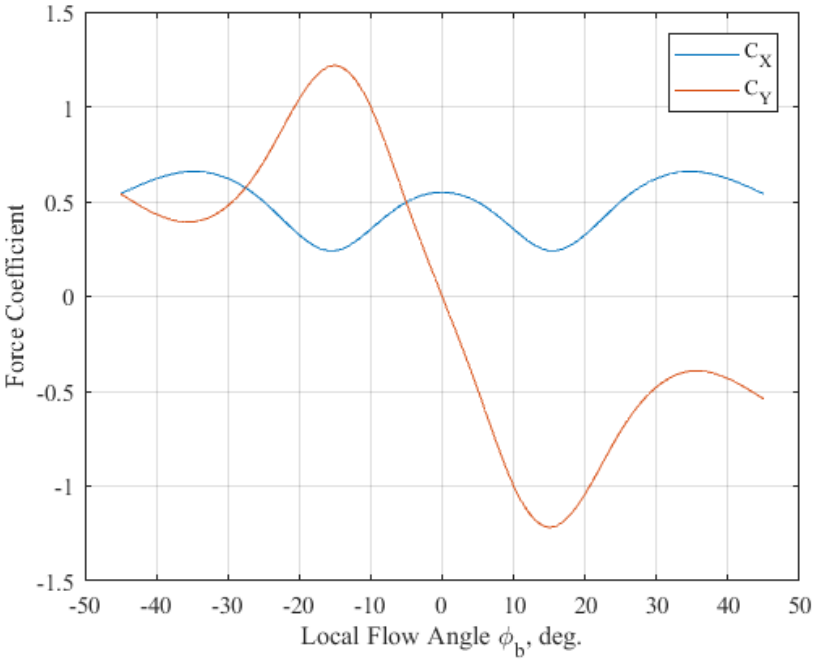

Figure 27: Cross-sectional force coefficients [141].

provided by Birhle et al. [24–26]. In general it is observed that while the trends exhibited by the fuselage aerodynamic model are consistent with experiment results there is a deviation in the magnitude of the forces and moments. Further investigation revealed that similar comparisons were noted by Pamadi and Taylor [128]. These discrepancies were deemed to be unacceptable in the context of the full dynamic model, as they ultimately lead to an inability to find suitable equilibrium points of the aircraft dynamic model in conditions of even moderate angles of attack and sideslip angle. Lacking this model of fuselage aerodynamics then it was decided that the LWGA fuselage aerodynamics would instead utilize the wind tunnel data for the similar aircraft model studied by Birhle et al. [24–26] in wind tunnel testing. These data were used to then construct the aerodynamic force and moment model for the LWGA fuselage, which is depicted in Figure 30.

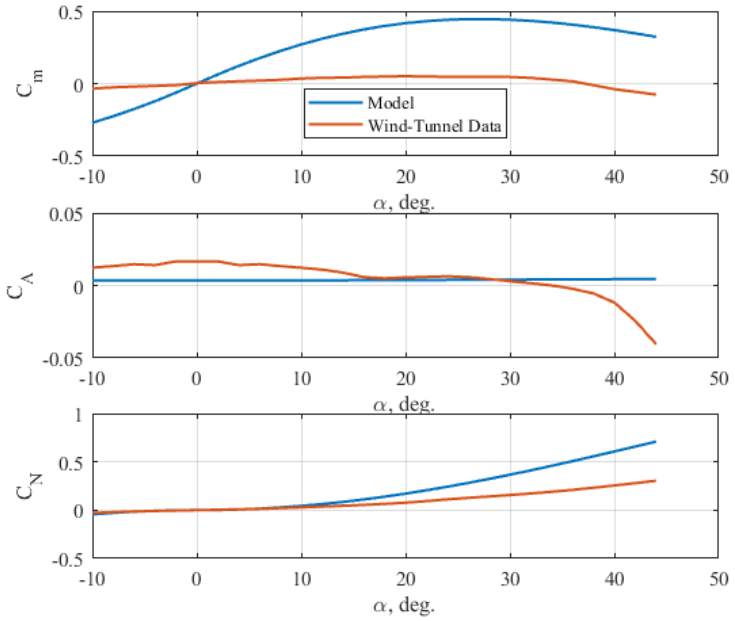

Figure 28: Fuselage longitudinal forces and moment comparison between model prediction and wind tunnel data.

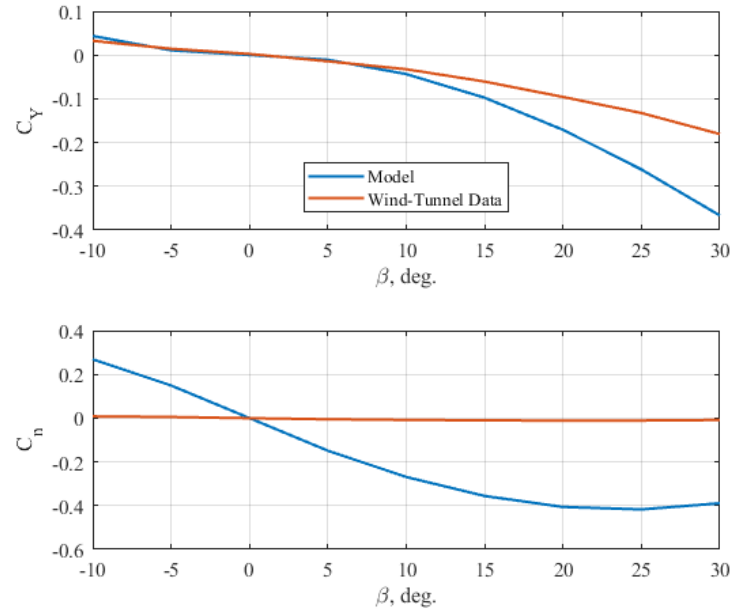

Figure 29: Fuselage lateral force and moment comparison between model prediction and wind tunnel data.

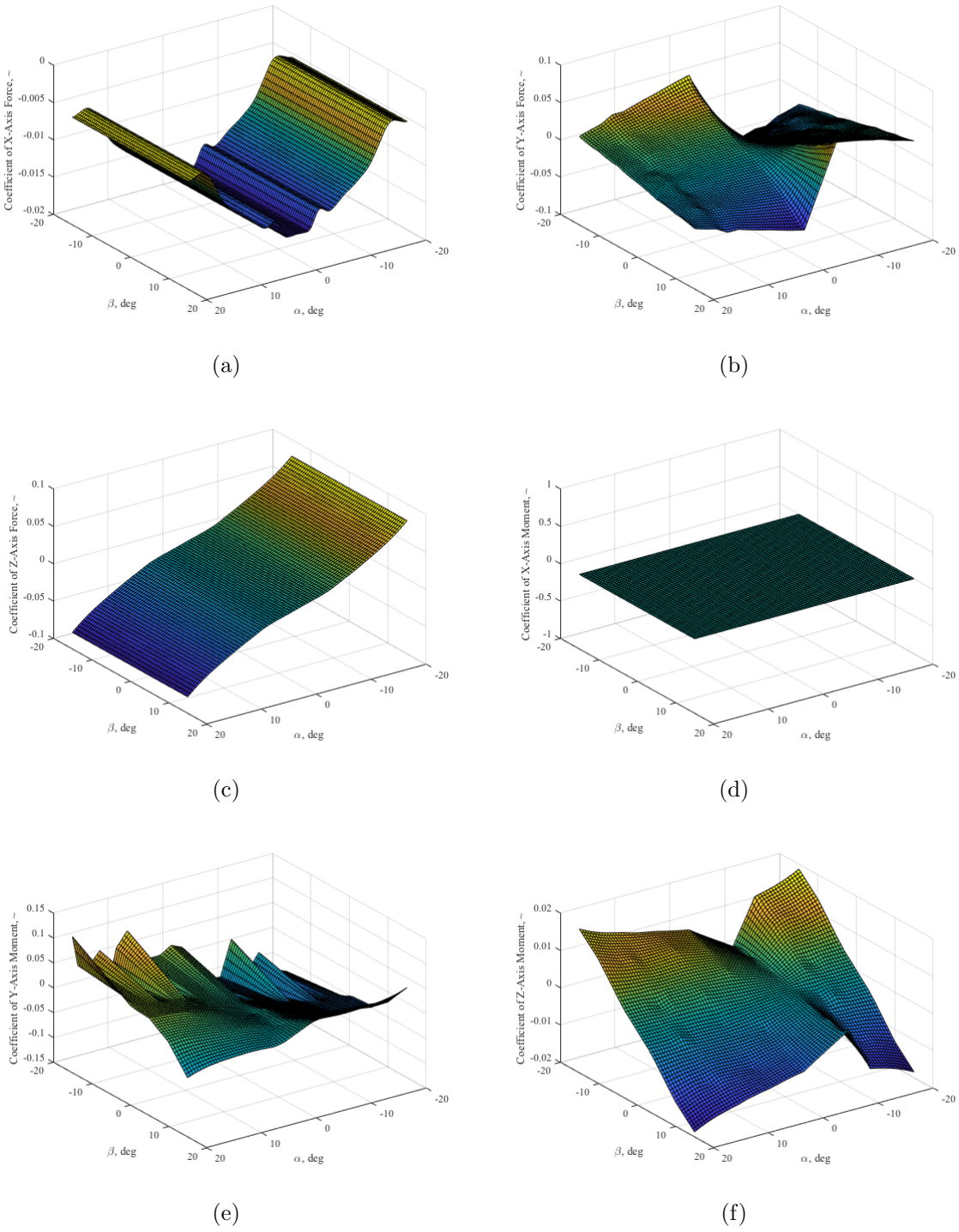

Figure 30: Force and moment coefficients for LWGA fuselage.

4.2.3 Propulsive Modeling

From the data summarized in Chapter 1 pertaining the GA fleet diversity, it was noted that the majority of the GA fleet consists of fixed-wing aircraft with a single piston-driven propeller [52]. To capture the propulsive properties of this class of vehicles, the vehicle model will individually model the performance of a piston engine and the performance of propellers.

Some notable options for modeling the performance of the types of internal combustion (IC) engines common to GA have been examined by Harrison et al. [79]. The two prominent methods observed are either the complete simulation of the engine cycle or the use of a semi-empirical, polynomial model. A brief overview of these two methods will be presented, and a comparison of their performance provided.

The internal combustion engines common to GA utilize the Otto cycle, which consists of the following four step process [59]:

- Isentropic compression of fuel, air, and residual gas
- Constant-volume heat addition
- Isentropic expansion of equilibrium combustion products
- Constant-volume heat rejection

The modeling of the above four thermodynamic processes is straightforward, allowing for the generation of engine cycle performance which in turn allows for the estimation of GA engine performance. In doing so, care must be given to the chemical composition of the fuel-air mixture present within to engine at various stages of the cycle. First, an assumed chemical composition of ambient air consisting primarily of oxygen and nitrogen is used, in the ratio

$$0.21O_2 + 0.79N_2 \tag{45}$$

Typical hydrocarbon fuels may be expressed generally as

$$C_\alpha H_\beta O_\gamma N_\delta$$

allowing then for mixtures of air, fuel, and common combustion products including CO_2, H_2O, N_2, O_2, CO, and H_2 to be expressed. The four integer parameters (α, β, γ, and δ) are fixed parameters for a given fuel type. To complete the analysis of the chemical reactions present within the cycle, 11 unknowns must be determined which represent the 10 mole fractions,y_i, for each combustion species present within the cycle and the total number of moles, N. Four of the required equations arise from conservation of mass equations, and a fifth is available from the definition of the total number of moles within the process. The remaining six equations can be gathered through a set of equations which represent the maximum entropy of possible reactions of the combustion process. In the work of Harrison et al. [79] a function which performs this cycle analysis was generated and validated both to published combustion cycle data and overall engine performance data for a GA engine.

Alongside the complete cycle analysis, an additional method of engine performance prediction is the application of polynomial relationships. A simple example of such a relationship provided by Raymer [149] and Gudmunsson [76] is seen as Eq. 46. This relationship models the local engine performance to rated sea-level performance as proportional to changes in local air density. An improvement version of this relationship known as the Gagg and Ferrar model is also given by Gudmunsson [76] and is shown as Eq. 47.

$$P = P_{SL}\left(\frac{\rho}{\rho_0}\right) \tag{46}$$

$$P = P_{SL}\left(1.132\left(\frac{\rho}{\rho_0}\right) - 0.132\right) \tag{47}$$

In Figure 31, a representative comparison of the above methods of engine performance estimation are shown along with published GA engine performance for the

same operating conditions. In general it is observed that the performance of the two estimation methods are quite similar. As noted by Harrison et al. [79], however, the computational expense of the two methods are quite different. In particular the cycle analysis require much higher computational time in comparison to the polynomial method. Due to the desire for speed alongside accuracy, the final version of the propulsion model estimates engine performance using a polynomial approximation of the form seen in Eq. 47.

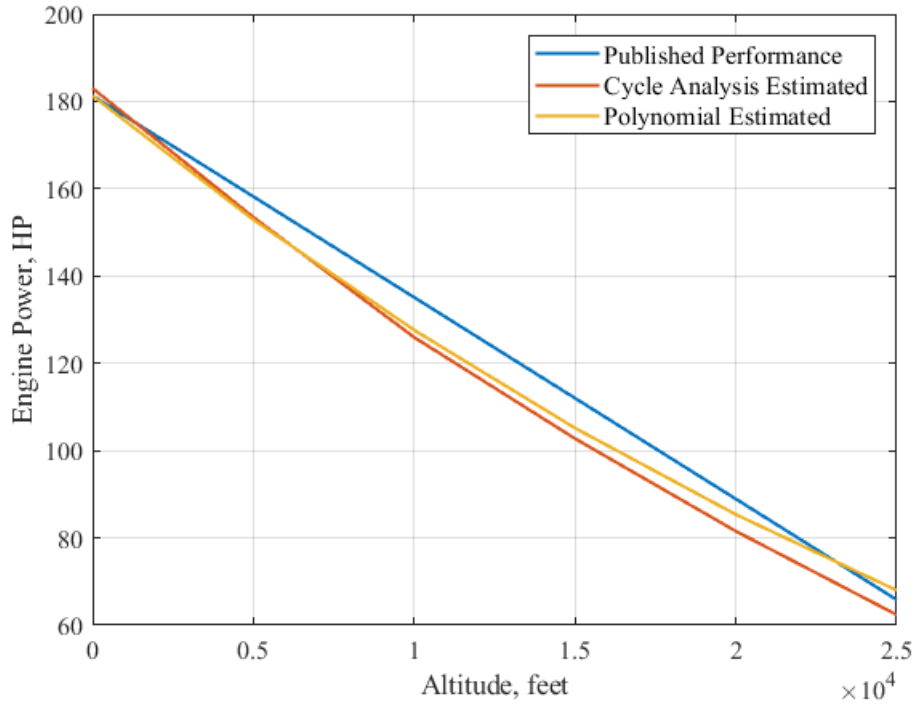

Figure 31: Comparison of engine performance estimation methods.

As with the engine performance model, several options are present within the literature for capturing the performance properties of propellers used on GA vehicles. A common empirical model used within the literature and employed by Harrison et al. [79] is the use of propeller performance curves generated by Hamilton Standard [175, 176]. This approach allows for rapid and accurate estimation of GA propeller performance through a range of typical operating conditions. However, this approach

is limited to the estimation of propeller thrust and torque as functions of the propeller advance ratio. While this limitation is often not critical for performance analysis, is it undesirable for the desired application of the propeller performance models within a dynamic vehicle simulation as off-nominal behavior is not captured.

In order to capture a more nuanced model of propeller performance a more theoretical approach must be explored. The most prominent theoretical methods of propeller performance modeling are actuator disk theory, which idealizes the propeller as a thin disk which accelerates flow as it passes through it, and blade element momentum theory (BEMT), which divides the propeller blade into many small sections and sums the effect of each of these sections. Of these two methods BEMT was chosen as the means of estimating propeller performance due to the capability of estimating the three-dimensional forces and moments induced by the propeller at any general inclination with the flow [136].

The fundamental theory of BEMT may be attributed to the work of Betz [23], Prandtl [144], and Goldstein [71]. More recently Phillips and Anderson [136] present a vortex-based derivation of BEMT for the prediction of propeller forces and moments. This theory which will be summarized briefly in the remainder of this section.

A depiction of a propeller at some velocity, V, rotation speed, ω, and at some inclination angle, α_p, to the local flow is given in Figure 32. The local velocity for a given element of the propeller blade at some radial location r and angle θ, as depicted in Figure 33, is then the vector sum of the free-stream velocity, rotation speed, and velocity induced by other elements of the propeller.

More specifically the velocity component due to free-stream velocity and propeller rotation is

$$V_e^2(r,\theta) = (\omega r - V_\infty \sin\alpha_p \sin\theta)^2 - (V_\infty \cos\alpha_p)^2 \tag{48}$$

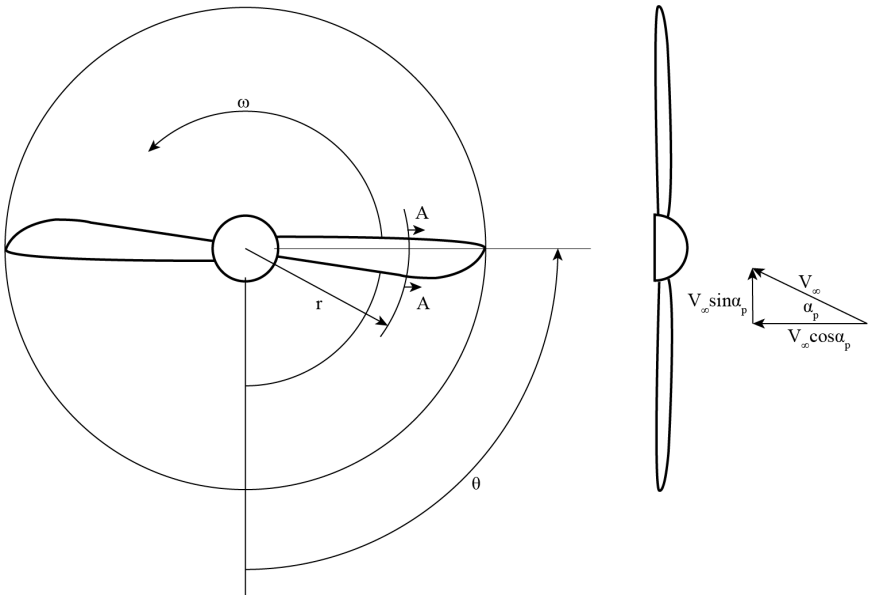

Figure 32: Front and side view of rotating propeller at some freestream velocity and orientation α_p, adapted from [136].

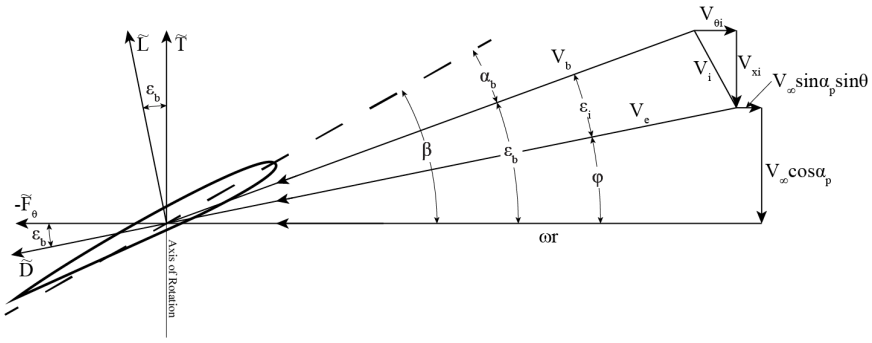

Figure 33: Local velocity components of propeller blade section A-A, adapted from [136].

The total velocity of each blade element (V_b) is then

$$V_b(r,\theta) = V_e \cos\epsilon_i \tag{49}$$

$$= \sqrt{(\omega r - V_\infty \sin\alpha_p \sin\theta)^2 - (V_\infty \cos\alpha_p)^2}\cos\epsilon_i \tag{50}$$

With the advance angle ϵ_∞ given by

$$\epsilon_\infty = \tan^{-1}\left(\frac{V_\infty}{\omega r}\right) \tag{51}$$

then the induced velocity angle, ϵ_i can be related to the total blade down-wash angle, ϵ_b, and as

$$\epsilon_b(r,\theta) = \epsilon_i + \phi \tag{52}$$

The angle ϕ results from the total forward motion and may be calculated along with the free-stream flow angle ψ as

$$\phi = \psi + \sin^{-1}\left[\frac{(V_\infty \sin\alpha_p \sin\theta)\sin\psi}{V_e}\right] \tag{53}$$

$$\psi = \tan^{-1}\left(\frac{V_\infty \cos\alpha_p}{\omega r}\right) \tag{54}$$

With the total blade down-wash angle known then the local blade element angle of attack is seen as

$$\alpha_b = \beta - \epsilon_b \tag{55}$$

allowing for the local lift and drag to be calculated as

$$\tilde{L} = \frac{1}{2}\rho V_b^2 c_b C_l(\alpha_b) \tag{56}$$

$$\tilde{D} = \frac{1}{2}\rho V_b^2 c_b C_d(\alpha_b) \tag{57}$$

The thrust and circumferential force generated at each blade element is then

$$\tilde{T} = \tilde{L}\cos\epsilon_b - \tilde{D}\sin\epsilon_b \tag{58}$$

$$\tilde{F_\theta} = -\tilde{D}\cos\epsilon_b - \tilde{L}\sin\epsilon_b \tag{59}$$

Integration along each blade radius (i.e. from hub radius R_h to blade tip R_t) and around the full propeller disk, along with multiplication by the number of propeller blades k yields the final expressions for the propeller forces and moments.

$$T = \int_{r=R_h}^{R_t} \frac{k}{2\pi} \int_{\theta=0}^{2\pi} \tilde{T} \mathrm{d}\theta \mathrm{d}r \tag{60}$$

$$N = \int_{r=R_h}^{R_t} \frac{k}{2\pi} \int_{\theta=0}^{2\pi} \tilde{F}_\theta \mathrm{d}\theta \mathrm{d}r \tag{61}$$

$$Q = \int_{r=R_h}^{R_t} \frac{k}{2\pi} \int_{\theta=0}^{2\pi} -\tilde{F}_\theta r \mathrm{d}\theta \mathrm{d}r \tag{62}$$

$$n = \int_{r=R_h}^{R_t} \frac{k}{2\pi} \int_{\theta=0}^{2\pi} \tilde{T} r \mathrm{d}\theta \mathrm{d}r \tag{63}$$

In developing an algorithm for estimating propeller performance, suppose that the flow properties V_∞, α_p, and ω are known along with the geometric and sectional properties of the propeller i.e. β, c_b, $C_l(\alpha_b)$, $C_d(\alpha_b)$ at a series of radial locations r. Then the unknown quantity in Equations 48-63 is the magnitude of the induced velocity angle ϵ_i. The angle may be estimated through an iteratively using the Newton-Raphson method. To do so, one may define the residual to be minimized as the difference between the sectional lift generated at each blade element its corresponding vortex strength [71]. After considering the tip loss factor f proposed by Prandtl and Betz [144] the residual R is seen as

$$f = \frac{\left(\beta\left(1 - \frac{r}{R_t}\right)\right)}{2\sin\beta_t} \tag{64}$$

$$R = \beta\frac{c}{16r}C_l(\alpha_b) - \cos^{-1}\left(\exp\left(-f\right)\right)\tan\epsilon_i \sin\left(\epsilon_\infty + \epsilon_i\right) \tag{65}$$

To generate the Newton step the gradient of the residual with respect to the induced velocity angle is required. Assume the sectional lift is assumed to be a linear function of α_b, corrected for Mach number effects with the Prandtl-Glaurt correction factor, that is

$$C_l = \left(C_{l,0} + C_{l,\alpha}\alpha_b\right)\left(\frac{1}{\sqrt{1 - M_b^2}}\right) \tag{66}$$

Then the gradient of section lift coefficient with respect to ϵ_i is

$$\frac{\partial C_l}{\partial \epsilon_i} = C_{l,\alpha} \frac{\partial \alpha}{\partial \epsilon_i} \left(\frac{1}{\sqrt{1 - M_b^2}} \right) + \frac{\partial M_b}{\partial \epsilon_i} \left[\left(C_{l,0} + C_{l,\alpha} \alpha_b \right) \left(1 - M_b^2 \right)^{(-3/2)} \right] \tag{67}$$

The gradient $\frac{\partial \alpha}{\partial \epsilon_i}$ can be observed from Equation (55) as unity, whereas the gradient $\frac{\partial M_b}{\partial \epsilon_i}$ arises from Equation (49) as

$$\frac{\partial M_b}{\partial \epsilon_i} = V_e \sin \epsilon_i \tag{68}$$

The gradient of the residual is then

$$\frac{\partial R}{\partial \epsilon_i} = \beta \frac{c}{16r} \frac{\partial C_l}{\partial \epsilon_i} - \cos^{-1} \left(\exp \left(-f \right) \right) \left[\tan \epsilon_i + \sec^2 \epsilon_i \sin \left(\epsilon_\infty + \epsilon_i \right) \right] \tag{69}$$

Using this method the performance of a propeller for the LWGA may be estimated. The propeller geometry was based off of measured properties of general aviation propeller, yielding the blade angle and blade chord length distributions given in Figure 34. Additionally the sectional aerodynamic properties were selected to be similar to common propeller airfoils like the Clark Y. The sectional lift is assumed to be linear with a cosine-shaped profile near the minimum and maximum sectional lift and the sectional drag is assumed to be quadratic with sectional lift. Data related to this assumed form of the lift and drag properties is given in Table 9. The resulting performance properties which were estimated within these geometric and aerodynamic properties in terms of both axial and tangential axis forces and moments is provided in Figure 35.

Table 9: Summary of propeller sectional aerodynamic properties.

Constant	**Value**
$C_{l,0}$	0.875
$C_{l,\alpha}$	6.30
$C_{l,max}$	1.27
$C_{l,min}$	-1.42
$C_{l,Cd0}$	0.250
$C_{d,0}$	000290
K	0.0046

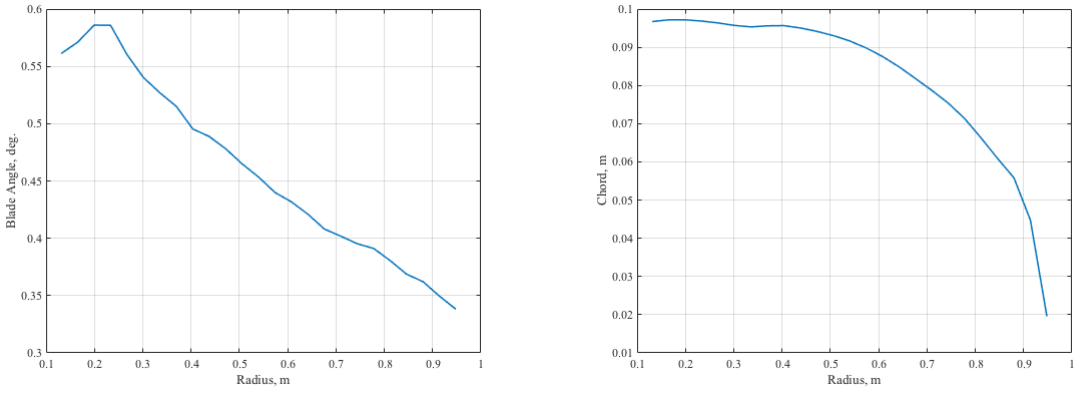

(a) (b)

Figure 34: Blade angle and chord distribution of LWGA propeller.

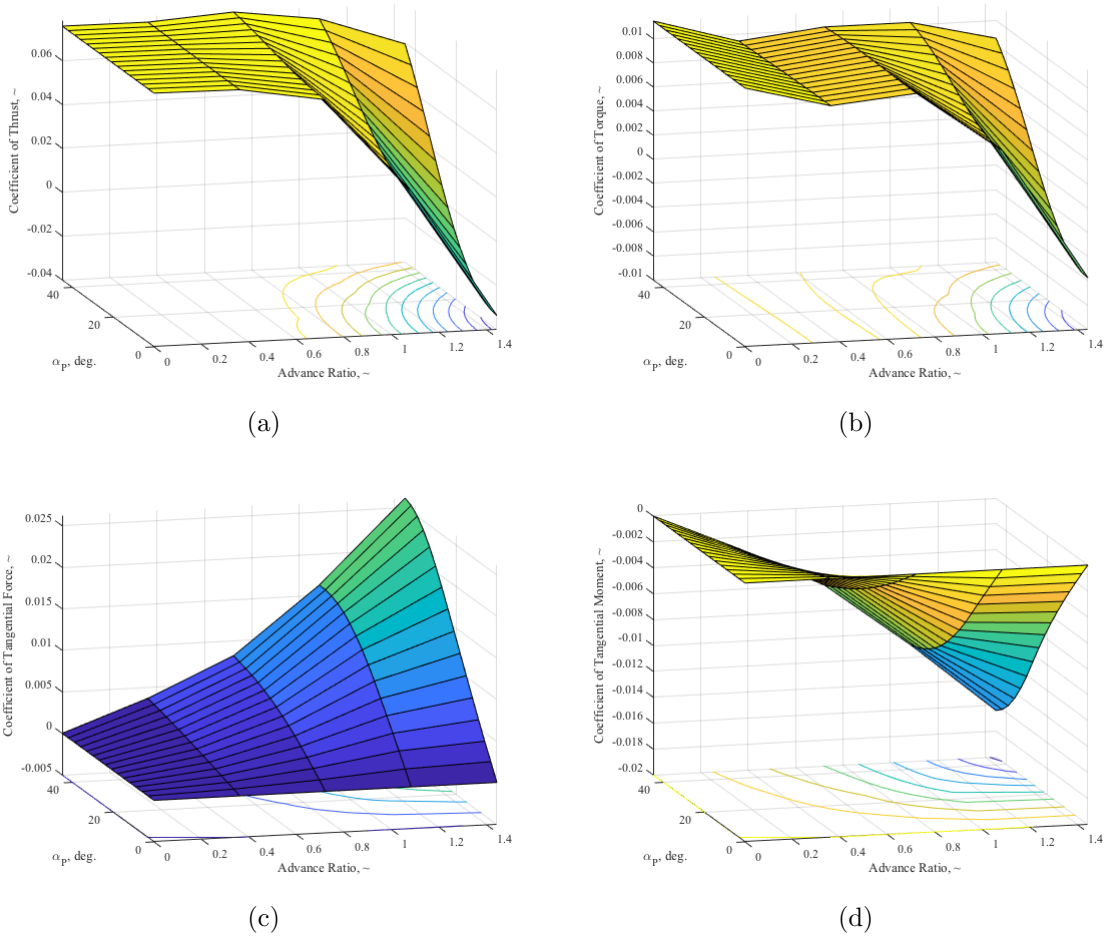

Figure 35: Force and moment coefficients for LWGA propeller.

4.2.4 Mass Properties

In addition to the aerodynamic and propulsive properties a description of the vehicle's mass properties is required. Determination of an aircraft's gross mass, and thus weight, can be estimated through comparison to similar vehicles. Aircraft characteristic data for 102 single-engine piston aircraft collected by the FAA [50] are displayed in Figure 36. These data indicate that the aircraft of this class typically have a maximum takeoff weight (MTOW) less than 5000 lbs., whereas most vehicles have MTOW between 2000 and 3000 lbs. This general trend can be observed to be in particular true for the Cessna 172 and PA-28 which have MTOW of 2550 lbs. and 2400 lbs., respectively. As the LWGA model is most similar to the PA-28 a MTOW of 2400 will be used for the LWGA.

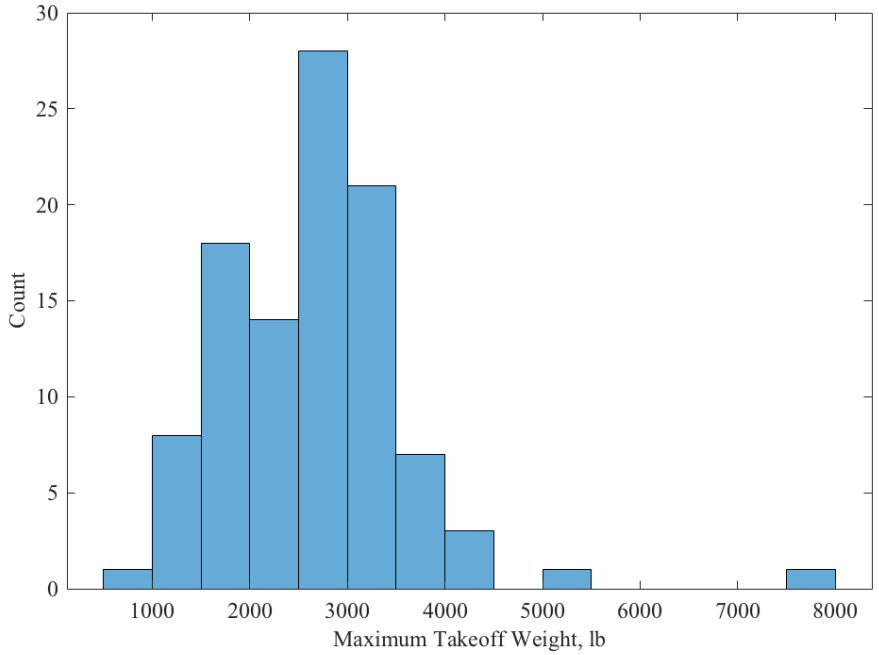

Figure 36: Single-engine piston aircraft maximum takeoff weight data [50]

As the LWGA is symmetric aircraft it is reasonable to assume that the location of the aircraft center of gravity is along the plane of symmetry. The forward and aft limits of the center of gravity along the plane of symmetry are dependent on stability

Table 10: LWGA inertial values.

Inertial Property	**Value** $[kg - m^2]$
I_{xx}	170
I_{yy}	1250
I_{zz}	1300
I_p	10

criteria, most notably maintaining positive static margin. Once the aerodynamic properties of the model are ascertained, then the static margin can be estimated for a given center of gravity location.

Finally, estimation of the mass moment of inertia tensor is required. For an aircraft with a plane of symmetry about the $x - z$ plane then the inertia tensor reduces to

$$J = \begin{bmatrix} I_{xx} & 0 & -I_{xz} \\ 0 & I_{yy} & 0 \\ -I_{zx} & 0 & I_{zz} \end{bmatrix} \tag{70}$$

The off-diagonal element $I_{xz} = I_{zx}$ can further be assumed to be negligible, reducing the inertia tensor further to consist of only the diagonal elements.

For the LWGA inertial values which are similar to the PA-28 will be utilized as a means of improving the similarity of the model to realistic aircraft performance. In addition to the aircraft body inertia the spinning propeller introduces an additional source of momentum. Estimation of the inertia of the propeller is performed through idealization to two similar rotating bodies. First consider the propeller as a rod of the same mass, m_p, and radius, R_p, as the true propeller, whose inertia about the axis of rotation is

$$I_{rod} = \frac{2}{3} m_p R_p^2 \tag{71}$$

Alternatively consider the propeller as a disk of the same mass and radius, whose inertia is

$$I_{disk} = \frac{1}{2} m_p R_p^2 \tag{72}$$

The inertia of the propeller can then be estimated as the average of I_{rod} and I_{disk}. The

estimated value of the propeller, along with the body inertial values for the LWGA, are provided in Table 10.

CHAPTER V

LOSS-OF-CONTROL ENVELOPE ESTIMATION

The first aspect of the prediction and mitigation efforts of this methodology are reliant upon the estimation of LOC onset through the application of a LOC envelope. This envelope and its attributes are the subject of the first research question, which is reproduced here:

Research Question 1:

What is the level of confidence afforded by a LOC envelope and how sensitive is this confidence to variability or uncertainty in the envelope generation process?

In general, an aircraft envelope is understood to be some set of quantified boundaries which delineate some safe and unsafe regions. Accordingly the basis of an LOC envelope rests upon the quantification of LOC onset. As part of the literature review presented in Chapter 2, several means of quantifying the onset of LOC are discussed in §2.2. In short, these methods include aircraft state envelopes, vehicle upset condition prediction, safe set generation, and identification of aircraft non-linearity effects. It was additionally observed upon consideration of these various quantification techniques that there is a degree of commonality or overlap, with each method providing some alternative perspective to some common event.

It is required of the LOC envelope that a clear distinction between normal, safe flight and LOC be defined. There are several envelopes which may be defined which satisfy this basic requirement, several of which were discussed in Chapter 2. In addition to this requirement the selected LOC envelope must be usable within the constraints of typical GA operations. These constraints restrict the selected envelope

to include only states of the vehicle. Additionally the computational burden imposed by the envelope must be within the limitations of typical GA PEDs. The limitations posed by GA operation are perhaps most restrictive, as it limits the use of many envelopes which rely upon extensive instrumentation in order to monitor the proximity of the vehicle to the LOC boundaries.

5.1 Development of LOC Envelopes

In demonstrating the present methodology, a subset of the identified methods in Chapter 2 to generate LOC envelopes for use in prediction and mitigation of GA LOC will be explored. This generation consists of two primary elements: aircraft state boundaries and safe set generation. The chosen envelope was selected due to the prominence of the selected methods within the existing LOC literature, attesting to their usefulness and applicability.

5.1.1 Performance Envelope Definition

Through selection of aircraft state boundaries in a fashion similar to Wilborn and Foster [174], the boundaries of the safe operating region can be directly identified. These boundaries were initially developed in earlier work by Harrison et al. [78], where they were used for retrospective analysis of GA vehicle safety. Using these state boundaries to generate the LOC envelope allows for the direct assessment of vehicle states for which vehicle upsets are likely to occur [174].

For the five envelopes which constitute the QLC a set of six upper and lower bounds are required. The adverse aerodynamics envelope requires upper and lower bounds for the aerodynamic angles α and β. For α upper and lower bounds may naturally be set based upon the stall onset, whereas Wilborn and Foster [174] recommend constraining β by means of the maximum demonstrated crosswind velocity. The second envelope, unusual attitude, presents constraints on the bank angle ϕ and pitch angle θ, the upper and lower bounds of which Wilborn and Foster [174] define

through "generally accepted industry definition". In addition to their application to the unusual attitude envelope, the upper and lower boundaries for ϕ and θ are additionally utilized in the dynamic roll control and dynamic pitch control envelopes as limitations on dynamic roll angle and dynamic pitch angle, respectively. The dynamic pitch and roll envelopes additionally utilize the maximum and minimum pitch and roll control input, each of which are defined according the limitations imposed by the vehicle. For the fifth envelope, the structural integrity envelope, upper and lower bounds are defined for the vehicle velocity and load factor. In their initial development Wilborn and Foster [174] define the limitations for load factor through the relevant transport category regulations i.e. Federal Aviation Regulations Part 25 [56]. For application to GA vehicles similar limitations may be drawn from the Federal Aviation Regulations Part 23 [55]. The velocity upper and lower bounds may similarly be defined by utilizing regulatory guidelines for the stall warning velocity and maximum operating velocity [55, 174].

The set of state boundaries which make up the QLC are proposed by Wilborn and Foster [174] to indicate LOC onset once three of the envelopes have simultaneously been violated. It is also noted however that in the course of normal operation it is rare that any single envelope is violated, as doing so indicates the excursion of the vehicle into unusual flight conditions. Further it may be noted that the safest course of action with respect to the defined LOC envelopes is to operate as far from any boundary as possible [14, 15]. Indeed, if one is able to prevent excursion from any single envelope of the QLC, then one further prevents the excursion of any three simultaneously.

It is noted that within this method of performance boundary estimation two key limitations arise. First when defining the limits of what is considered "normal operation" a blending of thresholds which are vehicle-dependent and vehicle-agnostic occurs. This reliance upon thresholds which are tied to the dynamics of the vehicles

introduces a level of uncertainty associated with the estimation of those limitations. For instance, the limits of normal operational velocity are defined relative to the stall warning and maximum operating velocities. While the methods of defining these velocities is established by the FAA [55] for any given GA vehicle there will nevertheless be variation in the values of such limits between different GA aircraft. This implies that in defining the GA QLC envelope a loss of generality occurs, such that a defined GA QLC envelope is applicable only to a single aircraft. That is, in defining the normal operation envelopes for multiple aircraft will result in an equivalent number of envelopes rather than some single envelope which may be applied to the set of aircraft. Further, use of this envelope within the MERLIN method implies that a given implementation of the MERLIN methodology is applicable to the single vehicle for which the envelope is defined.

The second limitation of this approach relates to the static nature of state limits in this approach. Within the range GA vehicle operations there may be envisioned some special operations which are simultaneously safe and outside what would be considered as "normal" operation. For instance, a pilot may perform an approach maneuver at pitch angle with is lower than normal in preparation for landing at a shorter runway. This operation is likely to exceed the lower limit on normal pitch angle which is included in the definition of the Unusual Attitude flight envelope, leading then to a violation of the defined LOC envelope. Such cases involving this identification of safe but special operations as unsafe is a inherent limitation of this implementation of the performance envelope which strives to define some "one-size-fits-all" set of constraints on the aircraft. Such a limitation may be overcome through the explicit definition of the allowable special conditions and subsequent development of particular performance envelopes for each. This set of performance envelopes would then include some normal or default envelope and an accompanying set of "special-case" envelopes that could then be either be interchanged by the end-user or in an

algorithmic fashion. Such an approach is likely to introduce further complications which should be considered, namely the difficulty in defining some complete set of special operations and the added potential for mode confusion on behalf of the user of such a system.

An important consideration noted by Kwatny et al. [97, 98, 98] is that operation within a defined boundary may not be sufficient to ensure that the vehicle remains within the envelope in some finite time in the future. Instead Kwatney et al. [98] observe the presence of regions within a defined aircraft envelope that should an aircraft trajectory begin within this region the ensuing trajectory will violate the envelope boundaries regardless of the control inputs. Therefore in order to provide a means of both predicting and avoiding GA LOC, the LOC envelope utilized within the MERLIN methodology will be the safe set defined relative to the GA QLC.

5.1.2 Safe Set Estimation

The computation of the safe set may be carried out in a variety of methods, such as the Hamitlon-Jacobi-based method utilized by Lygeros [106] and Kwatny et al [98]. Such an approach draws heavily from the numerical methods presented by Sethian [155] and implemented by Mitchell and Tomlin [117], which pose the safe set estimation problem as an application of the level-set method. In this approach the desired envelope boundary is selected as the zero-level set and a "terminal value" problem is performed using the level set method in order to generate the set of trajectories which terminate at the defined boundary. While this approach has been demonstrated for the generation of safe sets for two-dimensional longitudinal aircraft dynamics [98,106], significant computation time is required. In addition while level-set methods are well defined and tractable for two-dimensional problems, the added complexity of higher dimensional problems causes the computation time to grow to unacceptable levels.

A more expedient method of approximating the safe set is developed by McDonough and Kolmanovsky [111]. An overview of this method will be briefly provided here. Let the aircraft dynamic system be represented as a discrete-time linear system of the form

$$\begin{aligned} x(k+1) &= Ax(k) + Bu(k) \\ y(k) &= Cx(k) + Du(k) \end{aligned} \tag{73}$$

with $x \in \mathbb{R}^n$, $y \in \mathbb{R}^m$, $u \in \mathbb{R}^l$ $A \in \mathbb{R}^{n \times n}$, $B \in \mathbb{R}^{n \times l}$, $C \in \mathbb{R}^{m \times n}$, and $D \in \mathbb{R}^{m \times l}$. While the flight dynamics of aircraft are characteristically nonlinear, this linear representation can be applied to nonlinear dynamical systems through linearization about equilibrium conditions, though only in a small neighborhood about the equilibrium point.

Suppose the system is to be constrained to some region of the state-space. Then a set of n_g state constraints can be expressed as

$$y(k) \in Y = \{y : Gy \leq g\} \tag{74}$$

with $G \in \mathbb{R}^{n_g \times m}$ and $g \in \mathbb{R}^{n_g}$. The set of constraints, g, represent the full number of constraints imposed upon the system, which may include state constraints (i.e. flight envelope restrictions), control constraints, and constraints pertaining to the validity of the linearization of the nonlinear dynamics [111].

If it is supposed that a static feedback controller is implemented, taking the form

$$u(k) = -Kx(k) \tag{75}$$

then the closed-loop system dynamics reduce to

$$\begin{aligned} x(k+1) &= \tilde{A}x(k) \\ y(k) &= \tilde{C}x(k) \end{aligned} \tag{76}$$

with $\tilde{A} = A - BK$ and $\tilde{C} = C - DK$. Further, then the state at some time k in

response to some initial condition $x(0)$ can be observed as

$$\begin{aligned} x(k) &= \tilde{A}^k x(0) \\ y(k) &= \tilde{C}\tilde{A}^k x(0) \end{aligned} \tag{77}$$

This trajectory can be seen to satisfy the system constraints given as Equation (74) for some time k if

$$G\tilde{C}\tilde{A}^k x(0) \leq g \tag{78}$$

From these constraints the safe-set O_∞ can be expressed as [68, 94, 111]

$$O_\infty = \left\{ x(0) \in \mathbb{R}^n : y(k) = \tilde{C}\tilde{A}^k x(0) \in Y, \quad \forall k \geq 0 \right\} \tag{79}$$

If the control gain K is stabilizing, implying that $\tilde{A}$ is Schur, the pair $(\tilde{C}, \tilde{A})$ is observable, the output set Y is compact and $0 \in \int Y$, the Gilber and Tan [68] show that the safe-set O_∞ is a positively invariant set taking the shape of a bounded polyhedron. Additionally, this set is finitely determined which implies that there exists some time t^* for which $O_\infty = O_t \quad \forall t \geq t^*$ given as [68, 111]

$$O_t = \left\{ x(0) \in \mathbb{R}^n : y(k) = \tilde{C}\tilde{A}^k x(0) \in Y \text{for} k = 0, ..., t \right\} \tag{80}$$

A finitely determined O_∞ can in addition be represented with the system constraints given in Equation (74) for $k = t^*$ as [111]

$$\begin{bmatrix} G \\ G\tilde{C}\tilde{A} \\ G\tilde{C}\tilde{A}^2 \\ \vdots \\ G\tilde{C}\tilde{A}^k \end{bmatrix} \leq \begin{bmatrix} g \\ g \\ \vdots \\ g \end{bmatrix} \tag{81}$$

Each row of the safe-set representation given in Equation (81) applies the system constraints of Equation (74) to each discrete time of the trajectory, ensuring that the full trajectory satisfies the system constraints. This approach to estimation of

the safe-set has been demonstrated numerically within the literature [68, 94, 111] and has been observed to provide good approximations of the system's safe-set. The approximation is however directly dependent upon the selection of the control strategy (i.e. the feedback gain K in Equation (75)), and upon the sampling time. While the selection of sufficiently small sampling time may be trivially chosen such that the aliasing of aircraft dynamic behavior is avoided, the selection of the feedback gain K poses a more significant hurdle. In the implementation presented by McDonough and Kolmanovsky [111], the gain matrix K is generated using the linear-quadratic plus integrator (LQ-I) control theory. A similar approach will be proposed for this method, namely the use of the linear-quadratic regulator (LQR) control method, which will enable the design of control laws which provide optimal control strategies that may be tailored to fit the particular dynamics of the GA aircraft system.

In summary the following process is recommended for the generation of an LOC envelope for GA fixed-wing aircraft:

1. Define the set of upper and lower bounds on the constrained vehicle states
2. Construct the GA state envelopes
3. Determine set of trim conditions
4. Linearize aircraft dynamics about the trim conditions
5. Generate feedback gain matrix K
6. Perturb aircraft about trim conditions
7. Apply Equation (81) to estimate LOC envelope

A visual representation of this process is also provided in Figure 37, which provides a more particular application of this process which utilizes a GA-appropriate form the QLC envelopes developed by Wilborn and Foster [174].

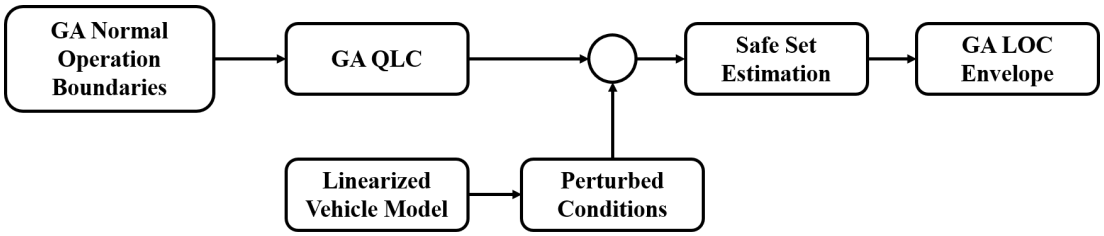

Figure 37: Summary of LOC envelope generation process.

The steps outlined above constitute both the particular method which will be utilized in the present work and a general process which may used in generating GA LOC envelopes. While the present method utilizes the set of envelopes which constitute the QLC [174], others may be selected given that the chosen envelope delineates between normal operation and LOC conditions. Steps 3-7, which approximate the safe set of flight conditions for the chosen envelope, may additionally be generally applied given that one is able to accurately linearize the aircraft about the set of desired flight conditions.

It should additionally be noted that use of the GA LOC envelope constructed in Steps 1 and 2 of the above process may be directly applied if additional considerations are made. From the definition of the safe set (i.e. Equation (81)) the defined GA LOC envelope boundary itself defines a safe set for a $k = 0$. In other words the GA LOC envelope provides an instantaneous assessment of flight conditions with respect to LOC proximity, though no assurances of future safety can be provided.

The process of envelope generation outlined above most directly relies upon assumed values of state threshold and a flight dynamic model. The state thresholds may be selected with a degree of confidence by following the recommendations of Wilborn and Foster [174] noted earlier in this section. While some uncertainty is likely to exist in the selection of these parameters the use of conservative values allows for the mitigation of this uncertainty's impact on the final LOC envelope, an effect which will be studied in §5.2. On the other hand, it is certain the flight dynamic model will

be subject to some degree of error which propagates to the final envelope and by extension to predictions made using this envelope. The sensitivity of the LOC envelope to this source of uncertainty will be the subject of experimentation presented in the following section.

5.2 Implementation and Testing of LOC Envelope

In implementing the LOC envelope generation process described previously a set of vehicle state and control boundaries were defined for the LWGA aircraft model. In this process the LWGA will be treated as a true representation of some nominal fixed-wing GA aircraft, such that it may be considered that the LWGA model represents some ideal error-free model of the LWGA aircraft. This assumption will enable later testing of the sensitivity of the LOC envelope generation process to sources of uncertainty, notably model error.

The process is initiated by the definition of various state and control boundaries. For this work the selected state bounds are provided in Table 11 and the defined control boundaries are shown in Table 12.

Table 11: Summary of state thresholds for LWGA LOC analysis.

State	Upper Limit	Lower Limit
Angle of Attack	15 deg.	-15 deg.
Sideslip Angle	15 deg.	-15 deg.
Bank Angle	45 deg.	-45 deg.
Pitch Angle	25 deg.	-10 deg.
Velocity	90 m/s	40 m/s
Load Factor	2.5 g	-1 g

Table 12: Summary of LWGA control limits for LWGA LOC analysis.

Control	Upper Limit	Lower Limit
Aileron Deflection	20 deg.	-20 deg.
Elevator Deflection	20 deg.	-20 deg.
Rudder Deflection	30 deg.	-30 deg.
Throttle	1	0

The state boundaries of Table 11 were defined according to observed model behaviors and various common safety recommendations. Limitations on the angle of attack arose from observation of the stall properties of the LWGA wing surface in both positive and negative stall conditions. Wilborn and Foster [174] suggest use of the maximum demonstrated crosswind landing speed in defining the limitations on the sideslip angle, suggesting a relationship between the sideslip angle limitations and rudder control authority. Using this guidance the sideslip angle limits were determined through testing of the limits of the LWGA control authority, evidenced by the relationship between rudder deflection and yawing moment at various sideslip angles. Limitations on roll angle and pitch angle were set to be consistent with recommendations provided by the FAA [54] regarding the limits of these parameters as they related to upset conditions. Additionally the load factor limits may be gathered through comparison to relevant aircraft regulation, which for GA aircraft is CFR Part 23 [55] which directly defines the acceptable limits on longitudinal load factor. Finally, the bounds on velocity are generated upon inspection of the velocity limits imposed by Wilborn and Foster's QLC [174]. The QLC defines a lower bound on velocity according to the stall warning velocity and an upper bound through the maximum operating velocity. This upper limit was attained through testing of the vehicle in progressively increasing steady velocity conditions until the upper limit of velocity was attained. Relevant FAA regulation once more guides the selection process, as the stall warning velocity is defined within CFR Part 23 [55] as "not less than 5 knots" above the stall velocity of the aircraft.

The control limitations defined within Table 12 were synthesized through comparison to the control limitations of aircraft which are similar to the LWGA. These limits are most reflective of the PA-28 [137–139] series of aircraft, due to the similarity of the lifting surfaces to this aircraft. While the QLC monitors deflection of only two of the control surfaces, aileron and elevator, the full set is required to ensure that the

control actions of various trajectories generated in the safe set calculation are within the control limitations.

Alongside the state limits imposed by the GA adaptation of the QLC [174] two additional sets of constraints were also imposed during the safe set generation process. The first set of constraints were the full set of control deflection limitations given in Table 12. In the state perturbation process the linearized aircraft system will be subjected to a trajectory generated by a pre-selected controller. The given form of the closed-loop system thus makes the direct enforcement of control limitations difficult, and it is likely that control limits will be violated for some extreme trajectories. As these trajectories would be infeasible for the true system then this additional set of constraints is appropriate.

The second additional set of constraints similarly arises due to the method by which the safe set is to be generated. As noted before the safe set will be estimated through application of a linearized form of the system model. This linearized form of the model may considered valid only in some neighborhood about the equilibrium condition used for the linearization. Given this concern the final set of constraints monitor the state trajectories to ensure that this closeness assumption is not violated.

The next phase of the LOC envelope estimation process is the definition of desired trim conditions and linearization of the model about those conditions. For demonstration of the methodology a general set of trim conditions is desired which will allow for exploration of various nominal flight conditions. Thus a range of velocities, flight path angles, and bank angles were defined, the extents of which are shown in Table 13. This set of vehicle conditions allow for flexible definition of trim conditions which include straight-and-level, level-turning, climbing, climbing-turning, descending, and descending-turning flight. An even grid of points was generated from these limits which constituted a set of trim point candidates.

To determine which of these flight conditions were feasible trim conditions the

Table 13: State test ranges for determining feasible trim conditions.

State	Lower Limit	Upper Limit
Velocity	55 m/s	70 m/s
Flight Path Angle	-10 deg.	10 deg.
Bank Angle	-30 deg.	30 deg.

trimming problem was posed as an optimization problem, similar to the approach presented by De Marco et al. [38]. The general objective of the trimming process is to identify the vehicle state and controls for which the vehicle is at equilibrium, that is to say the translational and rotational acceleration of the vehicle is zero. Neglecting the rate of the vehicle location with respect to the reference point $(\dot{x}, \dot{y}, \dot{z})$ then this reduces to a vector in $\mathbb{R}^6$ which is to reduced to zero. As the number of free controls is four, the optimization problem is over-determined and must be further developed if a unique solution is to be found.

Consider then that four parameters are known, namely the vehicle velocity, flight-path angle, bank angle, and the operating altitude. In addition, assume that the aircraft in trim is coordinated such that the yawing angle ψ is zero. Neglecting the relative positions the then unknown states and controls are $\{u, v, w, p, q, r, \theta, \delta_a, \delta_e, \delta_r, \delta_T\}$. The translational velocities in the body-axis frame are related to the translational velocity in the wind-axis frame as

$$u = V\cos(\beta)\sin(\alpha) \tag{82}$$

$$v = V\sin(\beta) \tag{83}$$

$$w = V\cos(\beta)\cos(\alpha) \tag{84}$$

Additionally the pitch angle is related to the flight-path angle, aerodynamic angles, and bank angle as

$$\theta = \gamma + \alpha\cos(\phi) + \beta * sin(\phi) \tag{85}$$

Finally the rotational rates can be related to the yawing rate $\dot{\psi}$, pitch angle, and bank

angle as

$$p = -\dot{\psi}\sin(\theta) \tag{86}$$

$$q = \dot{\psi}\sin(\phi)\cos(\theta) \tag{87}$$

$$r = \dot{\psi}\cos(\phi)\cos(\theta) \tag{88}$$

Thus the unknown states which will be considered as the optimization controls may be reduced to the set $\left\{\alpha, \beta, \dot{\psi}, \delta_a, \delta_e, \delta_r, \delta_T\right\}$. From the basic requirement of trim an optimization function may be posed which minimizes the rotational and translational acceleration vector $\{\dot{u}, \dot{v}, \dot{w}, \dot{p}, \dot{q}, \dot{r}\}$. As such the optimization problem is under-determined, thus the pitch angle rate $\dot{\theta}$ will be included in the final optimization vector $X = \left\{\dot{u}, \dot{v}, \dot{w}, \dot{p}, \dot{q}, \dot{r}, \dot{\theta}\right\}$. The optimization function may then be stated in standard quadratic form as

$$J = X^{\mathrm{T}} W X \tag{89}$$

When the weighting matrix $W \in \mathbb{R}^{7\times 7} = I_{7\times 7}$ then this function is noted to become the standard sum of the squared parameters to be minimized.

Using this method of determining trim conditions a set of trim conditions was determined for the LWGA at a nominal altitude of 1500 m. A total of 100 trim conditions were tested, consisting of all combinations of the velocity set $55, 60, 65, 70 m/s$, the bank angle set $-30, -15, 0, 15, 30 deg.$, and the flight path angle set $-10, -5, 0, 5, 10 deg.$ The subset of these conditions which are feasible are shown in Figure 38.

The LWGA model was then linearized about each feasible trim condition through finite differencing. Each linearized model was then simulated for many randomly generated perturbations. In simulating the conditions, a nominal control architecture was assumed which allowed for stabilization about the given trim conditions and the testing of the closed-loop system response to the various perturbation conditions. The chosen control architecture for the generation of the LOC envelopes in this work is the LQR controller, which requires the definition of the state weighting matrix Q and

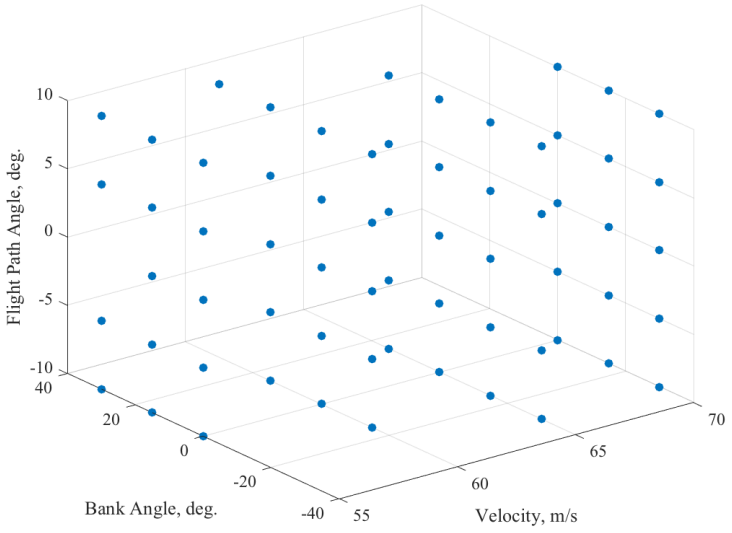

Figure 38: Set of feasible trim conditions for the LWGA.

control weighting matrix R.

Each of the weighting matrices were selected as diagonal matrices in order to simplify their definition. The weightings assigned to each vehicle state as the appropriate diagonal element of the matrix Q is given in Table 14. Similarly, the four controls (aileron, elevator, rudder, and throttle) were assigned the weighting values given in Table 15. These values were selected together to allow for satisfactory response to nominal initial conditions, such that reasonable settling times and state trajectories were generally attained while avoiding the violation of vehicle control constraints.

The perturbations were uniformly distributed between ± 15 m/s for translational velocities, ± 15 deg/s for rotational velocities, and ± 15 deg for attitude angles. The ensuing trajectories for these perturbed initial conditions were then compared to the state, control, and linearity constraints. Those initial conditions which did not violate any of these constraints were then used to construct the LOC safe set. This safe set is shown in Figure 39, along with the larger full set of tested flight conditions.

In constructing the safe set shown in Figure 39, the full set of non-violating perturbed conditions was examined to determine the convex hull which contained this

Table 14: State weighting values for LQR controller.

State	Value
u	1
v	1
w	1
p	1000
q	10000
r	1000
x	1
y	1
z	1
ϕ	1
θ	100
ψ	1

Table 15: Control weighting values for LQR controller.

Control	Value
δ_a	10000
δ_e	10000
δ_r	1000
δ_r	10000

set. Within this outer hull there are some tested conditions which do not satisfy the defined envelope conditions. As these points are within the convex hull of safe conditions it is the case then that these perturbed conditions are those for which safe recovery to the initial trim condition is not possible but it is possible to stabilize to some other trim condition within the trim set. Thus we may understand the safe set as representing the set of conditions for which it is possible to return to some safe trim condition without violating the defined envelope, whereas the points outside the safe set have no such guarantee.

This is not to say however that conditions which lie outside of the safe set may never return to a safe trim condition. Instead the theoretical development of general safe sets demonstrates that the safe set is itself a subset of a larger set known as the recoverable set [111]. This recoverable set represents the set of points relative to some envelope such that if a trajectory violates the envelope it is possible to return to a

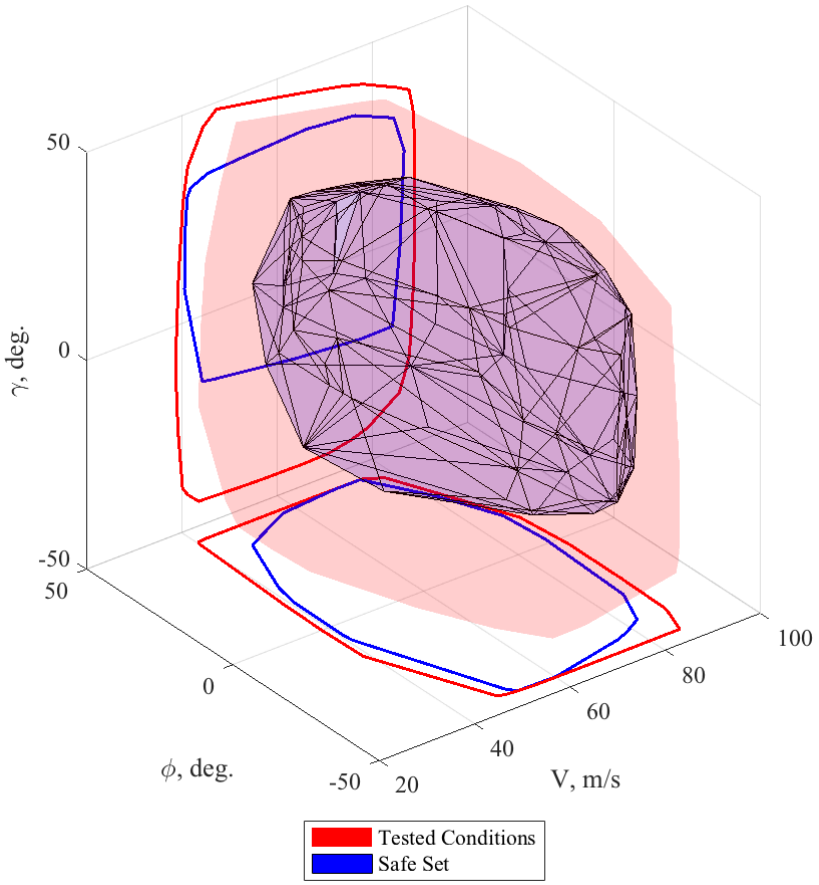

Figure 39: Baseline LOC envelope for LWGA.

condition within the envelope, that is to recover from the envelope violation. As this recoverable set is shown to contain the safe set it is quite possible, and in most cases likely, that several of the test points which lie outside the safe set can be returned to conditions which satisfy the envelope constraints.

Some key insights are gleaned from this baseline LOC envelope prior to further testing. The LOC envelope safe set shown in Figure 39 is additionally paired with two-dimensional projection views of the safe set in both the $V - \phi$ and $V - \gamma$ planes. These projections indicate that in general the $V - \gamma$ projection of the maximum cross-section is less constraining than the $V - \phi$ projection, implying that the selection of a desired bank angle is in general less constraining from a safety perspective than the velocity and flight-path angle. The overall shape of the estimated safe set can be

observed to taper at the extreme values of each parameter. That is, as one vehicle state (e.g. flight path angle) is nearer to the upper or lower limit, then a narrower range of the other states (e.g. velocity and bank angle) is tolerated. This observed behavior is not unexpected, as in general the combinations of flight states near "corner conditions" are known to be less safe.

Finally it should be noted that through this process of LOC envelope estimation that while the full QLC envelope was used to define the LOC boundary, the final safe set was expressible in terms of only three vehicle states. This basis for this reduction is somewhat evident in the formulation of the trim state solution provided above, as the three states shown for the final safe set are closely related to nearly the full set of vehicle flight states. The final three states observed, vehicle velocity, flight path angle, and bank angle, also are noted to be states which may easily estimated within the assumed data constraints imposed by this work. This implies that far fewer states are required within the state and control estimation portion of the proposed methodology if this safe set is utilized than originally anticipated, an effect which will be discussed further in §6.3.

An additional question arises upon further investigation of the derived LOC safe set: for the test conditions which are excluded from the final safe set, is there any trend or pattern that may be discerned regarding the LOC constraints which these conditions fail to satisfy? Put another way, if the safe set is violated in a particular region is it possible to predict the likely ways in which the ensuing trajectory may potentially violate the LOC boundaries if corrective action is not taken? To investigate this question, the set of test conditions which are excluded from the safe set are collected and the data regarding their various envelope violations were further investigated. Upon collection of this data, an initial filtering was performed to identify those trajectories which were not in violation of the linearity and control constraints but did violate one or more of the GA QLC envelopes. This subset presents data which

is limited to more reasonable representations of conditions which may be experienced by a physical system.

The data presented in Table 16 represent the various combinations of GA QLC envelopes which were violated for conditions that were tested and fall outside of the safe set. It is first noted that only four of the GA QLC envelopes appear in Table 16: the Adverse Aerodynamics (AA), Unusual Attitude (UA), Dynamic Pitch Control (DPC), and Dynamic Roll Control (DRC) envelopes. The fifth envelope, the Structural Integrity (SI) envelope, was observed to have not been violated by any of the non-safe set flight conditions. In addition to the envelope combinations presented in Table 16 the frequency with which each individual envelope was violated is given in Table 17.

Together the data given in Table 16 and Table 17 suggest that various combinations of AA, UA, and DPC envelope are the most commonly encountered LOC boundary violations. These types of combination suggest that for such conditions it is likely that while corrective action may be taken there is likely to be a LOC boundary violation involving the longitudinal axis. Further, as most of the non-safe set conditions are those with low flight path angle implying that flight in, or recovery from, such conditions is prone to LOC envelope violations. This finding is also supported by work presented by Kwatny et al. [98], which noted that tendency of a longitudinal model to violate imposed velocity and flight path angle limitations for combinations of low flight path angle and velocity.

Additionally while the DPC, UA, and AA envelopes are the most commonly violated, they are most likely violated in combination which some other envelope rather than individual violation of a given envelope. This observation is important in the context of the original application of the QLC, which described the onset of LOC as the simultaneous violation of at least three envelopes simultaneously [174]. Qualitative inspection of the trajectories reveals that the violation of LOC envelopes typically

occurs within the initial few seconds of a given trajectory. Thus it is likely that if multiple envelopes are indicated to have been violated that the violations occurred within a small window of time or simultaneously.

Table 16: Violated LOC envelopes for conditions outside safe set.

Violated Envelope Combinations	Percentage of Conditions
UA + DPC	40.45 %
DPC	16.26 %
AA + UA + DPC	13.81 %
AA	12.65 %
AA + DPC	4.78 %
DRC	3.72 %
UA + DPC + DRC	2.77 %
UA	2.11 %
DPC + DRC	1.33 %
AA + UA + DPC + DRC	0.67 %
AA + DRC	0.61 %
AA + UA	0.39 %
AA + DPC + DRC	0.33 %
UA + DRC	0.11 %

Table 17: Individual violated LOC envelope frequencies for conditions outside safe set.

Violated Envelope	Percentage of Conditions
DPC	79.74 %
UA	60.32 %
AA	33.24 %
DRC	9.54 %

With the baseline LOC envelope established, attention then turns to further investigation of the LOC envelope. Two key investigations are presented in the remainder of this section. First the sensitivity of the envelope to assumptions inherent within the envelope estimation process will be investigation. Then the effect of model uncertainty will assessed in a second experiment. Finally, a third experiment is presented which assesses the ways in which the envelope changes in the presence of both sources of uncertainty.

5.2.1 Experiment 1.1: LOC Envelope Sensitivity to Assumption Uncertainty

The sensitivity of the LOC envelope to the uncertainty implicit in the assumption of thresholds is the concern of Research Question 1.1. It is reasonable to assume that uncertainty in the assumed threshold values will undoubtedly propagate to the resultant LOC envelope. Indeed, should the LOC envelope consist of only these thresholds then the uncertainty of the assumptions would map directly to the uncertainty of the envelope itself. However, in the proposed methodology an additional phase of calculation is performed through the calculation of the safe set such that the final sensitivity of the LOC envelope to the assumptions uncertainty is not direct. It is hypothesized, though, that the generated LOC envelope is not overly sensitivity to this source of uncertainty, based upon the observed performance of similar envelopes within the literature. This assertion is expressed as Hypothesis 1.1. In order to measure the sensitivity of the LOC envelope with respect to the uncertainty in the assumptions, the methodology shall explicitly model this uncertainty and propagate it through to the final LOC envelope. The uncertainty of the assumed thresholds arises due to an imperfect level of knowledge. That is, this uncertainty does not primarily arise due to inherent randomness in the thresholds themselves but from lack of knowledge as to what the precise thresholds should be. This type of uncertainty is referred to by the International Organization for Standardization (ISO) as Type B uncertainty [85].

Guidance for modeling both Type A and Type B uncertainty is provided by the ISO through its *Guide to Estimation of Uncertainty in Measurement* (GUM) [85]. Based upon this guide, Castrup recommends the process pictured in Figure 40 for modeling both distribution and uncertainty of Type B uncertainty [33]. The fourth step of this process requires an assumption for the underlying distribution of error, which is then used to calculate the magnitude of standard uncertainty. While many

possible distributions could be used, Castrup recommends the use of a normal distribution for Type B uncertainty, particularly in cases when the output uncertainty distribution is desired [33].

In this application, however, the envelope threshold values that are selected are based upon estimates of vehicle normal operation envelopes. Selection of these thresholds additionally represent the desire of the operator to conservatively restrain the vehicle to some known safe envelope. This is to say that unlike other sources of error the uncertainty with regards to envelope assumptions may be directly accounted for through conservative selection of state or control thresholds. Thus the desired outcome of this student is not a distribution of the envelope's properties with respect to the input uncertainty distribution but rather the relationship between the two. Therefore a uniform distribution will be utilized such that no bias will be imparted into the outcome distribution.

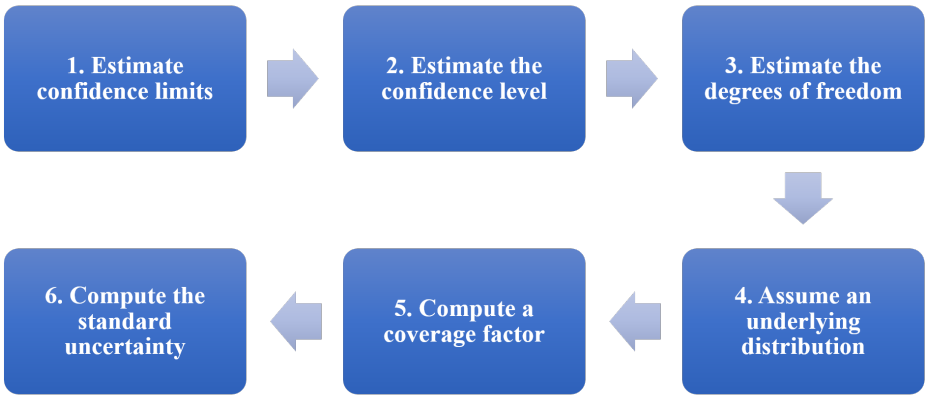

Figure 40: Process of estimating Type B uncertainty, adapted from [33]

With the distribution of uncertainty modeled, it was then numerically propagated through the generation of the LOC envelope. The ISO provides additional guidance for the propagation of the uncertainty distribution in a supplemental document to GUM [86]. This process involves propagation of the uncertainty of the estimated

values to calculate the resultant uncertainty of the final process. It was observed by Theodorou et al. however that this means of propagation tended to overestimate the magnitude of the final process when compared to propagation of the underlying error distribution through Monte Carlo simulation [168]. It is desirable to avoid this overestimation, as later experiments will include additional sources of error, so direct propagation of the assumed error distribution will be performed to ascertain the variability of the LOC envelopes.

The first experiment will test Hypothesis 1.1, which is related to the sensitivity of the LOC envelopes with respect to uncertainty in the estimation of thresholds. In performing this experiment, and later experiments described in §5.2.2 and §5.2.3, some means of assessing LOC envelopes is required. The general shape of the final LOC envelope is observed from Figure 39 to be a convex hull which encapsulates the set of conditions that do not violate any LOC constraint. In general internal volume of this hull is to be maximized, as a large internal volume represents a large envelope within which some flight may occur. Conversely a smaller volume indicates an envelope which is more restrictive such that the normal operation conditions are in closer proximity to LOC conditions. During the construction of the convex hull, this internal volume may be also be calculated and used an a measure of the goodness of a given LOC envelope. Using this measure for LOC envelopes, the sensitivity of the envelope's volume to each type of uncertainty can be tested.

With this measure of the LOC envelopes prepared, the following steps were performed as part of Experiment 1.1.

1. Define threshold uncertainties using a ISO-based process, like that described by Castrup [33]

2. Propagate uncertainty to LOC envelope

3. Calculate LOC envelope volume, V_{LOC}, and variability with respect to threshold

uncertainty

4. Calculate appropriate uncertainty bounds for satisfactory LOC envelope

In Figure 41 the uniform distribution used to model the threshold uncertainty is shown. This distribution displays values which vary from between a $\pm 25\%$ adjustment to all of the assumed GA QLC envelope thresholds. The application of this type of adjustment is based upon the application of various safety factors which are commonly used with safety analysis and FAA regulation [55, 56] to define conservative estimates of vehicle parameters.

Values in Figure 41 which are greater than unity represent a relaxation of the thresholds, while values less than unity represent a restriction of the thresholds. Relaxed threshold adjustments model the situation in which the threshold values which are "above" the true state or control thresholds, yielding a larger and less restrictive that the true state thresholds. The converse is true then for threshold adjustments which are less than unity, as these values represent an over-estimation of the threshold values which produce a smaller envelope. To apply these adjustment factors to the various state and control thresholds, the threshold adjustment factor was applied as

$$\tilde{X} = KX \tag{90}$$

where K is the threshold adjustment and X is one of the state or controls which constitutes the GA QLC.

This distribution of threshold adjustment factors was propagated through the LOC envelope following the LOC generation process. For this experiment, the propagated error was injected into the construction of the GA LOC envelope boundaries directly. Thus for this experiment the vehicle model and trajectories produced by the trim condition perturbations are unaffected by the selected error distribution. The direct adjustment of the LOC thresholds though would be anticipated to result in variations in the final LOC safe set.

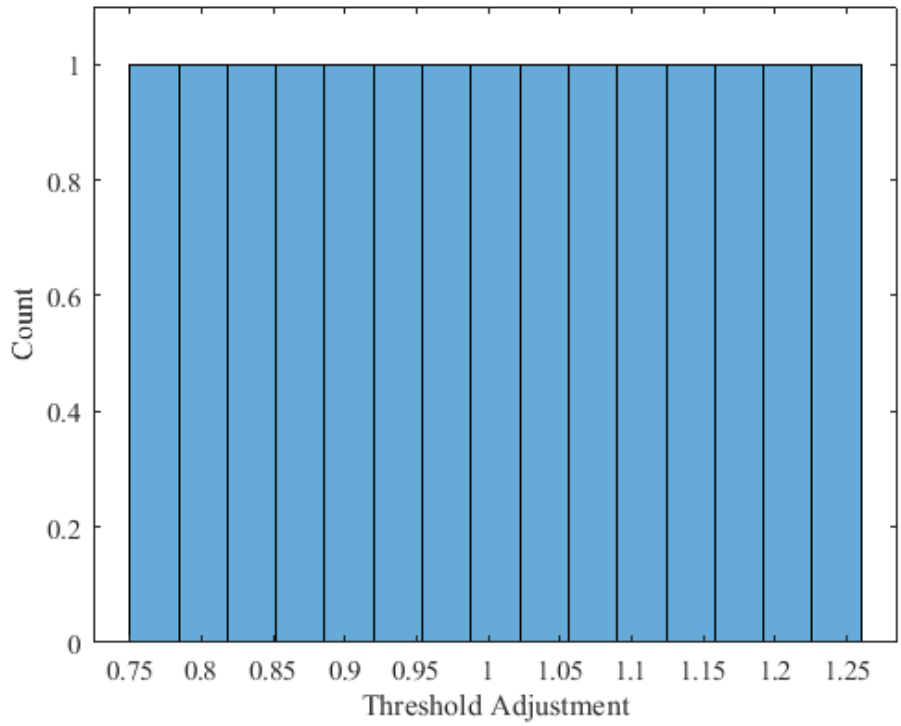

Figure 41: Distribution of threshold adjustment factor for Experiment 1.1.

Following the development of the baseline LOC envelope the key metric evaluated within this experiment is the volume of the final LOC safe set. In Figure 42 the resultant variation of the normalized safe set volume due to the propagated distributed of threshold adjustment values. This figure additionally contains a 2nd order polynomial fit to these data to aid in analysis, the equation for which is

$$f(x) = -4.924x^2 + 11.242x - 5.511 \tag{91}$$

The first observation which can be made is that this second-order polynomial is a good fit for the experimental data, with $R^2 = 0.998$. This good agreement suggests that the underlying trend behaves quadratically within the tested region and allows for some local conclusions to be drawn.

First an observed maximum safe set volume is observed for a threshold adjustment value of approximately 1.15. The LOC envelope which corresponds to this value of threshold adjustment is given in Figure 43. The general increase in the safe set volume

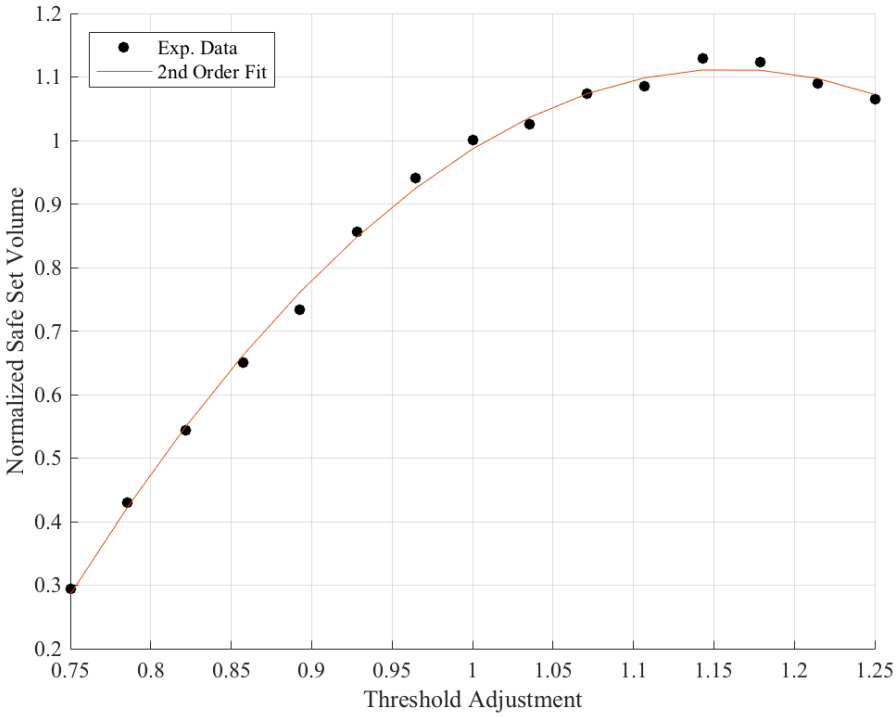

Figure 42: Variation of safe set normalized volume with threshold adjustment.

with increasing threshold adjustment is in agreement with the expectations for this experiment, as the increasing value corresponds to an expansion of the GA QLC envelope which would be expected to similarly expand the safe set. It is somewhat unexpected however that this increase would reach some maximal value.

Further investigation of the envelopes which result from threshold adjustments greater than or equal to 1.15 reveal that the volume of the safe set is driven primarily by the linearity and control constraints. This is to say, this maximal value observed near the threshold adjustment of 1.15 is indicative of some upper limit to the safe set volume. The upper limit represents the largest set of safe operating conditions which may be achieved for a given vehicle configuration, based upon the upper and lower control limits.

The data trend observed for threshold adjustments less than unity in Figure 42 is also in agreement with the initial expectations of the experiment. It is noted though

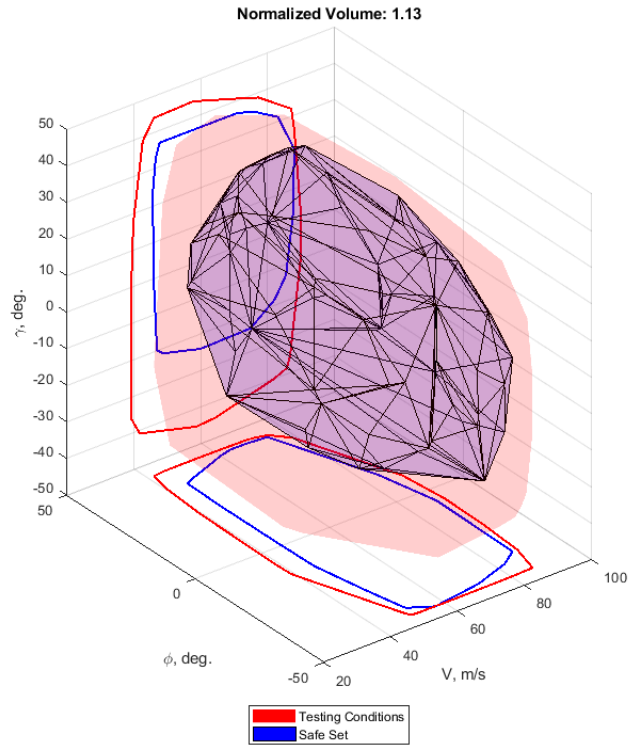

Figure 43: Sample LOC envelope with high threshold adjustment.

that reduction in safe set volume with decreasing threshold adjustment is non-uniform relative to the growth observed with increasing threshold adjustment. This is to say that for a uniform distance from unity in both directions, a non-uniform change in the safe set volume is observed, which is further demonstrated in Figure 44. This figure demonstrates a sample safe set corresponding to a threshold adjustment of approximately 0.85, and is therefore the converse of Figure 43. Interestingly, comparison of Figure 44 with the baseline safe set of Figure 39 reveals that the contraction of the safe set is such that the shrinking of the safe set also produces some slight translation of the centroid towards the origin point.

While this trend of uneven safe set volume growth may be obvious from the noted underlying fit, its interpretation within the broader effort is less so. Once implemented the various threshold values are to be indicative of various state and control thresholds

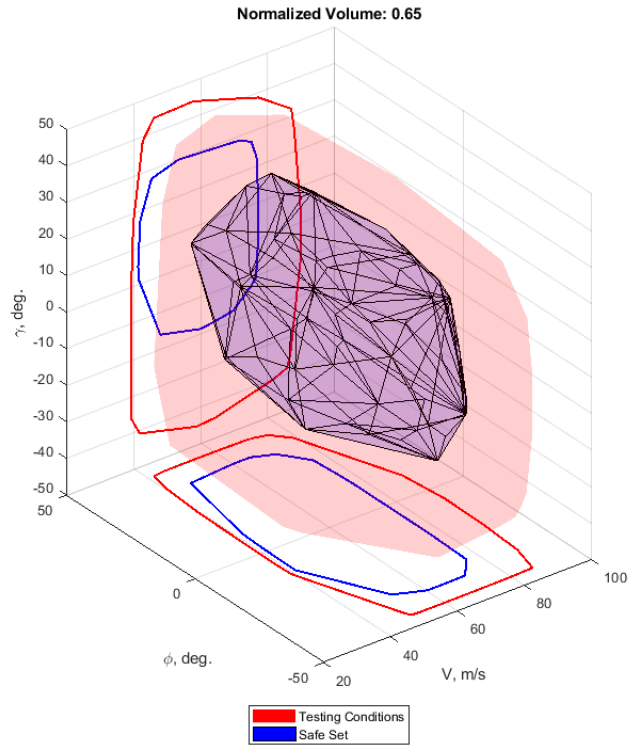

Figure 44: Sample LOC envelope with low threshold adjustment.

which are imposed to ensure safe operation of the vehicle. As such, there then exist some true set of thresholds which together constitute the true LOC envelope and corresponding safe set Consider the case in which it may be assumed that this true safe set corresponds to a threshold adjustment value of unity. Over-estimation (i.e. the chosen thresholds are two high) of these threshold values then corresponds to larger threshold adjustment values, which yield an estimated safe set which is larger than the true safe set. This situation is potentially quite grave, as it allows for flight conditions which are indicated by the safe set as safe with respect to LOC which may in fact represent unsafe conditions. Under-estimation on the other hand produces a conservative safe set that is both smaller than the true safe set, thereby limiting the vehicle to conditions which are somewhat "more" safe, and biased towards low flight-path and bank angle conditions due to the observed translational effects.

This capability to generate conservative approximations of the safe set is aided by the noted non-uniformity of the threshold adjustment trends. As the volume of the safe set is more sensitive to reductions in the threshold parameters, reasonable levels of uncertainty in the determination of the threshold parameters may be accounted for through inclusion of somewhat modest threshold adjustment. Further there is additional opportunity to use this form of adjustment to generate appropriately conservative approximations of the safe set which account for other sources of uncertainty, such as modeling error or uncertainty from observed states.

5.2.2 Experiment 1.2: LOC Envelope Sensitivity to Model Uncertainty

Alongside the uncertainty of the threshold assumptions, an additional source of uncertainty in the LOC envelope generation process is the aircraft dynamic model. This source of uncertainty and its effect on the LOC envelope is the subject of Research Question 1.2. Following a similar chain of reasoning as with Research Question 1.1, it is asserted that while the error inherent in the dynamical model will affect the LOC envelope, its impact will be reasonably bounded. This assertion was first provided as Hypothesis 1.2. Testing of the sensitivity of the LOC envelope to model error was tested in a similar fashion to that of Experiment 1.1. As before, this analysis will once measure the LOC envelopes using the volume of the resulting safe set under the influence of various assumed model error scenarios. In performing this experiment the following steps were conducted

1. Define dynamical model error distribution
2. Propagate error to LOC envelope
3. Calculate sensitivity of LOC envelope volume to model error

The manifestation of uncertainty in the aircraft dynamical model is less straightforward to model in comparison to the uncertainty present in threshold assumptions.

The uncertainty of the vehicle model arises primarily from various assumptions made within the modeling process which limit the accuracy of the model with respect to the true vehicle. Referring once more to the ISO's recommendations for uncertainty modeling [33] it may be noted that this type of uncertainty is categorized Type B uncertainty. In the development of the error distribution for the envelope thresholds the use of a normal distribution was passed over in favor of the use of an un-biased uniform distribution.

For modeling the error inherent to the model and its effect on the LOC envelope, the ISO's [33] recommendation to assume a normal distribution of uncertainty is utilized. This mean and standard deviation of the model error were chosen as zero and 15%, respectively, which results in a 95% confidence at ±30% model error. This selection of distribution parameters was guided by accepted modeling norms with regards to model accuracy. In general it is understood that an acceptable model has error which is typically within ±10%, a tolerance which is reflected by the selection of the given mean and standard deviation. Numerous samples were drawn from this distribution for propagation, and the resulting histogram of this sampling is given in Figure 45. The mean and standard deviation of this sampled distribution was calculated as $-2.603e^{-44}$ and 15.49%, respectively.

In the present method the vehicle model is responsible for estimating the forces and moments produced for some state and control configuration. These forces and moments are in general a summation of aerodynamic, propulsive, and inertial effects. To capture then the overall error of the vehicle model, several strategies may be used. One possibility is the direct modeling of the error contribution of each component of the vehicle model, which is then propagated through the LOC envelope process. Alternatively the gross error may be modeled, which models the total deviation of the forces and moments from their true values. Each approach may be useful in a particular context such that immediate exclusion of either option is not possible.

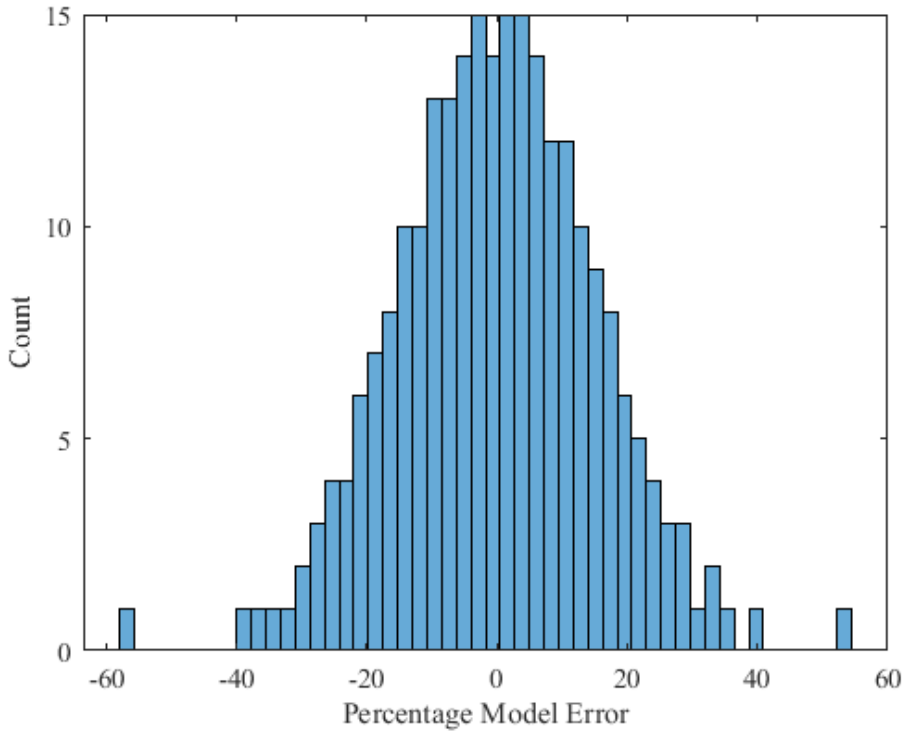

Figure 45: Distribution of model error for Experiment 1.2.

The intention of this experiment is to test the influence of general model error on the LOC envelope from an aggregate or high-level perspective. Building from this perspective the particular source of error, whether it be the aerodynamic, propulsive, or inertial portion of the model, is less prioritized with respect to the accuracy of the model as a whole. Therefore this experiment will model the total error of the vehicle model, rather than the error at the component model level.

With this selection, the means of error propagation was accomplished through comparison with the model error norm given as part of Equation (8), which poses the model error as some norm difference between the true vehicle dynamics and the modeled vehicle dynamics. In the LOC envelope synthesis process the true and estimated model dynamics are represented through the A and B matrices. For this experiment the model error with respect to the control matrix, B is neglected, such that the effects of any model error are applied solely to the system matrix A. Examination

of the system matrix A additionally reveals that the lower six rows correspond to the navigational and kinematic relationships (see Appendix C), and are not subject to modeling error. Therefore the model error is applied to the first six rows of the system matrix A, which correspond to the force and moment response estimation of the system. The model error is applied as a linear scaling of these rows as

$$\tilde{A}_{i\cdot} = (1 + K)A_{i\cdot}, \quad i = 1, ..., 6 \tag{92}$$

with K as the decimal percentage of model error and $A_{i\cdot}$ as the $i - th$ row of the system matrix A.

With the methods of model error propagation established, the propagation to the LOC envelope was then performed. The resulting distribution of normalized safe set volumes which were collected from this experiment is shown in Figure 46. Compared to the normal distribution of model error that served as the input for this experiment, the output distribution of normalized volumes is far less standard. There are two groupings of volumes, one about unity and a second, looser grouping between unity and 1.15.

The underlying phenomena which drives this unusual distribution seen in Figure 46 can be more easily described when paired with the data presented in Figure 42, which shows the variation in normalized safe set volume with changes in model error. From Figure 42 two trends can be noted corresponding to either positive or negative model error. The variation of normalized safe set volume for positive model error exhibits a linear trend with negative slope, consisting of values which are almost entirely negative. This trend indicates that if the model in general over-predicts, which is to say estimates forces and moments which are larger in magnitude than the true forces and moments, the resulting safe set tends to be smaller than the true safe set.

When the model error is negative, which would indicate a model which under predicts the vehicle forces and moments, the resulting safe set is larger than the safe set produced by the true model. The variation with negative error is not, however,

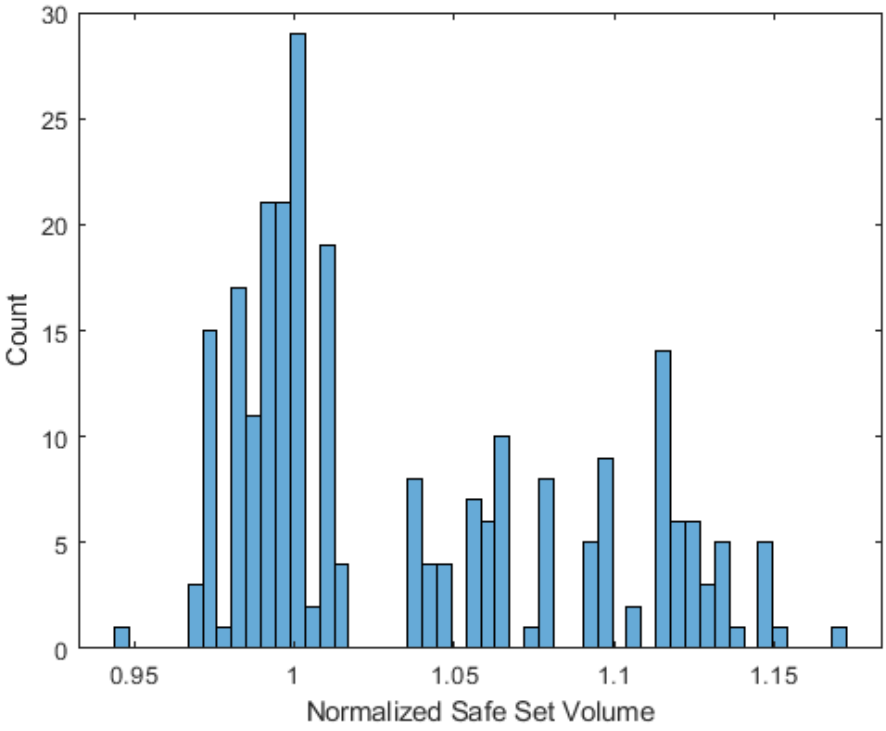

Figure 46: Distribution of normalized safe set volume for Experiment 1.2.

linear as with positive model error but rather exhibits a quadratic tendency with a maximal normalized safe set volume of 1.15. It is noted that this maximal value is quite close to the maximal value attained in Experiment 1.1, as seen in Figure 42. It may be surmised that this similarity is not merely coincidental, but is due to a similar nuance of the LOC envelope estimation process. As the safe set volume grows due to the relaxation of safety constraints, either directly in the case of the threshold adjustment or indirectly through less-severe force and moment reactions to state perturbations, an upper limit is met which is related to the maximal volume the safe set may attain given the imposed linearity and control authority constraints.

An additional behavior noted in Figure 47 is the dip in safe set volume observed for model error between -30% and -40%. It is theorized that in this region, the force and moment predictions become so low that for a given perturbation insufficient corrective forces and moments are produced by the body. As the vehicle begins

to fail in adequately contributing to the correction of the perturbation from the equilibrium condition, the closed loop system either more frequently exceeds the control constraints in order to compensate or the system "drifts" outside the established neighborhood of linearity due to insufficient corrective action.

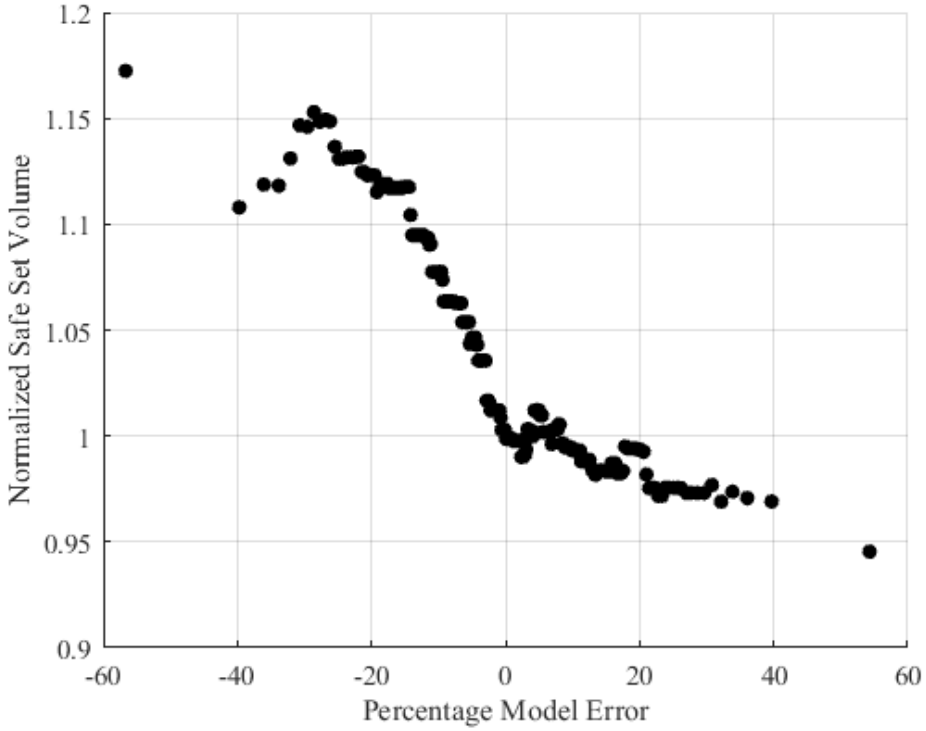

Figure 47: Variation of safe set normalized volume with model error.

Taken within the context of the full LOC mitigation methodology, it is pertinent to examine the sensitivity of the LOC envelope within a more localized range of model error values. It was noted during the definition of the model error distribution that models of this kind are typically considered to have errors within $\pm 10\%$ of the true value. Samples of the resultant LOC envelopes for both -10% and 10% error are shown in Figure 48 and Figure 49, respectively. Comparing these envelopes with the baseline LOC envelope shown in Figure 39 it is observed that there appears to be very little translation of the safe set towards the origin as the volume of the safe set decreases, in contrast to the translation observed during Experiment 1.1. Instead the

contraction of the safe set appears to be towards the center of the safe set, with little translation of the centroid of the safe set.

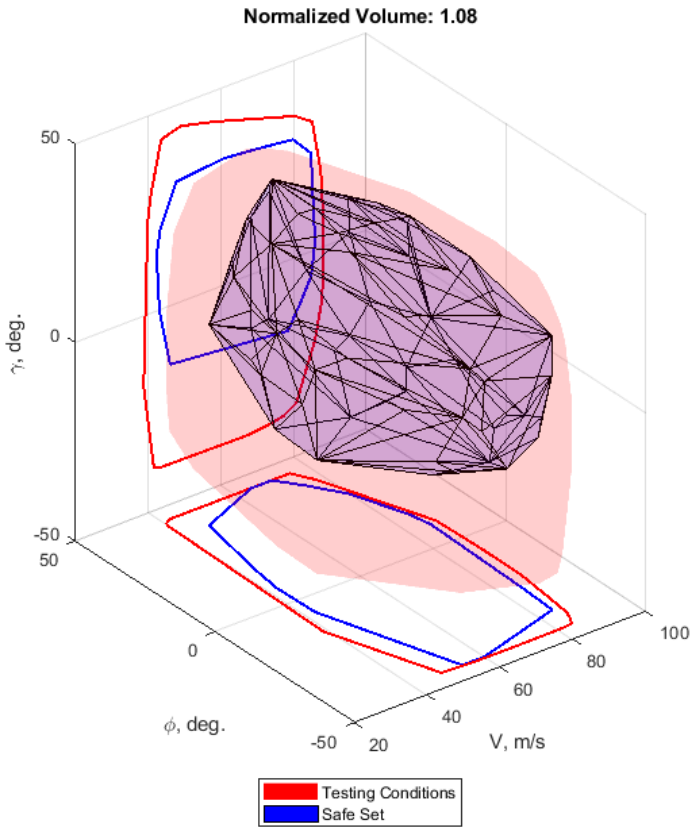

Figure 48: Sample LOC envelope with -10% model error.

Even within this more limited range of errors the non-uniform sensitivity of the safe set volume can be observed. While the contraction of the safe set in response to 10% model error is approximately 1% of the nominal safe set, the safe set volume grows by 8% in response to -10% model error. As discussed previously within the results of Experiment 1.1, the growth of the safe set volume is generally the more concerning of the two scenarios, as an estimated safe set which is larger than the true safe set allows for cases in which the estimated safe set provides false-positive assessments of some vehicle conditions. Given then the low sensitivity of the safe

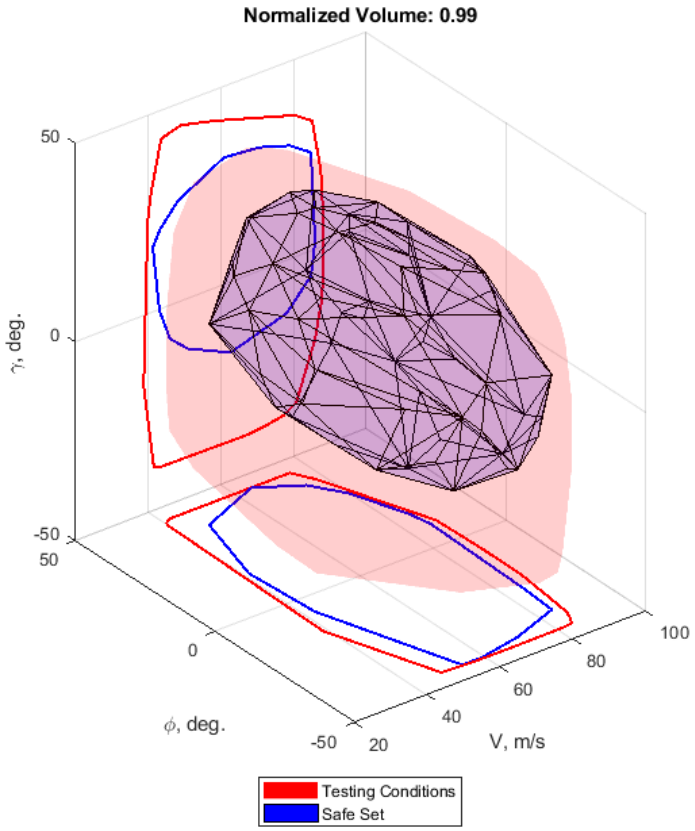

Figure 49: Sample LOC envelope with 10% model error.

set to positive model errors, a key observation that is drawn from this experiment is the preference towards zero or positive modeling error. That is, in the generation of models for the use in safe set estimation it is preferable to utilize a model which over-estimates the forces and moments by a reasonable amount rather than a model which under-estimates the true forces and moments by an equivalent percentage.

If a given model is known to produce under-estimations of the system's true response, then additional corrective effort would be advised based upon the results of this experiment. In this situation additional calibration of the model would be warranted, in hopes of yielding a vehicle model which is more accurate. Additionally, it is often the case that the creator of the system model is able to choose between various

methods of predicting the performance of the system. If this is the case for the vehicle model to be used in later LOC envelope estimation then preference should be given to models which in general provide an over-estimation of system performance at least insofar as the safe set generation is concerned.

It is also likely that little improvement can be made to a given vehicle model as it is understood that some level of error is expected due simply to the various assumptions inherent to the model. As such, a means of overcoming or countering the sensitivity of the model to this source of error is desired. In most cases the artificial inflation of the vehicle model is undesirable as doing so invalidates the model itself. Thus some corrective measure will be sought which is separate from the model itself that regardless allows for more conservative estimations of the safe set. The findings of Experiment 1.1 suggest that the use of threshold adjustments may be one means of accomplishing this goal, but the interaction between the level of threshold adjustment and the model error must be explored prior to any recommendation to this effect.

5.2.3 Experiment 1.3: LOC Envelope Level of Confidence Under Uncertainty

The final experiment related to Research Question 1 draws from the results of Experiments 1.1 and 1.2. In these experiments the sensitivity of the LOC envelope was ascertained for each primary source of uncertainty, namely the uncertainty in threshold values and the error in the aircraft dynamic model. As part of these experiments, bounds on permissible uncertainty for each source were generated and will serve as the starting point for Experiment 1.3. From these two independent bounds a joint propagation of uncertainty was performed that will allow for a more complete estimation of the confidence of the LOC envelopes under uncertainty. The steps that were performed during this experiment are listed below.

1. Based on Experiment 1.1, define limits in threshold values

2. Based on Experiment 1.2, define limits of model error

3. Construct distribution of threshold uncertainty and model error

4. Select combination of dual uncertainty and propagate to LOC envelope

5. Calculate LOC envelope volume for given combination of threshold uncertainty and model error

6. Repeat for various combinations of threshold uncertainty and modeling error

In Experiments 1.1 and 1.2 two different distributions were utilized in modeling the threshold adjustment and the model error. The threshold adjustment factor was assigned a uniform distribution in Experiment 1.1 whereas a normal distribution was utilized for the model error in Experiment 1.2. For Experiment 1.3 uniform distributions were utilized for both the threshold adjustment and the model error, based upon similar reasoning provided for Experiment 1.1. That is in Experiment 1.3 an unbiased evaluation of the underlying trends is preferred, such that the input of uniform distributions is deemed appropriate. For the threshold adjustment factor a uniform distribution is defined between 0.85 and 1.15, while a uniform distribution between $\pm 15\%$ is utilized for the model error.

These two distributions were then mixed to produce a full-factorial sampling which tested the full set of threshold adjustment and model error combinations. Each of these combinations was then used in the LOC envelope estimation process, resulting in an estimate of the the LOC envelope whose volume was calculated and recorded. The output distribution of these volumes is provided in Figure 50. The distribution of normalized volumes shown in Figure 50 a grouping of volumes between unity and 1.1, with a more gradual distribution of values less than unity. To better interpret this distribution of normalized volumes, an empirical CDF plot is also provided in Figure 51. In this CDF it is observed that 50% of the tested conditions result in a

normalized safe set volume that is greater than 1.02, while the remaining half produce a normalized volume that is below this volume.

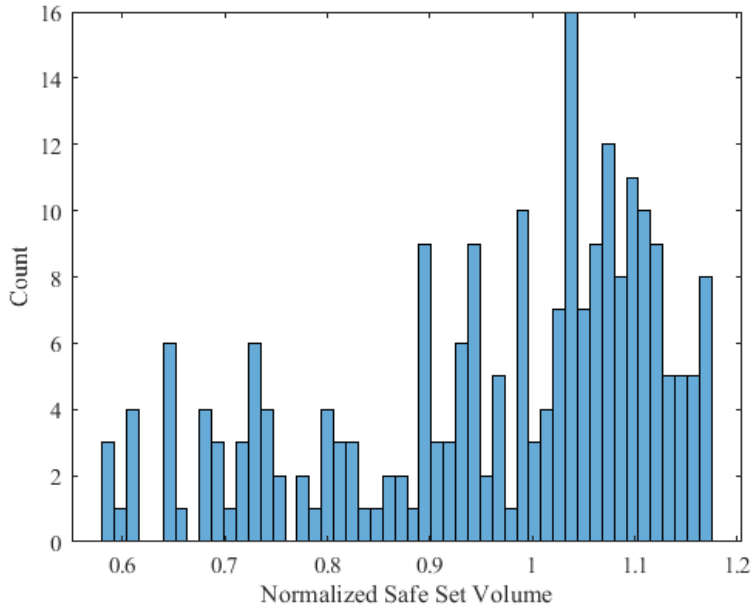

Figure 50: Distribution of normalized safe set volume for Experiment 1.3.

Thus while conditions which produce either an expansion or contraction of the safe set are observed to be equally common, the grouping of these two sets of conditions is quite dissimilar. The grouping of expanded safe set volumes is tightly grouped, indicating that the input conditions which produce expanded safe sets result in a range of values with somewhat low variability. Conversely the conditions which cause the safe set to contract produce an output distribution with higher variability, which implies that the normalized safe set is more sensitive to the input uncertainties in this region.

To identify the sets of conditions which produce either expanded or contracted safe sets, the normalized safe set volumes are plotted in each dimension of uncertainty. The variation of the volume with regards to threshold adjustment is first provided in Figure 52, which is similar to the results provided in Figure 42 which tested the

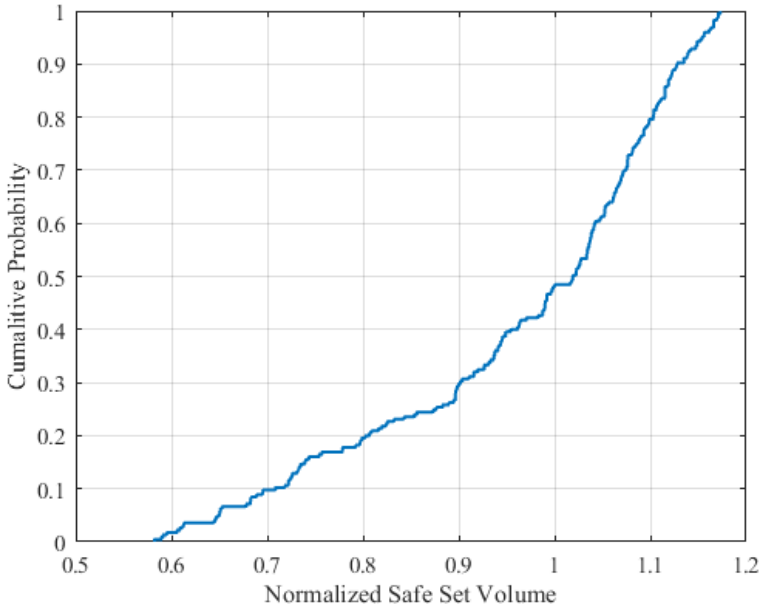

Figure 51: Empirical cumulative distribution function of normalized safe set volume for Experiment 1.3.

independent influence of threshold adjustment. Comparing the new results of Figure 52 with those observed previously in Figure 42 reveals that the overall trend is still present, though the influence of model error can be observed as the variability of points at each discrete threshold adjustment. Additionally it can be noted from this representation of the data the the normalized safe set volume is much more sensitive to the threshold adjustment factor than the model error within the ranges tested in this experiment.

The companion representation which depicts the variation of the safe set volume as a function of the model error is given in Figure 53. Comparison of this data with the corresponding representation given in Figure 47 is more difficult than the similar comparison performed for the threshold adjustment. The general trends observed in Experiment 1.2 can however still be noted, particularly the overall tendency for decreasing safe set volume with increasing model error.

In addition it can be noted both in Figure 52 and Figure 53 that there is some

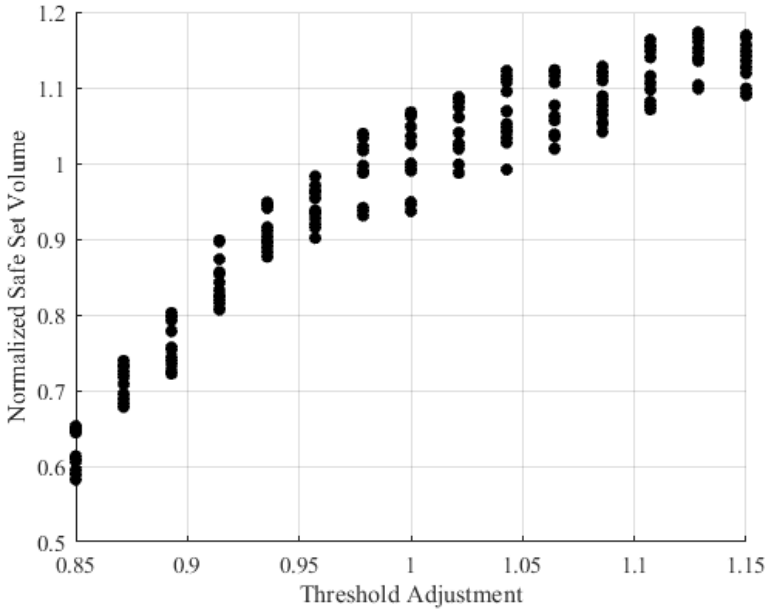

Figure 52: Variation of safe set normalized volume with threshold adjustments and varying model error.

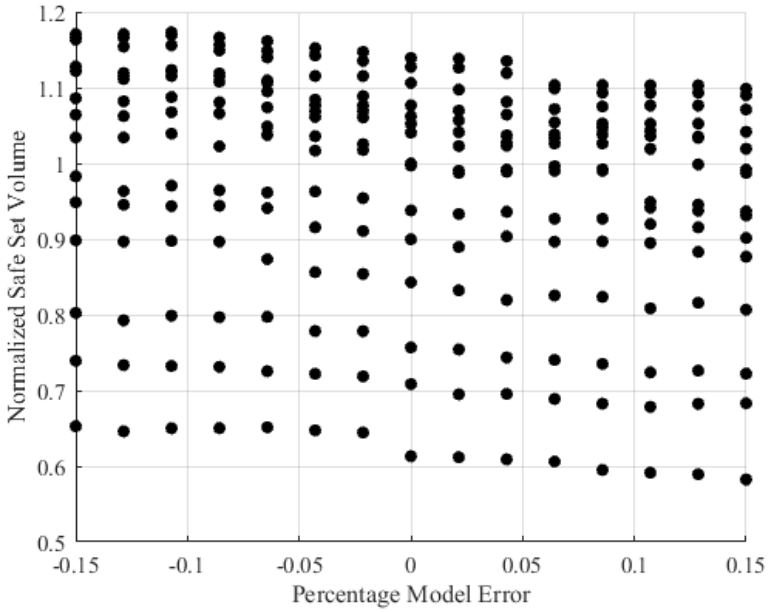

Figure 53: Variation of safe set normalized volume with model error and varying threshold adjustment.

interaction between the threshold adjustment factor and the model error. This interaction can also be observed in 54, which depicts the normalized safe set volume surface as a function of both threshold adjustment and model error, as a twisting of the depicted surface. From Figure 52 this interaction is observed as a tighter grouping of points as the threshold adjustment decreases, and similarly in Figure 53 as a flattening of the rows of points near the lower end of the normalized safe set volume axis. This interaction is likely driven by the larger variability of the volume response with respect to the threshold adjustment in comparison to the model error. For higher threshold adjustment, which yields a relaxation of the threshold constraints, the effect of model error may be more pronounced as there is more space within which the system may vary without violating the constraints. Conversely with lower threshold adjustment the LOC envelope begins the "choke" the perturbed trajectories, yielding more similar safe sets regardless of the magnitude of the model error.

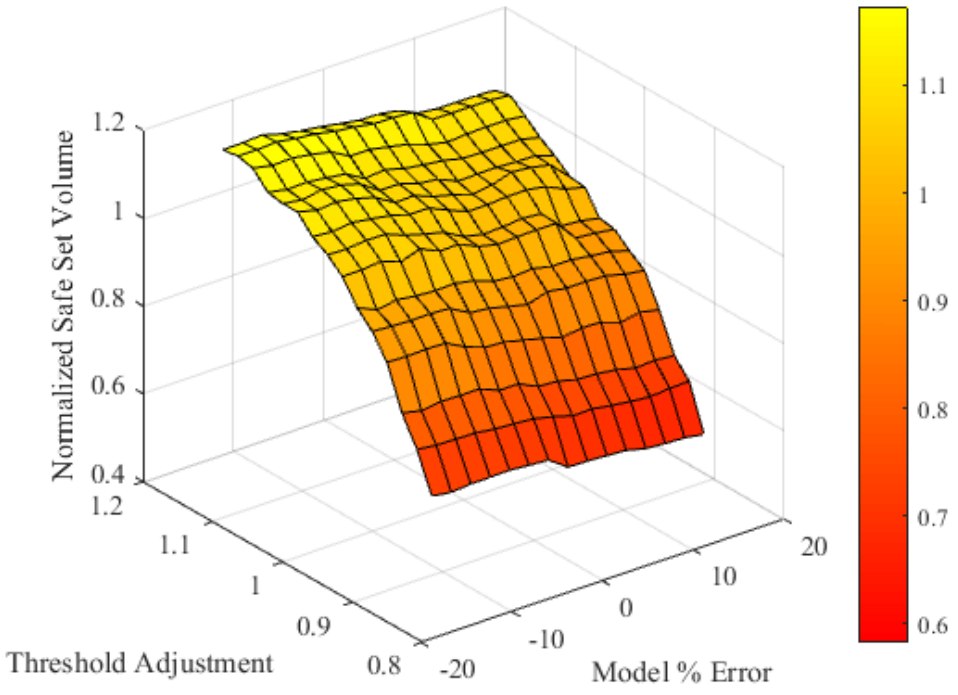

Figure 54: Surface of safe set normalized volume as a function of threshold adjustment and model error.

In the discussion of the results of Experiment 1.2 the observation was made that negative model error tended to produce an unacceptable LOC envelope, as indicated by a normalized volume value that was greater than unity. One potential means of avoiding this situation is through appropriate application of a threshold adjustment such that the final envelope has a volume which is less than or equal to unity. Observation of Figure 53 indicates that this approach is feasible, as there are numerous points at all model error values which have normalized volume less than or equal to unity. As an aside, these data also suggest that the converse may also be performed namely that if in some instance the model error was known to be too large that threshold adjustment could be utilized to re-inflate the final LOC envelope. This particular situation should be performed with great care, as such relaxation could allow for an envelope whose volume is of the appropriate volume but is inflated by including trajectories that are falsely identified as safe conditions. Returning to the means of correcting for negative model error, the appropriate level of threshold adjustment may be determined from the available data set through some means of interpolation such as a table-lookup or fitting the data to a surrogate function. If this approach is taken then the following process is recommended:

1. Determine magnitude of model error
2. Estimate threshold adjustment for model error contraction $K_T = f(\epsilon_{model}, V_{norm})$
3. Generate LOC envelope

From the collected data, an for the value of K_T as a function of the estimated model error and desired normalized volume can be constructed. Based upon the surface depicted in Figure 54, assume that the underlying function can be estimated by the polynomial

$$V_n = a_1 + a_2 K_M + a_3 K_T + a_4 K_M^2 + a_5 K_T^2 + a_6 K_M K_T \tag{93}$$

Table 18: Coefficients for fit of normalized volume as a function of K_M and K_T.

Coefficient	Value
a_1	-6.789
a_2	-0.102
a_3	14.019
a_4	0.0251
a_5	-6.2143
a_6	-0.217

where V_n is the normalized safe set volume, K_M is the estimated model error, and K_T is the threshold adjustment value. Using this assumed form a least-squares linear regression was performed to fit this model to the data of Experiment 1.3. The resulting coefficients are given in Table 18, which result in a fit to the experimental data with $R^2 = 0.99$.

At present an expression for K_T as a function of K_M and V_n is desired, so an inversion of this formula can be performed as

$$0 = a_5 K_T^2 + a_6 K_M K_T + a_3 K_T + \left(a_1 + a_2 K_M + a_4 K_M^2 - V_n\right) \tag{94}$$

$$K_T = \frac{-(a_3 + a_6 K_M) \pm \sqrt{(a_3 + a_6 K_M)^2 - 4a_5 \left(a_1 + a_2 K_M + a_4 K_M^2 - V_n\right)}}{2a_5} \tag{95}$$

$$K_T = \frac{-(a_3 + a_6 K_M) + \sqrt{(a_6^2 - 4a_4 a_5) K_M^2 + (2a_1 a_6 - 4a_1 a_2) K_M + a_3^2 - 4a_1 a_5 + 4a_5 V_n}}{2a_5} \tag{96}$$

In applying this relationship, care must be taken to avoid complex values resulting from negative values within the square root. This constraint may be expressed as

$$\frac{(4a_4 a_5 - a_6) K_M^2 + (4a_2 a_5 - 2a_3 a_6) K_M + 4a_1 a_5 - a_3^2}{4a_5} \geq V_n \tag{97}$$

Considering the experimental data in Figure 53 and the coefficients in Table 18 this constraint may be visualized as Figure 55. This visualization indicates that within the expected range of model error and the guiding principle to find K_T such that the normalized volume is no greater than unity there will be no combination of values which violate this constraint. Therefore it is established that the relationship for K_T given as eq. (96) will produce valid results within this range.

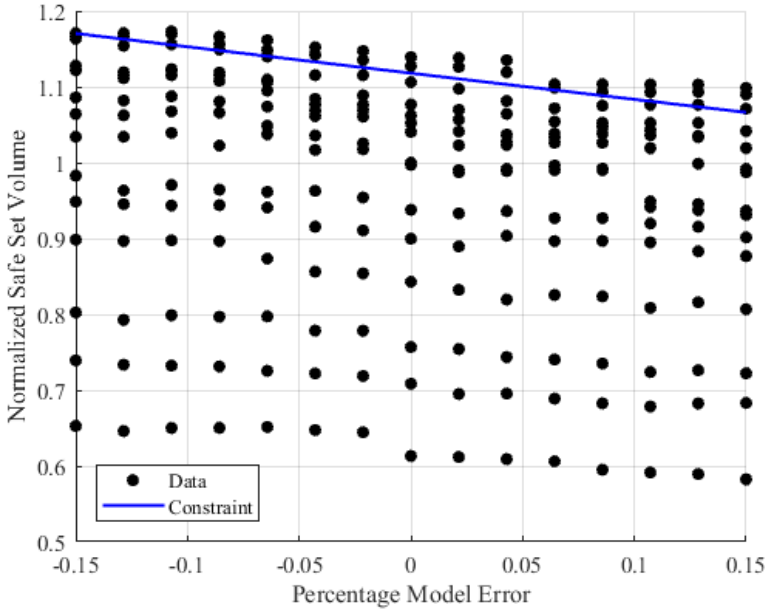

Figure 55: Experimental normalized safe set volume and percentage model error with expression constraint.

5.2.4 Summary of LOC Envelope Results

The first set of research question posed in Chapter 3 examine the proposed capability of the MERLIN methodology to predict impending LOC incidents through the definition of an LOC envelope. While the existing literature supports this general approach to LOC prediction further examination was performed to ascertain the sensitivity of the developed envelope to various sources of uncertainty. Following the process for LOC envelope definition displayed as Figure 37, a baseline envelope was first developed which is given as Figure 39. It was then noted that while the underlying envelope was comprised of six vehicle states, the final LOC envelope was reduced to only three: velocity, flight path angle, and bank angle.

Through the development of this process of LOC envelope definition two primary sources of uncertainty were identified that each were studied through additional experimentation. These sources of uncertainty are shown in Figure 56, which is a

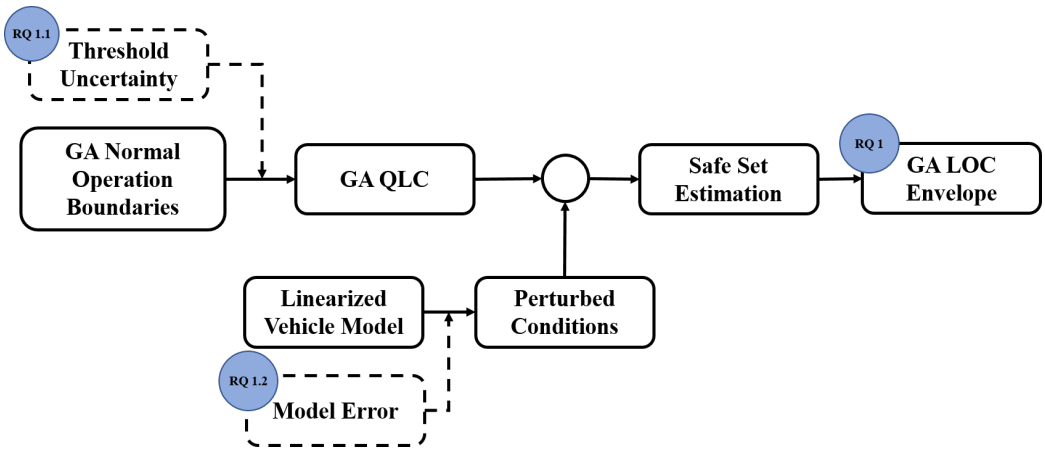

Figure 56: Summary of examined LOC envelope estimation method components with applicable research questions.

modified version of the GA LOC envelope generation process with included uncertainty sources. The first identified source of uncertainty, which was examined through Research Question 1.1, was the uncertainty related to the definition of the state and control thresholds which comprise the underlying GA operational envelope. Secondly, as a model of the vehicle is utilized in the estimation of the envelope's safe set an additional source of uncertainty is introduced due to the inherent error of the model. This source of error is examined through Research Question 1.2. Each of these research questions are also associated with relevant hypotheses which were tested through three experiments.

In the first experiment the assumed state and control thresholds of the GA normal operational boundaries were adjusted in order to test the sensitivity of the final GA LOC envelope to these changes. By either expanding or contracting the assumed thresholds it was observed that the volume of the resultant LOC envelope similarly expanded or contracted. The relationship between the level of threshold adjustment and the final volume is visualized in Figure 42. From this relationship it is was noted that the expected relationship between the threshold uncertainty and the final volume was present and that while there is a correlation between the uncertainty and the final volume, the sensitivity of the envelope to this uncertainty is not so severe as

to prevent effective practical implementation. An upper limit of approximately 10% to the growth of the LOC envelope was also noted which serves as an upper bound on the effect that the threshold uncertainty has on the generation process. This upper limit is particularly impart in the context of the LOC envelope as over-estimation of the envelope's size is noted as more concerning than under-estimation. Based upon these results it is observed that the conditions of Hypothesis 1.1 are satisfied, namely that the sensitivity of the LOC envelope is not only observed to within reasonable limits but is upper bounded and behaves in a predictable manner. Therefore the hypothesis posed for Research Question 1.1 is confirmed.

The second experiment followed suit in testing the sensitivity of the LOC envelope to an additional source of uncertainty. In this experiment the developed vehicle model was taken as a true representation of a fixed-wing GA vehicle such that modeling error could be artificially applied through prescribed deviation from the model predictions. This model error was then propagated through the LOC envelope estimation process, resulting in the relationship between model error and LOC envelope volume given in Figure 47. As expected the volume of the LOC envelope was observed to be sensitive to the variation in model error, with negative model error (i.e. under-estimation of forces and moments) causing an inflation of the envelope and positive model error causing a contraction. While the sensitivity was observed to be non-uniform for between positive and negative model error, in each case the rate at which the volume changed as a function of the model error was within a reasonable limit. An upper limit of the LOC envelope growth is also observed for variations due to model error, reaching a maximum normalized volume of approximately 1.15, similar to the upper limit noted for variations due to threshold uncertainty. Given these findings the assertion of Hypothesis 1.2 regarding the sensitivity of the LOC envelope to the model error is also confirmed.

The final experiment relating to the variation of the LOC envelope was to allow for the variation of both threshold adjustment and model error simultaneously in order to better understand the properties of the resulting safe set. These joint variations resulted in the variation of safe set volume described within Figure 54 which depicts the surface of normalized LOC envelope volumes as a function of both threshold adjustment. From these results it can be noted that in addition to the individual contributions of the threshold adjustment and the model error an additional interaction effect may be observed. These data additionally provided insight into a means of accounting for the uncertainty within the LOC envelope estimation process. As a LOC safe set which is larger than the true envelope is undesirable due to the implied safety concerns a means of ensuring that the envelope is either the same size as or smaller than the true safe set is desired. The results of this experiment showed that through a conservative shifting of the underlying state and control thresholds used to define the GA normal operating region, described by threshold adjustments less than unity, would be sufficient for generating a LOC envelope which meets this requirement within a range of expected model error. This insight was encapsulated in the description of a short process which relates the estimated model error to the required threshold adjustment to achieve a LOC safe set normalized volume of unity.

One noteworthy limitation of these results is related to means by which the model error is defined. While some overall estimate of model error may be quantified based upon the set of force and moment estimates produced by a model, it is somewhat likely that this error is not evenly distributed between all the force and moment predictions. Further the actual distribution of expected model error may not reflect a standard normal distribution as that utilized in Experiment 2.2, but may likely be skewed in one direction. Despite these limitations the results of the presented experiments nevertheless provide key insight into the behavior of the LOC envelope estimation process, and future work which more fully explores the impact of various

model error assumptions is recommended.

CHAPTER VI

STATE AND CONTROL ESTIMATION

In Chapter 3 a key assumption noted that the flight data available for this methodology is limited to that which can be collected through some electronic device brought on-board by the pilot. While the typical GA aircraft typically lacks an installed advanced avionics system, the use of PEDs such as tablet computers by GA pilots has become increasingly popular. These devices are often used as a digital flight bag [122] while also providing other services to the pilot. One such service is the observation and collection of flight data through applications such as GAARD [118]. The GAARD application, along with other similar applications, provide access to the GPS position of the aircraft which includes latitude, longitude, and altitude data alongside heading and ground speed. If in addition the pilot utilizes an external attitude and heading reference system (AHRS), such as the commercially available Stratus [60], then additional flight data can be collected by the application. Given the reasonable availability of these tools, it is assumed then that these data are available for the MERLIN methodology. A summary of the parameters assumed to be available is provided in Table 19.

Table 19: Summary of flight data available through external collection.

Parameter	**Source**
Longitude	GPS
Latitude	GPS
MSL Altitude	GPS
Heading	GPS
Ground Speed	GPS
Vertical Speed	GPS
Roll Angle	AHRS
Pitch Angle	AHRS
Yaw Angle	AHRS

With this subset of the aircraft state available for direct observation, some means of estimating the necessary states of the aircraft and the actions of the pilot are required. The extent to which various states and controls will be required within the MERLIN methodology is dependent directly upon the LOC envelope utilized within the particular application. In instantiations of the methodology which utilize a direct application of Wilborn and Foster's [174] QLC, then the vehicle states and pilot controls which must be collected are:

1. Angle of attack, α
2. Sideslip angle, β
3. Roll angle, ϕ
4. Roll angle rate, $\dot{\phi}$
5. Pitch angle, θ
6. Pitch angle rate, $\dot{\theta}$
7. Velocity, V
8. Longitudinal load factor, n
9. Pitch control (i.e. elevator angle), δ_e
10. Roll control (i.e. aileron angle), δ_a

If some other envelope is utilized then it is conceivable that other states may be required. At most an envelope may require the observation of the full set of vehicle states, their rates, and the control actions of the pilot. As such, investigations were performed which assessed the feasibility of collecting the required states from the available GA observation methods. This estimation effort relates to the subject of

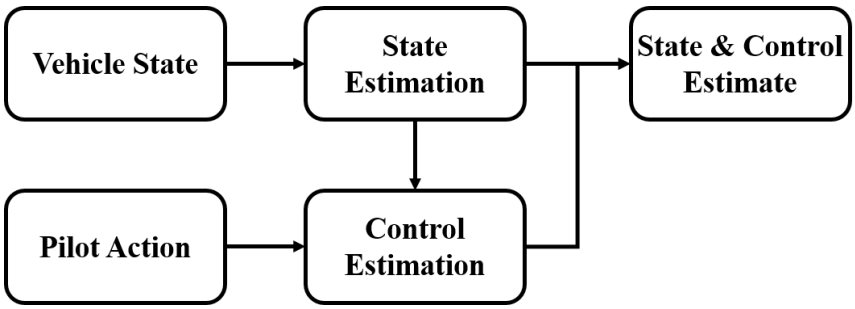

Figure 57: Overview of state and control estimation process.

the second research question, which is repeated here:

Research Question 2:

How can the proximity of a GA vehicle to a LOC situation be assessed in real-time while considering the constraints on available flight data for typical GA aircraft?

In addressing the second research question, the first sub-question addresses the methods available for performing the necessary estimation. It was hypothesized that through a combination of various approaches, the required information can be accurately estimated, stated specifically as Hypothesis 2.1. In investigating this research question, the tasks of estimating pilot actions and vehicle states were investigated separately. Various techniques were explored and tested for their accuracy and availability for use in the present method. Upon later experimentation, which is presented in Chapter 5, a particular GA LOC envelope is defined and a subsequent down-selection of estimation techniques is performed. Given a set of state and controls which are required for observation and the techniques selected for the estimation task, then the state and control estimation process will follow the process described in Figure 57.

6.1 Estimation of Pilot Control Action

There are typically five aspects of pilot control which are of interest for the current effort: flap deflection, thrust, elevator deflection, aileron deflection, and rudder deflection. Flap deflection angle is changed somewhat infrequently during a typical flight, yet with rather significant impact on the aerodynamic properties of the vehicle. The remaining four control states on the other hand are much more frequently altered and can be considered as the primary control actions available to the pilot. In light of this separation two separate algorithms were investigated, with one algorithm for the estimation of flap deflection and a second for the estimation of the remaining pilot-configured parameters.

The necessity of either of these algorithms in a particular implementation of the MERLIN methodology is not guaranteed, a point illustrated by the LOC envelope presented within §5.2 which requires only the estimation of three vehicle states and no pilot controls. The following algorithms are however included herein in order to enable a more general applicability of the MERLIN methodology to future applications which may require the estimation of pilot actions alongside vehicle states. At present no method of estimating flap activity for GA aircraft within the literature and methods for estimating other pilot actions are similarly limited. There exists then a gap between capability which may in general be required for the application of the MERLIN methodology and methods of satisfying this capability which is addressed with the inclusion of the following proposed algorithms.

6.1.1 Flap Activity Estimation Algorithm

While in recent years there has been an increase in the flight data collected during GA flights, there are very few capabilities for recording the flap deflection. Yet this information can be of vital importance for safety analysis as the phases of flight most prone to safety incidents are the phases in which flaps are more likely to be deployed.

In light of this, an algorithm for the estimation of flap deflection using collected flight data will be presented.

The core of this algorithm is based upon the concept of the total mechanical energy of an aircraft in flight. In their work, Puranik et al. [145] identify several energy-based metrics that are of use for flight-data based safety analysis. This work presents the *specific total energy* of an aircraft system as

$$E = h + \frac{V^2}{2g} \tag{98}$$

and the *specific total energy rate* as

$$\dot{E} = \dot{h} + \frac{V \times \dot{V}}{g} = \frac{(T - D)V}{W} \tag{99}$$

A convenient analogy for these metrics is the energy reservoir given by Amelink et al. [8] and represented in Figure 58. The specific total energy of the system represents a "tank" of energy which can be traded between either specific kinetic or specific potential energy "tanks" through appropriate control action, whereas the specific total energy rate indicates the rate at which energy is entering or leaving the "tank". As noted by Puranik et al. [145], both of these metrics have been used throughout the literature for various applications [8, 29, 115].

The basis for the algorithm for estimation of flap deflection can be found in Equation (99). In calculating the specific total energy rates, one may either use flight data (i.e. aircraft velocity, and altitude) or aircraft performance estimates (i.e. thrust and drag). By enforcing equality between these means of calculating the specific total energy rate, then an opportunity for estimating flap deflection is afforded. The steps of the algorithm will be described below and is also depicted in Figure 59.

To initiate the algorithm, the specific total energy rate is calculated from collected flight data. The required flight data is minimal, requiring at a minimum the altitude and velocity of the aircraft. Then the same calculation is performed using estimated aircraft performance parameters. The thrust of the vehicle will be estimated as a

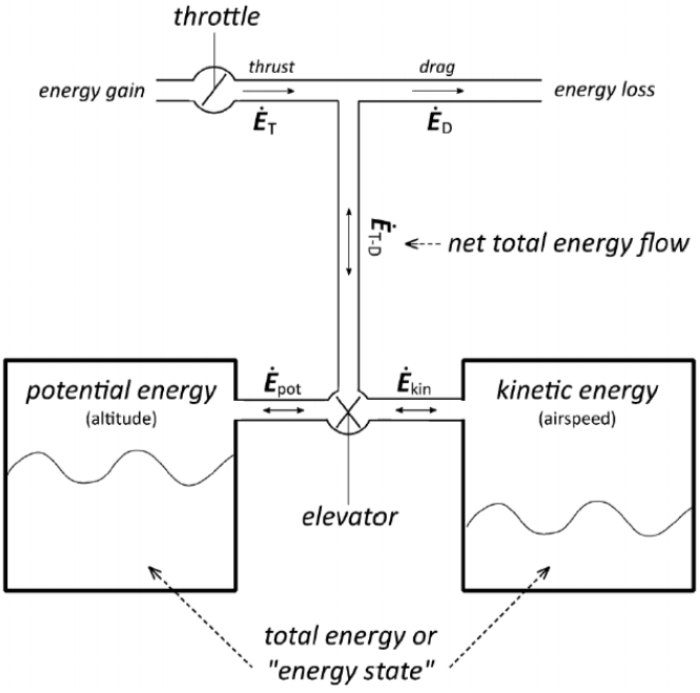

Figure 58: Depection of energy reservoir, adapted from [8].

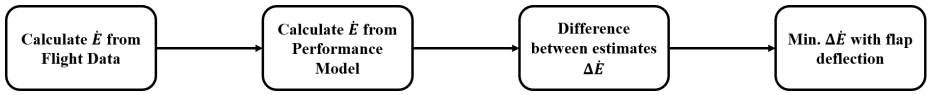

Figure 59: Steps of the FLAP algorithm.

control action of the pilot for this work, but in a more general effort the thrust of the aircraft may be estimated through calibrated performance models. Aerodynamic estimations needed to construct the dynamical model of the aircraft additionally provide the required estimates of the drag of the aircraft.

Next the difference between the two estimates of specific total energy rate is calculated. As these quantities should be identical, any difference is attributed to either error in the flight data or the performance model which includes error arising from the assumed flap deflection. Finally, the difference is minimized through selection of the flap deflection at every point in the flight. For GA aircraft, the flap deflection can be treated as a small number of discrete settings, such that the selection of the

error-minimizing flap deflection can be straightforward.

This algorithm has been tested on flight data collected from an actual flight of a Cessna 172. While flap deflection is not typically available, through coordination between partner researchers a record of the flap deflections used during an actual flight was acquired. A trace of the altitude and velocity profile is provided in Figure 60. The recorded flap deflection along with the predicted flap deflection made using the described algorithm are provided in Figure 61. It should be noted that it is known that not all flap deflections were recorded by the pilot during the flight, as appropriate safety precautions were taken such that no undue burden was inflicted on the pilots through manual recording of the flap deflection during the landing process. Post-flight interviews with the pilots do however indicate that flap usage occurred during the landing sequence, and that the flap usage identified by the algorithm but absent from the recorded flap deflection during the landing qualitatively matches the flap deflection used.

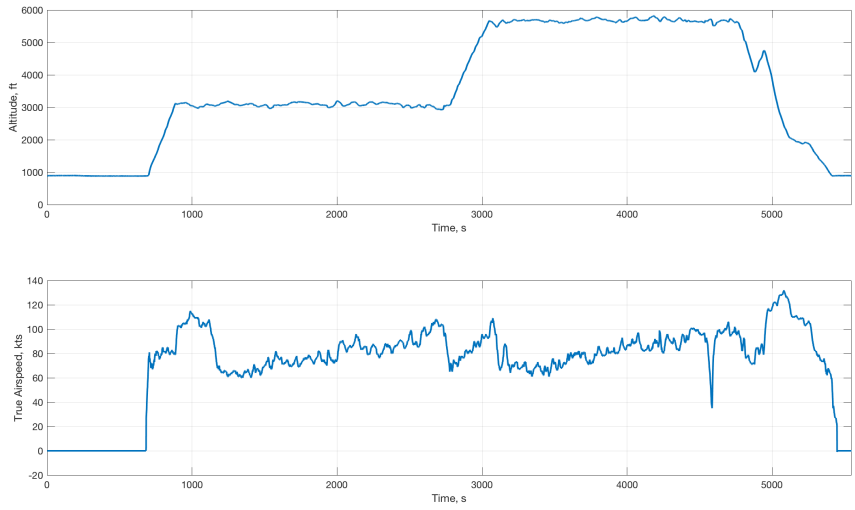

Figure 60: Altitude and velocity trace of flight used for FLAP algorithm testing.

In addition to the representation of the algorithm's performance shown in Figure 61, some statistics regarding the accuracy of the algorithm's estimations are

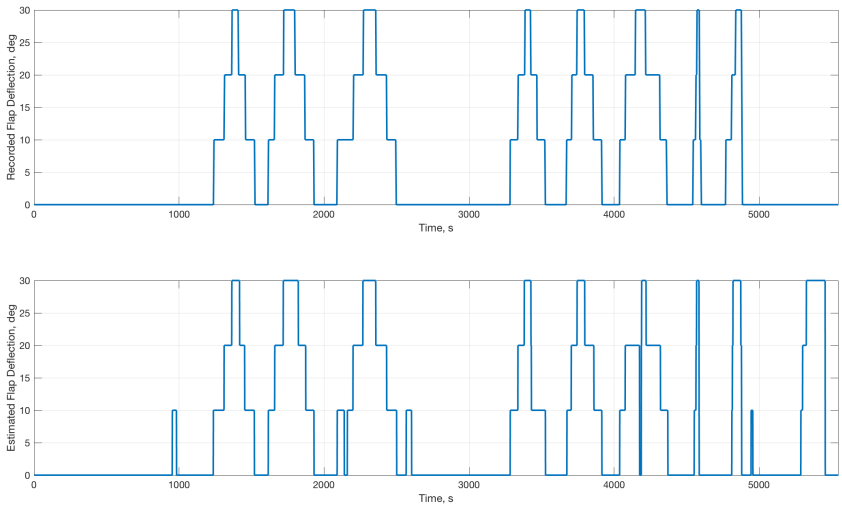

Figure 61: Recorded and estimated flap deflection from sample flight data.

given in Table 20. Taken together, these data suggest that the proposed algorithm is effective for predicting flap deflection activity for GA vehicles. There is some limitation, however, in the accuracy of the estimations produced by this algorithm. The algorithm is observed to be quite capable of estimating the absence of flap deflection but this accuracy diminishes when considering deployed flaps. Namely while it the algorithm demonstrates high accuracy in binary sense, it is less accurate in provides the particular degree to which flaps are utilized. It may also be anticipated that the accuracy of the method could be further degraded based upon additional error which arises from the prediction of thrust and drag, the estimation of aircraft weight, and noise in collected flight data.

From an algorithmic perspective it may be noted that the computational requirements of this algorithm are quite modest. As the velocity and altitude of the aircraft are assumed to already be collected for use in LOC proximity monitoring, the only additional computational burden imposed by this algorithm is the estimation of thrust and drag. This computational expense may be bounded from below by considering the approximation of these performance metrics through polynomial expressions, or

similarly with table look-ups.

Table 20: Overview of FLAP algorithm performance for sample flight.

Recorded Flap Condition	RMS Error (deg)	Percent Correct
All	5.67	88.9
0°	6.23	92.7
10°	3.50	87.7
20°	3.84	85.7
30°	6.12	88.4

6.1.2 Pilot Control Action Estimation Algorithm

In investigating methods of estimating the control actions other than the flap deflection, an expectation maximization (EM) algorithm was developed and tested. This algorithm uses the observed state of the aircraft along with a linearized dynamical model of the aircraft to estimate the most likely control action the pilot utilized. As these observations and the linearized vehicle model are likely to be developed in conjunction with other components of the methodology. The complete derivation of the proposed algorithm is provided in Appendix E, and some results will demonstrating the efficacy of the algorithm will be presented in this section.

For testing and demonstration of the EM algorithm, a toy problem is first constructed. The chosen problem is a cart pole system, which is depicted in Figure 62. This system has nonlinear dynamics which are given as

$$(m_c + m_p)\ddot{x} + m_p l\ddot{\theta}\cos\theta - m_p l\dot{\theta}^2 \sin\theta = f \tag{100}$$

$$m_p l\ddot{x}\cos\theta + m_p l^2\ddot{\theta} + m_p gl\sin\theta = 0 \tag{101}$$

A control strategy was developed for the cart pole system which results in the inversion of the pole from $\theta = 0$ to $\theta = 2\pi$. The states of the cart pole from this trajectory is shown in Figure 63. To simulate the presence of random noise which will be present within the final implementation of the estimation algorithm, the states of

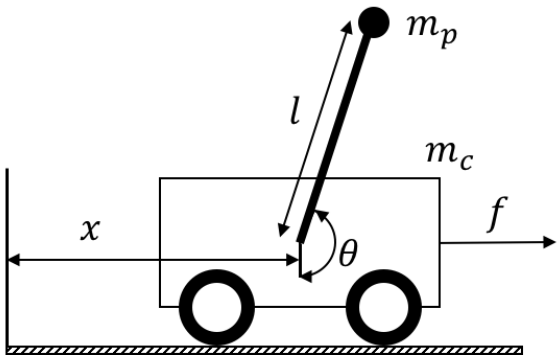

Figure 62: Depiction of cart pole system.

the cart pole system are corrupted using white noise. The corrupted system states trajectories are shown in Figure 64.

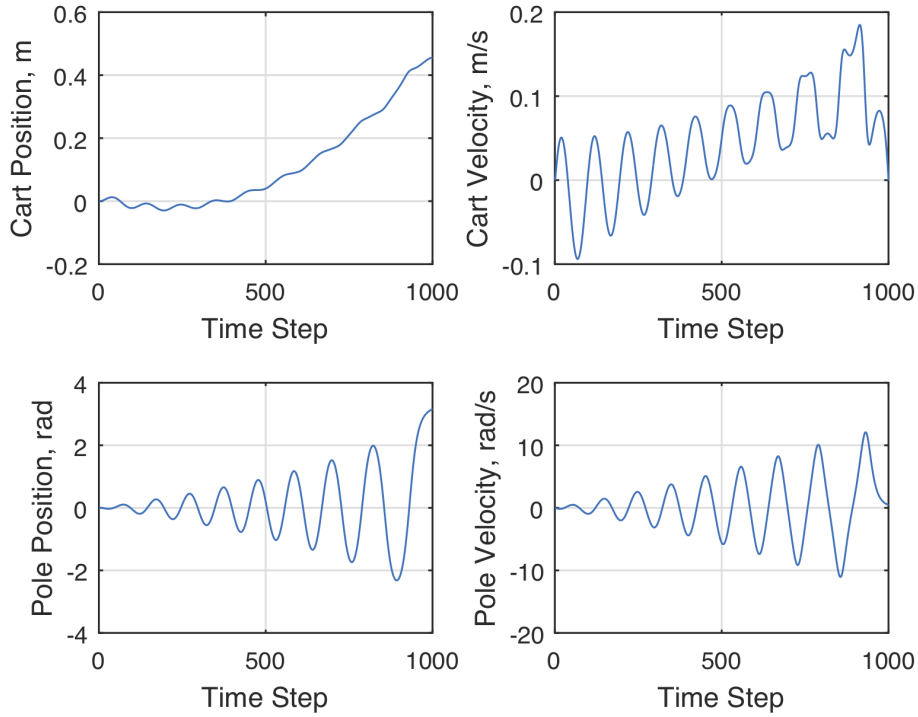

Figure 63: Simulation of cart pole system.

With the noise-corrupted state trajectories were provided to the EM algorithm to generate an estimate of the control input. These preliminary results are shown in Figure 65, which present a comparison of the input state trajectory and the trajectory

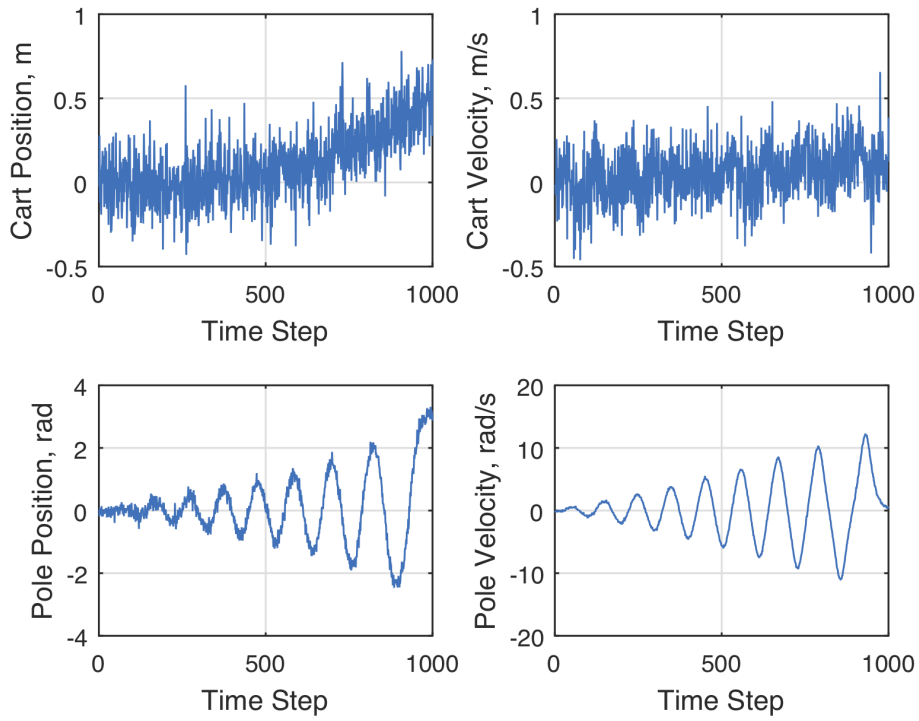

Figure 64: Trajectory of cart pole system with white noise corruption.

which arises from the estimated control. A good agreement is noted from these results, which suggest that the algorithm is capable of accurately estimating controls for nonlinear dynamical system.

In the implementation of the method, however, the requirement for multiple forward and backward recursions in the algorithm is computationally intensive. In its current form it is likely that the algorithm would require complete usage of a PED if used in a GA operational context, thereby limiting the efficacy of the methodology as a whole. Additionally the computations required limit the real-time applicability due to limitations of on-board computational power in a GA cockpit.

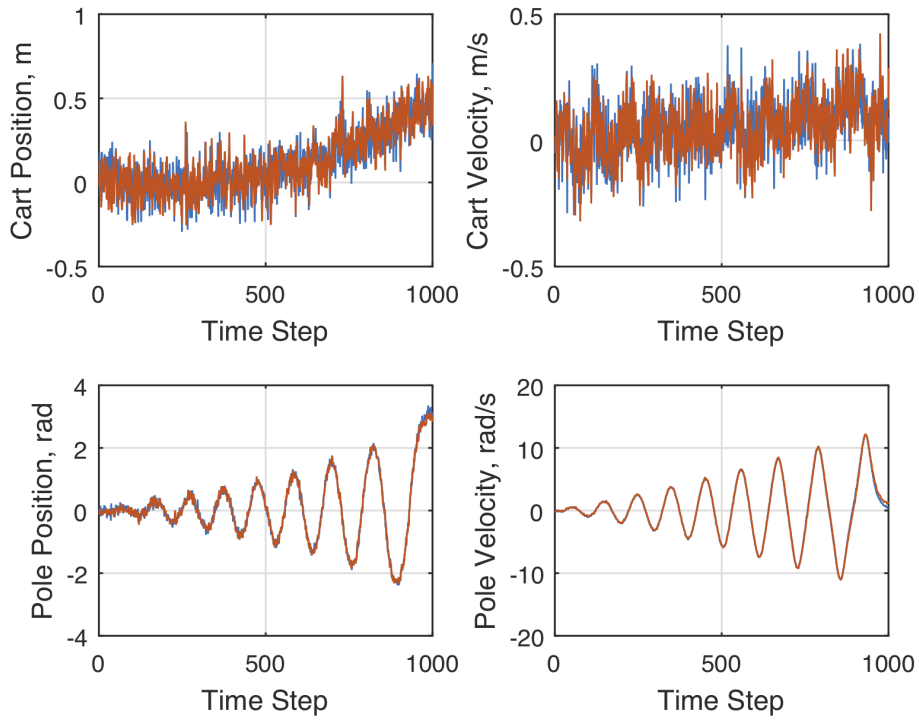

Figure 65: Comparison of true and estimated cart pole trajectory.

6.2 Estimation of Missing Aircraft States

The general task of full or partial state estimation from some observation is common across many fields, and as such has garnered a large body of relevant research. A full survey is beyond the scope of this effort, but an overview of the several prominent methods is provided by Simon [158]. In this overview, two key approaches are identified for state estimation, namely Kalman filtering and H_∞ filtering. In each approach the unobserved states of the aircraft are estimated using a combination of the observed system states, the dynamical model of the system, and some assumed noise distribution. In the case of Kalman filtering the noise for both controls and states is assumed to be standard white Gaussian noise whereas for H_∞ filtering the noise is assumed to be the worst-case noise. Along with the standard implementation of both filters for linear systems, Simon [158] presents variants of each algorithm intended to account for various changes in underlying assumptions, including non-linearity of the

system.

The progress in this field can be considered as largely mature, thus the methodology will not seek to generate a novel approach to state estimation. Instead, the various algorithms presented by Simon [158] and similar work within the literature may be considered as directly applicable to this work as required. In doing so, it is envisioned that little development is needed to develop an appropriate algorithm. Rather it is noted that the largely unresolved question with the application of these algorithms is the attainable level of accuracy of the outcome vehicle state.

In particular, it is noted that within the assumed set of available flight parameters provided by on-board PEDs only the ground speed of the vehicle may observed. The ground speed of the aircraft will match the airspeed of the aircraft only in the case of still air, leading to additional estimation error that may be anticipated in estimates of the vehicle's airspeed which rely upon the available ground speed. In light of this source of potential error a brief discussion on potential methods of estimating the wind speed, and thus the airspeed, from the available data will be provided.

6.2.1 Estimation of Wind Speed

In most aviation applications the wind speed experienced by an aircraft in flight is most often accomplished through comparison of airspeed measurements collected by Pitot tubes and inertial velocity (i.e. ground speed) measurements collected through inertial systems such as a GPS unit. This estimation is accomplished by leveraging the relationship between the total velocity (V_T), ground speed(V_G), and wind speed (V_W) known as the "velocity triangle". Namely these three velocities are related through vector addition as

$$V_T = V_G - V_W \tag{102}$$

Given the data constraints imposed for this work the standard means of wind estimation is hindered through the inaccessibility of the total velocity of the aircraft.

While this velocity is likely collected by installed instruments within the cockpit of the aircraft it is assumed that such data is not available within the MERLIN method. Therefore some alternative means of wind speed estimation, and by extension total velocity estimation, is required in order to account for the presence of wind during the flight.

Within the literature this problem of wind speed estimation in the absence of air data collection has been explored within two separate contexts outside of GA. In the implementation of advanced flight control systems on high-performance aircraft a heavy reliance on the full set of collected data emerges. The airspeed of the vehicle in particular is often quite important in such situations, as it is typically a key state in the implementation of feedback control systems or used for optimal gain scheduling [113]. There is concern, therefore, regarding the severe reduction in system capability which might occur in the event of air-data system failure which prevents access to this key data. In preparing for such eventualities techniques for "analytical redundancy" [150] have been developed which estimate the airspeed, and wind speed, using inertial data systems. A similar issue arises in the estimation of airspeed for Unmanned Aerial Vehicle (UAV) systems, which encounter the additional constraints of restricted capability for physical redundancy of air data systems due to weight limitations and limitations regarding on-board computational ability. From both of these fields two types of approaches have been suggested for the estimation of wind speed in the event that air-data is unavailable: model-based techniques and data-driven techniques.

In the use of model-based approaches knowledge regarding the system is leveraged alongside available data to estimate missing states. Such an approach is presented by McLaren [113] as an application of Dynamic Inversion techniques, which perform an inversion of the dynamic equations of motion, which are seen in Appendix C. For example, manipulation of the force relationship about the Z-axis in the wind-axis

frame, Equation (C.3), provides

$$V_T = -\left(\frac{g}{W q_W}\right)\left(T_{z_W} - L + W\cos\theta_W \cos\phi_W\right) \tag{103}$$

The application of this equation requires knowledge of the aircraft weight, thrust, and lift alongside estimates of the vehicle attitude. Further the aircraft lift is a function of pilot control, primarily the elevator deflection angle, implying that knowledge of pilot control action is required. From the development of the dynamic vehicle model provided in Chapter 4 it may be possible to predict this values, assuming that the required vehicle state data is accessible through either collection or separate estimation. Applied directly the use of this dynamic inversion method may be considered as a "perfect knowledge" like that presented by Fravolini et al. [62]. Alternatively a further process of parameter estimation may be performed which allows for the estimation of the unknown or uncertain vehicle parameters from collected flight data. Fravolini et al. [62] present a least-squares (LS) estimation approach which performs this task, but such an approach required access to a data set which includes the full set of parameters which was used offline to estimate vehicle parameters. In general parameter estimation methods are data-intensive [83] and assume access to the full set of flight states and controls in order to estimate the vehicle parameters.

Alongside the model-based methods a set of data-driven approaches are also present within the literature. McLaren [113] presents two related methods titled as the Three-Vector and Two-Vector approach which estimate the airspeed of the vehicle through repeated measurements of the vehicle's ground speed. In the Three-Vector method at least three measurements of the vehicle's ground speed are collected. By assuming that the true airspeed is held constant through pilot control and that the wind speed is also constant, then the true velocity is estimated through geometric relationship between the three ground speed vectors as the radius of the circle which touches the root of all three ground speeds following superposition of the three ground speeds such that their tips all intersect. An visualization of this process is given in

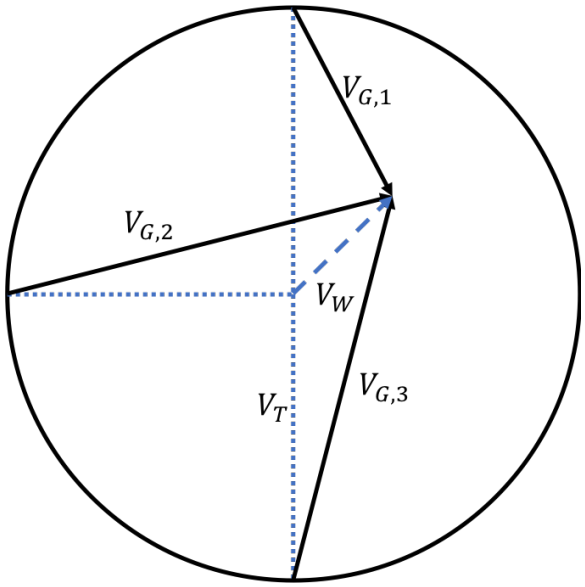

Figure 66: Representation of Three-Vector method of airspeed estimation, adapted from [113]

Figure 66. The Two-Vector approach a similar process is performed with the collection of two ground speed measurements alongside the collection of the true aircraft heading, which may be estimated using the inertial heading provided by the GPS and the vehicle attitude data provided by the AHRS. In both the Three-Vector and Two-Vector method McLaren [113] notes that additional samples may be taken in excess of the minimum required for each method and used in a least-squares estimation scheme to estimate the wind speed.

An additional data-driven approach presented by both McLaren [113] and Rhudy et al. [150] is the estimation of total velocity through Kalman filtering. McLaren presents an extended Kalman filter method which performs this estimation of wind speed using input true heading and ground speed data [113]. This approach however is envisioned for application in the aftermath of air-data system failure such that the initial estimate of the wind speed is assumed to be supplied by collected air-data. The nonlinear Kalman filter presented by Rhudy et al. [150] specifically avoid this complication, but do assume access to wind vane measurements of angle-of-attack

and sideslip angle in addition to inertial data.

Alongside the developments of the above model-based and data-driven methods of wind estimation various implementations available which provide some insight into the expected accuracy of such methods. In their work Fravolini et al. [62] utilized noisy velocity profiles collected from UAV flight simulations to test both perfect-knowledge and parameter-estimated forms of the model-based estimation method. Their data found that the perfect-knowledge approach yielded a total airspeed estimation error with mean of -1.49 m/s and standard deviation of 1.34 m/s while the parameter-estimation approach yielded a total airspeed estimation error with mean of -0.10 m/s and standard deviation of 1.53 m/s [62]. Similar results were observed by McLaren who utilized four T-38 pilot-in-the-loop simulations of a T-38 aircraft to test the dynamic inversion method of airspeed estimation, resulting in an average total airspeed estimation error of 3.99 m/s [113]. For this same data set McLaren additionally tested an extended Kalman filter approach which resulted in much better results, namely an average total airspeed estimation error of 0.51 m/s. This level of accuracy for the Kalman filtering approach is reflected Rhudy et al. who show that application of their nonlinear Kalman filter to a set of 16 flight data records resulted in total airspeed estimation error with a mean of 0.22 m/s and a standard deviation of 1.7 m/s. In additional experimentation McLaren additionally compares the performance of the Three-Vector, Two-Vector, and extended Kalman filter methods for the estimation of wind speed. This testing resulted in a mean wind speed error of 8.69 m/s for the Three-Vector method, 4.98 m/s for the Two-Vector method, and 0.038 m/s for the extended Kalman filter [113].

From the data presented by McLaren [113], Fravolini et al. [62], and Rhudy et al. [150] it is noted that in general both model-based and data-driven methods provide accurate estimates of total velocity and wind speed. Within each set, the data suggest that a method which utilized parameter estimation is preferable to a perfect

knowledge application, which is likely due to an advantage in estimating vehicle-specific characteristics. While more computationally intensive, an extended Kalman filter approach is suggested by the various data as the preferable data-driven approach. Between these two methods, namely a parameter-estimation driven model-based method and an extended Kalman filter method, experimental tests using actual UAV flight data provided by Fravolini et al. [63] suggest that the extended Kalman filter method provides more reliable and accurate estimates of wind speed.

In the developments of the extended Kalman filter [63, 113, 150] a key limitation is the reliance on data which is assumed to be unavailable within the GA context. Among the approaches the version of the extended Kalman filter presented by McLaren offers the least limiting case as it requires only some initial estimate of the wind speed. While no means of providing this estimate is considered to be available within the present context, future extensions may be envisioned which aid in overcoming this limitation. For instance, an initial estimate of wind speed may be collected from some external source and supplied to the wind estimation algorithm. This initial wind-speed estimate could be supplied by the pilot based upon air-data instrumentation within the cockpit, and may additionally be input by the pilot throughout the flight to aid in updating the experienced wind conditions. Alternatively several products available to GA operators have demonstrated the capability to query aviation weather data provided by National Weather Service. Thus some capability which automatically queries nearby weather reports, such as METAR data for the nearest airport to the vehicle based on its current GPS location, may be leveraged to provide an estimate of the expected wind condition.

6.3 Investigation and Testing of State and Control Estimation Methods

The second research question posed within this work examines the availability and accuracy of methods which allow for the observation of vehicle states and pilot control

actions for usage alongside the implemented LOC envelope. While several methods were introduced in §6.3 it was noted there that the down-selection process would be reliant upon the states and controls which constitute the implemented LOC envelope. Within the present demonstration and testing of the MERLIN method, the developed envelope is similar to the baseline depicted in Figure 39. This envelope was generated through simulation of the vehicle dynamics in numerous flight conditions, but is observed to consist in its final form of only three vehicle states: (1) vehicle velocity V, (2) vehicle bank angle ϕ, and (3) vehicle flight path angle γ. It is this subset of the vehicle states that then must be estimated in order to enable real-time monitoring of the vehicle's proximity to LOC conditions.

It is important to recall that for the given work it is assumed that the only sources of flight data available for data collection are those external devices which are brought into the cockpit by the pilot. These devices include some GPS enabled PED and an AHRS system, which together allow for the collection of the flight parameters listed in Table 19. Given these available data the required vehicle states may then be derived, and later investigation will ascertain the level of accuracy and impact on the usage of the LOC safe set.

Of the three required parameter the vehicle bank angle may be directly gathered from the AHRS unit, such that further analysis is required solely for the vehicle velocity and flight path angle. As the AHRS unit reports only the vehicle attitude the velocity of the vehicle must be collected through the data provided by the GPS. The horizontal component of the velocity, which corresponds to the vehicle velocity projected onto the $x - y$ plane of the vehicle-carried reference frame, is reported directly as the ground speed of the vehicle. To gather the total vehicle velocity then additional information must be collected, namely the velocity of the vehicle in the vertical plane which is also reported as the vertical speed of the vehicle. The total velocity then may be calculated simply as the vector sum of these two components.

An important caveat to this estimation of the vehicle velocity is that is based upon an approximately inertial measurement of the vehicle's position and derived velocity. Thus this velocity will suffer some loss of accuracy in the presence of non-zero atmospheric velocity i.e. wind. In the present analysis it is assumed that the atmosphere is still, so this source of error will not be included in the analysis of velocity error, though some discussion will be included in the next subsection on some potential methods of adapting the method to account for this source of error.

The flight path angle of the aircraft is defined as the angle between the velocity vector and the vertical component of the velocity, as expressed in the vehicle-carried reference frame. This relationship is expressed as

$$\gamma = \sin\left(\frac{V_v}{V}\right) \approx \frac{V_v}{V} \tag{104}$$

From this relationship it can be noted that the flight path angle can be approximated with information gathered from the GPS unit.

In addition, the flight path angle is related to the local angle of attack and the vehicle pitch angle as

$$\gamma = \theta - \alpha \tag{105}$$

As the pitch angle of the vehicle is reported by the AHRS system, then an additional opportunity arises to monitor the angle of attack of the vehicle. While this parameter is not explicitly included in the present LOC envelope this parameter may nevertheless provide some additional insight into the current state of the vehicle. Similarly, as both the heading and yaw angle of the vehicle are provided by the GPS and AHRS, respectively, then an approximation of the sideslip angle may be made using

$$\psi_W = \psi + \beta \tag{106}$$

As with angle of attack, the sideslip angle is not explicitly included in the LOC envelope but may be a useful parameter to monitor in addition to the LOC envelope states.

As the velocity, flight path angle, and bank angle can be either directly measured or analytically determined from the available flight data there is then little motive to pursue further means of state or control estimation. This further implies that the proposed experiments to ascertain the estimation accuracy and downstream impact on the LOC envelope monitoring may be streamlined. Rather than performing simulated flights which include the simulated state and control estimation techniques, the various data sources may be directly modeled and their typical error included in later simulation. In §6.3.1 an analysis of the two data sources, GPS and AHRS, will be presented and from this analysis the bounds of error for each observed state will be determined. Following this analysis the means by which this error may be accounted for is also analyzed and is presented in §6.3.2.

6.3.1 Experiment 2.1: State and Control Estimation Accuracy

The second research question evaluates the capability of the proposed methodology to accurately estimate the state of the aircraft and control actions of the pilot. Experiment 2.1 first examines the accuracy of the proposed estimation techniques as required by the developed LOC envelope as a means of testing Hypothesis 2.1. Throughout this work, it is assumed that the available flight data which may be collected is limited, presenting an obstacle to the testing of the estimation capability in the general case. It was envisioned that should some general set of flight states and controls be required the following experiment would allow for the testing of the various implemented estimation methods.

1. Perform simulated flight of GA aircraft in nominal conditions
2. Collect necessary states of aircraft alongside set of pilot actions
3. Generate assumed flight data from full simulated data set
4. Perform state and control estimation using limited data set

5. Compare true and estimated states

6. Iterate for desired atmospheric noise levels

This experimental setup leverages the vehicle simulation capability to act as both the truth model of the aircraft, which includes all of the aircraft states and controls. In simulation the number of available states and controls may then be artificially restricted to a set like that shown in Table 19. Any remaining states would then be estimated using an appropriate set of estimation techniques and the demonstrated accuracy of these methods used to generate the desired error bounds.

It was later determined however that the states included in the LOC envelope do not exceed the set of states assumed to be available within the GA cockpit. Thus the above experimental process may be streamlined to simply the direct quantification of the expected error for the observed states, as driven by the collection devices themselves. Additionally, as these error bounds are determined by the GPS and AHRS hardware rather than algorithmic estimation of the vehicle states then testing of these bounds through vehicle simulation is unwarranted. Instead an analysis of the expected GPS and AHRS errors is performed and the results are used in later states of experimentation.

The primary source of data that is collected for this effort is through some GPS connected PED. Such devices have become remarkably common in modern society, with basic GPS functionality often considered by many as a standard capability of mobile devices such as smartphones or tablet computers. Operation of the GPS system is conducted by the United States Department of Defense, who have maintained specified levels of performance for their end users since the service was initiated in 1993 [170]. This level of performance is regularly monitored and reported on by several other agencies, thereby helping to ensure consistently high levels of performance for the GPS system.

While data directly received through transponders only includes data regarding

the position of the receiver as reported by the GPS satellite array, there are well-established techniques for the accurate estimation of the velocity of the user. These techniques include direct differencing of the position data, or some relationship regarding the Doppler shift of the received signals. Greater accuracy has been attained however through time-differenced carrier phase (TDCP) approaches, which augment the velocity estimation through additional consideration of the carrier phase of the signal [134]. These methods of velocity estimation have become a commonplace feature of most GPS-equipped devices that the capability to accurately estimate the velocity of the receiver may be safely assumed.

Given this availability the accuracy of GPS-based velocity measurement is also included in the GPS specifications of performance, outlined with the GPS Standard Positioning System (SPS) Performance Standard report [170] for Signal in Space (SiS) operation. This report specifies that the accuracy of GPS measurements for Position, Velocity, and Time (PVT) estimates is the product of the User Range Rate Error (URRE) and the Dilution of Precision (DoP). The first factor, URRE, is a measure of the global average accuracy of the GPS system with regards to the rates reported to end users and is one of the primary metrics which is monitored to ensure the ongoing accuracy of the GPS system. The second factor additionally takes into account local factors which may further degrade GPS accuracy, such as full or partial blockage of the GPS signal or local atmospheric distortion.

The standard threshold for the global average of URRE is ≤ 0.006m/s at a 95% confidence, which must be attained for any three-second interval of nominal operation [170]. For the local DoP, an additional division may be made between horizontal dilution of precision (HDoP) and vertical dilution of precision (VDoP) which measure the various local factors which diminish the accuracy of horizontal velocity and vertical velocity measurements, respectively. Reported global average values of HDoP and VDoP within the same DoD report suggest a 90% probability of the HDoP value

being approximately 1.2 and similarly a 90% probability of a VDoP value of approximately 2.0. As these values are global averages it is also useful to note that this report additionally details the expected "worst-case" range for both of these values as approximately 1.4 for HDoP and 2.5 for VDoP, again with a 90% probability and assuming the full array of GPS satellites are available [170].

Considering this range of values for DoP in both the horizontal and vertical ranges then the expected local accuracy of the GPS velocity measurement may be estimated between 0.0072 m/s and 0.015 m/s for a given component (either horizontal or vertical) of the velocity with a confidence of 95%. For the typical operating velocities of the vehicle, between 40 and 75 m/s, this deviation is far less than 1% of the velocity. Nevertheless this information allows for the direct modeling of the error properties of typical GPS measurements. As a 95% confidence intervals are provided by the GPS data, it will be assumed in future stages of experimentation that the GPS velocity error is normally distributed with mean zero. The 95% confidence interval is known to be approximately 1.96 standard deviations from the mean, such that the standard deviation may be quickly defined once the 95% confidence interval is chosen. Given the data provided by the DoD, a value of 2.0 is selected from both HDoP and VDoP to represent a somewhat conservative estimate of the expected dilution. This selection yields a total error of less than or equal to 0.012 m/s at 95% confidence.

While this level of error is quite low it should be recalled that this level of accuracy accounts only for the uncertainty arising from the measurement of the vehicle's velocity. In this work it is assumed that the vehicle is operating in still air, but in a reality the atmosphere can be quite turbulent. This is especially true for smaller GA aircraft which are in general more susceptible to various atmospheric disturbances. The general approach taken to quantify the GPS measurement error herein, namely the estimation of the error based empirical observation and modeling, could additionally be extended to atmospheric variability as well.

Alongside the measurement of vehicle rates through GPS measurements the attitude of the vehicle can be gathered directly through the data supplied by an AHRS unit. While many GA aircraft produced recently are equipped with AHRS units, often integrated within larger avionics suites, legacy aircraft are less likely to include such installations. Recently however there has been an influx of portable AHRS units which provide the same attitude data without permanent installation on-board the aircraft. Some trade-off is made however in accuracy with such portable units, which tend to be smaller for portability and thus offer less processing power and do not have access to other aircraft instrumentation for additional calibration or computation.

A brief survey of commercially available AHRS devices is provided in Table 21 to provide some context to some existing AHRS devices currently on the market. These devices typically range in price from $250 to $1200, which while somewhat costly is also comparable with the current price for modern electronics such as smartphones or tablets. In addition, these devices all offer additional sensing or communication capabilities alongside the AHRS including ADS-B and GPS and typically allow for the transmission of the collected data to a visualization platform on a separate PED. As an additional aside the final two entries in Table 21 consist of "kit" units which offer a kit of parts which are assembled by the customer, allowing for a reduction in the overall cost while maintaining similar performance. Further the software of these kit units is often open-source such that an individual may create their own AHRS-equipped hardware and install the required software to operate it, potentially at a much lower cost that the

As with the GPS data it is known that some error will be present in the estimation of vehicle attitude. Unlike the data gathered from GPS units, however, this error is less well defined due to the decentralization of the the data. Instead this estimate may be drawn from data provided from various manufacturers for their units. Some representative data for four vehicle-mounted AHRS units produced by Inertial Labs

Table 21: Sample of commercially available AHRS-equipped devices.

Manufacturer	Product	Cost
Stratus [60]	Stratus 3	$699
Dual [47]	XGPS170D	$599
iLevil [103]	iLevil 3 SW	$1,195
iLevil [104]	iLevil Sport	$855
Stratux [164]	Stratux	$239
Open Flight Solutions [126]	Flight Box	$239.95

[84] is shown in Table 22. Surveys of other commercial units, both fixed and portable, reveals that this level of accuracy is typical of commercial AHRS units.

Table 22: Representative AHRS unit accuracy, provided by Inertial Labs [84].

Measurement	Value
Heading Accuracy	0.2 - 0.8 deg.
Pitch and Roll Accuracy	0.1 - 0.2 deg.
Gyroscope Bias	1 - 8 deg./hr
Accelerometer Bias	0.005 mg

For AHRS units which are constructed by the user rather than bought pre-assembled have also been shown to exhibit similar levels of accuracy. A survey of AHRS accuracy conducted by Cordero et al. [36] which focused on the effect of the algorithms driving the AHRS unit experimentally determined the root-mean-square (RMS) of error of the pitch and roll estimates to be between 0.43 and 0.78 deg. and have a standard deviations between 0.63 and 0.82 deg. with corresponding RMS error of heading measurements between 1.37 and 3.09 deg. with standard deviations between 0.97 and 1.48 deg. Additionally a study into the accuracy of low-cost AHRS units conducted by Gebre-Egziabher et al. [65] which found that errors of less than 0.2 deg. could be attained through algorithms which mitigate sensor bias through GPS calibration during operation.

These data suggest that the accuracy of AHRS units is fairly consistent across the various available products currently available. As such an assumed distribution of AHRS error may be defined which may be trusted as representative of the general

performance of existing AHRS units. Similar to the error model used with GPS collected data it will be assumed that the error is normally distributed. A mean error of zero deg. will be assumed along with a standard deviation of 0.5 deg., consistent with error estimates for pitch, roll, and heading measurements for various AHRS units. As with the GPS error distribution this AHRS data error distribution will be implemented in future demonstration of the system and the joint impact on the LOC estimation process will be considered in the following subsection.

6.3.2 Experiment 2.2: LOC Onset Prediction Accuracy

In Experiment 2.1 a method of assessing the accuracy of the estimation capability was presented, alongside more specific development corresponding to the expected error for GPS and AHRS data. To satisfy the uninvestigated portions of Research Question 2, namely the impact of state and control estimation on the LOC estimation process, an additional phase of experimentation was performed. The purpose of this experiment is to not only ascertain the impact of estimation error on the LOC estimation accuracy, but also glean insight into means by which this impact might be mitigated within the MERLIN methodology.

In accordance with the previous experiment a general experimental plan may be envisioned which allows for this assessment. Given some pre-defined LOC envelope and set of estimation methods, further simulation of the aircraft system may be performed which includes the proposed real-time monitoring of the vehicle flight state based upon estimation of required flight states. In this simulation both the true and estimated state is accessible, such that the estimation error may be readily computed for a given flight condition. Then two LOC predictions may be performed simultaneously: a "true" estimation which bypasses the state and control estimation process and evaluates the LOC boundaries based on the actual flight condition and an "test"

estimation which instead uses the generated state and control estimates. The impact then of the estimation error on the LOC estimation process can be ascertained through comparison of the two LOC onset predictions, and then repeated for various flight conditions. This process may be summarized as follows:

1. Perform simulated flight of GA aircraft in nominal and LOC conditions
2. Perform state and control estimation to estimate necessary states and controls using limited flight data set
3. Apply pre-defined LOC envelope to predict LOC onset with combination of collected and estimated flight data
4. Compare predicted and actual LOC onset
5. Repeat for various simulated flight conditions

Building upon the findings of previous work it is observed that while in general the state and control estimation error may be difficult to *a priori* define, the LOC envelope developed in §5.2 allowed for significant down-selection of the required estimation methods. Rather than requiring the implementation of some stochastic means of state or control estimation it was found that the states required by the LOC envelope consist of a set which may be directly observed from data assumed to be present on-board the aircraft. The expected error of these sources then may be estimated explicitly, a process which is presented in §6.3.1, resulting in *a priori* definitions of the estimation error. As such, the described process for the present experiment may once more be streamlined for this special case.

Rather than perform explicit simulation of the vehicle, LOC envelope, and estimation system a thought experiment is performed to gather insight into the impact of the defined estimation error on the LOC estimation process. Suppose an estimate of some vehicle state is performed such that the true value of the state is related to

the estimated value by some error, $\delta \in \mathbb{R}$. If we assume that the random distribution of the estimate error is known then for a given estimate we may construct upper and lower bounds about the estimate such that the true value may be assumed to be within the range of the upper and lower bound with some defined level of confidence. Taking the distance between the state estimate and the upper or lower bound as ϵ_u and ϵ_l, respectively, then the above statement may expressed as $\delta \leq \epsilon_u, \epsilon_l$. In particular assume that the error is normally distributed with mean μ and standard deviation σ^2. In this case then $\epsilon_u = \epsilon_l = \epsilon$ and therefore $\delta \leq \epsilon$.

Consider that this state is additionally defined such that it has some threshold which is monitored, and additionally consider that values below or equal to the threshold are acceptable and above the threshold are unacceptable. For any value of the true state then evaluated against this threshold will be either above, below, or equal to the given threshold. Thus if the estimate of the state is known then the likelihood of the true value of the state being above, below, or equal to the defined threshold may be assessed and the distance between the estimated state and the state threshold as $\tilde{\delta}$. With the assumed normal distribution of error, this distance $\tilde{\delta}$ allows for an assessment of the probability that the true value is in the acceptable region. Namely the probability that the error δ is less than or equal to the distance between the state estimate and the threshold, $P(\delta \leq \tilde{\delta})$, can be related directly to the standard normal distribution probability as

$$P\left(\delta \leq \tilde{\delta}\right) = P\left(\frac{\delta - \mu}{\sigma} \leq \frac{\tilde{\delta} - \mu}{\sigma}\right) = P\left(Z \leq z\right) \tag{107}$$

where Z is a random variable having a standard normal distribution of mean zero and standard deviation of one. The converse value may also be computed in this fashion, with $P\left(\delta > \tilde{\delta}\right) = 1 - P\left(\delta \leq \tilde{\delta}\right)$.

Consider then the possible relationship between the estimated state and the state threshold. First, if the estimated state is equal to the threshold then $\tilde{\delta} = 0$ and therefore the probability of true acceptable value of the state is $P\left(\delta \leq 0\right) = P\left(Z \leq \frac{-\mu}{\sigma}\right)$.

For error of mean zero this probability is 0.5, such that it is equally likely that the true value is acceptable or unacceptable. If the mean of error is some positive (or negative) value then this probability will be less than (or greater than) 0.5.

Consider then the second case for state estimates within the acceptable region, that is $\tilde{\delta} > 0$. From Equation (107) then the value of z will be positive for $\mu \leq 0$ and therefore the probability of the true value also in the acceptable region is greater than 0.5. If the mean of the error is positive then three sub-cases emerge:

$$\begin{cases} P(\delta \leq \tilde{\delta}) > 0.5 & \tilde{\delta} > \mu \\ P(\delta \leq \tilde{\delta}) = 0.5 & \tilde{\delta} = \mu \\ P(\delta \leq \tilde{\delta}) < 0.5 & \tilde{\delta} < \mu \end{cases} \tag{108}$$

Finally consider that the error estimate is above the state threshold, which is to say that $\tilde{\delta} < 0$. The probability of an acceptable true state is then given by Equation (107) for $z < 0$ if the mean of error is zero or positive, which suggests that the probability of acceptable values is less than 0.5. If the mean of the error is negative, then the inverse of the sub-cases for positive mean error emerge.

From this set of possible scenarios and their likelihoods we may further construct the likelihood that a given assessment regarding the acceptability of the true state is correct, given an estimate of the state and the state threshold. This assessment may be posed as probabilities of four constructed scenarios, which relate the probability that a correct or incorrect identification of the acceptability of the true value is made given some estimate of the state. In addition we now assume that the mean of the error distribution is zero, which implies that $P(\delta \leq \tilde{\delta}) = P(Z \leq \frac{\delta}{\sigma})$. If the estimated state is less than or equal to the threshold, then the probability of the true value being acceptable is $P(\delta \leq \tilde{\delta}) \geq 0.5$. By extension then the probability that the true value is not acceptable is $P(\delta > \tilde{\delta}) = 1 - P(\delta \leq \tilde{\delta}) \leq 0.5$. In these two cases, the probability of each is equal to 0.5 only when $\tilde{\delta} = 0$. When the estimated state is greater than

the threshold then the probabilities are flipped, that is $P(\delta \leq \tilde{\delta}) < 0.5$ and $P(\delta > \tilde{\delta}) = 1 - P(\delta \leq \tilde{\delta}) > 0.5$. These four general scenarios are summarized in Table 23. Of these situations, the case of most concern is the case for which the estimate is acceptable while the true case is unacceptable. This situation indicates the possibility of a scenario in which the LOC envelope does not indicate an unsafe condition even though an unsafe condition has been encountered. The converse situation, when a true value that is acceptable is paired with an unacceptable estimate, is a "cry-wolf" scenario which does not pose serious immediate threat but may cause alarm fatigue to users if the occurrence of such events is too frequent.

Table 23: Summary of state assessment probabilities given state estimates and threshold.

	Estimate Acceptable	**Estimate Unacceptable**
True Acceptable	$P(\delta \leq \tilde{\delta}) \geq 0.5$	$P(\delta \leq \tilde{\delta}) < 0.5$
True Unacceptable	$P(\delta > \tilde{\delta}) \leq 0.5$	$P(\delta > \tilde{\delta}) > 0.5$

Given the cases summarized in Table 23, one insight gleaned is that the major transition in the probability of a correct prediction of true state acceptability occurs near the threshold. For example, when $\tilde{\delta} = \sigma$ then the probability of $P(\delta \leq \tilde{\delta}) \approx 0.84$ and further increases to $P(\delta \leq \tilde{\delta}) = 0.90$ for $\tilde{\delta} \approx 1.28\sigma$. For the error distribution assumed for the AHRS, this indicates that the probability that the true value of some attitude value is acceptable relative to its threshold is greater than 90% if the distance between the estimate of the state is at least 1.28 deg. away from the threshold. As such we may observe that in most of the vehicle's operating range the probability of false-positives, that is the chance that the estimated state is acceptable when the true is unacceptable, is quite low. While this probability increases nearer to the boundary, the low magnitude of the error distribution deviations suggests that these larger probabilities are quite near to the threshold values. From this then one may reason that the influence of the estimation error on the final distribution is negligible within the interior of the envelope but should be accounted for at the threshold

Table 24: Sample of false-positive probabilities for given ratios of $\frac{\tilde{\delta}}{\sigma}$.

$\frac{\tilde{\delta}}{\sigma}$ **Ratio**	$P(\delta > \tilde{\delta})$
0	0.5
0.39	0.35
0.67	0.25
0.84	0.20
1.00	0.16
1.03	0.15
1.28	0.10
1.64	0.05

boundary.

Further, a direct condition is seen which relates the magnitude of the error to increased probability of false-positive scenarios. Given the assumption of an underlying normal distribution of error with mean zero then the probability of any condition occurring may be gathered as a function of the ratio $\frac{\tilde{\delta}}{\sigma}$. A sample of such values for the false-positive scenario is shown in Table 24. This ratio may be thought of from two perspectives. First if the standard deviation is known then this ratio provides the probability of false-positive estimates as a function of the distance between the estimated state and the threshold. Secondly for a set threshold distance this ratio describes the variation of this probability with shifting standard deviation, with increasing probability for increasing standard deviation.

Beyond the quantification of the impact of the estimation error on the LOC estimation, this insight additionally presents some guidance towards effective strategies for mitigating this impact. In Experiment 1.1 and 1.3 presented in §5.2.1 and §5.2.3, the variance of the LOC safe set with shifting state and control thresholds was observed. In the later portion of Experiment 1.3, observations were made that this shift was capable of accounting for adverse expansion of the LOC envelope due to model error, such that the final LOC safe set's normalized volume may be brought closer to unity. It is additionally feasible to use this approach to not merely bring the

safe set volume to a value near unity but to some other arbitrary value which is less than unity. Such an adjustment may be used to account for other sources of error or uncertainty that may be encountered in the usage of the LOC envelope within the larger LOC mitigation method, namely the estimation error which is assumed to be present within the MERLIN methodology.

In doing so, consider that the error for a given state or control action that is estimated is bounded. This bound could be either a firm threshold, such as some physical bounding, or the threshold for a given level of confidence. To account for the level of error then the corresponding state threshold should be adjusted conservatively by a similar magnitude, creating a "buffer" threshold. This specification is visualized in Figure 67. With a known bounds for the error for a given state (ϵ), then the estimate of that state may be considered as a small neighborhood of possible values around the true value of the state, within which the reported value will likely reside. If the distance between the threshold buffer and the true state buffer (τ) is less than the state error then it is possible that a given state may exceed the given state threshold even while no infraction is indicated. Thus a simple constraint can be defined for this buffer distance as

$$\tau \geq \epsilon \tag{109}$$

In general the relationship between this buffer distance τ and the final safe set volume is difficult to define, as the present instantiation of the methodology has expressed the safe set with a different set of states than those used in generating the LOC envelope (i.e. the GA QLC states). If a some other envelope form is generated, however, then it may be feasible to directly generate a relationship between this constrained buffer distance and the output safe set volume. At present however the definition of the buffer distance and the application of the threshold adjustment in this series of experiments are analogous in that each perform direct manipulation of some state threshold. It is proposed then that one means of determining the

appropriate level of threshold adjustment be tied directly to the constrained buffer distance, such that the minimum level of the threshold required to account for state and control estimation error be equivalent to the maximum expected error of the state and control estimate.

From this development and the results of Experiment 1.3 the general process for selecting the appropriate level of threshold adjustment may be re-formulated as follows to account for both the adverse model error and estimate error:

1. Determine error bound for state and control estimate
2. Determine magnitude of model error
3. Calculate threshold adjustment required for threshold estimation buffer: $K_{T,1} = \max(\epsilon_j)$ for j observed states and controls
4. Estimate threshold adjustment for model error contraction $K_{T,2} = f(\epsilon_{model})$
5. Select threshold adjustment as $K_T = \min(K_{T,1}, K_{T,2})$

Note that in the present process the minimum value of the threshold adjustment is suggested as it is assumed that the value of the threshold adjustment is less than unity, corresponding to values which generate more conservative estimates of the LOC envelope.

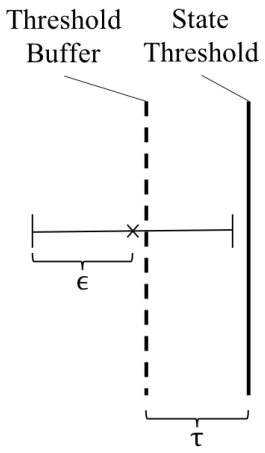

Figure 67: Depiction of threshold buffer to account for state or control estimation error.

6.3.3 Summary of State and Control Estimation Results

The second research question and its associated sub-questions examines the state and control estimation capability within the MERLIN methodology. Once an LOC envelope is implemented the necessary state and controls for monitoring this envelope are known, at which time the required state and control techniques may then be selected. For the LOC envelope developed and tested in the study of Research Question 1 the necessary states are the vehicle velocity, flight path angle, and bank angle. These states are such that no additional state estimation is required, as each state may be directly gathered from available flight data provided by a GPS and AHRS system.

As such the subject of Research Questions 2.1 and 2.2 were refined somewhat to reflect the quantification and subsequent impact of this observation process within the MERLIN framework. These research questions are associated with the state and control estimation process in the manner shown in Figure 68. Research Question 2.1 first examines the methods by which the required states and controls may be gathered and the associated accuracy of these estimations. Following this, Research Question 2.2 studies the effect of the estimation error within the MERLIN methodology, in particular how the error in the state and control estimate may be expected to affect

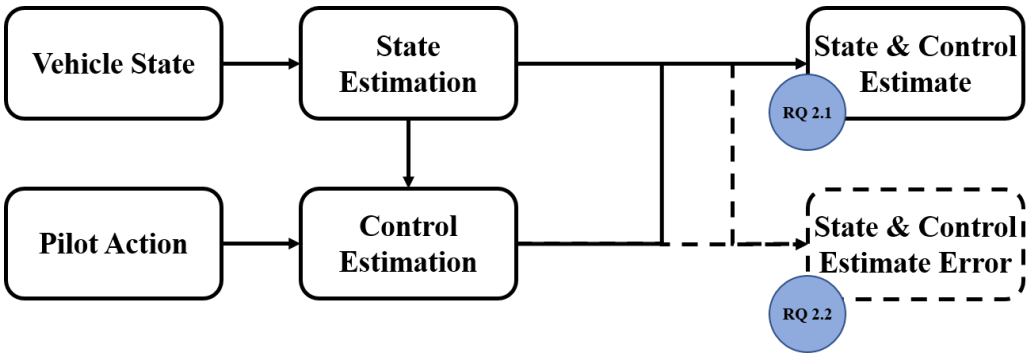

Figure 68: Summary of examined state and control estimation method components with applicable research questions.

the LOC monitoring capability.

The process of Experiment 2.1 was proposed as a means of testing the hypothesis of Research Question 2.1. Due to the direct estimation of the required states allowed by the generated LOC envelope, however, this process was streamlined to include a direct analysis of the expected error distribution for each source of assumed flight data. The vehicle velocity and flight path angle were shown to be available through location and rate data provided by a GPS unit, whose accuracy may be estimated through relationships provided by the US DoD. These relationships were found to result in an error distribution for velocity measurements which was normally distributed with a mean of zero and a standard deviation defined by a 95% confidence interval of 0.012 m/s. An additional survey of typical portable AHRS units used for GA fixed-wing aircraft provided more insight into the expected performance of such devices. This study resulted in an error distribution on the pitch, roll, and yaw angles provided by the AHRS unit which is normally distributed with a mean of zero and a standard deviation of 0.5 deg. As it is shown that the required aircraft states may not only be estimated but also furnished with accuracy expectations, Hypothesis 2.1 may be conditionally confirmed. The caveat of this confirmation is that as the developed LOC envelope required such a simple set of states, it may be reasoned that some other LOC envelope may require a broader set of states which may be more difficult to estimate

with the given tool-set. Nevertheless for the given LOC envelope it is observed that the required states can be accurately estimated, in which case the Hypothesis 2.1 is confirmed.

The following experiment, Experiment 2.2, examined the effect of the estimation error on the LOC monitoring task. As the vehicle's proximity to LOC condition is monitored using a defined LOC envelope, the effect of the estimation error on the use of such an envelope was explored. As with Experiment 2.1 a general process for performing this study was first developed, but due to the special nature of the particular estimation task at hand a more streamlined version was performed. Through a thought experiment which analyzed the probability with which the true vehicle state satisfies a particular envelope was explored, assuming only that an estimate of the state and its proximity to the threshold is available. Application of this approach to the expected error distributions of the GPS and AHRS systems revealed that the estimation error has the most impact on the accuracy of the LOC condition identification in a small region near the state threshold. Thus it is seen that the LOC identification is largely unaffected while the vehicle is well into the interior of the envelope, as the likelihood of false-positive identification is quite low, and the trends of the increase in likelihood can be quantified in terms of the ratio between the distance to the envelope boundary and the standard deviation of the error. This relationship is tabulated within Table 24. From this relationship and the exhibited error behavior a method of accounting for this error within the LOC envelope estimation process is also presented, which utilizes a reduction in the state and control thresholds in the same manner used to account for the estimated model error. These findings are evidence that given some assumption of estimation error the propagated impact on the LOC prediction process can be quantified and subsequently accounted for. Therefore Hypothesis 2.2 is considered to be confirmed.

In these results it is assumed that the vehicle is operating in still atmosphere,

such that the ground speed and airspeed of the aircraft are equivalent. Should this assumption be relaxed then additional error would be anticipated due to the mismatch between the vehicle's ground speed and airspeed. Assuming that some technique for estimating the airspeed is utilized, such as one of the approaches given in §6.2.1, then an additional distribution of error may be incorporated alongside the GPS and AHRS unit error. This error may be similarly propagated forward to the LOC proximity evaluation, and it may be noted that in this case then the process for developing appropriate threshold buffers may still be employed and would be expected in general to produce more conservative estimates of the state thresholds.

CHAPTER VII

RECOVERY STRATEGY GENERATION

The final piece of the MERLIN methodology is the generation and application of a strategy for LOC recovery. This portion of the methodology is associated with the third research question:

Research Question 3:

What is an appropriate strategy for LOC avoidance or recovery and how can this strategy be leveraged to synthesize real-time recommendations for a GA pilot?

In Chapter 2, several methods for creating LOC recovery strategies were presented and a summary of some of the most common methods from the literature was provided in Figure 11. Given the constraints associated with GA aircraft, it was noted that the direct application of the strategies is difficult, given the need to provide a recommended strategy to a pilot without the assistance of automated flight control. As such the following development will address both the synthesis and later communication of a simplified recovery strategy.

7.1 Synthesis of Simplified Recovery Strategy

The creation of an appropriate strategy for LOC avoidance or recovery is expressed in Research Question 3.1. In Table 3 and Table 4, the recommended recovery strategies for both stall and spins as provided by the FAA are provided. For both of these strategies, it is noted that the strategy has been divided into a series of steps which consist of simple and direct application of a single control. This advisement by the FAA is corroborated by recent work by Stepanyan et al. [163], who suggest a system

simple cues which are provided to the pilot in order to mitigate or recover from LOC conditions. These notions of simplified strategies consisting of some combination of discrete control actions serves as the foundation for Hypothesis 3.1. In the present methodology, a set of "control archetypes" is defined. These archetypes consist of the application of each degree of control at appropriate upper, lower, and neutral settings, as summarized in Table 25. In selecting these archetypes, it is noted that the archetypes in Table 25 consist of general directional settings of each control. This restriction is seen to coincide with the general recommendations for stall and spin recovery by the FAA, and qualitatively with many of the control strategies generated within the literature. It is reasoned that in the event of a some upset condition, the emphasis of the strategy is the expedient recovery of the vehicle such that the vehicle returns to a safe operating condition as quickly as possible while avoiding over correcting. Given this, it is reasonable to assert that application of controls is made such that as much effect is gained in as short a time as is reasonable through brisk application of the controls while moderated in degree by the response of the aircraft.

Table 25: Set of control action archetypes.

	Control	**Setting**
1	Throttle	MAX
2	Throttle	IDLE
3	Throttle	NEUTRAL
4	Aileron	LEFT
5	Aileron	RIGHT
6	Aileron	NEUTRAL
7	Elevator	AFT
8	Elevator	FORWARD
9	Elevator	NEUTRAL
10	Rudder	LEFT
11	Rudder	RIGHT
12	Rudder	NEUTRAL

Hypothesis 3.1 states that from the set of control archetypes given in Table 25 one may generate a control strategy which provides a recovery trajectory from an

impending LOC event. Further it is asserted that using this set of archetypes any given control strategy can be expressed. For example the spin recovery strategy in Table 4 can be constructed as the sequence $3 \rightarrow 6 \rightarrow 10/11 \rightarrow 8 \rightarrow 12$ followed by a return to level flight. Similarly, other recovery strategies can be approximated using an appropriate sequence of archetypes.

To gather guidance in synthesizing appropriate mitigation strategies further study was performed of the various upset recovery algorithms present within the literature. For each studied upset recovery algorithm the demonstrated recovery strategies were analyzed and mapped using a sequence of control archetypes. A summary of these sequences is provided in Table 26 and Table 27 which separate the various recovery strategy methods into stall and spin recovery, respectively. In each of the sequences, the symbol "$\rightarrow$" is utilized to indicate a temporal transition from one phase of the recovery to the next, a transition which typically occurs relatively quickly. Additionally the symbol "+" indicates a combination of control actions which occur simultaneously within a given phase while two archetypes separated by the "/" symbol indicates a state-dependent selection between directional control actions. For example, in the FAA spin recovery technique sequence provided in Table 27 the first phase is 10/11, indicating that the appropriate rudder deflection is dictated by the direction of the impending spin to be corrected.

Two additional methods considered in this effort that do not neatly fall into either category are the methods presented by Garcia et al. [64] and Zhang and Chen [178]. The receding horizon control strategy developed by Garcia et al. was applied to two upset cases, first a high bank angle scenario and second a high bank angle paired with very low pitch angle. For the first recovery scenario the method of Garcia et al. maps to the sequence $8 + 4/5 \rightarrow 9 + 6$ while the second sequence is $7 + 4/5 \rightarrow 9 + 6$ [64]. The upset condition studied by Zhang and Chen reflects a stall condition with the addition consideration of high sideslip angle. Recovery from this condition was

Table 26: Stall recovery strategies mapped to archetype sequences.

Author	Generation Method	Archetype Sequence
FAA [54]	Stall Recovery Template	$8 \rightarrow 6 \rightarrow 3 \rightarrow 9$
Dongmo [42]	Feedback Linearization and High Order Sliding Mode	$8 \rightarrow 3 \rightarrow 9$
Dongmo [41]	Nonlinear Smooth Feedback Regulator	$8 \rightarrow 3 \rightarrow 9$
Dongmo [45]	Hybrid	$8 \rightarrow 9$
Dongmo [43]	Nonlinear Smooth Trackers	$8 \rightarrow 3 \rightarrow 9$
Dongmo [44]	Nonlinear Smooth Feedback Regulators	$8 \rightarrow 3 \rightarrow 9$
Lombaerts et al. [105]	Energy-Based Control	$8 \rightarrow 6 \rightarrow 3 \rightarrow 9$
Richards et al. [151]	Constrained Nonlinear Optimal	$8 \rightarrow 6 \rightarrow 3 \rightarrow 9$
Schuet et al. [152]	Model Predictive Control	$8 \rightarrow 4/5 \rightarrow 3 \rightarrow 9$

Table 27: Spin recovery strategies mapped to archetype sequences.

Author	Generation Method	Archetype Sequence
FAA [54]	Spin Recovery Template	$2 \rightarrow 6 \rightarrow 10/11 \rightarrow 8 \rightarrow 12$
Lee and Nagati [102]	Optimal Control	$10/11 \rightarrow 9 \rightarrow 5/4$
Martin and Hill [107]	Direct Allocation	$10/11$
Raghavendra [146]	Nonlinear Dynamic Inversion	$10/11 \rightarrow 8 \rightarrow 5/4$
Rao and Sinha [148]	Sliding-Mode Control	$10/11 + 5/4 \rightarrow 8$

achieved through the sequence $8 + 4/5 \rightarrow 3 \rightarrow 2 + 6 + 9$.

The key observation drawn from the data presented in Table 26 and Table 27 is the general convergence of the various control strategies to the guidance provided by the FAA for both stall and spin recovery [54]. Consideration of the underlying physics of aircraft recovery aids in accounting for this finding. In a given upset condition, there is often a small number of flight states which are deemed to be unacceptable. For stall these states are primarily the angle of attack whereas in spin conditions the states of concern are the yaw rate, r. Correction of these unsatisfactory states may also be mapped to a specific control state e.g. negative elevator deflection in order to quickly reduce the pitch angle and by extension the angle of attack. This direct mapping between the given unsatisfactory state and the control action which corrects it thus yields a similarity between various methods which seek to provide recovery

strategies for similar upset conditions.

Some addition insight may also be gleaned by comparing and contrasting the various phases present in the sequences for each upset condition. For stall recovery sequences, the initial recovery action is a forward elevator command which initiates a pitch down maneuver. In the FAA's recommended recovery strategy particular care is given to specify that the aircraft should remain wings-level, indicated as the "Aileron NEUTRAL" archetype. Several of the strategies which neglect this phase do so implicitly, as the recovery strategy is presented as a purely longitudinal maneuver such that lateral states are presumed to remain at equilibrium. The remaining strategies explicitly include aileron action in the second phase of the recovery. In particular, the methods of Schuet et al. [152] and Zhang and Cheng [179] include explicit wing-leveling maneuvers for reducing the roll angle during the stall recovery. In the final phases of the recovery thrust commands are often utilized to aid in regulating the aircraft's velocity following by a return to stable flight condition by returning the elevator to a neutral position.

Taken together a general sequence that incorporates these various considerations for stall recovery may be constructed as: $8 \rightarrow 4/5/6 \rightarrow 3 \rightarrow 9$. This sequence emphasizes immediate corrective elevator action to reduce the angle of attack. Then an appropriate aileron command is issued to either attain or maintain wings-level condition. The final two phases then utilize the thrust and subsequent elevator commands to stabilize the aircraft and facilitate a return to a nominal flight condition.

Comparison of the spin recovery strategies reveals a consistent deviation from the recommended FAA spin recovery procedure, namely the absence of the initial reduction of the thrust to idle and neutralizing of the aileron deflection. Instead the strategies from literature utilize an initial rudder deflection to counteract the aircraft spin, presumably while maintaining a constant throttle setting. In two strategies this rudder deflection is followed by elevator action, one to maintain neutral pitch and

the other to cause a nose down pitching moment. These two strategies additionally specify the application of ailerons in the opposite direction of the rudder deflection following the elevator command, whereas this aileron action is specified as coincident with the rudder action in the strategy developed by Rao and Sinha [148].

Consolidation of these observations into a general outline is less straightforward as compared to the stall recovery sequences due to the more notable differences in the various strategies. While the initial sequences of the FAA spin recovery strategy are neglected in other strategies within the literature, this absence may be due to simplifications in the analyses performed by the various authors. Additionally, the FAA notes that these two steps are included in order to improve the characteristics of the impending spin should it fully develop. It is noted that increased propulsive power may induce a higher spin rotational rate, while improper aileron usage may delay spin recover or prevent recovery altogether [54]. Therefore these two steps, while not directly improving the aircraft condition, enable improve recovery characteristics in later steps and are reasonable to include at the outset of the recovery sequence. Later phases of the recovery sequence are then much more consistent, consisting of full opposite rudder deflection with a subsequent pitch down elevator input. The sequence then ends with a neutralizing these surfaces in order to return to nominal flight. This general recovery sequence is then identical to the FAA spin recovery template sequence: $2 \rightarrow 6 \rightarrow 10/11 \rightarrow 8 \rightarrow 12$.

The strategies developed by Garcia et al. [64] present a third class of sequence which is made distinct from the others examined largely due to the uniqueness of the examined upset condition. In each case studied by Garcia et al. the high bank angle condition is immediately addressed within the recovery strategy by opposite direction aileron commands. Simultaneously to the aileron command is a command for either forward or aft elevator. In particular it is observed that in the case when the pitch angle is nominal a pitch down command is given. With this command given, the

sequence then reflects a the FAA guidance for stall recovery with the order of the first and second commands reversed. The second case which includes an initial low pitch angle includes an aft elevator command instead, consistent with the general strategy of correcting undesirable flight conditions.

Consideration of the three above classes of control sequences together allows for the generation of an algorithm which will synthesize a mitigation strategy for an impending upset condition. The initial decision point of the algorithm is the determination of whether the upset condition involves primarily some unusual pitch attitude or unusual yaw attitude. In the case of pitch, then either the stall avoidance sequence or the similar variant observed from the work of Garcia et al. [64] should be utilized. Otherwise a spin avoidance strategy would be the appropriate strategy to recommend. In either case it can be observed that the sequence of control actions is to first improve secondary aircraft conditions, such as bank angle and propulsive power, if deemed prudent followed by direct corrective control action. This corrective action is then aided by subsequent actions which maintain favorable aircraft conditions during the recovery.

Algorithm 1 LOC Mitigation Sequence

if Unusual Yaw Attitude **then**
    Cmd. 2
    Cmd. 6
    Cmd. 10/11 ▷ Rudder command in corrective direction
    Cmd. 8
    Cmd. 12
else if Unusual Pitch Attitude **then**
    Cmd 7/8 ▷ Elevator command in corrective direction
    Cmd 4/5/6 ▷ Aileron command to wings level
    Cmd 3
    Cmd 9
end if

In addition to the particular recovery sequence it is prudent to determine the starting and stopping criteria for the full recovery strategy. These questions were

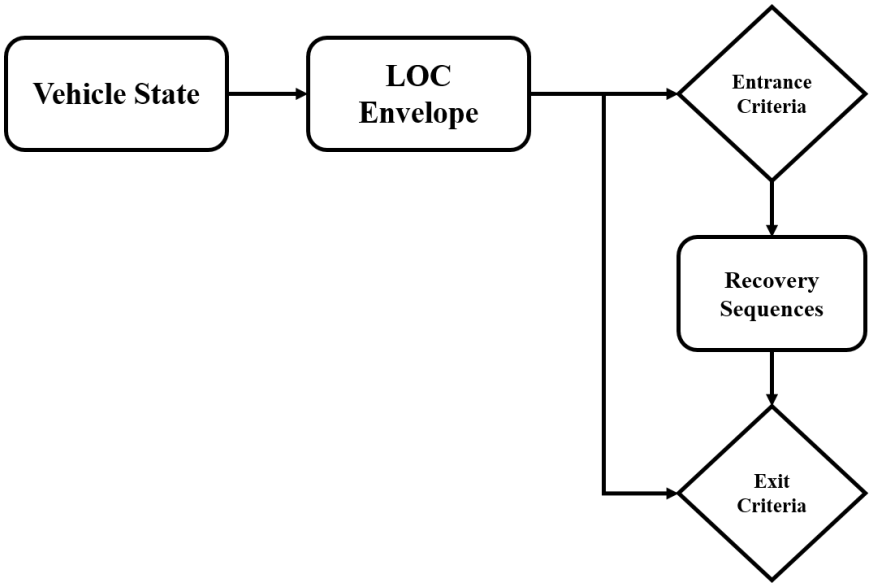

Figure 69: Summary of recovery strategy process.

addressed by Lombaerts et al. [105] in developing their stall recovery strategy. Lombaerts et al. initiated their algorithm based on proximity to the stall condition as monitored through an angle of attack threshold and exited the algorithm once a target flight condition was deemed to be have been attained. This threshold-based entrance criteria is a subset of an envelope evaluation criteria, that is to say initiation of the recovery strategy upon violation of a pre-specified envelope. Such an entrance criteria is well-suited for the current effort which intends to perform LOC mitigation in part with a pre-defined flight envelope. Similarly the exit criteria utilized Lombaerts et al. is straightforward and indicative of a logical transition point out of the recovery strategy and back to regular flight. It is noted that in application is likely that convergence to this exit condition may take some time. In this case then it will be assumed that the algorithm will continue to monitor the condition of the aircraft and provide recommendations which aid in the stabilization of the vehicle to the desired safe state. With these conditions then a general overview of the steps which are taken for application of a recovery strategy alongside LOC envelope monitoring is shown in Figure 69.

In application of this process of LOC mitigation it is noted that two scenarios emerge. Through the definition of the given entrance criteria, which is tied to the boundaries of the LOC envelope, the initial intent of the LOC mitigation sequences is to prevent the aircraft from exiting the performance envelope, thereby avoid upset conditions and by extension LOC. In this sense then the mitigation sequences act as a means of envelope restriction, attempting to aid the pilot in restricting the aircraft to remain within the normal operating envelope. It is noted then that in this scenario, namely in the initial case of envelope restriction and LOC mitigation, some deviation from the standard recovery techniques may occur in pursuit of the general objective of envelope restriction. Should the mitigation actions recommended to pilot prove ineffective, however, such that an upset condition occurs then the control actions recommended by the algorithm should align completely with the standard recovery techniques. In this second scenario then the LOC recovery sequence capability is thus restricted to only suggest the standard stall or spin recovery sequence, as these sequences are well known to provide recovery from fully developed upset conditions.

In general the boundary between these two scenarios, namely the pre-upset region and the upset region, is somewhat difficult to define. One approach which may be envisioned leverages some characteristics of the defined LOC envelopes provided in Chapter 5. The defined LOC envelope consists of two components, the set of defined state thresholds and the corresponding safe set. For the present LOC mitigation method the primary focus is on the latter portion of the envelope, that is the boundaries of the safe set are those which are leveraged in the definition of the entrance criteria. A second "entrance criteria" may additionally be defined which indicates the transition from the pre-upset LOC mitigation scenario and the developed upset LOC recovery scenario. It is proposed then that the trigger for this transition, which will be referred to as the "transition criteria", be defined as the violation of the outer set of state thresholds which constitute the normal flight envelope.

7.2 Communication of Simplified Recovery Strategy

Alongside the generation of an appropriate mitigation strategy, the proposed methodology must also address the communication of this strategy to the pilot. This requirement is a direct result of the assumed limitations posed by implementation on GA aircraft i.e. the lack of automated flight control systems. The final research question is posed to address this need for communication:

Research Question 3.2:

How can a specific set of control actions be efficiently communicated to a pilot during LOC conditions?

In consideration of the means by which information may be communicated to a human pilot, three avenues present reasonable alternatives: auditory cues, visual cues, and tactile cues. For each category there exist some historical which yields insight into the efficacy and limitations of each method.

Tactile feedback systems are already commonplace on many transport category aircraft. The most common example is the stick-shaker, which causes the control yoke to vibrate as the aircraft nears stall conditions. This behavior mimics the vibratory phenomena which naturally occurs on simple control systems, like those on most GA aircraft, where the control surfaces begin to vibrate as the air becomes more turbulent in stall thereby causing a direct motion of the yoke though their physical connection. In modern fly-by-wire control systems, this physical connection is no longer present but the behavior is still mimicked to provide a recognizable tactile feedback to the pilot. While the implementation of stick-shakers or other modifications to the vehicle are assumed to be infeasible for this work, other options are available such as vibratory wrist-bands [159] or some other device which is separate from the vehicle. The use of tactile feedback has been observed to complement other forms of feedback, allowing

for faster recognition of some specified condition when paired with visual cues while not interfering with the ability to detect visual stimuli [159]. Some concern is noted however with the use of tactile feedback during active motion, such vibration felt through the hands during active manipulation of the control yoke as it has been observed that while some part of the body is being actively used it is less sensitive to tactile stimuli [35]. This decreased sensitivity suggests that the use of tactile feedback in LOC situations would be less effective, where the pilot is likely to be engaging their arms and feet in manipulation of the aircraft controls. In addition GA aircraft are known to be somewhat "bumpy" in normal flight and more so during upset conditions, presenting a situation in which tactile cues may be "washed out" by the operating environment.

Visual representation is likely the most common means of information transfer present within aviation. In Figure 70 a pilot's view of the cockpit of a typical GA aircraft, the Cessna 172, is provided. In this view, numerous dials and displays are clearly present, each presenting some visual representation of aircraft data which is pertinent for safe operation of the aircraft. By comparison to more complex and modern aircraft cockpits such as the the Boeing 787 Dreamliner, shown in Figure 71, a clear preference for visual presentation of information in all types of aviation systems is suggested. In terms of LOC mitigation, visual communication of information also has a strong presence. Many authors within the literature have proposed various display concepts which seek to present a set of pertinent information to the pilot in the hopes of either mitigating unsafe condition or aiding in the recovery from them. Some examples of such concepts include the work by Amelink et al. [8], Glaab et al. [70], and Stepanyan et al. [163]. In general these concepts often represent a system which would serve as consolidation of much of the information already present within the cockpit's visual field through integration as a "glass cockpit", rather than an additional source of visual information. For the current methodology, however, a

direct replacement of the existing cockpit systems cannot be performed, so any visual cues must be designed alongside existing visual information. This limitation presents additional concerns related to the saturation of the pilot's attention, that is to say that for a given amount of time a human may only view and process a limited amount of information. Given the amount of visual information already present within the cockpit, it must be considered that additional cues may either be ignored or consumed at the detriment of some existing visual source due to information overload.

Figure 70: View of the Cessna 172 cockpit.

Figure 71: View of the Boeing 787 Dreamliner cockpit.

The final method of communication to be considered is auditory. As with tactile and visual cues, there is already some precedent for auditory cuing in the aviation system. Many monitoring systems such as angle of attack indicators provide some auditory cues, such as simple beeps or chimes, to indicate the imminent violation of some threshold or boundary. These aural cues are often paired with simple visual cues such as blinking lights [163]. More sophisticated systems have also been implemented in the aviation system, particularly for transport aircraft. One example is the Traffic Alert and Collision Avoidance System (TCAS II), which provides aural cues to pilots in the event of impending aircraft proximity. These aural cues are provided as Traffic Advisories (TA) or Resolution Advisories (RA), and pilots are instructed that RA provided by the TCAS II take precedence over other instructions. As shown in Table 28, this system is capable of providing a number of aural cues to pilots which consist of short phrases to indicate desired courses of actions.

Table 28: Set of TCAS II aural cues, adapted from [51].

Type of Advisory	Annunciation
TA	"Traffic, Traffic"
RA	"Climb, Climb"
RA	"Descend, Descend"
RA	"Climb, Crossing Climb; Climb, Crossing Climb"
RA	"Descend, Crossing Descend; Descend, Crossing Descend"
RA	"Level Off, Level Off"
RA	"Climb, Climb NOW; Climb, Climb NOW"
RA	"Descend, Descend NOW; Descend, Descend NOW"
RA	"Increase Climb, Increase Climb"
RA	"Increase Descent, Increase Descent"
RA	"Maintain Vertical Speed, Maintain"
RA	"Maintain Vertical Speed, Crossing Maintain"
RA	"Monitor Vertical Speed"
RA	"Clear of Conflict"

Upon consideration of the three available methods of strategy communication, it is assumed that auditory cues provide the best means of communicating LOC recovery strategies to the pilot. While effective in some situations it is observed from literature that tactile feedback may be limited in effectiveness during LOC recovery, as the pilot will be actively operating in an environment that is prone to environmental vibration. Likewise, during emergency situations such as LOC recovery the pilot is likely to be attending to existing visual cues within the cockpit or outside the aircraft, such that additional visual information may either cause a distraction or be neglected. Therefore it is reasoned that auditory cues present the most appropriate method for LOC recovery strategy communication. This conclusion is also reflected in Hypothesis 3.2:

Hypothesis 3.2: *A segmented control strategy consisting of properly arranged control archetypes can be recommended in stages with auditory prompts to the pilot at the appropriate time through real-time evaluation of aircraft state.*

Given the segmentation of the recovery strategy into archetypal components, the

verbal cues that are suggested in this methodology will consist of aural versions of the archetypes given in Table 25. Using these archetypes as direct aural cues allows for the clear communication of the generated control strategy while aligning with precedent set by other means of aural cuing such as the TCAS II. From the set of TCAS cues in Table 28 it is observed that the provided instructions communicate the intent of a given maneuver rather than the specific control actions. While this type of guidance could also be applied to the twelve archetype sequences, such that each command is translated into some command intent rather than the control action, it is envisioned that the improper translation of this intent by a pilot during a stressful situation may cause unnecessary deviation. Instead the developed commands aim to clearly describe the direct control action which the pilot is recommended to take. One noted deviation from this general development regards neutral yoke commands. As the yoke is used for both aileron and elevator commands, an instruction for "Yoke Center" may not clearly distinguish between these two control surfaces. Thus a command for neutral aileron is included as "Aileron NUETRAL" and neutral elevator as "Elevator NEUTRAL" An initial version of such commands are provided in Table 29.

Table 29: Sample aural commands for control archetype sequences.

	Control Action	**Aural Command**
1	Throttle MAX	"Power ON, Power ON"
2	Throttle IDLE	"Power OFF, Power OFF"
3	Throttle NEUTRAL	"Maintain Power, Maintain Power"
4	Aileron LEFT	"Yoke LEFT, Yoke LEFT"
5	Aileron RIGHT	"Yoke RIGHT, Yoke RIGHT"
6	Aileron NEUTRAL	"Aileron NEUTRAL, Aileron NEUTRAL"
7	Elevator AFT	"Yoke AFT, Yoke AFT"
8	Elevator FORWARD	"Nose Down, Nose Down"
9	Elevator NEUTRAL	"Elevator NEUTRAL, Elevator NEUTRAL"
10	Rudder LEFT	"Pedals LEFT, Pedals LEFT"
11	Rudder RIGHT	"Pedals RIGHT, Pedals RIGHT"
12	Rudder NEUTRAL	"Pedals CENTER, Pedals CENTER"

In the present study the primary focus is upon the efficacy of this method of

recovery such that at this stage it will be first assumed that the aural issuing of commands is performed such that the pilot both hears and understands the issued command. Once communicated to the pilot there is likely to be some delay between the communication of the desired command and initiation of the command. This delay and any inaccuracy on behalf of the pilot may inhibit the efficacy of the recovery strategy. This aspect of the recovery strategy is explored through experimentation, which incorporates the recovery strategy into a vehicle simulation which includes a simulated pilot.

7.3 Implementation and Testing of LOC Mitigation Strategies

The final research question examines the methodology's capability to generate appropriate recovery strategies for LOC events. From the review of the literature performed in Chapter 2 several methods for LOC recovery were identified and a methodology for generating a simplified strategy was described in Chapter 7. In this development it was shown that a simplified recovery strategy may be synthesized in accordance with existing recovery methods through comparison of these methods with various control strategy archetypes. It remains to be shown that such an implementation would allow for an effective strategy for LOC mitigation within the broader MERLIN methodology. Thus a final phase of experimentation is presented which constructs a full demonstration of the MERLIN method, which includes an estimated LOC envelope, state estimation, and an implementation of a simplified control strategy. The setup of this demonstration and the series of tests performed with the constructed apparatus will be described in the remainder of this section.

7.3.1 Construction of MERLIN Demonstration

To allow for the testing of recovery strategy efficacy within the context of the MERLIN methodology a full demonstration of the model is required. This demonstration

will also serve to exercise the efficacy of the methodology as a whole, as the other sets of experiments thus far have tested portions of the method in isolation. This demonstration includes each of the elements shown in the MERLIN overview provided in Figure 12, some of which were developed in earlier phases of the work. The vehicle model used for the demonstration is the LWGA model whose development is outlined within Chapter 4. For demonstration purposes a nominal condition of steady, wings-level cruise of 65 m/s and 1500 m. is selected.

The basic motivation of the MERLIN methodology is provide a system which aids in preventing LOC events. That is, given that the aircraft is initially in some safe condition is the MERLIN method sufficient to prevent excursion outside of the normal operating envelope? The focus then of this experiment and demonstration is on the capability of the full method in providing a framework for mitigating LOC events should the vehicle begin to deviate from safe conditions. From the qualitative and quantitative descriptions of LOC provided in Chapter 2 this desired restriction of the aircraft to a nominal performance envelope may be observed as simultaneously seeking to avoid adverse flight conditions and vehicle dynamics. In particular should the vehicle be constrained to the normal operational envelope, and further still to the corresponding safe set, it is expected that the vehicle should remain within the linear flight regime. For this initial testing and demonstration of the MERLIN method then a linear vehicle model will be used, taken as the nonlinear model which is linearized about a known trim condition.

This linear simulation will allow for testing of the mitigation capability, taking constraint to the linear regime using a linear control strategy as the fundamental capability which will be tested. However the secondary scenario envisioned within the recovery strategy, the recommendation of control actions for recovery from a fully-developed upset condition, is not testable within a strictly linear simulation. It

is asserted however that these upset recovery sequences, being constrained to conform to the FAA recommended stall and spin recovery techniques, have already been demonstrated numerous times both within the literature and in practice. Thus their efficacy in providing for upset recovery is known, whereas the capability of the present method in preventing envelope excursion remains to be shown. Further still, experimentation presented by McDonough and Kolmanovsky [111] developed vehicle trajectories that were constrained to defined envelope using a safe-set approach using a linearized vehicle model. These trajectories were then also demonstrated to satisfy the set of constraints when a nonlinear vehicle simulation was utilized [111] . Therefore it may be expected that should the present testing demonstrate a capability to mitigate envelope excursion using a linear model then similar mitigation should be observed upon extension to a nonlinear model.

To provide LOC mitigation an appropriate LOC envelope is also defined in accordance with the process developed in Chapter 5 and tested through the first series of experiments. In doing so, the process introduced in §5.2.3 and later refined in §6.3.2 for accounting for sources of uncertainty will be utilized. A model error of -5% will be assumed, which is selected to represent an adverse model error scenario which artificially inflates the LOC safe set. Additionally the demonstration will include the GPS and AHRS error models identified in §6.3.1, namely error which is normally distributed with zero mean and a standard deviation of 0.012 m/s for the GPS and 0.5 deg. for the AHRS. With these levels of model uncertainty a threshold adjustment of 0.95 is selected, in accordance with the process for threshold adjustment determination given in §6.3.2. The LOC safe set which results from these assumptions, and will be used in the demonstration is given in Figure 72.

The simulation of the vehicle and the MERLIN demonstration was performed through a MATLAB Simulink model which is shown in Figure 73. The core elements of this model is the vehicle model which is represented in state-space form following

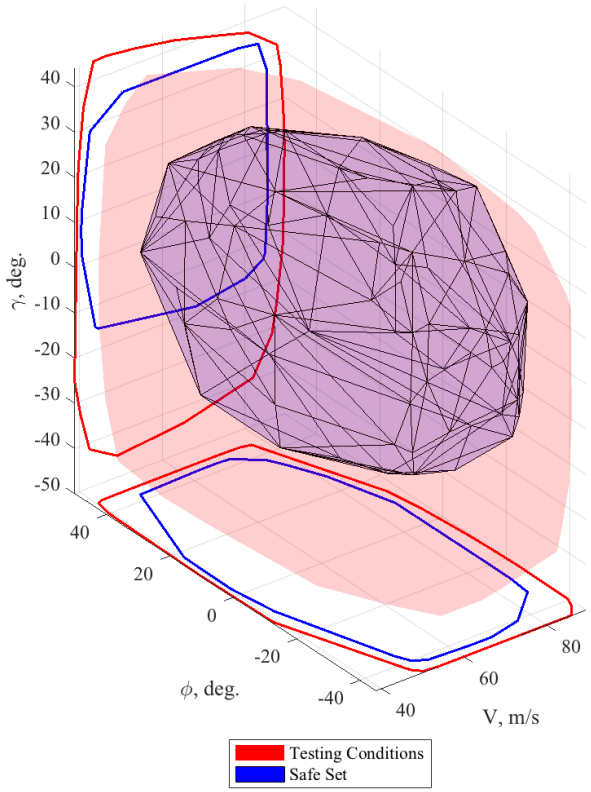

Figure 72: LOC envelope for MERLIN demonstration.

linearization about the selected trim condition. Feedback control is used both to improve stability of the model and to enable the tracking of control commands. This feedback controller includes both a feedback gain controller and a pilot dynamic model in series, that is

$$u(t) = -G_P K x(t) \tag{110}$$

The feedback gain is selected as the LQR gain, at this form of feedback control is also used in the generation of LOC envelope.

A model of pilot performance is included in the demonstration in order to reflect the assumed context of the MERLIN methodology, which includes the assumption

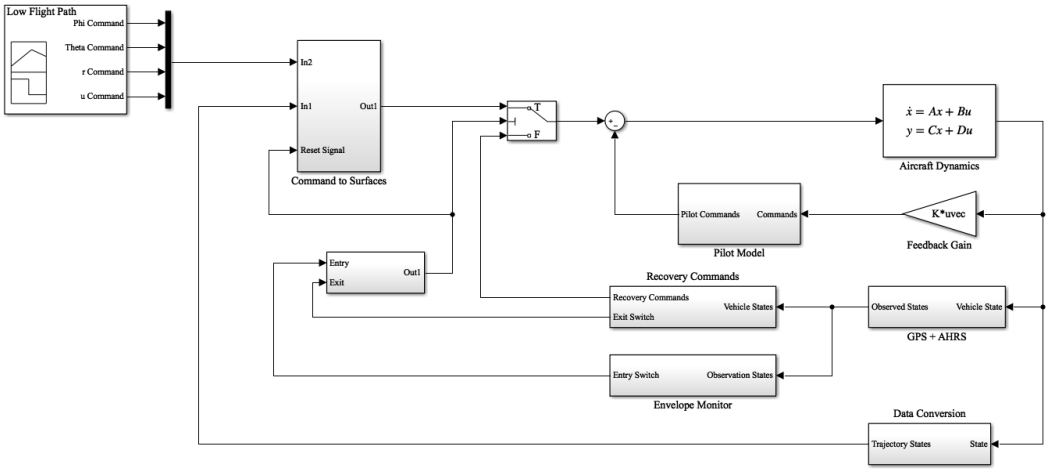

Figure 73: MATLAB Simulink model constructed for MERLIN demonstration and recovery strategy testing.

that any recovery strategy must be communicated to a human pilot for implementation. As such it can be assumed that a given recovery strategy will be perfectly implemented by the pilot, but that some deviation may be expected as the pilot responds to the recovery suggestions. Further, it may be expected that the pilot may elect to take some set of control actions in addition to those commanded by the recovery commands in order to maintain the stability of the aircraft throughout the maneuver. These factors then lead to the inclusion of the given form of the aircraft feedback controller. The pilot model that will be used is presented by Richards et al. [151] which models the transfer function of the pilot as

$$Y_P(s) = \frac{K_p\,(s + 1/T_{lead})}{(s + 1/T_{lag})} e^{-\tau_e s} \tag{111}$$

The four parameters of the pilot model shown in Equation (111) determine the effectiveness of the pilot in responding to the communicated control strategy. In the testing of the recovery strategies various gain scenarios will be constructed to test the efficacy of the recovery strategy in varying pilot scenarios.

To allow for the simulation of various test trajectories a set of nominal control

commands are generated in accordance with pre-defined trajectories. As there are four control dimensions the test trajectories are similarly constructed as variations of four parameters: x-axis velocity u, bank angle ϕ, pitch angle θ, and yaw rate r. For a given trajectory specified as some combination of these four states control commands are synthesized using proportional-integral (PI) compensation which seeks to minimize the error between the commanded trajectory and the simulated vehicle state. The trajectory PI gains used for each control dimension are shown in Table 30.

Table 30: Gains for trajectory PI compensators.

Control	Gain	Value
Aileron	K_p	1
	K_i	10
Elevator	K_p	1
	K_i	10
Rudder	K_p	1
	K_i	10
Throttle	K_p	1
	K_i	0.25

Alongside the components needed for the simulation of the vehicle those components which implement the various parts of the MERLIN methodology are also shown in Figure 73 as the GSP + AHRS, Envelope Monitor, and Recovery Strategy blocks. The GPS + AHRS block simulates the observation of the vehicle state which is assumed to be available within a GA cockpit, which includes the restriction of the visible states to only those provided by GPS or AHRS devices and inclusion of the normally distributed random error. These states are then provided to both the Envelope Monitor and Recovery Strategy blocks, as it is assumed that these methods may only perceive the state of the vehicle in this manner.

To provide evaluation of the vehicle state with respect to some given envelope a means of evaluation was defined which could be efficiently computed. This evaluation is an instance of the general problem of determining whether or not some point is contained within a given convex polygon, a problem which has been well developed in

other applications. As the dimension of the polygon is low, there is no need to utilize an approach such as linear programming, which has been demonstrated within the literature for high-dimensional polygons. Instead, a dot-product method is utilized which evaluates the inclusion of the point according using a series of dot products. First each face of the convex hull, in this case the pre-calculated LOC envelope, is considered an its inward-facing normal vector $\vec{n}$ is computed. For some candidate point x and point along the face a, then the point can be observed to be interior of the given face if the dot product of the difference $(\vec{x} - \vec{a})$ and $\vec{n}$ is non-negative, that is

$$(\vec{x} - \vec{a}) \cdot \vec{n} \geq 0 \tag{112}$$

If this condition is satisfied for all faces of the convex polygon, then it is inside the polygon. This method is advantageous as it allows for pre-computation of the normal vectors $\vec{n}$ and the dot product $\vec{a} \cdot \vec{n}$, such that during the simulation only the dot products $\dot{\vec{x}}\vec{n}$ must be evaluated and compared for evaluation.

The final block is then the Recovery Strategy block, which generates control commands that are issued to the pilot in the event that the LOC envelope is violated. Per the development of the recovery strategy in Chapter 7, the entry conditions, exit conditions, and definitions of the implemented sequence archetypes are required. The definition of the entry condition will be selected as simply the detection of LOC envelope violation. From the method of evaluating the inclusion of a given condition within the envelope this may be specified more clearly as

$$(\vec{x} - \vec{a}) \cdot \vec{n} = 0 \tag{113}$$

Following the development of Lombaerts et al. [105] an exit condition is defined relative to proximity to a pre-selected target condition. This condition is selected as a steady, wings-level cruise condition, and will be monitored through the same estimation techniques used for envelope monitoring. Thus the exit condition will be

said to be satisfied once the aircraft state satisfies

$$V - V_S \leq \epsilon_V \tag{114}$$

$$\phi - \phi_S \leq \epsilon_\phi \tag{115}$$

$$\gamma - \gamma_S \leq \epsilon_\gamma \tag{116}$$

The defined safe state and the associated convergence tolerances which are used throughout the demonstration is shown in Table 31.

Table 31: Defined safe state for aircraft recovery and exit condition tolerances.

State	**Value**	**Tolerance**
Velocity, V	65 m/s	1 m/s
Bank Angle, ϕ	0 deg.	2.5 deg.
Flight Path Angle, γ	0 deg.	2.5 deg.

The various control sequences defined in Table 25 must be defined relative to the control limitations selected in Table 12 in order to be communicated within the simulation framework. For each control the "NEUTRAL" archetype will be taken as the control action required to maintain the trim condition. From these trim settings then the difference between the trim condition and the upper and lower control limits shown in Table 12 can be computed. These differences provide upper and lower limits on the allowable control deflection in each control dimension. The remaining archetype sequences (i.e. "AFT", "FORWARD", etc.) are then defined as 90% of the allowable difference in the appropriate direction for the aileron, elevator, and rudder while the throttle actions were limited to 75% of the allowable difference.

From the development of the simplified control strategy archetypes it can be noted that the general strategy suggested by the FAA and implemented within the literature for recovery from upset conditions primarily involves control surface deflection. Throttle settings are typically either left at a neutral setting or involved in the latter stages of the recovery sequence. This preference is reflected in the chosen control limits, which affords more control authority to control surface deflections than to

throttle action. It was decided, however, not to command full surface deflections for each of the archetypes which are non-neutral. This decision leaves some margin above or below each of the control actions which will allow for small control perturbations to aid the feedback controller in satisfying the control commands while remaining stable.

In the present framework the various control archetypes will be allowed to be simultaneously communicated to the pilot. It is reasoned that even if a single command is issued verbally to a pilot in a given situation it is likely that the pilot will continue to operate the remaining control actions in a manner which will aid in the recovery of the aircraft. Therefore in the present demonstration commands will be issued in all four control dimensions simultaneously. Additional logic is included however within the recovery command generation sub-routine which gives preference to the most important control deflections.

For instance, if the aircraft is in a low flight path angle condition, then longitudinal control commands are more likely to be given as extreme commands while lateral control commands are more likely to be given as neutral commands. The opposite is also true for lateral recovery situations, namely cases of high bank angle. This control command preference is handled by implementing a "dead-band" about the desired safe state, such that if the aircraft state is somewhat close to the safe state in the lateral or longitudinal direction while the opposite direction is given priority then a neutral command will be issued. The width of this zone of low-command priority is notionally set at twice the safe state tolerance both above and below the safe state, resulting in a band whose width is roughly four times the state tolerance level.

With this recovery command strategy in place the full demonstration may then be carried out. In the remainder of this section a series of experiments will be performed which simulated an aircraft which engages in maneuvers which approach the boundary of the LOC envelope. The real-time monitoring of the envelope the violation of the

threshold is identified and appropriate control commands are issued to the simulated pilot. Through this sequence of experimentation the full MERLIN method may be demonstrated, with particular attention given to the performance of the simplified recovery strategies in mitigating loss of control incidents.

7.3.2 Experiment 3: Efficacy of Simplified Recovery Strategy Method

The final set of experimentation primarily tests the LOC recovery strategy portion of the MERLIN methodology, though in doing so the full capability is also demonstrated. In this experiment the efficacy of the simplified recovery strategy will be examined in two ways, in accordance with Research Questions 3.1 and 3.2, and will allow for testing of Hypotheses 3.1 and 3.2. The first of these research questions, Research Question 3.1, is concerned primarily with the efficacy of the simplified recovery strategy in mitigating LOC situations. To satisfy this question and to assess Hypothesis 3.1 it must be shown that the recovery strategy which consists of the simplified control archetypes is an effective means of LOC mitigation. The second question extends this question of efficacy to include not only the recovery strategy itself but also its application by a human pilot. Therefore to satisfy this second hypothesis it must be shown that this strategy, if shown to be effective in a nominal scenario, remains so under some degradation due to pilot performance.

During this experiment, it will be assumed that the strategy will be correctly comprehended by the pilot, restricting the experiment to testing of the response time and effectiveness of the pilot in implementing the communicated strategy. This assumption further implies that auditory prompting is sufficient for communicating the desired control action to the pilot. Each of these assumptions are based upon evidence afforded by similar systems which exist within the aviation system, such as TCAS or stall warning indicators. In both instances it is observed that given appropriate training and clear verbal instruction there is little issue on behalf of the

pilot in comprehending and acting upon the verbal instructions of these systems. It may be noted here as an aside that one avenue of future research in this topic would be cases in which the pilot clearly hears and comprehends a given command but either knowingly or unknowingly fails to heed the provided suggestion. Such a study is likely to involve studies into various human factors such as training culture, and could be important for future real-world implementations of the MERLIN methodology. At present however these cases will be neglected.

Using the vehicle simulation paired with the instantiation of the MERLIN methodology described earlier in this section the experiment will be performed according to the following steps:

1. Simulate GA aircraft in nominal and LOC conditions
2. Recommend recovery strategy to simulated pilot model and record resulting performance
3. Repeat Steps 2 for varying pilot assumptions
4. Repeat Steps 1 through 3 for various LOC conditions

In this experiment three assumptions of pilot performance will be made, drawn from the model of pilot performance presented by Richards et al. [151]: nominal, high gain, and low gain. Nominal values of the pilot model parameters for each control are shown in 32. This version of the pilot model will be considered as the baseline performance of the pilot with respect to the recovery sequences. It is noted that while a time delay is included in the pilot model (τ_e) presented by Richards et al. [151] it was found during preliminary testing of the flight demonstration that even small delays caused the simulation to become rather fragile, if not unstable, even for rather mild maneuvers. This sensitivity may arise from a few sources within the simulation, including the selected form of the feedback controller or the means

by which the trajectory commands have been implemented. It is further reasoned that some delay already exists within the system, as the current implementation will current implementation has some inherent delay in satisfying the commanded trajectories even without the inclusion of additional pilot delay. Thus it is elected then to simply reduce the pilot delay to zero in order to allow for the present experiment to more clearly examine the efficacy of the control strategy.

Table 32: Nominal pilot model parameters, adapted from [151].

Parameter	Pitch and Roll Yoke	Rudder Pedals	Throttle
K_p	0.1	1.0	0.21
$1/T_{lead}$	20	20	20
$1/T_{lag}$	0.01	0.01	0.01
τ_e, ms	0	0	0

The high gain set of parameters, given in Table 33, represents a situation in which the pilot responds to the control commands with too much aggression. In general for each control dimension this model of pilot performance will tend to overshoot given control commands followed by the stronger presence of oscillations in later efforts to correct. The aggressive response modeled by this pilot model may be thought of as representing a pilot who is somehow distressed or anxious, perhaps due to stress or inexperience.

Table 33: High gain pilot model parameters, adapted from [151].

Parameter	Pitch and Roll Yoke	Rudder Pedals	Throttle
K_p	0.16	2.0	0.42
$1/T_{lead}$	20	20	20
$1/T_{lag}$	0.01	0.01	0.01
τ_e, ms	0	0	0

The final set of parameters corresponding to a low gain pilot model is shown within Table 34. This variation of the pilot model represents a pilot who reacts slowly to communicated commands. Such may be the case when the pilot distracted by other stimuli in the environment or otherwise inattentive to the vehicle state or the recovery

commands.

Table 34: Low gain pilot model parameters, adapted from [151].

Parameter	Pitch and Roll Yoke	Rudder Pedals	Throttle
K_p	0.025	0.25	0.05
$1/T_{lead}$	20	20	20
$1/T_{lag}$	0.01	0.01	0.01
τ_e, ms	0	0	0

These pilot models will be exercised within the simulation environment through a set of trajectories which each deviate from the trim condition towards some edge of the LOC boundary. Trajectories were selected such that each dimension of the LOC boundary could be tested and provide an opportunity to evaluate the performance of the recovery strategy in each of these dimensions. The first trajectory is a deviation towards a low velocity while seeking to maintain nominal flight path angle and bank angle, representing a common exercise performed in stall recovery practice. A high velocity trajectory is neglected from this set as it is deemed that this case is less likely to be encountered as defined (i.e. over-speed with zero flight path angle and wings level) unintentionally in normal operation. The second and third trajectories then seek to achieve low and then high flight path angles, respectively, while maintaining nominal airspeed and bank angle. These trajectories reflect instances in which either descent or climb is performed that begins to deviate into the unsafe region. Fourth and final is a commanded high bank angle trajectory while maintaining constant velocity and flight path angle, representative of attempting to enter a turn which is too steep and becomes unsafe. Only one direction of high bank angle is examined in this study, though it is likely that some small differences between each direction may exist due to propeller-induced effects.

These four selected trajectories allow for the response to single-dimension envelope excursions to be examined. Many more trajectories may be envisioned with are combinations of the above trajectories such that corner conditions of the envelope are

violated. It is assumed that the present trajectories allow for sufficient exploration of the capabilities of the recovery strategies in order to ascertain whether or not it represents an effective means of suggesting LOC mitigation. In preparing some future implementation of the MERLIN methodology suited for real-world application the present trajectories should be supplemented with additional studies of the combinatorial space such that any gaps in the capability may be identified and rectified.

For each of the twelve combinations of trajectory scenario and pilot model two sets of results will be presented. The first is the set of state trajectories which are observed by the LOC monitoring capability alongside an indicator of the recovery mode onset and termination. This indicator is represented as a binary value in which a value of unity represents nominal flight and zero indicates that the vehicle is being provided with recovery commands. The three LOC states, velocity, flight path angle, and bank angle, are shown as they are seen by the LOC monitor which includes the error imparted on the signal by the GPS and AHRS observation. The second set of results presented for each case is the set of pilot control actions and the associated control commands. In each the actual pilot action is given as a solid blue line whereas the control command is represented by a dashed black curve. Within this section the trajectories produced by the nominal pilot model in each scenario are presented, while the performance of the low gain and high gain pilot models are provided in Appendix F.

The time histories for the first trajectory, a low speed maneuver, is represented in Figures 74, 102 and 103. In each figure the commanded trajectory can be seen in the first few seconds of the velocity trajectory, in which a decrease from the trim velocity of 65 m/s to approximately 40 m/s is observed. While this trajectory was commanded to maintain a constant flight path angle and bank angle a slight decrease in flight path angle prior to the recovery sequence is observed, consistent with the nose beginning to droop due to insufficient pitch moment produced by the tail in

order to maintain the zero flight path angle at low speeds.

Examining first the nominal pilot response given in Figure 74 it is observed that once the recovery sequence is initiated at approximately five seconds the initial response is to command a pitch-down maneuver which allows for the velocity to be quickly gained. By ten seconds into the trajectory sufficient velocity has been restored and the remainder of the recover appears to slowly bring the flight path angle and velocity to the desired trajectory. While there is some lateral motion present early in the maneuver and near the end, it is observed that the aileron and rudder deflection is mostly commanded as neutral though the maneuver. This general arrangement of sequences is noted as consistent with the identified LOC recovery process for unusual pitch attitude shown in Algorithm 1 and the FAA recommendation for stall recovery.

These trends are present for the high and low gain pilot model shown in Figures 102 and 103 though some other trends also emerge in each of these cases. Across all three pilot models it is observed that the recovery sequence is quite lengthy, lasting approximately 35 seconds from the detected onset of the recovery commands. It is observed that while the high gain pilot exits the recovery phase approximately five seconds faster than the nominal pilot model there is overall much more oscillation in the control response. This is particularly true for the lateral controls which exhibit a slight wing-rock tendency throughout the recovery sequence driven by the aileron and rudder oscillations about the trim deflections. For this trajectory the low gain pilot model also recovers in slightly less time than the nominal pilot but in other respects is qualitatively similar to the recovery of the nominal pilot for this trajectory.

The second trajectory scenario, which examines the recovery response to a low flight path angle scenario, is given for the three pilot models in Figures 75, 104 and 105. This trajectory starts with steady decrease in the flight path angle for approximately ten seconds before the LOC envelope is violated. During this decrease in the flight path angle the vehicle velocity and bank angle remain constant at their trim

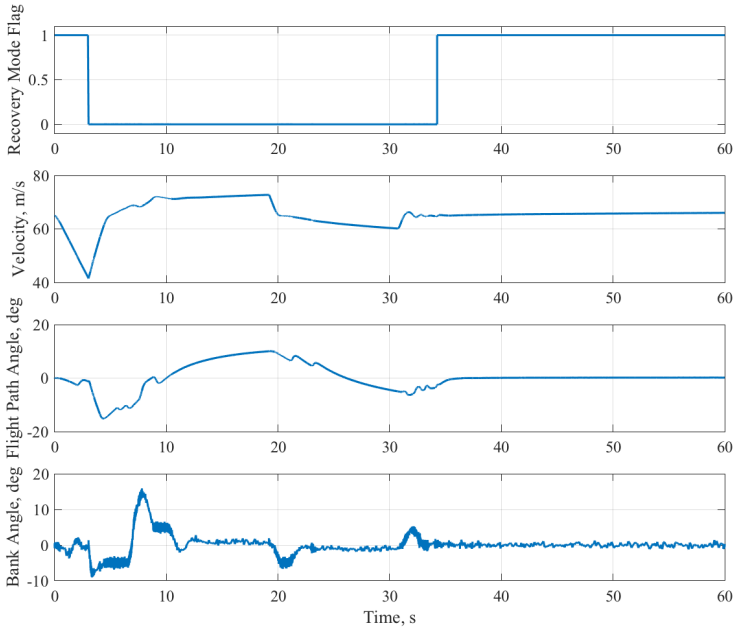

(a)

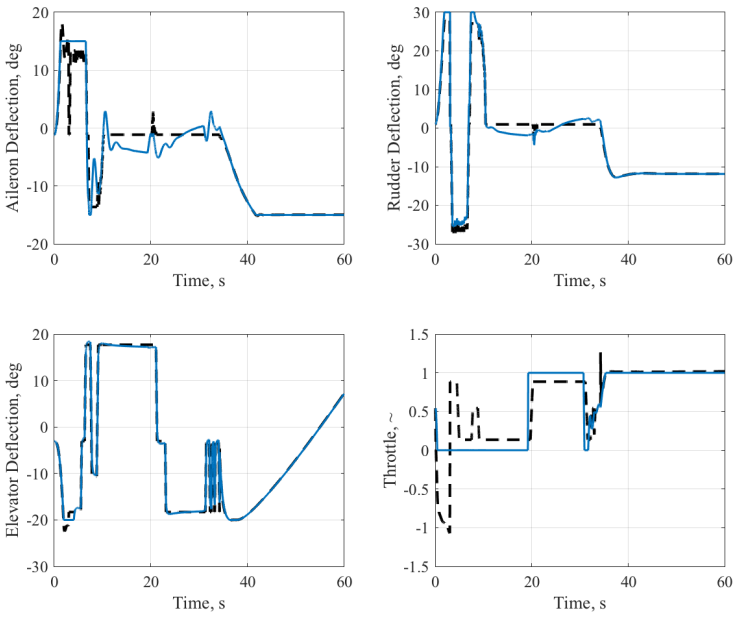

(b)

Figure 74: Trajectory and control history for low velocity scenario with nominal pilot model.

values as commanded by the trajectory generator. This adherence to the commanded trajectory is aided by the favorable dynamics of the maneuver between the flight path angle and velocity.

The nominal pilot model recovery is achieved in approximately ten seconds, which is more in line with typical recovery times. This recovery is primarily driven by a elevator command in the recovery direction, nose up in this case, with a coordinated increase in the throttle setting from idle to full throttle. Laterally there is some curious behavior which occurs approximately five seconds in to the maneuver. This deviation in the bank angle occurs at the same time that there is a drop and leveling off in the flight path angle of aircraft. As this maneuver is performed while the throttle setting is somewhat high it may be inferred that some of the behavior is due to coupling between the longitudinal and lateral motion from the gyroscopic motion of the propeller and is possibly exacerbated by the commanded aileron and rudder commands. Regardless it is observed that while this event occurs it is quickly resolved and the vehicle soon achieves the safe operating condition.

Differences between the nominal pilot model and the other two models for this trajectory are similar to those observed in the previous trajectory. Once more the high gain model shown in Figure 104 recovers more quickly than the other two pilot models. Unlike the low velocity recovery however there are in fact fewer oscillations present in the high gain pilot recovery trajectory, though this is likely due to the short time of the recovery overall. The low gain pilot model exhibits similar recovery characteristics as the nominal pilot model with slightly smoother convergence to the safe condition in the later portion of the recovery. In all three cases of this trajectory one other notable feature of the recovery trajectory is the overshoot of the flight path angle beyond the desired zero flight path angle.

For this trajectory such an overshoot is permissible as the range of acceptable positive flight path angles is larger than the range of negative flight path angles (see

72). The presence of the overshoot may however help to identify a limitation of this implementation of the recovery strategy method. The control archetypes primarily include extreme applications of each control surface, which in turn creates larger restorative moments. In a real-world scenario it may be envisioned that a pilot would "ease-off" of the control once it was apparent that enough effective action had been taken. Such a maneuver may be possibly be translated through a neutral control command, but it is also likely that this behavior is an artifact of the implemented definition of the control archetype. That is to say since the recovery strategy is oriented towards more extreme control commands it likely that overshoot is more likely to occur in the ensuing trajectory.

The third control trajectory is the opposite scenario to the second, namely the response to the a high flight path angle. This trajectory proceeds in the opposite fashion to that before in the pre-recovery phase, with a steadily increasing flight path angle which exceeds the LOC envelope after about ten seconds. The three recovery histories for this trajectory are given in Figures 76, 106 and 107. While a successful recovery is indicated for each model recovery, observation of the trajectory histories casts some doubt on the legitimacy of this indication. During the recovery for this trajectory it is observed that the aircraft once more overshoots the desired flight path angle. In this instance however this overshoot into the negative flight path angle regime exceeds the LOC envelope on the opposite side, due to the smaller range of permissible negative flight path angles. With this result then these recovery sequences, though they do eventually converge to the desired condition, do not do so in a satisfactory manner.

The fourth and final trajectory which was tested in this experiment is provided in Figures 77, 108 and 109. This maneuver simulates a commanded high bank angle maneuver with constant velocity and flight path angle. As may be observed in the time histories of the responses this desired trajectory was adhered to quite well in

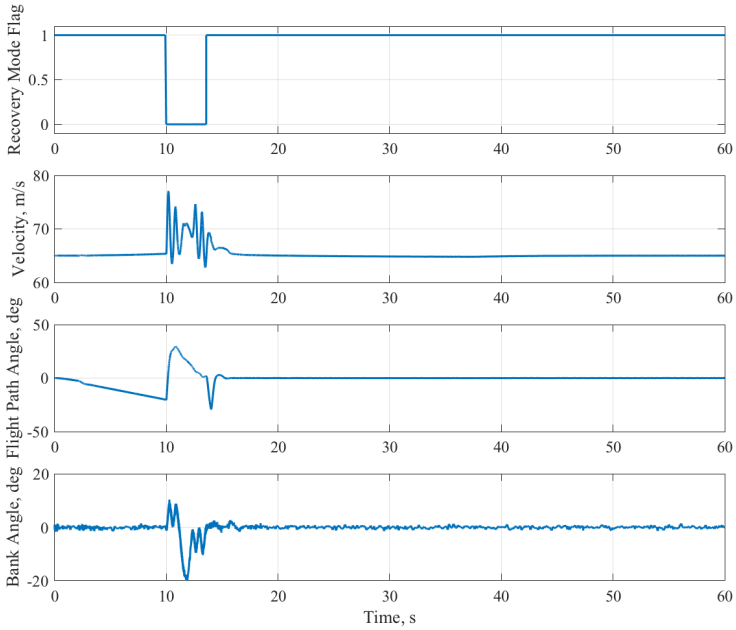

(a)

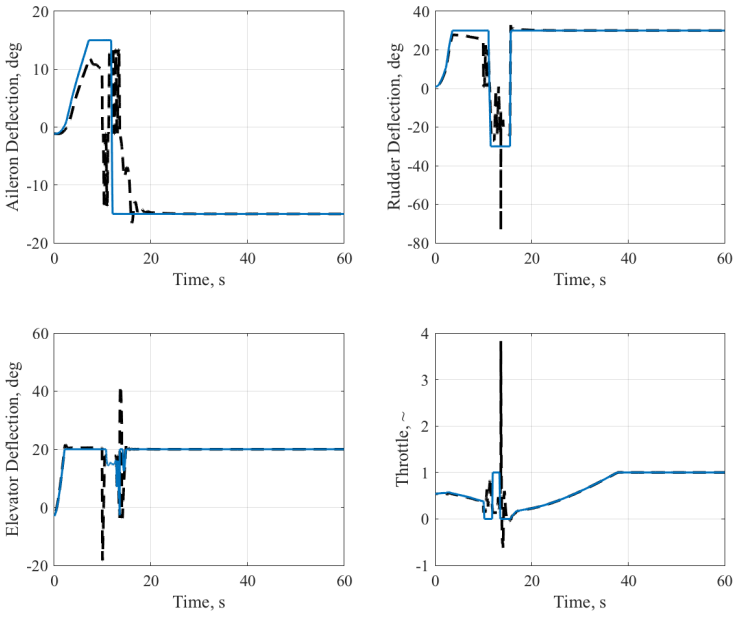

(b)

Figure 75: Trajectory and control history for low flight path angle scenario with nominal pilot model.

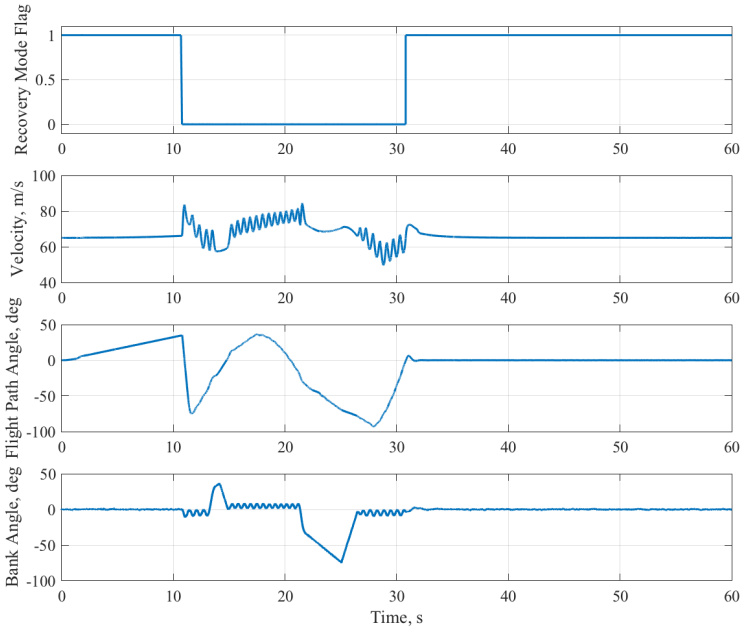

(a)

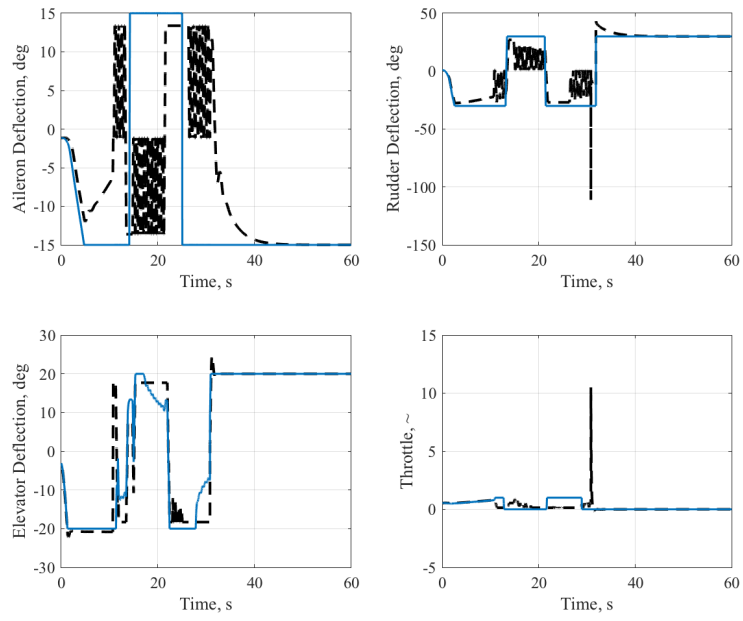

(b)

Figure 76: Trajectory and control history for high flight path angle scenario with nominal pilot model.

each of the pilot model cases, with very little deviation in vehicle velocity and flight path angle.

The recovery of the vehicle in these cases is very brief for the nominal pilot model shown in Figure 77. Recovery in this situation is driven by coordinated action between the aileron and rudder, which agrees with the expected sequences previously developed. Though brief there is also present some longitudinal control action, which is initiated in response to the drop in flight path angle and associated increase in velocity which occurs as a secondary result of the lateral control actions.

One interesting feature which distinguishes this trajectory from the first two is that the high gain control requires much more time to recover when compared to the nominal and low gain control. This result is likely driven by the aggressive action associated with this pilot model which in this trajectory produces adverse recovery characteristics relative to the less aggressive pilot models. Additionally the high gain model exhibits some longitudinal oscillations which initially grow before being rectified by appropriate action. Such tendency was noted within the spin recovery literature as a tendency for inappropriate elevator action to inhibit the recovery from a fully developed spin and possibly to hinder recovery altogether.

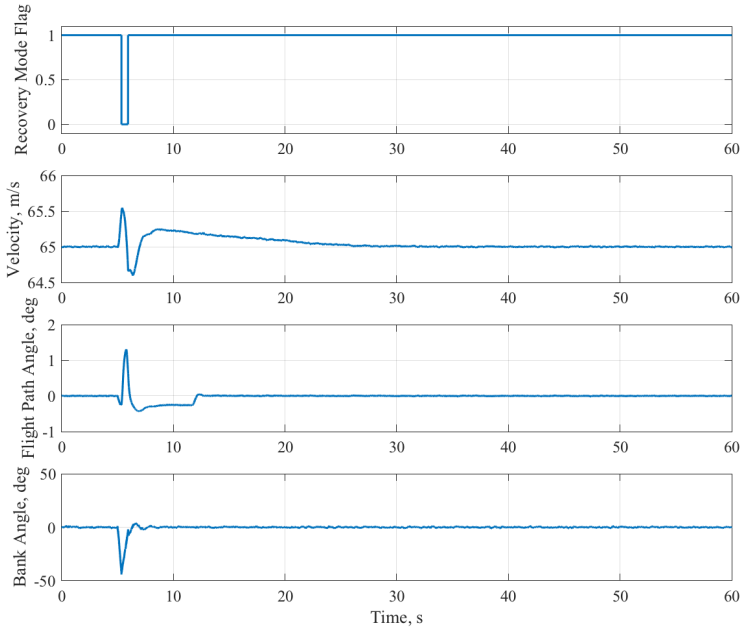

(a)

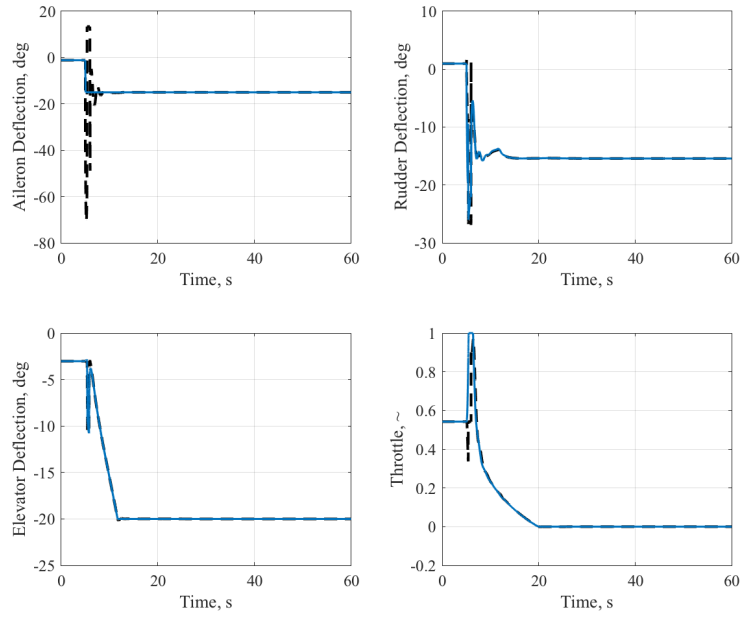

(b)

Figure 77: Trajectory and control history for high bank path angle scenario with nominal pilot model.

7.3.3 Summary of Mitigation Strategy Results

The final research question focuses on the efficacy of the simplified recovery strategy in providing recovery commands which produce effective recovery of the aircraft from detected envelope violations. This investigation focused on two related aspects: the ability of the recovery strategy to produce a recovery trajectory from detected envelope infraction and then sufficient robustness to ensure that this recovery is accomplished by a pilot who may inaccurately apply the provided commands. These two aspects are the subject of Research Question 3.1 and 3.2 respectively, and are seen to be related to the LOC recovery process as shown by Figure 78.

To test these questions a final experiment was developed which generated a full demonstration of the MERLIN methodology within a simulation of the LWGA aircraft's dynamics. An overview of this demonstration was provided in 73, which depicts the MATLAB Simulink model of these components. Within this model various trajectories could be simulated which drove the aircraft from an initial safe condition towards the boundary of a pre-defined LOC envelope. Once violation of the envelope was detected a set of recovery commands were then provided to the pilot model according to the simplified recovery strategy developed in §7.1. The resulting time histories were then recorded and studied to reveal the extent to which these commands were sufficient in aiding in the recovery of the aircraft from impending envelope violation.

From the results for the twelve test cases shown in Figure 74 through Figure 109, some conclusions relating to the efficacy of the recovery strategy may be drawn. It may first be noted that in all of the tested trajectories expect for the high flight path angle scenario, the recovery sequence method developed within this work was capable of achieving recovery from identified violation of LOC envelope thereby providing a means of LOC mitigation. In the case of the third trajectory it is observed that while the trajectory produced is unsatisfactory the final result is observed to be that

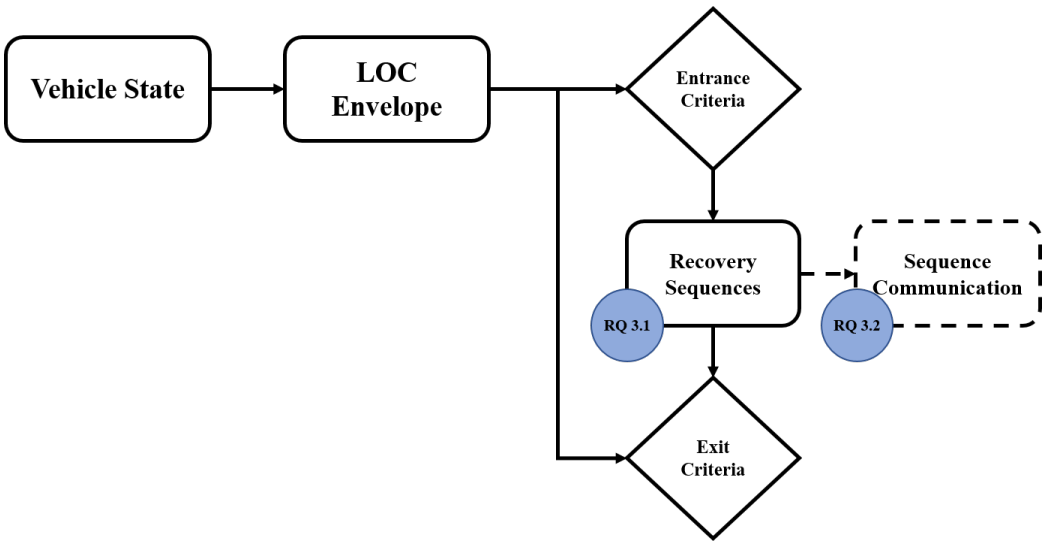

Figure 78: Summary of examined LOC mitigation method components with applicable research questions.

some measure of recovery was achieved. This indicates that with some additional safeguards developed which ward against extreme overshoots that this situation too may be expected to be appropriately recovered. On this basis then it is observed that Hypothesis 3.1 is confirmed, as the application of a simplified recovery strategy is sufficient for the mitigation of the identified conditions.

Further the results shown within this experiment were all implemented with some assumed pilot model. In each case of pilot model assumptions the recovery of the aircraft from the unsafe conditions was achieved, which suggests some degree of robustness of the recovery strategy method to varying pilot conditions. These results then suggest that not only is the simplified recovery strategy provide sufficient instructions for LOC mitigation but also that these instructions remain effective even when implemented by a separate human pilot. This finding then suggests that Hypothesis 3.2 may also confirmed.

Alongside the results of this experiment some key limitations are also noted. As previously discussed, the simplification of the simulation to a linear model allows for initial testing of the mitigation capability but prevents full testing of the capability

of full upset recovery. Thus in future work these results should be supplemented with a full nonlinear simulation which confirms the capability to mitigate LOC envelope violation and also to aid in upset recovery in the event that it occurs. An additional limitation of this experiment is the inclusion of a statistical pilot model. While the pilot model is known to be in good agreement with observed pilot behavior [151], it is nevertheless an approximation of the response of an actual human pilot. Further testing of the present recovery strategy method, and the full MERLIN method, using pilot-in-the-loop simulation would allow for a more realistic representation of how this framework may be expected to perform when used in tandem with human operators.

CHAPTER VIII

CONCLUSION

While aviation is known to be safest mode of transportation, numerous incidents occur each year involving GA vehicles. These incidents most commonly involve LOC, a phenomena that is known to be a pervasive issue for all classes of aircraft. In review of existing efforts for mitigating LOC for aircraft it was found that no existing methodology suitably addresses LOC for GA fixed-wing aircraft, though this particular class of aircraft is most likely to be involved in an LOC-related event. This gap in preventative assistance for LOC incidents among GA aircraft prompted the objective of this research which was:

Research Objective:

Develop a methodology for the prediction and mitigation of LOC incidents for fixed-wing GA aircraft within the typical GA operation limitations.

To meet this objective it was hypothesized that a model-based methodology which provided a means of LOC detection and mitigation through observation of a defined LOC envelope and the suggestion of appropriate control actions in the event that the envelope is violated. This methodology primarily consists of three components: the definition of LOC envelopes, the estimation of vehicle states in order to monitor the envelope, and formulation and recommendation of recovery actions in the event that the envelope is violated. These key components of the MERLIN methodology were each developed by building upon methods and techniques within the literature in order to formulate a set of tools which is tailored for use within the given context. Following their development each component was further examined according to the

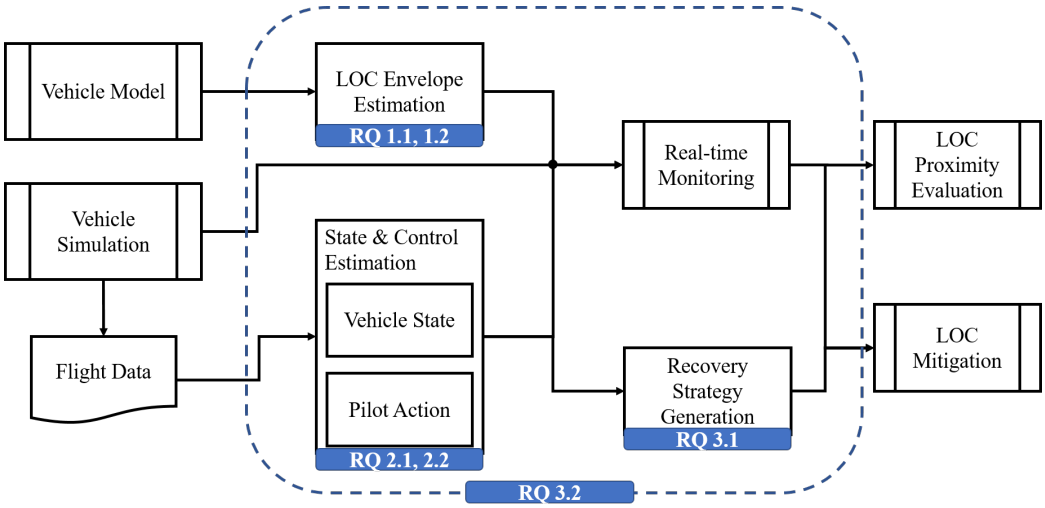

Figure 79: Summary of MERLIN methodology with examined research questions.

set of research questions formulated within Chapter 3. A summary of these research questions and their relative relationship to the major components of the MERLIN methodology is provided in Figure 79.

Research Question 1, which included the supplemental Research Questions 1.1 and 1.2, was tested through Experiments 1.1, 1.2, and 1.3. This first research question stated:

Research Question 1:

What is the level of confidence afforded by a LOC envelope and how sensitive is this confidence to variability or uncertainty in the envelope generation process?

These three experiments examined the ways in which the developed LOC envelope varied under two sources of uncertainty, the uncertainty associated with the state and control thresholds and the uncertainty due to dynamic vehicle model error. Each source of uncertainty was modeled and propagated through the envelope estimation procedure to produce a range of LOC envelope estimates. These envelopes were compared to a baseline envelope by examining the normalized volume of each envelope's safe set. It was observed that while each source of uncertainty does affect the size

of the resultant envelope, the relative changes could be bounded. Additionally the third of these experiments revealed that when considered together the total effect on the LOC envelope can additionally be quantified in a manner which allows for more conservative approximations of the LOC envelope to be developed even in the presence of adverse model error. These results together demonstrate the bounded and quantifiable sensitivity of the LOC envelope to both threshold uncertainty and model error and that the a conservative approximation of the LOC envelope may always be constructed. Therefor Hypothesis 1.1 and 1.2 were each confirmed, providing the required sensitivity quantification and level of confidence assessment in order to satisfy Research Question 1.

The second set of presented experiments tested the research questions which were concerned with the state and control estimation capability, based upon Research Question 2:

Research Question 2:

How can the proximity of a GA vehicle to a LOC situation be assessed in real-time while considering the constraints on available flight data for typical GA aircraft?

These questions and their hypotheses were focused on both the required techniques for providing accurate state and control estimates within the MERLIN methodology and also for examining how this accuracy, or lack thereof, may influence the downstream monitoring of the aircraft state relative to the LOC envelope. Based upon the states required by the LOC envelope, methods of estimating the vehicle velocity, flight path angle, and bank angle from only GPS and AHRS collected data were developed within Experiment 2.1, alongside estimates of the expected distribution of estimation error from these sources. Following this estimation Experiment 2.2 examined the ways in which this error may affect the accuracy of LOC envelope excursion identification, resulting in an approach for preemptively restricting the LOC envelope in order to

account for the anticipated estimation error. These experimental results were used to test Hypothesis 2.1 and 2.2, thereby demonstrating the capability of the MERLIN method to assess LOC proximity in real-time using only the available flight data. It can thus be seen that Research Question 2 is satisfied.

The final research question first focused on the efficacy of the recovery strategy, stated as:

Research Question 3:

What is an appropriate strategy for LOC avoidance or recovery and how can this strategy be leveraged to synthesize real-time recommendations for a GA pilot?

Through Research Question 3.1 the generation of the strategy and the impact that the generated strategy would have within the full contextual implementation of the MERLIN methodology was examined, while Research Question 3.2 examined the efficacy of such a strategy given communication to a human pilot. To test these two research questions a full demonstration of the MERLIN method was constructed which included an estimate of the LOC envelope for the LWGA vehicle model, simulated observation of the vehicle state through a GPS and AHRS unit, and recovery recommendations delivered to a simulated pilot in control of a GA aircraft simulation. Through this demonstration a series of simulated flights were performed which involved the deviation of the aircraft from an initial safe condition towards a set of unsafe conditions. In the results of Experiment 3 the responses of the pilot model to issued recovery commands were provided, which demonstrated both the overall efficacy of the recovery strategy generation method and the capability MERLIN method to mitigate LOC conditions. With this simulated demonstration of the MERLIN method a LOC mitigation method was both generated in real-time to provide pilot recommendations, satisfying Research Question 3.

Through interpretation of the results of the six experiments the six proposed hypotheses were confirmed, and in so doing the three primary research questions were each satisfied. By their confirmation it is found then that the MERLIN methodology is capable of achieving the prediction and mitigation of LOC incidents for GA vehicles. In addition this conclusion is further supported by the range of test conditions through which the methodology was tested, which accounted for uncertainty in dynamic vehicle modeling, uncertainty in the definition of state and control thresholds on flight operation, state estimation error, and inaccurate recovery strategy implementation due to simulated human application of control commands. From these findings it is concluded that the Overarching Hypothesis is confirmed and thus the Research Objective is satisfied.

8.1 Contributions

During the course of this work several contributions have been developed which will be identified. The primary contribution of this work is the development and testing of the MERLIN methodology, a framework which satisfies a gap which exists in the domain of fixed-wing GA flight safety. This methodology is a novel method which combines model-based estimation of LOC envelopes, state estimation techniques, and the generation of simplified recovery strategies for the purpose of providing a framework for predicting and mitigating LOC incidents for GA aircraft. Throughout its development the MERLIN methodology was formulated with the constraints of the existing GA fleet in mind such that it can be reasonably envisioned for future application to existing GA vehicles without the need for costly modification to the vehicle itself. Additionally while the method was synthesized with these GA-specific constraints in mind the same framework may similarly be applied to other classes of aircraft.

In addition to the MERLIN framework as a whole a second set of contributions

made by this work include the implemented and tested forms of each of the major components. The implemented LOC envelope tested within this work represents a novel approach within GA fixed-wing aircraft safety analysis that combines a defined set of LOC boundaries with an estimation of the envelope's safe set. Further, it was demonstrated that this envelope has several attractive properties included the dimensional reduction to only three vehicle states and provision for robustness to various sources of uncertainty. During the exploration of state and control estimation techniques, a novel method for estimating the flap deflection of a GA aircraft through energy-based metrics and performance estimation and the derivation of a novel algorithm for the estimation of pilot control actions from observed flight data and dynamical models were presented. While these two techniques were not ultimately required within the present demonstration of the MERLIN method, other work which seeks to estimate these parameters may benefit from their development. Finally, a methodology for the synthesis and communication of LOC recovery strategies consisting of simplified control archetype sequences was developed and demonstrated by this work, and offers a novel approach to providing recovery recommendations to GA pilots prior to or during upset conditions.

A third contribution of this work is the summary and development of a set of methods and techniques for generating a dynamic model of a GA aircraft. While many of the individual methods within this dynamic modeling approach exist within the literature, this work provides an identification of an appropriate set of methods from the larger set of techniques which balances the required level of fidelity and computational burden. In the context of this effort this modeling work was focused on the synthesis of a dynamic model which would be used within the MERLIN methodology. Other uses may be conceived for such an approach, including the design or analysis of fixed-wing aircraft in a manner which includes the capability to examine the static and dynamic properties of the design.

8.2 Recommendations for Future Work

During the development and testing of the MERLIN method a number of limitations were identified, many of which are candidates for future research. Within the definition of the LOC envelope it was noted that the defined envelope, labeled as the GA QLC, was a set of general conditions which may be considered as nominal but may inappropriately identify some special flight conditions as unsafe when they are in fact safe operations. Thus is recommended that future work should expand the definition of the original performance envelope to either include such conditions within some single envelope or to define a set of envelopes which each correspond to some specific flight condition. In either case the resulting LOC envelope(s) may be estimated through the presented safe set analysis. Implementation of this expanded envelope approach would also call for the definition of some means of selecting the situation-appropriate envelope, either with some manual selection by the pilot, algorithm selection, or a combination of the two. Additionally within the envelope estimation work presented in Chapter 5 testing it was observed that the means by which model error was applied was limited to uniform scaling of the set of forces and moments. It is recommended that future experimentation be performed which more closely explores the effect of model error on the LOC envelope estimation process. In this experimentation the contribution of model error from each portion of the vehicle dynamic model may be estimated and propagated through the envelope estimation process.

In the exploration and testing of state estimation methods it was assumed that the vehicle was operating in a still atmosphere, which limited the examined error to only that arising from the data collection devices. While some methods of estimating the wind speed using only the available PED collected data were introduced, further development is recommended to determine their operational viability. Following this

development then an additional set of experimentation may be performed which follows the general experimental process provided with Experiments 2.1 and 2.2, which describe an approach which simulates the data collection and state estimation process within a flight simulation framework.

In future efforts associated with these developed methods it is also recommended that additional refinement and testing of the recovery strategy method be performed. The results of Experiment 3 identified some limitations inherent to the means by which the recovery strategy was defined for that testing, most notably the state overshoot of the vehicle during some mitigation procedures. It is likely that this overshoot is due to a combination overly extreme control commands which are applied too "sharply" which leads to overly fast vehicle rotations. Further refinement of the particular limits of these control archetypes and the means by which they are intended to be interpreted during the recovery may alleviate these concerns while potentially improving the performance of the recovery strategy overall.

In addition later testing of this recovery strategy should be conducted in an more realistic environment. As the simulation of the vehicle in Experiment 3 was linear it is recommended that future work test both the recovery strategy method and the full MERLIN method within a nonlinear framework. Further, future work should strive to include the aural communication of the control commands to actual human pilots within a pilot-in-the-loop simulation of the aircraft. Such additional study would not only further test the efficacy of the method in a better approximation of the intended environment but would also allow for additional study of associated human factors.

Another avenue of future work involves the considerations which would be necessary for implementing the MERLIN method on some PED within a GA cockpit. This future work would likely include an evaluation of the memory and computational load required by this method and a comparison of those requirements to the resources available on a PED. It is also additionally assumed that the data is collected

by some external GPS and AHRS device, which would require additional development to ensure proper interfacing. Alternatively an extension of the method could be investigated which examines the feasibility of utilizing a single device to both monitor the flight state and execute the MERLIN methodology. Such a device could be envisioned as a new device designed for this purpose which contains GPS and AHRS capability while also providing an implementation of the MERLIN method. Another alternative is the use PED such a smartphone or tablet computer which could monitor the state using its on-board GPS and accelerometers.

One of the key assumptions of this work is that the monitored vehicle is unimpaired. Trends of common LOC incidents however indicate that LOC is commonly precipitated by some failure of the aircraft. A expanded form of the MERLIN methodology could be utilized to address such situations through the inclusion of means of vehicle fault detection. This detection capability would allow for the dynamic redefinition of the relevant LOC envelope and potentially modify the pertinent recovery strategies for maintaining the operating envelope.

Finally while the MERLIN method was developed with application to GA aircraft loss-of-control in mind it is observed that the methodology may be extended to various other applications. The core means by which LOC incidents are mitigated is through the definition of the LOC envelope. As such that the incorporation of some other undesirable flight condition to be avoided instead of, or in addition to, LOC may be performed through the redefinition of the normal operation envelope. Such an envelope must be defined such the extents of normal operation are defined as upper and lower bounds on some subset of the vehicle states, from which a safe set may then be estimated. The MERLIN method could be also extended to other air vehicles through appropriate adaptation of the vehicle model and by appropriate adaptation of the LOC envelope to the new vehicle. In addition this method could also be adapted for general flight safety assessment purposes, as it allows for the explicit exploration

of vehicle flight conditions which satisfy a set of safety constraints and the feasibility of maintaining the vehicle within the safe region for a set of operational limitations.

APPENDIX A

DYNAMIC MODEL VERIFICATION

In order to test various aspects of the MERLIN methodology a dynamic vehicle model was developed which reflects the attributes of a fixed-wing GA aircraft. The various assumptions and models used to construct the LWGA model are provided in Chapter 4. The models which used to construct the LWGA were each drawn from various sources within the literature and in large part these works additionally contain the independent verification and validation of the given modular components. As this particular union of the gathered models is unique, then an additional step of model verification is presented which confirms that the constructed model reasonably reflects the expected performance of a GA aircraft.

Attention will first be turned to verification of the propulsive model, which consists of a polynomial model of engine performance and a BEMT model of propeller performance. The polynomial of engine power lapse is provided as Equation (47), and a sample of the accuracy of the model to other models of engine performance is shown in Figure 31. In addition the force and moment coefficients of the propeller model at a range of operating conditions is shown in Figure 35. As this propulsive system is rather straightforward, the verification process will involve sampling of the steady state RPM between the engine and propeller for a range of nominal cruise conditions. This sampling is shown in Figure 80 with gives the balanced RPM for a range of free-stream velocities and throttle settings, assuming that a constant propeller angle of attack of zero degrees. The expected trends are noted, primarily that as the throttle setting is increased for a given velocity the RPM also increases. This is consistent with an increase in torque absorbed by the propeller to match the

increased torque supplied by the engine. As this test is performed in isolation of the aerodynamic model it can not be determined which of these conditions would be sufficient to satisfy some desired trim condition, though it may be surmised from the range of conditions present that such conditions are at feasible.

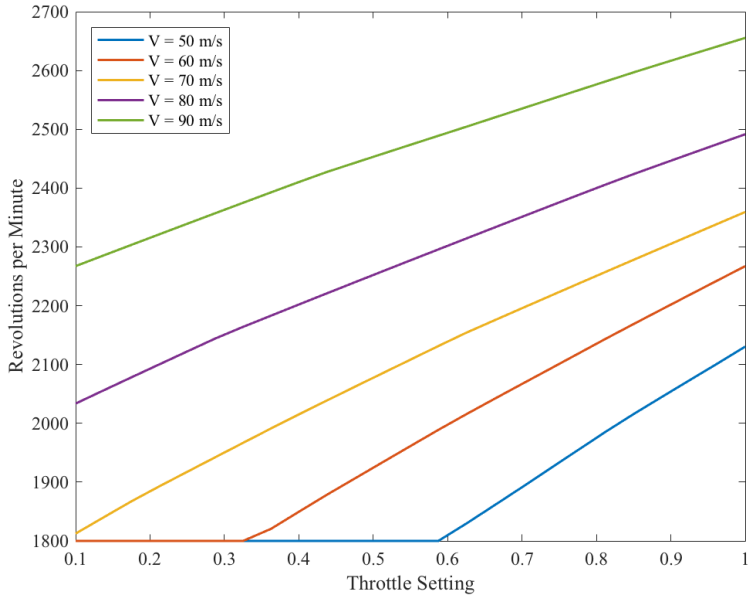

Figure 80: Steady state RPM for engine-propeller system at 1500 m and a range of velocities.

Verification of the aerodynamic model is performed in a more granular fashion, as this model consists of several model components which may interact in unexpected ways. To gain insight into the model then a wide range of aerodynamic conditions were tested, spanning a combination of angle of attack and sideslip angle states for various combinations of aileron, elevator, and rudder deflections. The data for these tests was then used to fit response surfaces to each component of the force and moment coefficients, which allowed for enhanced visualization of the present trends and clearer depiction of the interactions between various state changes. Note however that these response surface models were only used within this verification exercise. While

the response surfaces were in general well behaved and found to be accurate representations of the underlying model, the inherent error introduced by their use would present an additional level of uncertainty into later testing. Thus in all other applications of the vehicle model the aerodynamic model is directly sampled in determining the aerodynamic performance of the model for a given condition.

The response surface representation of the x-axis force coefficient is shown in Figure 81, and the interactions of the tested states with respect to this direction of the force is shown in Figure 82. This body-axis force is closely related to the drag of the aircraft, which generally speaking is related is aligned in the negative x-axis direction for small aerodynamic angles. As aerodynamic drag is primarily a function of angle of attack, the quadratic relationship which emerges as a function of the state is an indicator of correct functioning. The angle of attack is also observed to most strongly interact with the other independent variables in Figure 82, with strong interaction noted between the angle of attack and the elevator deflection angle. This interaction is likely a behavior which is attributed to the down-wash effects of the wing on the aft tail which shifts direction relative to the tail as the is alternately above or below the wing surface.

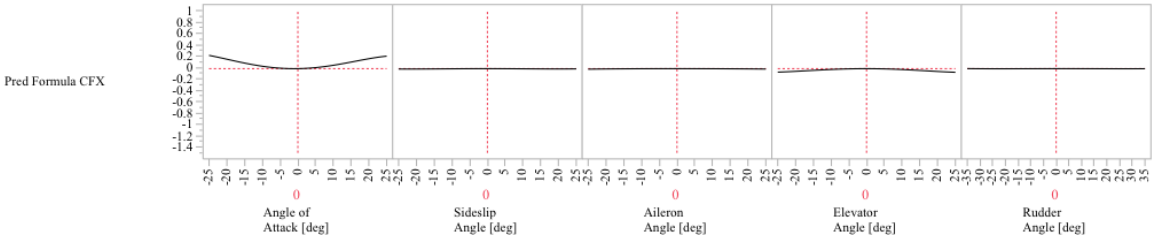

Figure 81: Aerodynamic force about x-axis with varying state and control deflections.

The second set of figures given as Figure 83 and Figure 84 demonstrates the y-axis force response to the tested variables. Overall the side-force coefficient is observed to be very low in the nominal condition depicted in Figure 83. This is another expected result as the side force for aircraft is typically quite low in normal operation,

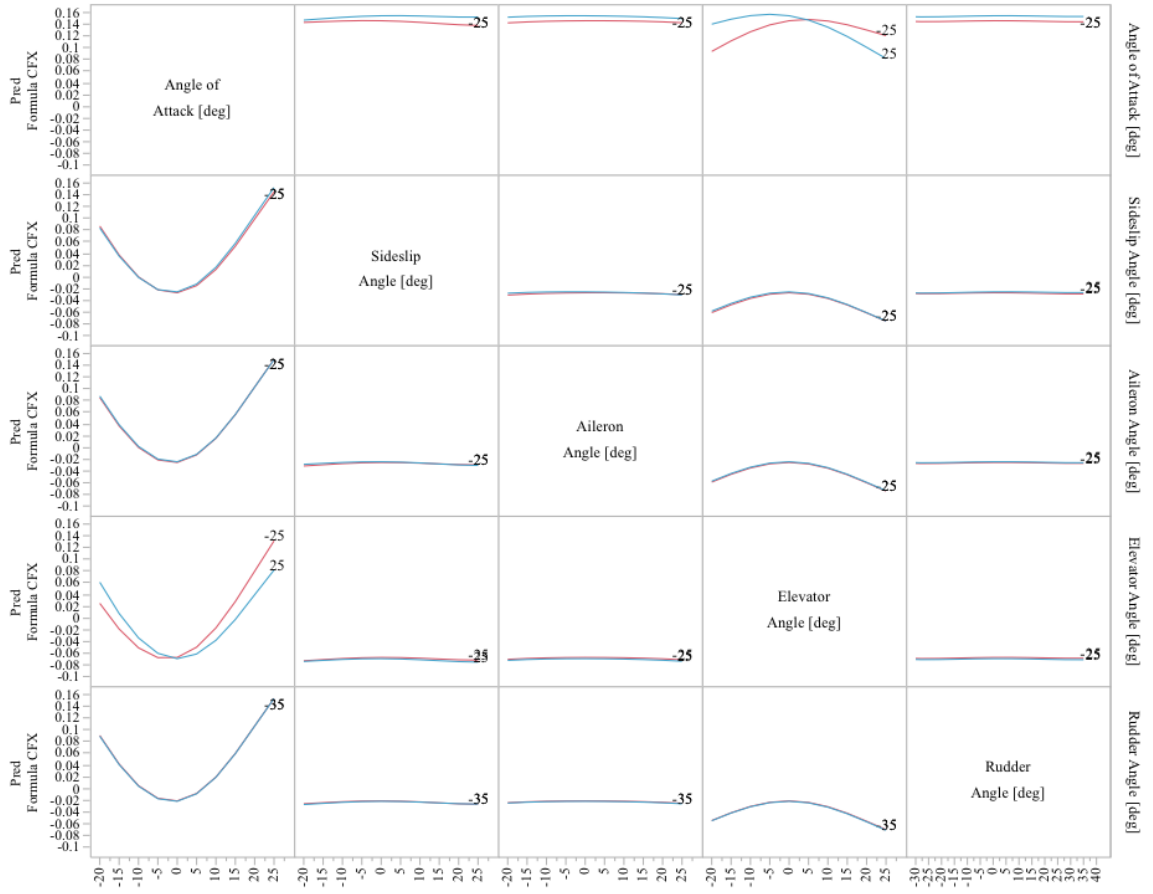

Figure 82: State interactions for aerodynamic force about x-axis.

particularly during symmetric flight conditions. The interactions between the states and control deflections do indicate that while the side force is normally quite low it may become more significant in certain flight conditions. When the aircraft is in non-symmetric flight, for instance, a more significant side force is generated at all angles of attack. There is additional variation in the side force with the application of the lateral control surfaces with rudder deflection developing the larger shifts in this force coefficient. Across these various combinations however it is observed that the maximum magnitude of the side force is approximately 0.15, which is still rather small in comparison to the lift coefficient of the aircraft.

The final force coefficient behavior, that which is about the z-axis, is shown in

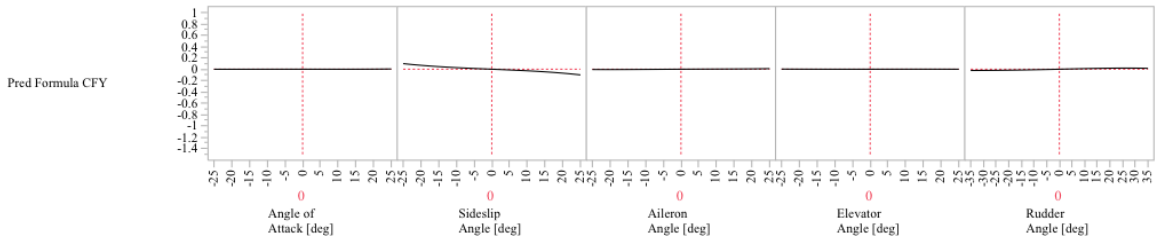

Figure 83: Aerodynamic force about y-axis with varying state and control deflections.

Figure 85 and Figure 86. Just as the drag is primarily along the x-axis the aerodynamic lift is generally aligned with the negative z-axis for small aircraft angles. This connection between the lift and z-axis force is consistent with the strong linear relationship between the z-axis force and the angle of attack. It is noted that the z-axis force coefficient is negative for at zero angle of attack, which is consisting the positive incidence angle of approximately four degrees at the wing root. Alongside the strong effect of the angle of attack the other notable sensitivity is related to the elevator deflection angle. This sensitivity is primarily a vertical translation of z-axis force coefficient with a minimal change in slope. Such a trend indicates that a deflection of the elevator slightly shifts the angle of attack at which a given value of z-axis force occurs, but otherwise does not dramatically alter the relationship between this force and the other angles or deflections.

Following the force coefficient relationships the similar set of moment coefficients is then examined for the same set of operating conditions. The first of these results displays the relationships associated with the x-axis moment coefficients, which are shown in Figure 87 and Figure 88. As would be expected the primary variations in the rolling moment coefficient are the sideslip angle and the aileron deflection, with each have similar magnitudes of sensitivity. In Figure 88 the relationship between the rolling moment and the sideslip angle can be most clearly observed to be linear with negative slope. This negative slope indicates that the aircraft has a stable roll stability through the secondary effect of sideslip experienced at non-zero bank

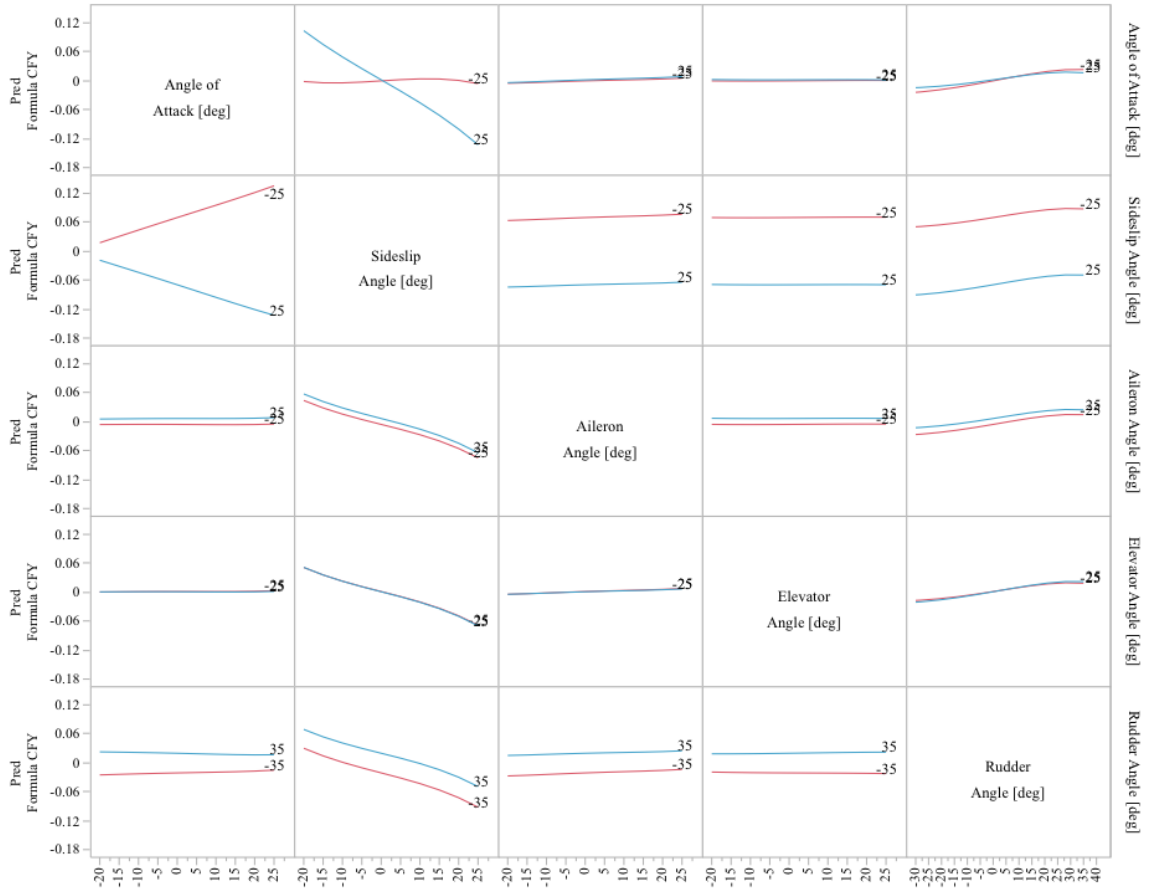

Figure 84: State interactions for aerodynamic force about y-axis.

angles. In addition it is seen from the interaction effect between the sideslip angle and the aileron deflection that there is almost always sufficient control authority along the x-axis. While the effectiveness of the ailerons becomes somewhat small at extreme sideslip angles, the restorative tendency of the aircraft with respect to sideslip implies that this reduction in control effectiveness would likely be aided by the aircraft's dynamics. An additional strong interaction for this moment is that between the angle of attack and sideslip angle, which is strong at extreme angles in each dimension.

The longitudinal moment about the y-axis is demonstrated in Figure 89 and Figure 90 which similarly display agreeable stability characteristics for this aircraft. As the slope of the relationship between the angle of attack and the pitching moment

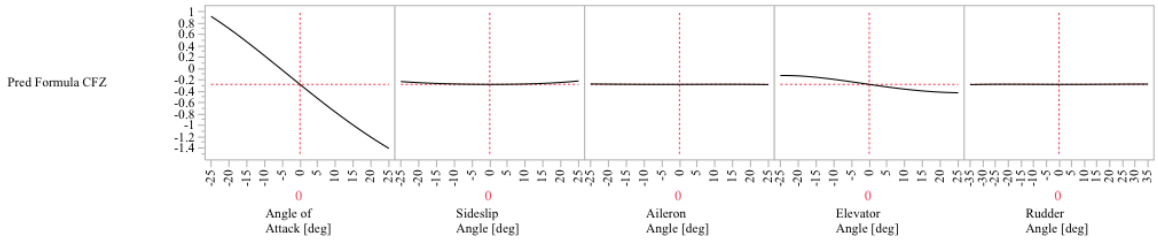

Figure 85: Aerodynamic force about z-axis with varying state and control deflections.

is negative then the aircraft is statically stable about the y-axis. Inspection of the interaction between the angle of attack and the elevator deflection for the pitching moment provides some additional insight into the range of trimmable vehicle conditions. It is noted that for almost all angles of attack there is an elevator deflection which may be utilized to bring the pitching moment to zero. At very low angles of attack it is seen that the elevator effectiveness is reduced sufficiently such that the pitching moment cannot be brought to zero. However the general static stability in this axis will once more aid in overcoming this deficiency.

The final study in this verification exercise is the examination of the z-axis moment relationships, which are shown in Figure 91 and Figure 92. This moment is observed to primarily vary as a function of the sideslip angle and the rudder deflection. Studying the sideslip relationship with the yawing moment reveals that a linear relationship with a positive slope. Therefore the aircraft can be observed to have static directional stability. In addition to the primary effects of sideslip and aileron deflection there is a secondary effect due to the deflection of the aileron. Finally, observation of the interaction between sideslip angle and rudder deflection indicates that for the tested range of these two variables there is sufficient rudder control authority in order to maintain a total of zero sideslip angle.

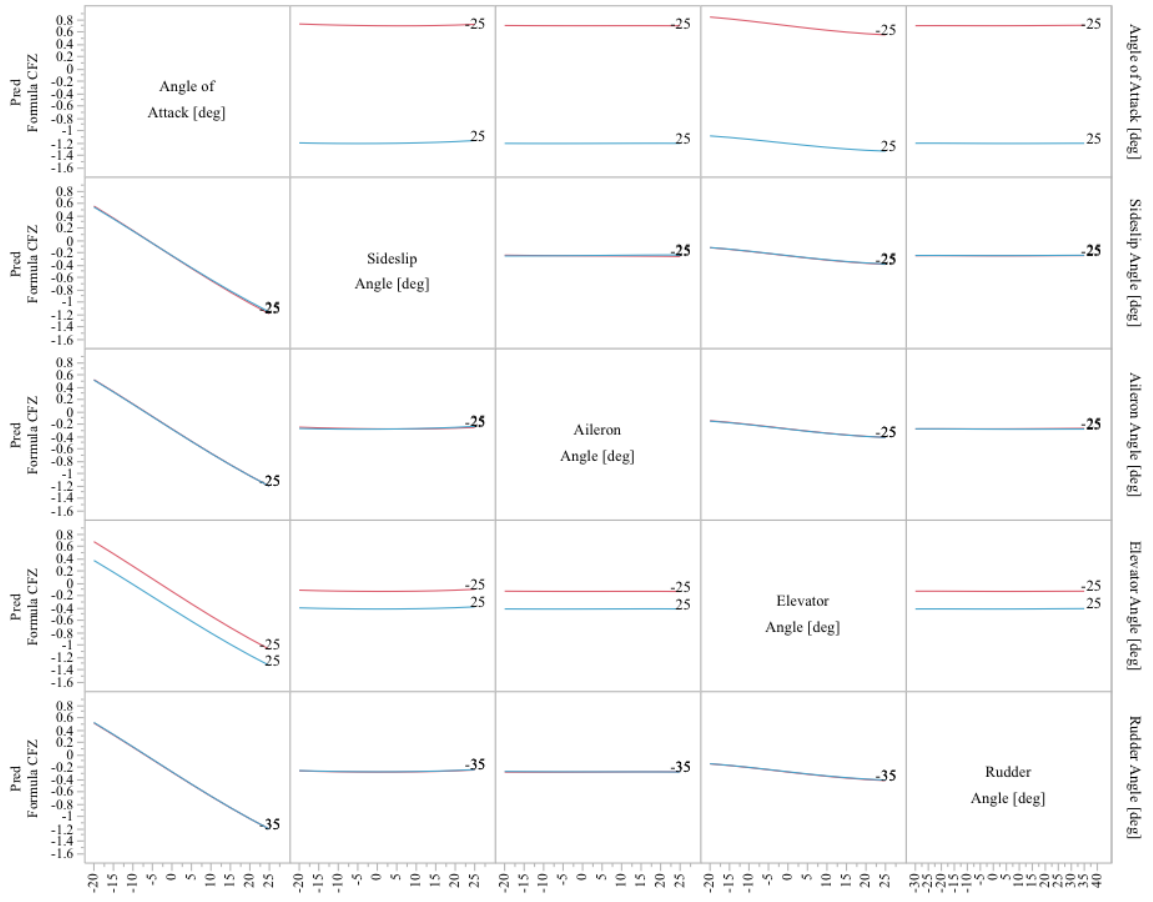

Figure 86: State interactions for aerodynamic force about z-axis.

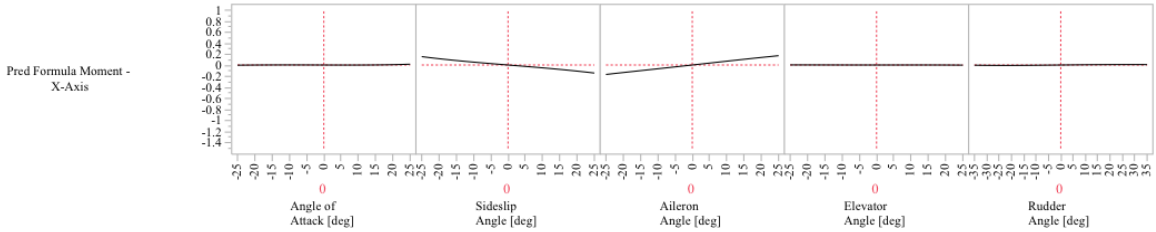

Figure 87: Aerodynamic moment about x-axis with varying state and control deflections.

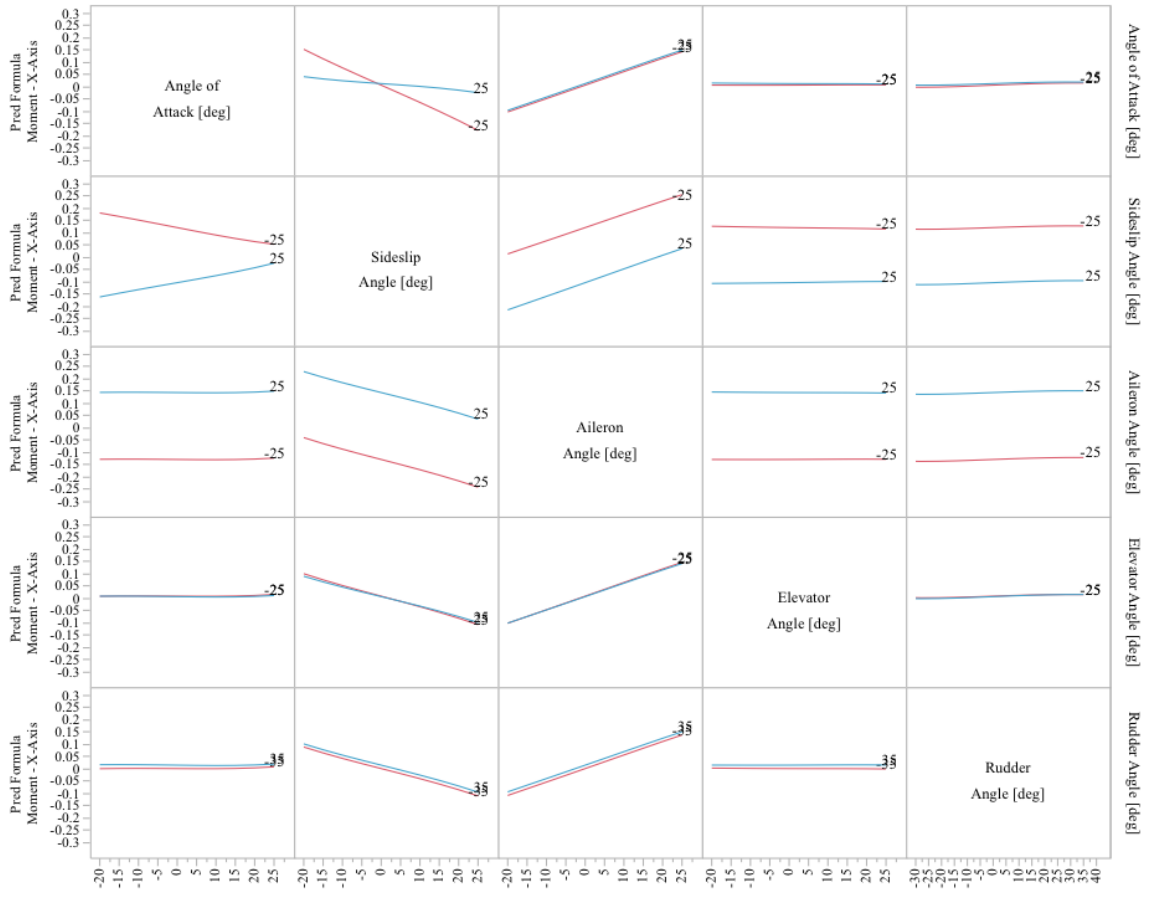

Figure 88: State interactions for aerodynamic moment about X-axis.

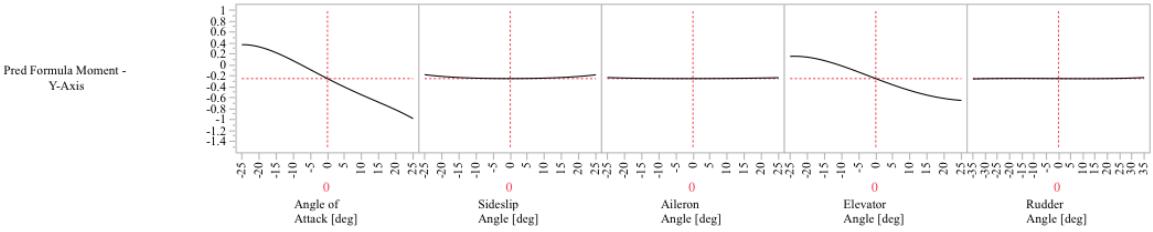

Figure 89: Aerodynamic moment about y-axis with varying state and control deflections.

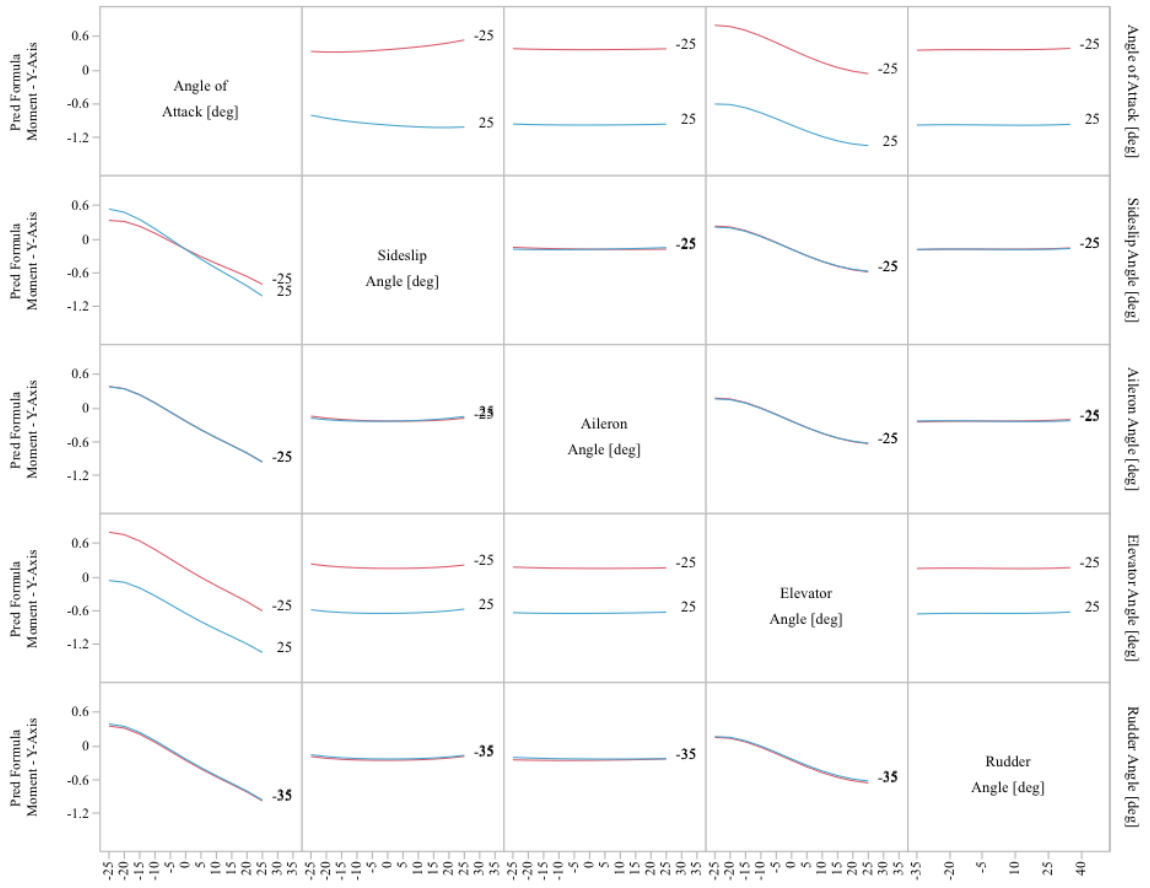

Figure 90: State interactions for aerodynamic moment about y-axis.

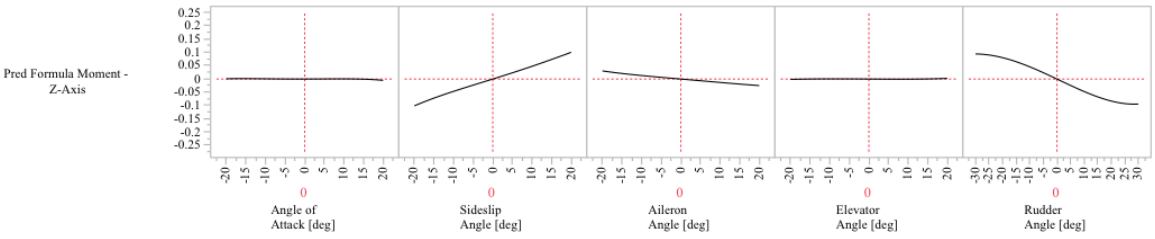

Figure 91: Aerodynamic moment about z-axis with varying state and control deflections.

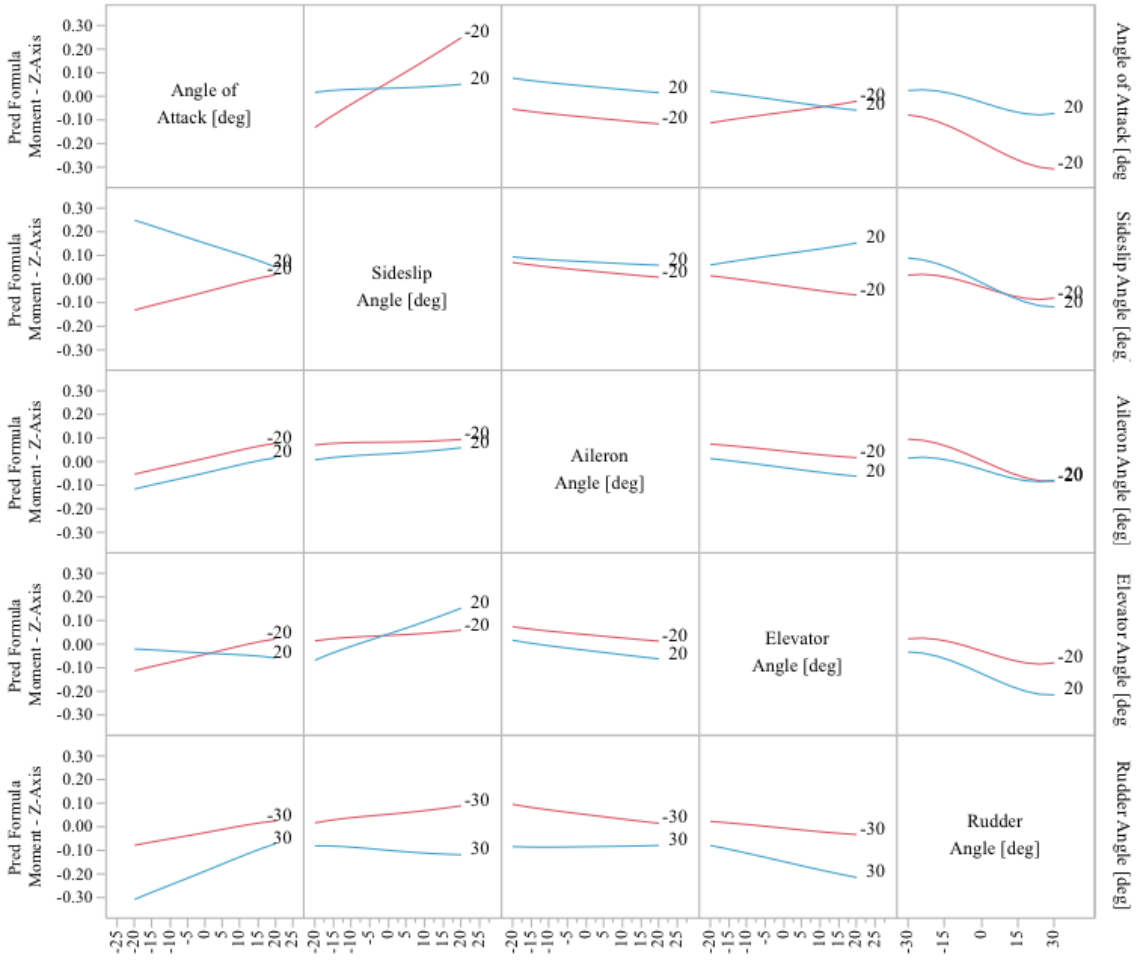

Figure 92: State interactions for aerodynamic moment about z-axis.

The overarching observation drawn from this set of aerodynamic data is that alignment of the model with typical expectations for this class of aircraft. The expected stability characteristics, namely positive static stability in both the longitudinal and lateral motion, is observed for the LWGA and is consistent with the stability characteristics of most GA aircraft. Further, there is evidence that the appropriate interactions between lifting surfaces is present such that a realistic depiction of GA aerodynamics is modeled. With these observations alongside the verified propulsive model it is concluded that the developed model is functioning appropriately and therefore may serve as an appropriate model for the testing and experimentation performed within this work.

APPENDIX B

OVERVIEW OF LIFTING LINE THEORY ALGORITHM

The analytical lifting line method developed by Prandtl [143, 144] in the early twentieth century has seen extensive application throughout the aerospace engineering literature. While this method has proven to provide accurate estimates of aerodynamic surface aerodynamics, it's limitation to single lifting surfaces of non-swept wings with no dihedral presents a hindrance to many modern applications. In light of this more recent adaptations of Prandtl's lifting line method have been presented within the literature, including that of Phillips and Snyder [135]. This method allows for the aerodynamic estimation of a system of lifting surfaces, the members of which may include swept surfaces with non-zero dihedral. The generalization provided by Phillips and Snyder utilizes a three-dimensional vortex law that explicitly includes the down-wash effects of both the bound and free segments of the typical horseshoe vortices used in the lifting line method. In their work Phillips and Snyder [135] provide a theoretical overview of this generalized lifting line method which will not be fully included in this work. Instead an algorithmic perspective will be presented which presents the various steps and modifications taken to develop a computational algorithm which is used in the method described in this work to estimate the aerodynamic properties of a GA aircraft.

First consider a single lifting surface, such as that shown in Figure 93, which has some pre-defined geometry. Each half-span of the surface may be divided into n panels or strips, such that the number and location of the panels is symmetric about the center-line of the lifting surface. For each section a control point is also defined at some span-wise location within the section along the quarter-chord line of the lifting

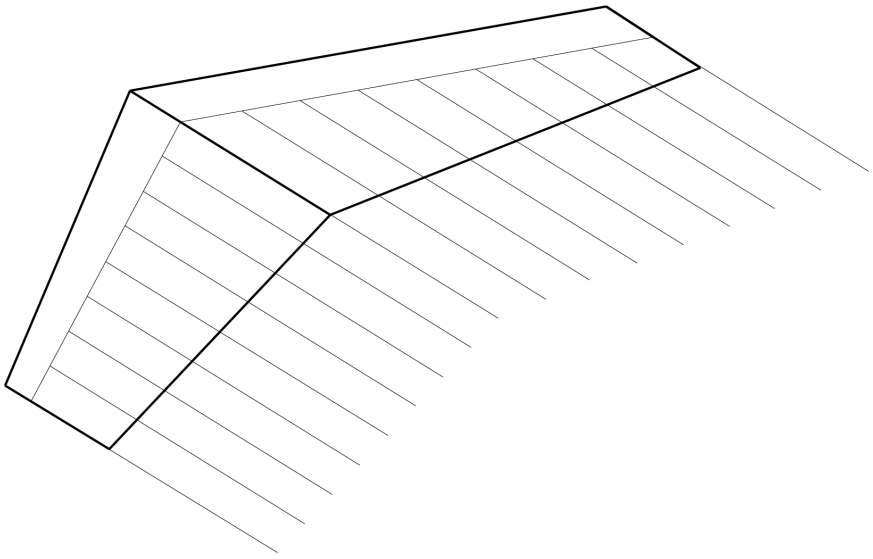

Figure 93: Sample lifting surface with evenly sections and horseshoe vortices, adapted from [135].

surface. This control point serves as a representative location for the lifting surface section at the aerodynamic properties of the section will be evaluated. The simplest method of defining the lifting surface sections and their respective control points is to evenly divide the lifting surface into n desired sections and to simply select the control point location to be at the midpoint of the span of the section. An alternative method of assigning the section locations is through cosine clustering of the sections near the edges of each semispan, a method which is noted by Phillips and Snyder to improve the efficiency of the overall algorithm [135]. Taking the temporary variable ϕ to vary from 0 to π as the span-wise coordinate s varies from zero to the half-span length $\frac{b}{2}$, then the location of each section edge is defined as

$$\frac{s_i}{b} = \frac{1}{4}\left[1 - \cos\left(\frac{i\pi}{n}\right)\right], \quad 0 \leq i \leq n \tag{B.1}$$

Placement of the control points midway in ϕ for each section can similarly be achieved with

$$\frac{s_i}{b} = \frac{1}{4}\left[1 - \cos\left[\left(\frac{i\phi}{n}\right) - \left(\frac{\pi}{2n}\right)\right]\right], \quad 1 \leq i \leq n \tag{B.2}$$

Along each section a horseshoe vortex is defined whose bound segment is aligned

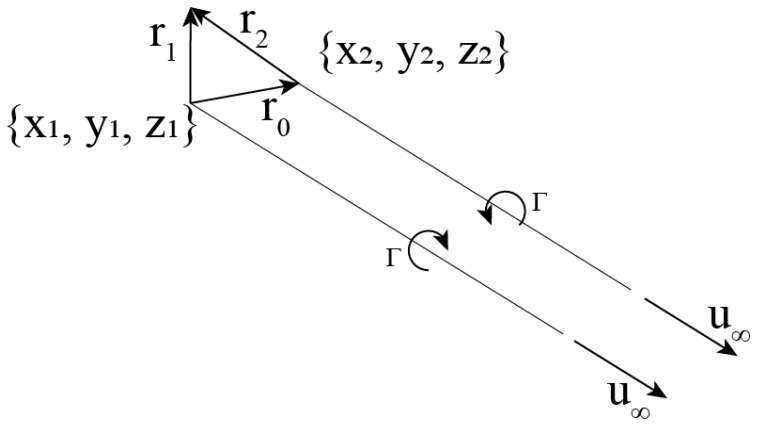

Figure 94: Sample horseshoe vortex geometry, adapted from [135].

with the local quarter-chord line, implying that the bound portion of the vortex is also aligned with the local sweep and dihedral of the lifting surface. The two trailing vortices of the horseshoe are aligned with the trailing vortex sheet downstream of the lifting surface (assumed to be in the direction of the free-stream flow) and coincident with the bound vortex at the two outer edges of the each section. A representation of this spatial arrangement for a sample horseshoe vortex is shown in Figure 94, which represents a horseshoe vortex anchored between section points $\{x_1, y_1, z_1\}$ and $\{x_2, y_2, z_2\}$. The vector $\vec{r}0$ seen in Figure 94 represents the vector between the two section points, whereas the vectors $\vec{r}1$ and $\vec{r}2$ depict the vector between these sectional boundary points and some arbitrary vector in space $\{x, y, z\}$.

At each control point a set of geometric parameters must be defined: the dimensionless span-wise length vector, ζ_i, sectional aerodynamic mean chord length, $\bar{c}_i$, and three orientation vectors u_n, u_a, u_s. Assuming that the chord length of the lifting surface is known as a function of span the the area of each section is found as

$$\delta A_i = \int_{s=s_1}^{s_2} c \mathrm{d}s \tag{B.3}$$

It is common that the chord length varies linearly over each section, or may be

reasonably approximated as such, thus this integral may be carried out as

$$\delta A_i = \frac{c_{i1} + c_{i2}}{2} \left(s_{i2} - s_{i1} \right) \tag{B.4}$$

With the sectional area then the aerodynamic mean chord length, assuming once more a linear variation of chord over the section, can be computed as

$$\bar{c}_i = \frac{1}{\delta A_i} \int_{s=s_1}^{s_2} c^2 \mathrm{d}s = \frac{2}{3} \frac{c_{i1}^2 + c_{i1} c_{i2} + c_{i2}^2}{c_{i1} + c_{i2}} \tag{B.5}$$

The dimensionless span-wise length is computed by normalizing the span-wise length vector, $\mathrm{d}l_i$, for each section. By definition of the vector $\vec{r}_0$ depicted in Figure 94 this normalization can be carried out as

$$\zeta_i \equiv \bar{c}_i \frac{\mathrm{d}\vec{l}_i}{\delta A_i} = \bar{c}_i \frac{\vec{r}_0}{\delta A_i} \tag{B.6}$$

The orientation vectors for each control point are defined according to the convention depicted in Figure 95. These three vectors describe the orientation of the local airfoil located at each section's control point, which are aligned to with the direction of the local chord and dihedral angle. For an unswept surface with no dihedral these vectors can be simply defined as a rotation of the coordinate system unit vectors.

Consider that the free-stream velocity $\vec{V}_{fs}$ which has magnitude V_∞ and is at some angles α and *beta* in relation to the zero-lift line of the system of lifting surfaces. The normal free-stream velocity, namely the unit vector in the direction of the free-stream flow, is taken as

$$\vec{v}_\infty = \frac{\vec{V}_{fs}}{V_\infty} \tag{B.7}$$

The normal and axial directions of the local velocity at each i control point due to the free-stream flow may be found as

$$v_{ni} = \vec{v}_\infty \cdot u_{ni} \tag{B.8}$$

$$v_{ai} = \vec{v}_\infty \cdot u_{ai} \tag{B.9}$$

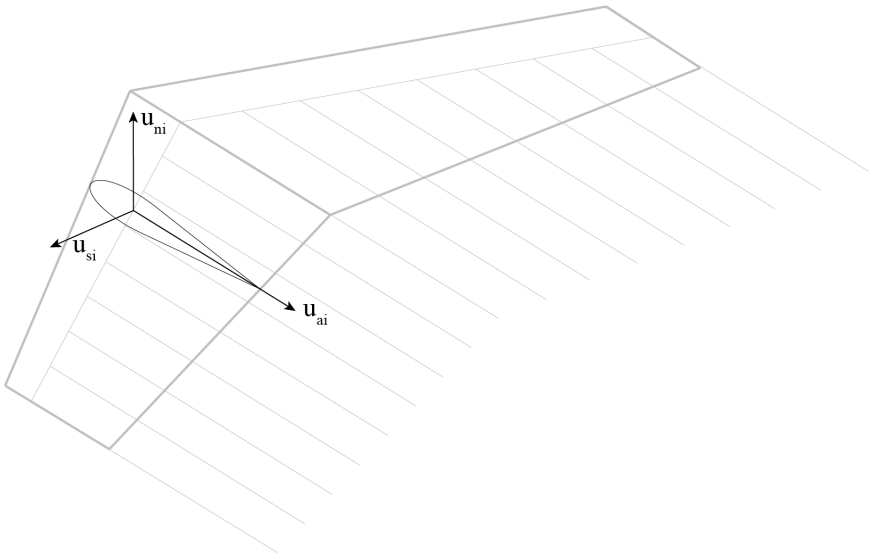

Figure 95: Orientation vectors for sample airfoil at i-th control point, adapted from [135].

These dot products then allow for the calculation of the local angle of attack at each control point as

$$\alpha_i = \tan^{-1}\left(\frac{v_{ni}}{v_{ai}}\right) \tag{B.10}$$

The local flow at each section is additionally affected by flow which is induced by the other vortices, both bound and free, that are present within the system of lifting surfaces. For some point in space the induced velocity due to a complete horseshoe vortex can be calculated through application of the Biot-Savart law. Referencing the vectors depicted in Figure 94 this induced velocity is given as

$$\vec{V}_{ind} = \frac{\Gamma}{4\pi}\left[\frac{\vec{u}_\infty \times \vec{r}_2}{r_2\left(r_2 - \vec{u}\infty \cdot \vec{r}_2\right)} + \frac{\left(r_1 + r_2\right)\left(\vec{r}_1 \times \vec{r}_2\right)}{r_1 r_2\left(r_1 r_2 + \vec{r}_1 \cdot \vec{r}_2\right)} - \frac{\vec{u}_\infty \times \vec{r}_1}{r_1\left(r_1 - \vec{u}_\infty \cdot \vec{r}_1\right)}\right] \tag{B.11}$$

where $\vec{u}_\infty$ is the unit vector in the direction of the trailing vortex (assumed to be equal to the free-stream flow) and the scalars r_1 and r_2 are the magnitudes of the vectors $\vec{r}_1$ and $\vec{r}_2$ respectively.

For an assumed vortex strengths Γ the velocity induced by all of the vortices in the system on each control point may be calculated, providing then an estimate of the total velocity at each control point. Looking to Prandtl's assumptions regarding

the sectional lift of a surface we may estimate the force generated at each section due to its vortex as

$$\mathrm{d}\vec{F} = \rho\Gamma\vec{V} \times \mathrm{d}\vec{l} \tag{B.12}$$

This sectional force should equal the sectional lift, which is in general a function of the local angle of attack and local surface deflection i.e. $C_{li} = C_{li}(\alpha_i, \delta_i)$. The residual of this relationship can be written as a function of the local vortex strengths Γ_i, and thus the lifting line analysis may be posed as an iterative algorithm which estimates the unknown vortex strengths by minimization of this sectional force residual.

In generating this algorithm, it is convenient to further follow the direction of Phillips and Snyder [135] in first developing non-dimensional forms of the key equations. First consider the non-dimensional induced velocity at control point j as induced by vortex located at control point i as

$$\vec{v}_{ij} \equiv \begin{cases} \frac{\bar{c}_i}{4\pi}\left[\frac{\vec{u}_\infty \times \vec{r}_{i2j}}{r_{i2j}(r_{i2j} - \vec{u}_\infty \cdot \vec{r}_{i2j})} + \frac{(r_{i1j}+r_{i2j})(r_{i1j}\times r_{i2j})}{r_{i1j}r_{i2j}(r_{i1j}r_{i2j} + \vec{r}_{i1j} + \cdot \vec{r}_{i2j})} - \frac{\vec{u}_\infty \times \vec{r}_{i1j}}{r_{i1j}(r_{i1j} - \vec{u}_\infty \cdot \vec{r}_{i1j})}\right], & i \neq j \\ \frac{\bar{c}_i}{4\pi}\left[\frac{\vec{u}_\infty \times \vec{r}_{i2j}}{r_{i2j}(r_{i2j} - \vec{u}_\infty \cdot \vec{r}_{i2j})} - \frac{\vec{u}_\infty \times \vec{r}_{i1j}}{r_{i1j}(r_{i1j} - \vec{u}_\infty \cdot \vec{r}_{i1j})}\right], & i = j \end{cases} \tag{B.13}$$

Taking the non-dimensional vortex strength $G_i \equiv \frac{\Gamma_i}{\bar{c}_i V_\infty}$ then the total non-dimensional velocity at a control point i due to the induced velocity of N total sections is

$$\vec{v}_i = \vec{v}_\infty + \sum_{j=1}^{N} v_{ji} G_j \tag{B.14}$$

The local angle of attack can be computed as

$$\alpha_i = \tan^{-1}\left(\frac{\vec{v}_i \cdot u_{ni}}{\vec{v}_i \cdot u_{ai}}\right) \tag{B.15}$$

Defining $\vec{w}_i$ as

$$\vec{w}_i \equiv \vec{v}_i \times \zeta_i \tag{B.16}$$

then the residual vector $\vec{R} \in \mathbb{R}^{N\times 1}$ is defined element-wise by

$$\vec{R}_i = 2\left|\vec{w}_i\right| G_i - C_{li}\left(\alpha_i, \delta_i\right) \tag{B.17}$$

If a Newton-based iterative scheme is used to minimize the residual vector, then the Jacobean matrix $\mathbf{J} \in \mathbb{R}^{N \times N}$ of the residual with respect to the non-dimensional vortex strength is required. This matrix can be determined analytically as

$$\mathbf{J}_{ij} = \begin{cases} \left[\frac{2\vec{w}_i \cdot (\vec{v}_{ij} \times \zeta_i)}{|\vec{w}_i|} G_i - \frac{\partial C_{li}}{\partial \alpha_i} \frac{v_{ai}(\vec{v}_{ji} \cdot \vec{u}_{ni}) - v_{ni}(\vec{v}_{ji} \cdot \vec{u}_{ai})}{v_{ai}^2 + v_{ni}^2} \right], & i \neq j \\ \left[2\,|\vec{w}_i| + \frac{2\vec{w}_i \cdot (\vec{v}_{ji} \times \zeta_j)}{|\vec{w}_i|} G_i - \frac{\partial C_{li}}{\partial \alpha_i} \frac{v_{ai}(\vec{v}_{ji} \cdot \vec{u}_{ni}) - v_{ni}(\vec{v}_{ji} \cdot \vec{u}_{ai})}{v_{ai}^2 + v_{ni}^2} \right], & i = j \end{cases} \tag{B.18}$$

The update for the non-dimensional vortex strength is then

$$\Delta \vec{G} = -\mathbf{J}^{-1} \vec{R} \tag{B.19}$$

providing the update equation

$$\vec{G} = \vec{G} + \Omega \Delta \vec{G} \tag{B.20}$$

with Ω as a factor of relaxation.

Once this minimization has been performed then the total vector force and moment can be computed as follows

$$\vec{\Gamma} = G \bar{c}^{\mathrm{T}} * V_\infty \tag{B.21}$$

$$\vec{F}_i = \vec{\Gamma}_i \vec{V}_{fs} + \sum_{j=1}^{N} \frac{\vec{\Gamma}_i \vec{\Gamma}_j}{\bar{c}_j} \vec{v}_{ji} \tag{B.22}$$

$$\vec{F} = \rho \sum_{i=1}^{N} \vec{F}_i \tag{B.23}$$

$$\delta \vec{M}_i = -\frac{1}{2} \rho V_\infty^2 C_{mi}(\alpha, \delta) \bar{c}_i \vec{u}_s \tag{B.24}$$

$$\vec{M} = \rho \sum_{i=1}^{N} \vec{r}_{cg} \times \vec{F}_i + \delta \vec{M}_i \tag{B.25}$$

Using these relationships an lifting line algorithm was defined for use in estimating the aerodynamic properties of the LWGA lifting surfaces. The algorithm mirrors the presented equations with modifications included to directly compute most dot products and cross products in scalar form in order to avoid the computational overhead required for direct calculation. In the algorithm the variables $\mathbf{r}_1$ and $\mathbf{r}_2$ will be

considered as three-dimensional arrays i.e. $\mathbf{r}_1, \mathbf{r}_2 \in \mathbb{R}^{N\times N\times 3}$, which may considered as a set of three $N \times N$ matrices. In this from each matrix relates to each Cartesian direction component of the vector $\vec{r}_1$ between the section edge and the full system control points. Indexing of the form $\mathbf{r}_1(i)$ refers then to the matrix corresponding to the i-th Cartesian direction. Similar indexing will be used for the matrices $\mathbf{u}_n, \mathbf{u}_a, \mathbf{u}_s, \zeta \in \mathbb{R}^{3\times N}$, with the indexed result yielding a vector of the appropriate dimension. This algorithm is provided herein as Algorithm 2.

Algorithm 2 Lifting Line

procedure LIFTINGLINE($\vec{V}_{fs}, \mathbf{r}_1, \mathbf{r}_2, \mathbf{r}_{cg}, \zeta, \bar{c}, \mathrm{d}\vec{l}, \mathbf{u}_n, \mathbf{u}_a, \mathbf{u}_s, \delta, \epsilon, \Omega$)
- $Vinf \leftarrow ||V_{fs}||$
- $vinf \leftarrow \frac{V_{fs}}{Vinf}$
- $uinf \leftarrow vinf$ ▷ Assume trailing vortices aligned with free-stream
- $G \leftarrow 0$
- $nr1 \leftarrow \sqrt{\mathbf{r}_1(1)^2 + \mathbf{r}_1(2)^2 + \mathbf{r}_1(3)^2}$ ▷ $||\vec{r}_1||$
- $nr2 \leftarrow \sqrt{\mathbf{r}_2(1)^2 + \mathbf{r}_2(2)^2 + \mathbf{r}_2(3)^2}$ ▷ $||\vec{r}_1||$
- $uidr1 \leftarrow uinf(1) * \mathbf{r}_1(1) + uinf(2) * \mathbf{r}_1(2) + uinf(3) * \mathbf{r}_1(3)$ ▷ $\vec{u}_\infty \cdot \vec{r}_1$
- $uidr2 \leftarrow uinf(1) * \mathbf{r}_2(1) + uinf(2) * \mathbf{r}_2(2) + uinf(3) * \mathbf{r}_2(3)$ ▷ $\vec{u}_\infty \cdot \vec{r}_2$
- $uicr1(1) \leftarrow uinf(2) * \mathbf{r}_1(3) - uinf(3) * \mathbf{r}_1(2)$ ▷ $\vec{u}_\infty \times \vec{r}_1$
- $uicr1(2) \leftarrow -uinf(1) * \mathbf{r}_1(3) + uinf(3) * \mathbf{r}_1(1)$
- $uicr1(3) \leftarrow uinf(1) * \mathbf{r}_1(2) - uinf(1) * \mathbf{r}_1(1)$
- $uicr2(1) \leftarrow uinf(2) * \mathbf{r}_2(3) - uinf(3) * \mathbf{r}_2(2)$ ▷ $\vec{u}_\infty \times \vec{r}_2$
- $uicr2(2) \leftarrow -uinf(1) * \mathbf{r}_2(3) + uinf(3) * \mathbf{r}_2(1)$
- $uicr2(3) \leftarrow uinf(1) * \mathbf{r}_2(2) - uinf(1) * \mathbf{r}_2(1)$
- $r1cr2(1) \leftarrow \mathbf{r}_1(2) * \mathbf{r}_2(3) - \mathbf{r}_1(3) * \mathbf{r}_2(2)$ ▷ $\vec{r}_1 \times \vec{r}_2$
- $r1cr2(2) \leftarrow -\mathbf{r}_1(1) * \mathbf{r}_2(3) + \mathbf{r}_1(3) * \mathbf{r}_2(1)$
- $r1cr2(3) \leftarrow \mathbf{r}_1(1) * \mathbf{r}_2(2) - \mathbf{r}_1(1) * \mathbf{r}_2(1)$
- $r1dr2 \leftarrow \mathbf{r}_1(1) * \mathbf{r}_2(1) + \mathbf{r}_1(2) * \mathbf{r}_2(2) + \mathbf{r}_1(3) * \mathbf{r}_2(3)$ ▷ $\vec{r}_1 \cdot \vec{r}_2$

while $R \geq \epsilon$ **do** ▷ Stopping criteria based on minimization of residual

$vind \leftarrow \frac{\bar{c}}{4\pi}\left(\frac{uicr2}{nr2*(nr2-uidr2)} + (nr1+nr2)\frac{r1cr2}{nr1*nr2(nr1*nr2+r1dr2)} - \frac{uicr1}{nr1*(nr1-uidr1)}\right)$

$vinddiag \leftarrow \frac{\bar{c}}{4\pi}\left(\frac{uicr2}{nr2*(nr2-uidr2)} - \frac{uicr1}{nr1*(nr1-uidr1)}\right)$

$vind(i,i) \leftarrow vinddiag(i,i)$

$vi \leftarrow G * vind$

$vl \leftarrow vinf + vi$

$$w \leftarrow \begin{bmatrix} vlocal(2)*\zeta(3) - vlocal(3)*\zeta(2) \\ -vlocal(1)*\zeta(3) + vlocal(3)*\zeta(1) \\ vlocal(1)*\zeta(2) - vlocal(2)*\zeta(1) \end{bmatrix}$$

$vn \leftarrow vl(1)*\mathbf{u}_n(1) + vl(2)*\mathbf{u}_n(2) + vl(3)*\mathbf{u}_n(3)$ ▷ $\vec{v}_n = \vec{v}_{local} \cdot \vec{u}_n$

$va \leftarrow vl(1)*\mathbf{u}_a(1) + vl(2)*\mathbf{u}_a(2) + vl(3)*\mathbf{u}_a(3)$ ▷ $\vec{v}_a = \vec{v}_{local} \cdot \vec{u}_a$

$\alpha \leftarrow \tan^{-1}\left(\frac{vn}{va}\right)$

$nw \leftarrow \sqrt{w(1)^2 + w(2)^2 + w(3)^2}$ ▷ $||\vec{w}||$

$Cl \leftarrow Cl(\alpha, \delta)$

$dCla \leftarrow dCl(\alpha, \delta)$

$R \leftarrow 2nw * G^{\mathrm{T}} - Cl$

$$vjicz \leftarrow \begin{bmatrix} vind(2)*\zeta(3) - vind(3)*\zeta(2) \\ -vind(1)*\zeta(3) - vind(3)*\zeta(1) \\ vind(1)*\zeta(2) - vind(2)*\zeta(1) \end{bmatrix}$$ ▷ $\vec{v}_{ji} \times \zeta$

$vjidun \leftarrow vind(1)*un(1) + vind(2)*un(2) + vind(3)*un(3)$ ▷ $\vec{v}_{ji} \cdot \vec{u}_n$

$vjidua \leftarrow vind(1)*ua(1) + vind(2)*ua(2) + vind(3)*ua(3)$ ▷ $\vec{v}_{ji} \cdot \vec{u}_a$

$Jn1 \leftarrow 2w(1)*vjicz(1) + w(2)*vjicz(2) + w(3)*vjicz(3)$

$J \leftarrow G\frac{Jni}{nw} - dCla * \frac{va*vjidun - vn*vjidua}{va^2+vn^2}$

$J(i,i) \leftarrow J(i.i) + 2nw$

$DelG \leftarrow -J^{-1}R$ ▷ $\Delta G = -J^{-1}R$

$G \leftarrow G + \Omega DelG$

end while

$Gam \leftarrow G * \bar{c} * Vinf$ ▷ $\Gamma = G\bar{c}V_\infty$

$fiVG \leftarrow V_{fs} + Gam\frac{vind}{\bar{c}}$

$$fiGcdl \leftarrow \begin{bmatrix} fiVG(2)*\mathrm{d}\vec{l}(3) - fiVG(3)*\mathrm{d}\vec{l}(2) \\ -fiVG(1)*\mathrm{d}\vec{l}(3) + fiVG(3)*\mathrm{d}\vec{l}(1) \\ fiVG(1)*\mathrm{d}\vec{l}(2) - fiVG(2)*\mathrm{d}\vec{l}(1) \end{bmatrix}$$

$Fi \leftarrow Gam * fiGcdl$

$F \leftarrow \rho\sum_{i=1}^{N} Fi$

$Cm \leftarrow Cm(\alpha, \delta)$

$dMi \leftarrow -0.5\rho * Vinf^2 * Cm * \bar{c} * \mathbf{u}_s$

$$rcFi \leftarrow \begin{bmatrix} \mathbf{r}_{cg}(2)*Fi(3) - \mathbf{r}_{cg}(3)*Fi(2) \\ -\mathbf{r}_{cg}(1)*Fi(3) + \mathbf{r}_{cg}(3)*Fi(1) \\ \mathbf{r}_{cg}(1)*Fi(2) - \mathbf{r}_{cg}(2)*Fi(1) \end{bmatrix}$$

$M \leftarrow \rho\sum_{i=1}^{N} rcFi + dMi$

end procedure

APPENDIX C

EQUATIONS OF MOTION

For the case of fixed-wing aircraft design, some common assumptions serve to greatly simplify the relevant equations of motion. In particular, the equations provided below utilize the flat-earth approximation, thereby neglecting effect of the Earth's rotation on the dynamics of the vehicle. The vehicle itself is treated as a rigid body and is assumed to have a plane of symmetry about the x-axis. With these assumptions, the nonlinear force equations expressed in wind axis are [48]

$$T_{x_W} - D - mg\sin\theta_W = m\dot{V} \tag{C.1}$$

$$T_{y_W} - C + mg\cos\theta_W \sin\phi_W = mVr_W \tag{C.2}$$

$$T_{z_W} - L + mg\cos\theta_W \cos\phi_W = -mVq_W \tag{C.3}$$

Similarly the nonlinear force and moment equations in body axis are [48]

$$X - mg\sin\theta = m\left(\dot{u} + qw - rv\right) \tag{C.4}$$

$$Y + mg\cos\theta\sin\phi = m\left(\dot{v} + ru - pw\right) \tag{C.5}$$

$$Z + mg\cos\theta\cos\phi = m\left(\dot{w} + pv - qu\right) \tag{C.6}$$

$$L = I_x\dot{p} - I_{zx}\left(\dot{r} + pq\right) - \left(I_y - I_z\right)qr \tag{C.7}$$

$$M = I_y\dot{q} - I_{zx}\left(r^2 - p^2\right) - \left(I_z - I_x\right)rp \tag{C.8}$$

$$N = I_z\dot{r} - I_{zx}\left(\dot{p} - qr\right) - \left(I_x - I_y\right)pq \tag{C.9}$$

Various transformations between wind axis angular rates, Euler angular rates, and

aerodynamic angles are often useful for dynamic analysis and are presented here [48]

$$\dot{\phi}_W = p_W + q_W \sin\phi_W \tan\theta_W + r_W \cos\phi_W \tan\theta_W \tag{C.10}$$

$$\dot{\theta}_W = q_W \cos\phi_W - r_W \sin\phi_W \tag{C.11}$$

$$\dot{\psi}_W = (q_W \sin\phi_W + r_W \cos\phi_W) \sec\theta_W \tag{C.12}$$

$$\dot{\alpha}_x = q - q_W \sec\beta - p\cos\alpha_x \tan\beta - r\sin\alpha_x \tan\beta \tag{C.13}$$

$$\dot{\beta} = r_W + p\sin\alpha_x - r\cos\alpha_x \tag{C.14}$$

$$\alpha_x = \tan^{-1}\frac{w}{u} \tag{C.15}$$

$$\beta = \sin^{-1}\frac{v}{V} \tag{C.16}$$

$$p_W = p\cos\alpha_x\cos\beta + (q - \dot{\alpha}_x)\sin\beta + r\sin\alpha_x\cos\beta \tag{C.17}$$

$$\dot{x}_E = V\cos\theta_W\cos\psi_W \tag{C.18}$$

$$\dot{y}_E = V\cos\theta_W\sin\psi_W \tag{C.19}$$

$$\dot{z}_E = -V\sin\theta_W \tag{C.20}$$

$$\begin{bmatrix} \dot{x}_E \\ \dot{y}_E \\ \dot{z}_E \end{bmatrix} = \mathbf{L}_{VB} \begin{bmatrix} u \\ v \\ w \end{bmatrix} \tag{C.21}$$

APPENDIX D

PROPAGATION OF MODEL UNCERTAINTY IN TRAJECTORY PREDICTION

In Chapter 5 the impact of dynamical model error on predicted trajectories was given as Equation (10). The related theorem and its proof are shown by Haddad and Chellaboina [77], and is repeated here for completeness.

Theorem 1. *Consider the nonlinear dynamical systems*

$$\dot{x}(t) = f(x(t)), \quad x(t_0) = x_0, \quad t \in [t_0, t_1] \tag{D.1}$$

$$\dot{y}(t) = g(y(t)), \quad y(t_0) = y_0, \quad t \in [t_0, t_1] \tag{D.2}$$

Assume that $f : \mathcal{D} \to \mathbb{R}^n$ is uniformly Lipschitz continuous on the domain $\mathcal{D}$ with some Lipschitz constant L. Additionally assume that $g : \mathcal{D} \to \mathbb{R}^n$ is Lipschitz continuous on the domain $\mathcal{D}$.

Suppose that

$$||f(x) - g(x)|| \leq \epsilon, \quad x \in \mathcal{D}$$

and that the initial conditions x_0 and y_0 are close to each other, such that

$$||x_0 - y_0|| \leq \gamma$$

Then the solutions $x(t)$ and $y(t)$ to systems f and g, respectively, on some time interval $\mathcal{I} \in \mathbb{R}$ are such that

$$||x(t) - y(t)|| \leq \gamma e^{L|t-t_0|} + \frac{\epsilon}{L}\left(e^{L|t-t_0|} - 1\right) \tag{D.3}$$

Proof. For some $t \in \mathcal{I}$ then

$$x(t) - y(t) = x_0 - y_0 + \int_{t_0}^{t} [f(x(s)) - g(y(s))]\, \mathrm{d}s. \tag{D.4}$$

Then,

$$||x(t) - y(t)|| \leq ||x_0 - y_0|| + \int_{t_0}^{t} ||f(x(s)) - g(x(s))|| \, \mathrm{d}s \tag{D.5}$$

$$\leq \gamma + \int_{t_0}^{t} ||f(x(s)) - f(y(s)) + f(y(s)) - g(y(s))|| \, \mathrm{d}s \tag{D.6}$$

$$\leq \gamma + \int_{t_0}^{t} ||f(x(s)) - f(y(s))|| \, \mathrm{d}s + \int_{t_0}^{t} ||f(y(s)) - g(y(s))|| \, \mathrm{d}s \tag{D.7}$$

$$\leq \gamma + \int_{t_0}^{t} L \, ||x(s) - y(s)|| \, \mathrm{d}s + \int_{t_0}^{t} \epsilon \mathrm{d}s, \quad t \in \mathcal{I}. \tag{D.8}$$

Let $q(t) \triangleq ||x(t) - y(t)||$, which implies

$$q(t) \leq \gamma + L \int_{t_0}^{t} \left[q(s) + \frac{\epsilon}{L} \right] \mathrm{d}s, \quad \in \mathcal{I} \tag{D.9}$$

$$q(t) + \frac{\epsilon}{L} \leq \gamma + \frac{\epsilon}{L} + L \int_{t_0}^{t} \left[q(s) + \frac{\epsilon}{L} \right] \mathrm{d}s, \quad \in \mathcal{I} \tag{D.10}$$

Using Gronwall's Lemma then

$$q(t) + \frac{\epsilon}{L} \leq \left(\frac{\epsilon}{L} + \gamma \right) e^{L|t - t_0|}, \quad t \in \mathcal{I} \tag{D.11}$$

Rearranging then yields

$$||x(t) - y(t)|| \leq \gamma e^{L|t - t_0|} + \frac{\epsilon}{L} \left(e^{L|t - t_0|} - 1 \right) \tag{D.12}$$

□

APPENDIX E

DERIVATION OF EXPECTATION-MAXIMIZATION ALGORITHM FOR CONTROL ESTIMATION

In general, the dynamics of a system can be expressed simply as Eq. (E.1).

$$\frac{\mathrm{d}\mathbf{x}}{\mathrm{d}t} = F(\mathbf{x}, \mathbf{u}, t) \tag{E.1}$$

By expanding this expression with a Taylor series expansion to first order terms, Eq. (E.1) can be rewritten as

$$\begin{aligned} \frac{\mathrm{d}\mathbf{x}}{\mathrm{d}t} &= F(\bar{\mathbf{x}} + \delta\mathbf{x}, \bar{\mathbf{u}} + \delta\mathbf{u}, t) = F(\bar{\mathbf{x}}, \bar{\mathbf{u}}, t) + \nabla_x F\delta\mathbf{x} + \nabla_u F\delta\mathbf{u} \\ \frac{\mathrm{d}\mathbf{x}}{\mathrm{d}t} &- F(\bar{\mathbf{x}}, \bar{\mathbf{u}}, t) = \nabla_x F\delta\mathbf{x} + \nabla_u F\delta\mathbf{u} \\ \frac{\mathrm{d}\delta\mathbf{x}}{\mathrm{d}t} &= \nabla_x F\delta\mathbf{x} + \nabla_u F\delta\mathbf{u} \end{aligned} \tag{E.2}$$

Utilizing the Euler method for the linearization and discretization of this expression yields

$$\begin{aligned} \frac{\mathrm{d}\delta\mathbf{x}}{\mathrm{d}t} &= \nabla_x F\mathrm{d}t\delta\mathbf{x} + \nabla_u F\mathrm{d}t\delta\mathbf{u} \\ \delta\mathbf{x}(t_{k+1}) - \delta\mathbf{x}(t_k) &= \nabla_x F\mathrm{d}t\delta\mathbf{x}(t_k) + \nabla_u F\mathrm{d}t\delta\mathbf{u}(t_k) \\ \delta\mathbf{x}(t_{k+1}) &= (I + \nabla_x F\mathrm{d}t)\,\delta\mathbf{x}(t_k) + \nabla_u F\mathrm{d}t\delta\mathbf{u}(t_k) \\ \delta\mathbf{x}(t_{k+1}) &= \mathbf{A}(t_k)\delta\mathbf{x}(t_k) + \mathbf{B}(t_k)\delta\mathbf{u}(t_k) \end{aligned} \tag{E.3}$$

Finally, with the inclusion of an observation output and some assumed noise for both the state and observation gives

$$\begin{aligned} \delta\mathbf{x}(t_{k+1}) &= \mathbf{A}(t_k)\delta\mathbf{x}(t_k) + \mathbf{B}(t_k)\delta\mathbf{u}(t_k) + \mathbf{w}(t_k) \\ \mathbf{y}(t_{k+1}) &= \mathbf{C}\delta\mathbf{x}(t_{k+1}) + \mathbf{n}(t_{k+1}) \end{aligned} \tag{E.4}$$

The noise signals $\mathbf{w}(t_k)$ and $\mathbf{n}(t_{k+1})$ are both assumed Gaussian distributed with zero mean and variances $\mathbf{Q}$ and $\mathbf{R}$, respectively.

Consider the feedback control policy expressed as

$$\delta\mathbf{u}(t_k) = \mathbf{L}(t_k)\delta\mathbf{x}(t_k) \tag{E.5}$$

This control parametrization assumes that the control is linked to the state of the system by some feedback matrix $\mathbf{L}$. In consideration of GA vehicles, this parametrization of the control seems an appropriate approximation, as there are typically no complex control systems on board. Rather, the pilot initiates various control commands in response to the current state of the vehicle, leading naturally to a proportional feedback parametrization of the control policy. With this parametrization, then the linearized system is

$$\begin{aligned}
\delta\mathbf{x}(t_{k+1}) &= \mathbf{A}(t_k)\delta\mathbf{x}(t_k) + \mathbf{B}(t_k)\mathbf{L}(t_k)\delta\mathbf{x}(t_k) + \mathbf{w}(t_k) \\
&= \left[\mathbf{A}(t_k) + \mathbf{B}(t_k)\mathbf{L}(t_k)\right]\delta\mathbf{x}(t_k) + \mathbf{w}(t_k) \\
\mathbf{y}(t_{k+1}) &= \mathbf{C}\delta\mathbf{x}(t_{k+1}) + \mathbf{n}(t_{k+1})
\end{aligned} \tag{E.6}$$

A similar expression of system dynamics was considered by Akyildiz [3] and in earlier work by Ghahramani et. al [67]. In his work, Akyildiz assumed a controlled linear dynamical system which is time-invariant and submitted an algorithm which estimated the feedback gain $\mathbf{L}$ given knowledge of the system parameters $\mathbf{A}, \mathbf{B}, \mathbf{C}, \mathbf{Q}$, and $\mathbf{R}$. However, typical aviation systems are non-linear and time-variant systems. Local linearization of aircraft dynamics is often feasible, yet the further assumption of time-invariance is typically far too restrictive. Yet, the method taken by Akyildiz does hold some promise for the problem at hand. Therefore, the derivation provided by Akyildiz will be mirrored, but adapted for the more general case of a non-linear system which is linearized at each time step.

The goal of the Expectation Maximization (EM) algorithm is to maximize the log likelihood of the random data $\mathbf{x}$ and $\mathbf{y}$, given the feedback gain matrix $\mathbf{L}(t_k)$. Considering some set of data with length T, this probability can be expressed with

the implicit Markov property as

$$P(\mathbf{x}_{1:T}, \mathbf{y}_{1:T}|\mathbf{L}_{1:T}) = P(x_1) \prod_{k=1}^{T-1} P(x_{k+1}|x_k, \mathbf{L}_k) \prod_{j=1}^{T} P(y_j|x_j) \tag{E.7}$$

Taking the log of this expression then yields

$$\log P(\mathbf{x}_{1:T}, \mathbf{y}_{1:T}|\mathbf{L}_{1:T}) = \log P(x_1) + \sum_{k=1}^{T-1} \log P(x_{k+1}|x_k, \mathbf{L}_k) + \sum_{j=1}^{T} \log P(y_j|x_j) \tag{E.8}$$

We are concerned with the second term of the final equation above, namely due to its dependence on the parametrization $\mathbf{L}$. The EM algorithm consists of two steps: estimation and maximization. During the estimation step (E-Step), the expected log likelihood is calculated based upon the current estimate of the system parameters, then during the maximization step (M-Step) the system parameters are updated by maximizing this expectation. After some iterations, an accurate estimate of unknown system parameters is acquired. For this particular application, the system parameter of interest is the feedback gain matrix, $\mathbf{L}$.

E.1 M-Step

For a simplification of notation, it is noted that several vectors and matrices are indexed by time t_k. To simplify, identification of the value for time t_k will be denoted simply by the subscript k.

By assuming that the random state variable, $\mathbf{x}_k$, is Gaussian distributed, then the probability $P(\mathbf{x}_{k+1}|\mathbf{x}_k, \mathbf{L}_k)$ is

$$P(\mathbf{x}_{k+1}|\mathbf{x}_k, \mathbf{L}_k) = \mathcal{N}(\mathbf{x}_{k+1}; (\mathbf{A}_k + \mathbf{B}_k\mathbf{L}_k), \mathbf{Q}) \tag{E.1}$$

where $\mathbf{A}_k$, $\mathbf{B}_k$, and $\mathbf{Q}$ are assumed to be known. Rewriting this expression yields

$$P(\mathbf{x}_{k+1}|\mathbf{x}_k, \mathbf{L}_k) = \frac{1}{\sqrt{(2\pi)^n |Q|}} \exp\left[-\frac{1}{2} \left(\mathbf{x}_{k+1} - (\mathbf{A}_k + \mathbf{B}_k\mathbf{L}_k)\, \mathbf{x}_k\right)^{\mathrm{T}} \mathbf{Q}^{-1} \left(\mathbf{x}_{k+1} - (\mathbf{A}_k + \mathbf{B}_k\mathbf{L}_k)\, \mathbf{x}_k\right)\right] \tag{E.2}$$

To find an update rule for $\mathbf{L}_k$, we will minimize the cost function

$$\mathcal{Q}(\mathbf{L}_k, \mathbf{L}_{k,old}) = -\frac{T-1}{2}\log|Q| - \mathbb{E}_{\mathbf{x}_{1:T}|\mathbf{L}_{old}}\left[\frac{1}{2}\sum_{k=1}^{T-1}\left(\mathbf{x}_{k+1} - \left(\mathbf{A}_k + \mathbf{B}_k\mathbf{L}_k\right)\mathbf{x}_k\right)^{\mathrm{T}}\mathbf{Q}^{-1}\left(\mathbf{x}_{k+1} - \left(\mathbf{A}_k + \mathbf{B}_k\mathbf{L}_k\right)\mathbf{x}_k\right)\right] \quad \text{(E.3)}$$

Taking the derivative of this cost function with respect to $\mathbf{L}$ provides

$$\frac{\partial\mathcal{Q}(\mathbf{L}_k, \mathbf{L}_{k,old})}{\partial\mathbf{L}} = -\frac{1}{2}\mathbb{E}_{\mathbf{x}_{1:T}|\mathbf{L}_{old}}\left[\sum_{k=1}^{T-1}\frac{\partial\left(\mathbf{x}_{k+1} - \left(\mathbf{A}_k + \mathbf{B}_k\mathbf{L}_k\right)\mathbf{x}_k\right)^{\mathrm{T}}\mathbf{Q}^{-1}\left(\mathbf{x}_{k+1} - \left(\mathbf{A}_k + \mathbf{B}_k\mathbf{L}_k\right)\mathbf{x}_k\right)}{\partial\mathbf{L}}\right] \quad \text{(E.4)}$$

Expanding the term within the numerator yields

$$\mathbf{x}_{k+1}^{\mathrm{T}}\mathbf{Q}^{-1}\mathbf{x}_{k+1} - \mathbf{x}_{k+1}^{\mathrm{T}}\mathbf{Q}^{-1}\left(\mathbf{A}_k + \mathbf{B}_k\mathbf{L}_k\right)\mathbf{x}_k - \mathbf{x}_k^{\mathrm{T}}\left(\mathbf{A}_k + \mathbf{B}_k\mathbf{L}_k\right)^{\mathrm{T}}\mathbf{Q}^{-1}\mathbf{x}_{k+1} + \mathbf{x}_k^{\mathrm{T}}\left(\mathbf{A}_k + \mathbf{B}_k\mathbf{L}_k\right)^{\mathrm{T}}\mathbf{Q}^{-1}\left(\mathbf{A}_k + \mathbf{B}_k\mathbf{L}_k\right)\mathbf{x}_k \quad \text{(E.5)}$$

$$\mathbf{x}_{k+1}^{\mathrm{T}}\mathbf{Q}^{-1}\mathbf{x}_{k+1} - \mathbf{x}_{k+1}^{\mathrm{T}}\mathbf{Q}^{-1}\mathbf{A}_k\mathbf{x}_k - \mathbf{x}_{k+1}^{\mathrm{T}}\mathbf{Q}^{-1}\mathbf{B}_k\mathbf{L}_k\mathbf{x}_k - \mathbf{x}_k^{\mathrm{T}}\mathbf{A}_k^{\mathrm{T}}\mathbf{Q}^{-1}\mathbf{x}_{k+1} - \mathbf{x}_k^{\mathrm{T}}\left(\mathbf{B}_k\mathbf{L}_k\right)^{\mathrm{T}}\mathbf{Q}^{-1}\mathbf{x}_{k+1} + \mathbf{x}_k^{\mathrm{T}}\mathbf{A}_k^{\mathrm{T}}\mathbf{Q}^{-1}\mathbf{A}_k\mathbf{x}_k + \mathbf{x}_k^{\mathrm{T}}\mathbf{A}_k^{\mathrm{T}}\mathbf{Q}^{-1}\left(\mathbf{B}_k\mathbf{L}_k\right)\mathbf{x}_k + \mathbf{x}_k^{\mathrm{T}}\left(\mathbf{B}_k\mathbf{L}_k\right)^{\mathrm{T}}\mathbf{Q}^{-1}\mathbf{A}_k\mathbf{x}_k + \mathbf{x}_k^{\mathrm{T}}\left(\mathbf{B}_k\mathbf{L}_k\right)^{\mathrm{T}}\mathbf{Q}^{-1}\left(\mathbf{B}_k\mathbf{L}_k\right)\mathbf{x}_k \quad \text{(E.6)}$$

As this term is scalar, one may take the trace of the entire expression and leverage trace properties to find

$$\mathrm{tr}\left[\mathbf{Q}^{-1}\mathbf{x}_{k+1}\mathbf{x}_{k+1}^{\mathrm{T}} - \mathbf{Q}^{-1}\mathbf{A}_k\mathbf{x}_k\mathbf{x}_{k+1}^{\mathrm{T}} - \mathbf{Q}^{-1}\mathbf{B}_k\mathbf{L}_k\mathbf{x}_k\mathbf{x}_{k+1}^{\mathrm{T}} - \mathbf{A}_k^{\mathrm{T}}\mathbf{Q}^{-1}\mathbf{x}_{k+1}\mathbf{x}_k^{\mathrm{T}} - \left(\mathbf{B}_k\mathbf{L}_k\right)^{\mathrm{T}}\mathbf{Q}^{-1}\mathbf{x}_{k+1}\mathbf{x}_k^{\mathrm{T}} + \mathbf{A}_k^{\mathrm{T}}\mathbf{Q}^{-1}\mathbf{A}_k\mathbf{x}_k\mathbf{x}_k^{\mathrm{T}} + \mathbf{A}_k^{\mathrm{T}}\mathbf{Q}^{-1}\mathbf{B}_k\mathbf{L}_k\mathbf{x}_k\mathbf{x}_k^{\mathrm{T}} + \left(\mathbf{B}_k\mathbf{L}_k\right)^{\mathrm{T}}\mathbf{Q}^{-1}\mathbf{A}_k\mathbf{x}_k\mathbf{x}_k^{\mathrm{T}} + \left(\mathbf{B}_k\mathbf{L}_k\right)^{\mathrm{T}}\mathbf{Q}^{-1}\mathbf{B}_k\mathbf{L}_k\mathbf{x}_k\mathbf{x}_k^{\mathrm{T}}\right] \quad \text{(E.7)}$$

Recalling that $\mathrm{tr}A = \mathrm{tr}A^{\mathrm{T}}$, this can be reduced to

$$\mathrm{tr}\left[\mathbf{Q}^{-1}\mathbf{x}_{k+1}\mathbf{x}_{k+1}^{\mathrm{T}} - 2\mathbf{Q}^{-1}\mathbf{A}_k\mathbf{x}_k\mathbf{x}_{k+1}^{\mathrm{T}} - 2\mathbf{Q}^{-1}\mathbf{B}_k\mathbf{L}_k\mathbf{x}_k\mathbf{x}_{k+1}^{\mathrm{T}} + \mathbf{A}_k^{\mathrm{T}}\mathbf{Q}^{-1}\mathbf{A}_k\mathbf{x}_k\mathbf{x}_k^{\mathrm{T}} + 2\mathbf{A}_k^{\mathrm{T}}\mathbf{Q}^{-1}\mathbf{B}_k\mathbf{L}_k\mathbf{x}_k\mathbf{x}_k^{\mathrm{T}} + \mathbf{L}_k^{\mathrm{T}}\mathbf{B}_k^{\mathrm{T}}\mathbf{Q}^{-1}\mathbf{B}_k\mathbf{L}_k\mathbf{x}_k\mathbf{x}_k^{\mathrm{T}}\right] \quad \text{(E.8)}$$

Applying the partial derivative gives

$$-\frac{\partial\left[2\mathbf{Q}^{-1}\mathbf{B}_k\mathbf{L}_k\mathbf{x}_k\mathbf{x}_{k+1}^{\mathrm{T}}\right]}{\partial\mathbf{L}}-\frac{\partial\left[2\mathbf{A}_k^{\mathrm{T}}\mathbf{Q}^{-1}\mathbf{B}_k\mathbf{L}_k\mathbf{x}_k\mathbf{x}_k^{\mathrm{T}}\right]}{\partial\mathbf{L}}+\frac{\partial\left[\mathbf{L}_k^{\mathrm{T}}\mathbf{B}_k^{\mathrm{T}}\mathbf{Q}^{-1}\mathbf{B}_k\mathbf{L}_k\mathbf{x}_k\mathbf{x}_k^{\mathrm{T}}\right]}{\partial\mathbf{L}} \quad \text{(E.9)}$$

In order to proceed, consider the following derivative definitions:

$$\frac{\mathrm{d}}{\mathrm{d}\mathbf{X}}\mathrm{tr}\mathbf{A}\mathbf{X}=\mathbf{X} \quad \text{(E.10)}$$

$$\frac{\mathrm{d}}{\mathrm{d}\mathbf{X}}\mathrm{tr}\mathbf{A}\mathbf{X}\mathbf{B}=\mathbf{B}\mathbf{A} \quad \text{(E.11)}$$

With these definitions, the previous partial derivative is seen to be

$$-2\mathbf{x}_k\mathbf{x}_{k+1}^{\mathrm{T}}\mathbf{Q}^{-1}\mathbf{B}_k-2\mathbf{x}_k\mathbf{x}_k^{\mathrm{T}}\mathbf{A}_k^{\mathrm{T}}\mathbf{Q}^{-1}\mathbf{B}_k+2\mathbf{x}_k\mathbf{x}_k^{\mathrm{T}}\mathbf{L}_k^{\mathrm{T}}\mathbf{B}_k^{\mathrm{T}}\mathbf{Q}^{-1}\mathbf{B}_k \quad \text{(E.12)}$$

This expression can now be replaced in the full expression for the partial derivative of the cost function to give

$$\frac{\partial\mathcal{Q}(\mathbf{L}_k,\mathbf{L}_{k,old})}{\partial\mathbf{L}}= \mathbb{E}_{\mathbf{x}_{1:T}|\mathbf{L}_{old}}\left[\sum_{k=1}^{T-1}\mathbf{x}_k\mathbf{x}_{k+1}^{\mathrm{T}}\mathbf{Q}^{-1}\mathbf{B}_k+\mathbf{x}_k\mathbf{x}_k^{\mathrm{T}}\mathbf{A}_k^{\mathrm{T}}\mathbf{Q}^{-1}\mathbf{B}_k-\mathbf{x}_k\mathbf{x}_k^{\mathrm{T}}\mathbf{L}_k^{\mathrm{T}}\mathbf{B}_k^{\mathrm{T}}\mathbf{Q}^{-1}\mathbf{B}_k\right] \quad \text{(E.13)}$$

To find the maximal L, we set $\frac{\partial\mathcal{Q}(\mathbf{L}_k,\mathbf{L}_{k,old})}{\partial\mathbf{L}}=0$. To further simplify, let the following matrices be defined

$$E_{k|k+1}=\mathbb{E}_{\mathbf{x}_{1:T}|L_{old}}\left[x_kx_{k+1}^{\mathrm{T}}\right] \quad \text{(E.14)}$$

$$E_{k|k}=\mathbb{E}_{\mathbf{x}_{1:T}|L_{old}}\left[x_kx_k^{\mathrm{T}}\right] \quad \text{(E.15)}$$

This results in the equation

$$\sum_{k=1}^{T-1}\left[E_{k|k+1}\mathbf{Q}^{-1}\mathbf{B}_k+E_{k|k}\mathbf{A}_k^{\mathrm{T}}\mathbf{Q}^{-1}\mathbf{B}_k\right]=\sum_{k=1}^{T-1}E_{k|k}\mathbf{L}_k^{\mathrm{T}}\mathbf{B}_k^{\mathrm{T}}\mathbf{Q}^{-1}\mathbf{B}_k \quad \text{(E.16)}$$

Considering that the summations are satisfied by setting each corresponding term to be equal, then

$$E_{k|k+1}\mathbf{Q}^{-1}\mathbf{B}_k+E_{k|k}\mathbf{A}_k^{\mathrm{T}}\mathbf{Q}^{-1}\mathbf{B}_k=E_{k|k}\mathbf{L}_k^{\mathrm{T}}\mathbf{B}_k^{\mathrm{T}}\mathbf{Q}^{-1}\mathbf{B}_k \quad \text{(E.17)}$$

Denoting the matrices

$$\mathbf{M}_k = \mathbf{B}_k^{\mathrm{T}} \mathbf{Q}^{-1} \mathbf{B}_k \tag{E.18}$$

$$\mathbf{N}_k = E_{k|k} \tag{E.19}$$

$$\mathbf{Z}_k = E_{k|k+1} \mathbf{Q}^{-1} \mathbf{B}_k + E_{k|k} \mathbf{A}_k^{\mathrm{T}} \mathbf{Q}^{-1} \mathbf{B}_k \tag{E.20}$$

then,

$$\mathbf{Z}_k = \mathbf{N}_k \mathbf{L}_k^{\mathrm{T}} \mathbf{M}_k \tag{E.21}$$

Then solving for $\mathbf{L}_k$, we find

$$\mathbf{L}_k = \mathbf{M}_k^{-1} \mathbf{Z}_k^{\mathrm{T}} \mathbf{N}_k^{-1} \tag{E.22}$$

E.2 E-Step

With an estimate of the feedback gain $\mathbf{L}_k$ and knowledge of the matrices $\mathbf{A}_k, \mathbf{B}_k, \mathbf{C}, \mathbf{Q}$, and $\mathbf{R}$, an estimation of the log likelihood can be derived. The derivation of this step is readily available within the literature. Specifically, Ghahramani et. al [67] have provided the appropriate relationships needed for the E-Step. These step will be repeated here, with some minor modifications. Primarily, the system matrix $\mathbf{A}$ used by Ghahramani et. al is replaced with the dynamics derived previously with the form $\mathbf{A}+\mathbf{BL}$, and will be considered in general to be time-dependent. In doing so, consider the matrix $\tilde{A}_k$ as

$$\tilde{A}_k = A_k + B_k L_k$$

Hence $\tilde{A}_k$ can be directly substituted into the steps outlined by Ghahramani et. al.

First, define $\mathbf{x}_t^\tau$ to denote $\mathbb{E}\left(\mathbf{x}_t | \{\mathbf{y}\}_1^\tau\right)$ and V_t^τ to denote $\mathrm{Var}\left(\mathbf{x}_t | \{\mathbf{y}\}_1^\tau\right)$. With these

definitions, then the Kalman filter forward recursions are

$$\mathbf{x}_{k+1}^{k} = \tilde{A}_k \mathbf{x}_k^k \tag{E.1}$$

$$V_{k+1}^{k} = \tilde{A}_k V_k^k \tilde{A}_k{}^{\mathrm{T}} + \mathbf{Q} \tag{E.2}$$

$$K_{k+1} = V_{k+1}^{k} \mathbf{C}^{\mathrm{T}} \left(\mathbf{C} V_{k+1}^{k} \mathbf{C}^{\mathrm{T}} + \mathbf{R} \right)^{-1} \tag{E.3}$$

$$\mathbf{x}_{k+1}^{k+1} = \mathbf{x}_{k+1}^{k} + K_{k+1} \left(\mathbf{y}_{k+1} - \mathbf{C} \mathbf{x}_{k+1}^{k} \right) \tag{E.4}$$

$$V_{k+1}^{k+1} = V_{k+1}^{k} - K_{k+1} \mathbf{C} V_{k+1}^{k} \tag{E.5}$$

Next, the state estimate (i.e. $\mathbf{x}_k^T = \mathbb{E}\left(\mathbf{x}_T | \{\mathbf{y}\}_1^T \right)$) is made using a backward pass from the equations

$$J_k = V_k^k \tilde{A}_k{}^{\mathrm{T}} (V_{k+1}^k)^{-1} \tag{E.6}$$

$$\mathbf{x}_k^T = \mathbf{x}_k^k + J_k (x_{k+1}^T - \tilde{A}_k x_k^k) \tag{E.7}$$

$$V_k^T = V_k^k + J_k \left(V_{k+1}^T - V_{k+1}^k \right) J_k^{\mathrm{T}} \tag{E.8}$$

Additionally, an expression for the variance $V_{k,k-1}^T$ is needed for the M-Step. This expression can be calculated with a backward propagation as

$$V_{k,k-1}^T = V_k^k J_{k-1}^{\mathrm{T}} + J_k \left(V_{k-1}^T - \tilde{A}_k V_{k-1}^k \right) J_k^{\mathrm{T}} \tag{E.9}$$

initialized as $V_{T,T-1}^T = (I - K_T \mathbf{C}) \tilde{A}_k V_{T-1}^{T-1}$.

APPENDIX F

DATA VISUALIZATION

In this appendix, various figures are collected which aid in the interpretation and demonstration of the presented methods. The first set of figures are those which visualize aspects of the developed vehicle model. A second set is collected from the results of Experiment 3 for the low gain and high pilot models.

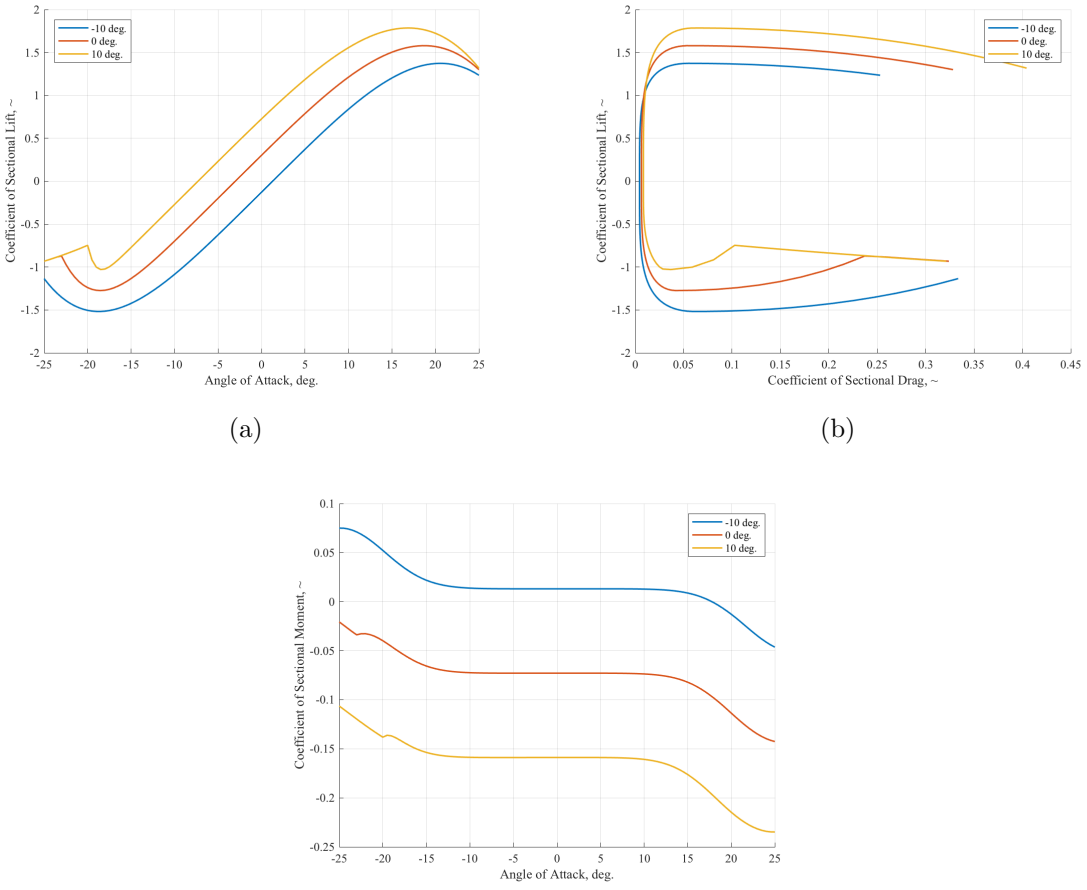

(a) (b)

(c)

Figure 96: Sectional lift, drag, and moment coefficient for LWGA wing airfoil, NACA $65_2 - 415$.

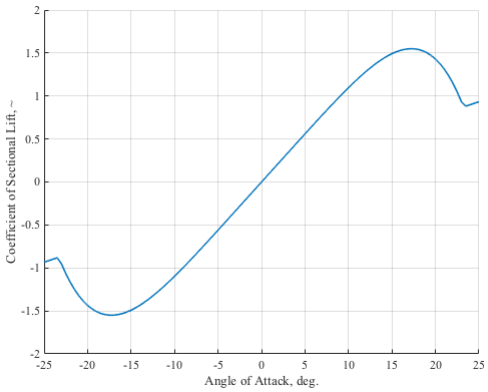

(a)

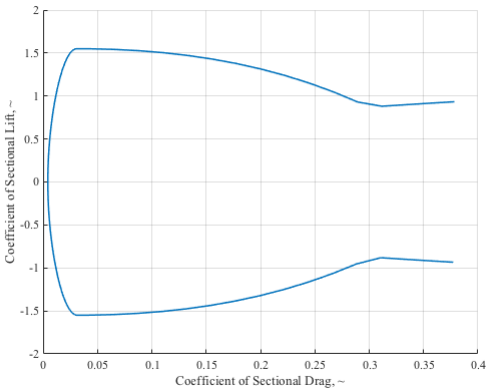

(b)

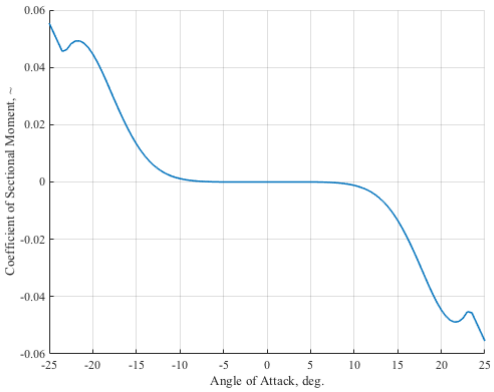

(c)

Figure 97: Sectional lift, drag, and moment coefficient for LWGA horizontal tail airfoil, NACA 0012.

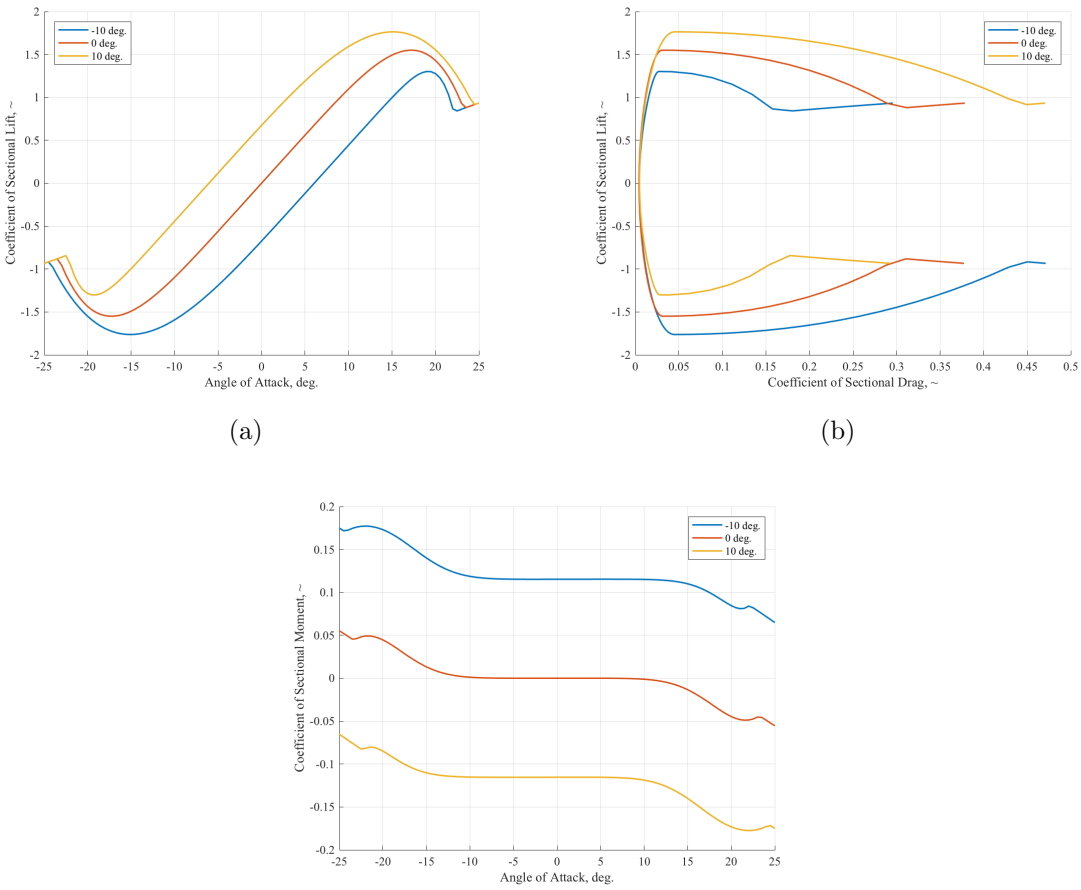

(a) (b)

(c)

Figure 98: Sectional lift, drag, and moment coefficient for LWGA vertical tail airfoil, NACA 0010.

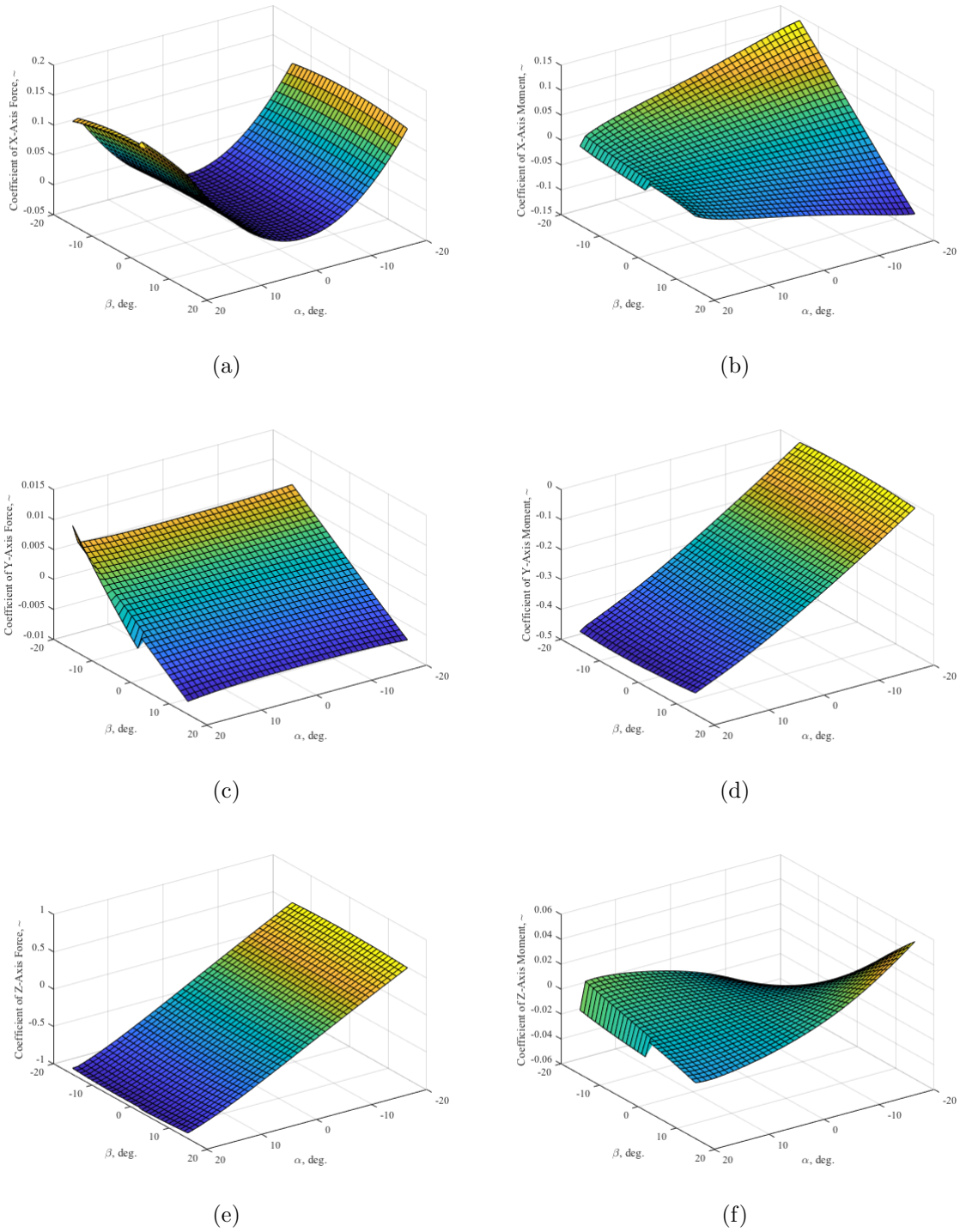

Figure 99: Force and moment coefficients for LWGA wing.

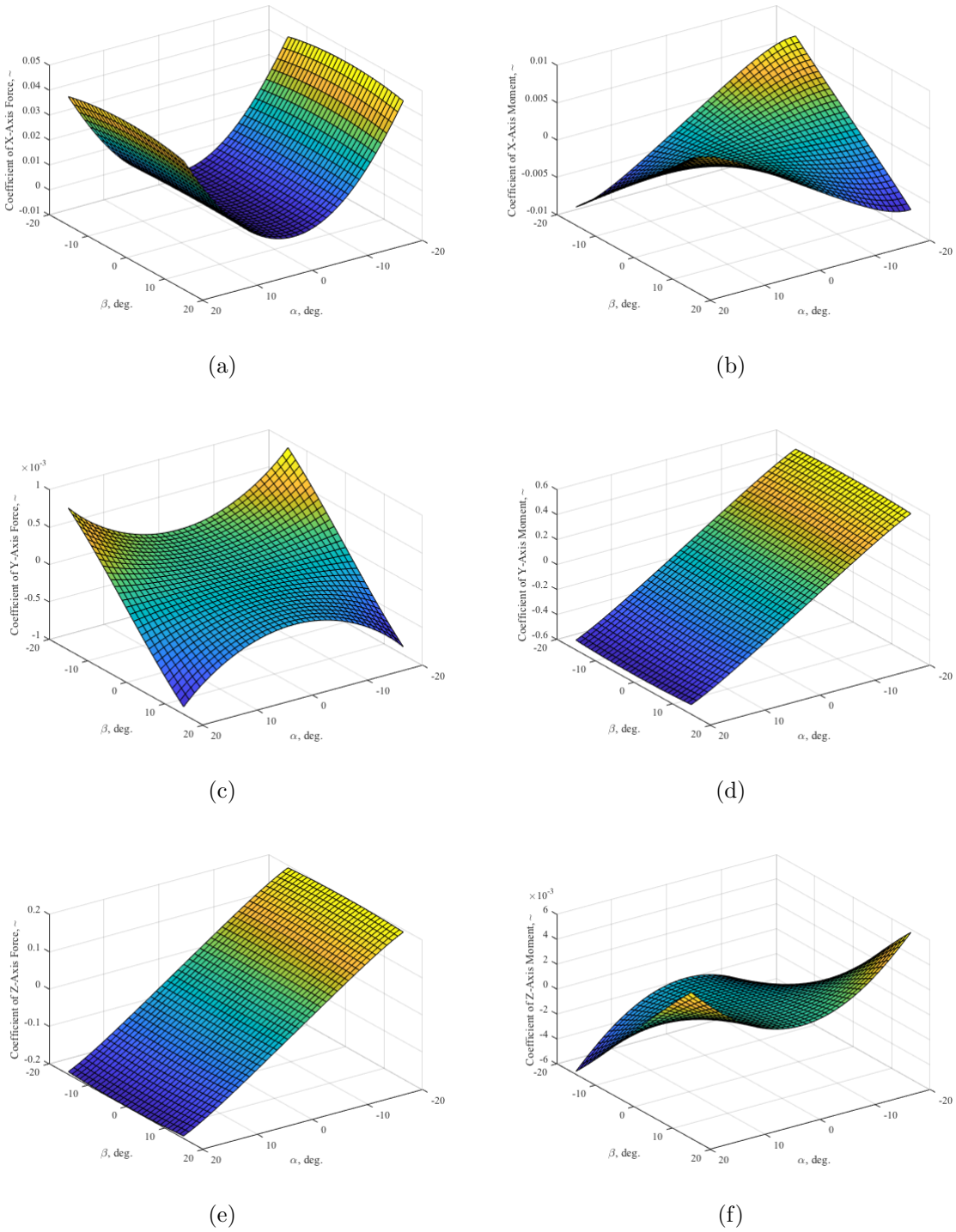

Figure 100: Force and moment coefficients for LWGA horizontal tail.

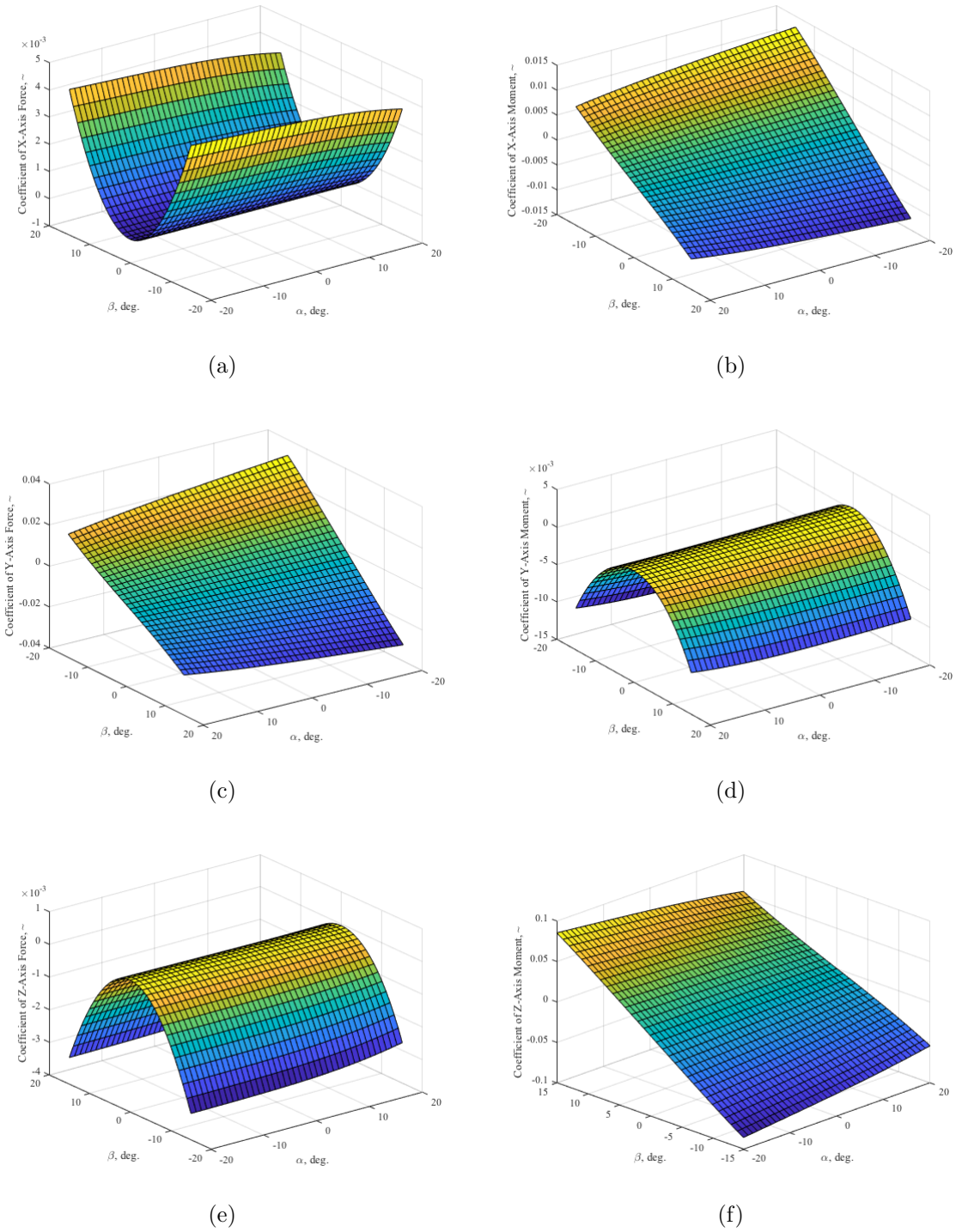

Figure 101: Force and moment coefficients for LWGA vertical tail.

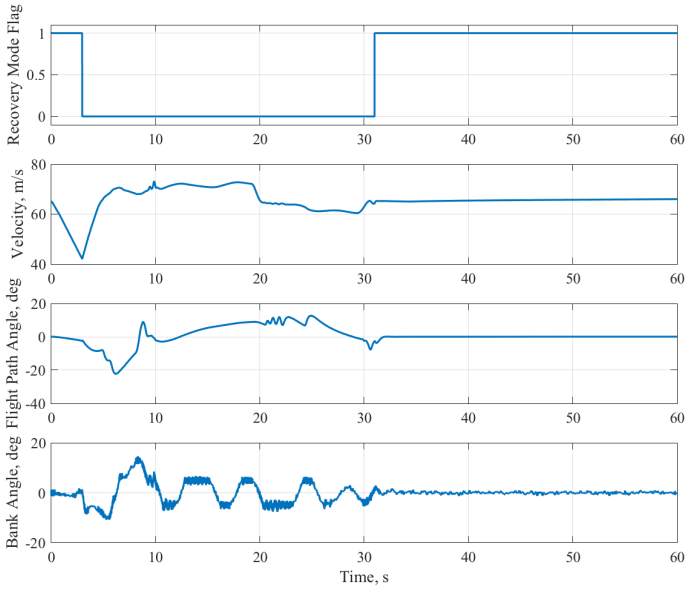

(a)

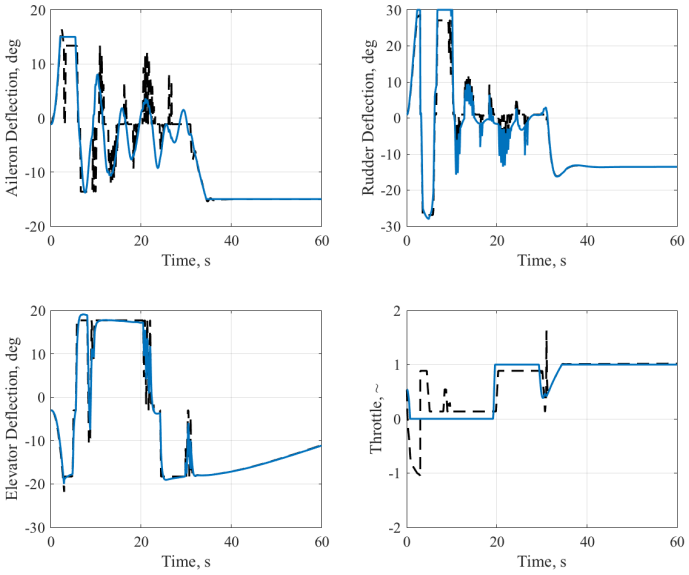

(b)

Figure 102: Trajectory and control history for low velocity scenario with high gain pilot model.

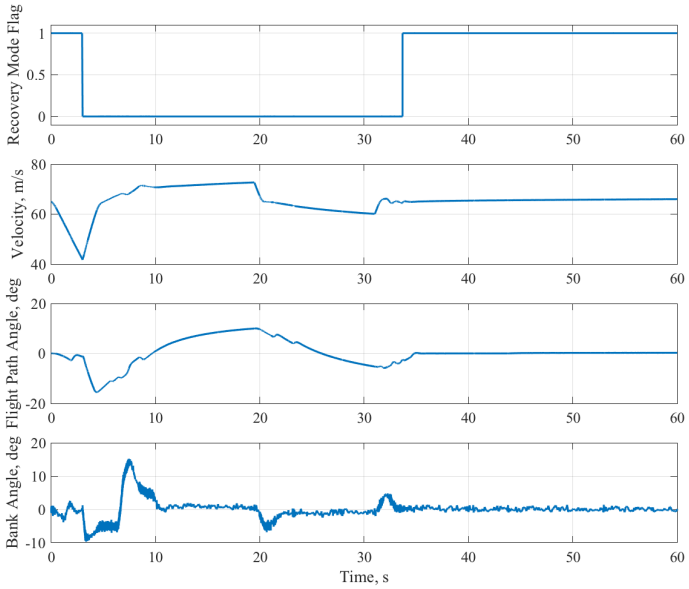

(a)

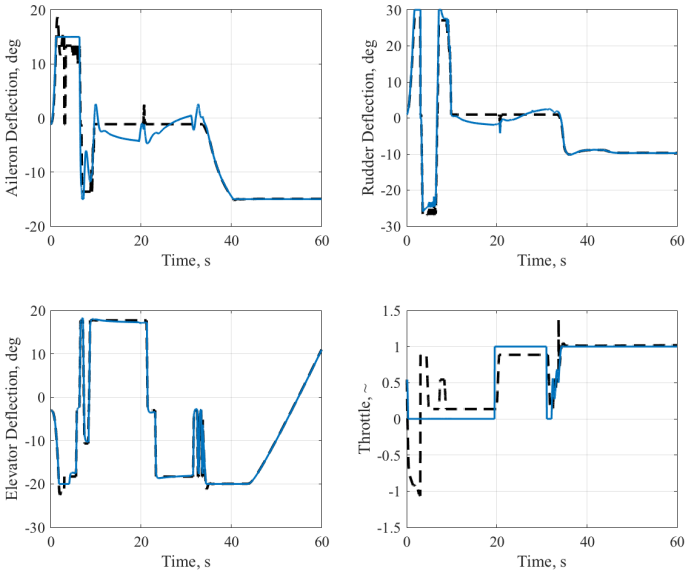

(b)

Figure 103: Trajectory and control history for low velocity scenario with low gain pilot model.

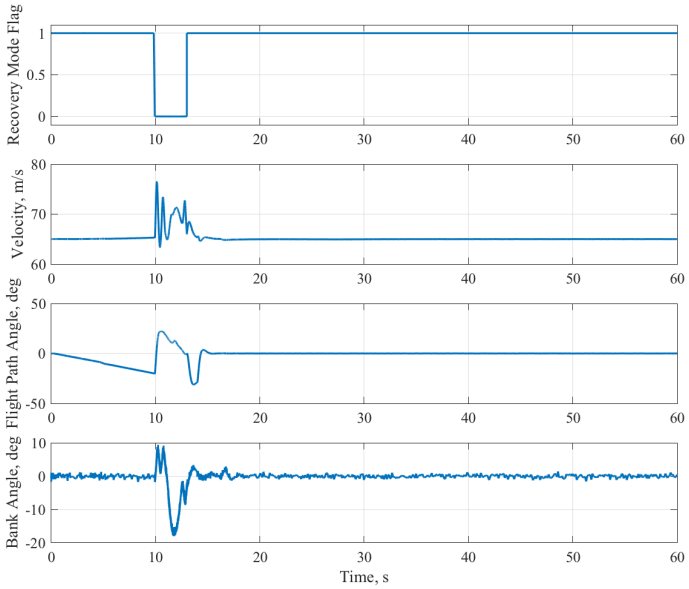

(a)

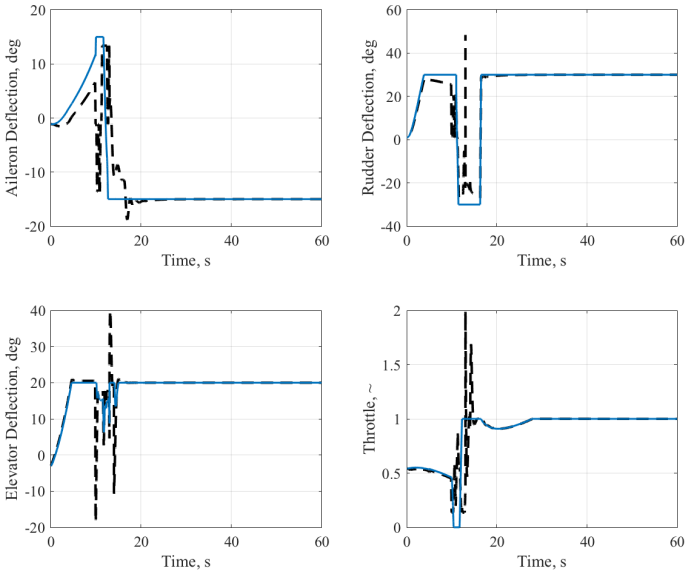

(b)

Figure 104: Trajectory and control history for low flight path angle scenario with high gain pilot model.

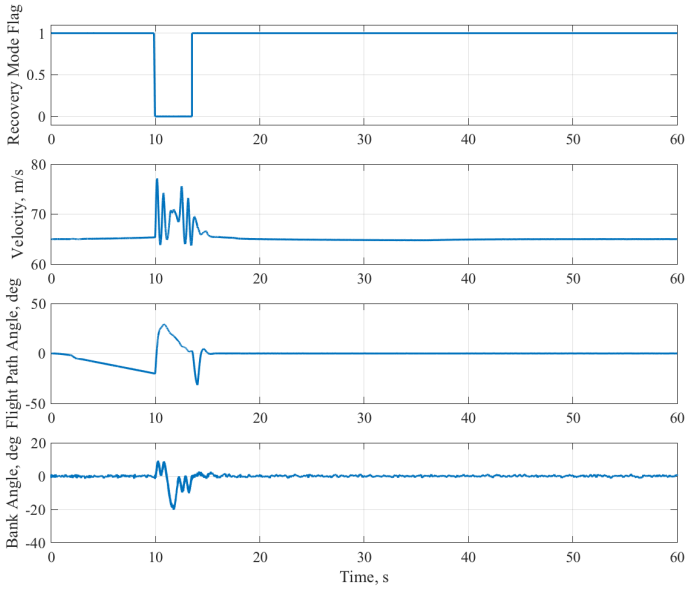

(a)

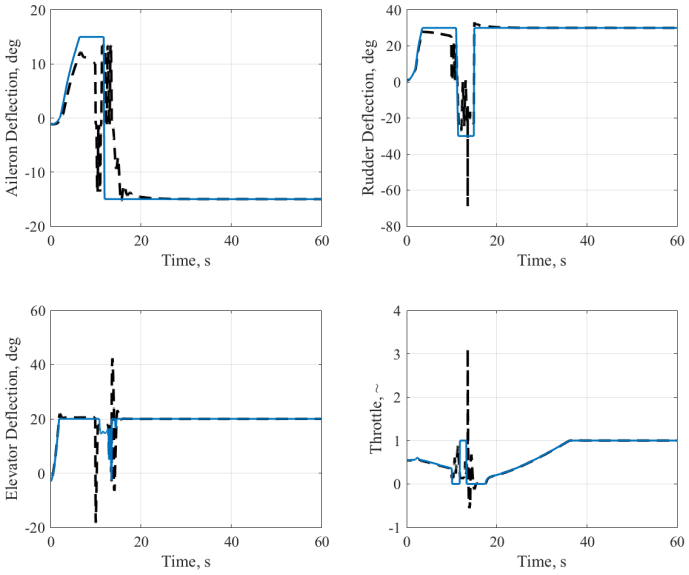

(b)

Figure 105: Trajectory and control history for low flight path angle scenario with low gain pilot model.

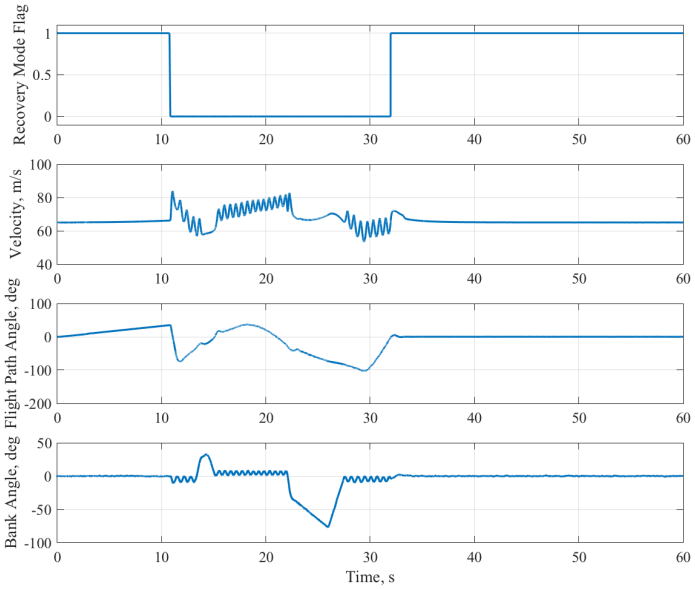

(a)

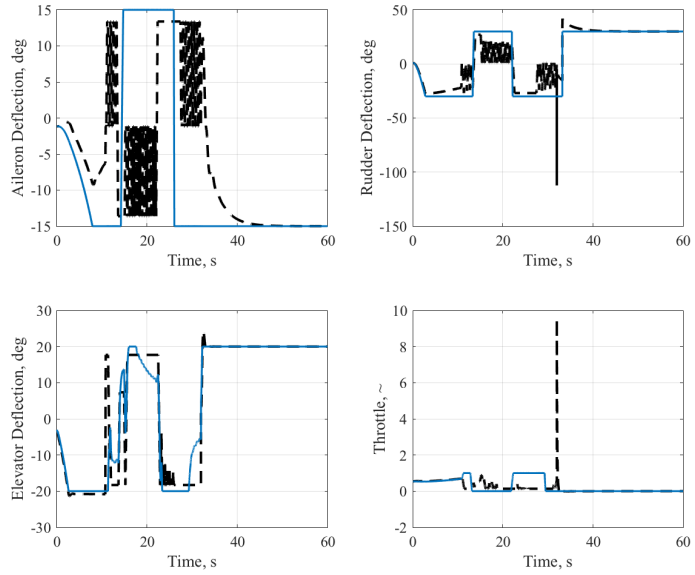

(b)

Figure 106: Trajectory and control history for high flight path angle scenario with low gain pilot model.

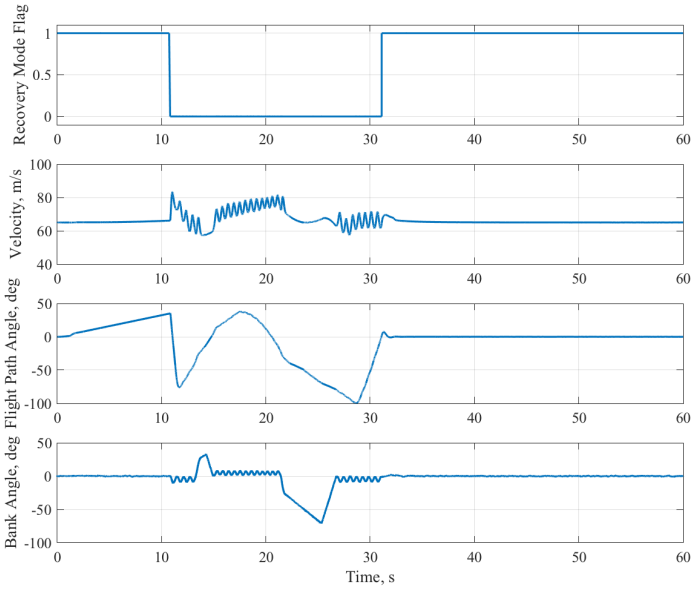

(a)

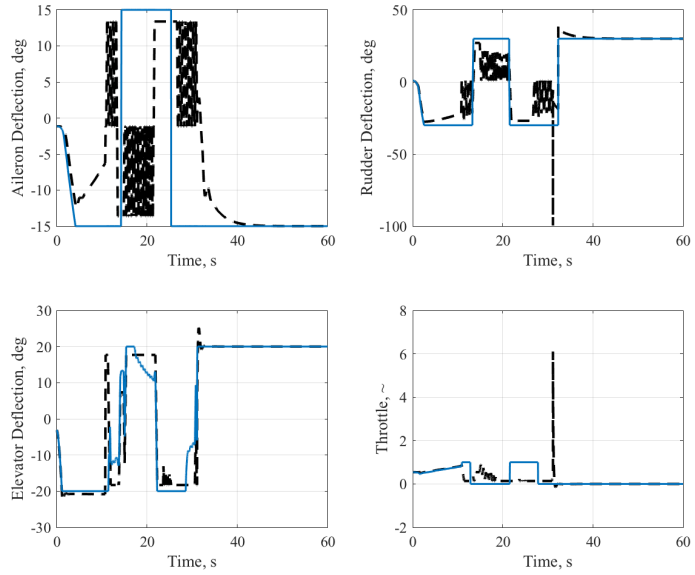

(b)

Figure 107: Trajectory and control history for high flight path angle scenario with low gain pilot model.

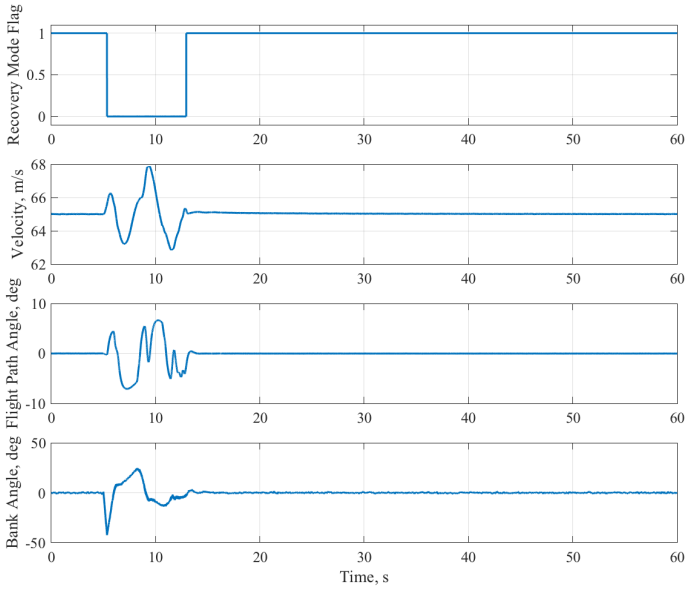

(a)

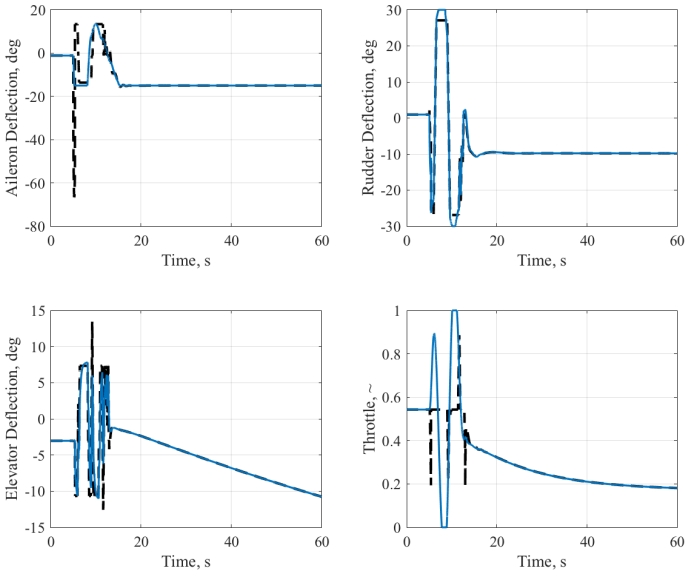

(b)

Figure 108: Trajectory and control history for high bank path angle scenario with high gain pilot model.

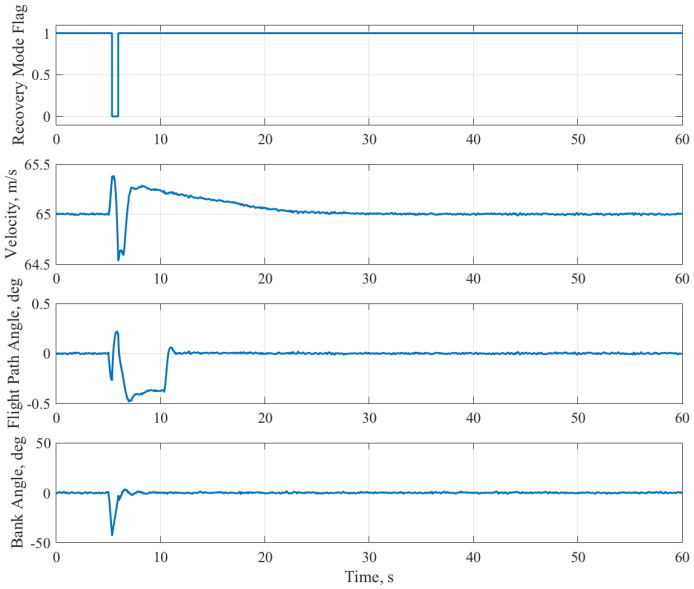

(a)

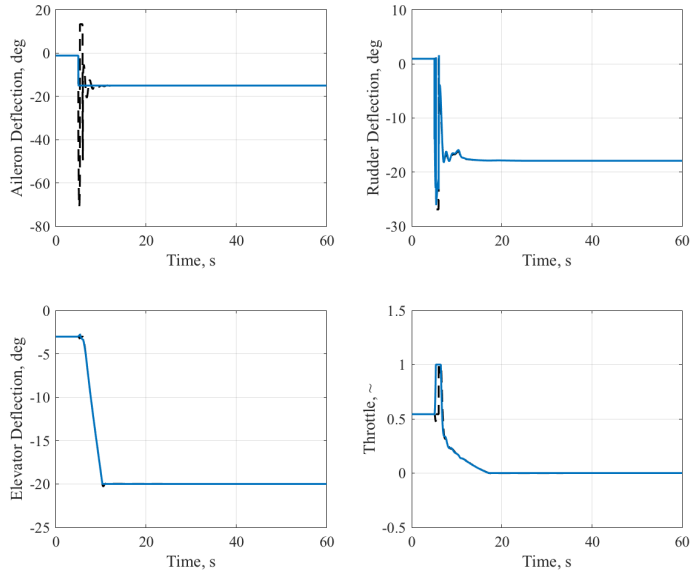

(b)

Figure 109: Trajectory and control history for high bank angle scenario with low gain pilot model.

REFERENCES

[1] Abbott, I. H. and von Doenhoff, A. E., *Theory of Wing Sections*. 1949.

[2] Abdallah, A., Newman, B., and Omran, A., "Measuring aircraft nonlinearity across aerodynamic attitude flight envelope-revisited with symmetrized aerodynamics," in *AIAA Aviation*, 2014.

[3] Akyildiz, O. D., "An em algorithm for learning in controlled linear dynamical systems," 2013.

[4] Allen, H. J., "Estimation of the forces and moments acting on inclined bodies of revolution of high fineness ratio," Tech. Rep. NACA-RM-A9I26, NACA, 1949.

[5] Allen, R. C. and Kwatny, H. G., "Maneuverability and envelope protection in the prevention of aircraft loss of control," in *Proceedings of 2011 8th Asian Control Conference*, 2011.

[6] Althoff, M., Stursberg, O., and Buss, M., "Reachability analysis of linear systems with uncertain parameters and inputs," in *Proceedings of the 46th IEEE Conference on Decision and Control*, 2007.

[7] Althoff, M., Stursberg, O., and Buss, M., "Reachability analysis of nonlinear systems with uncertain parameters using conservative linearization," in *Proceedings of the 47th IEEE Conference on Decision and Control*, 2008.

[8] Amelink, M. H. J., Mulder, M., Passen, M. M. R. V., and Flach, J., "Theoretical foundations for a total energy-bared perspective flight-path display," *The International Journal of Aviation Psychology*, vol. 15, no. 3, pp. 205 – 231, 2005.

[9] Ananda, G. K. and Selig., M. S., "Stall/post-stall modeling of the longitudinal characteristics of a general aviation aircraft," in *AIAA Atmospheric Flight Mechanics Conference, AIAA AVIATION Forum*, 2016.

[10] Ananthkirshnan, N. and Sinha, N. K., "Level flight trim and stability analysis using extended bifurcation and continuation procedure," *Journal of Guidance*, vol. 24, no. 6, 2001.

[11] Anderson Jr., J. D., *Fundamentals of Aerodynamics*. McGraw-Hill Education, 2010.

[12] Asarin, E., Dang, T., and Girard, A., *Reachability Analysis of Nonlinear Systems Using Conservative Approximation*, pp. 20–35. Berlin, Heidelberg: Springer Berlin Heidelberg, 2003.

[13] Baghdadi, N., Lowenberg, M. H., and Isikveren, A. T., "Application of bifurcation and continuation methods to nonlinear flexible aircraft dynamics," in *AIAA Guidance, Navigation, and Control Conference*, 2009.

[14] Barlow, J. S., Stepanyan, V., and Krishnakumar, K., "Estimating loss-of-control: a data-based predictive control approach," *AIAA Guidance, Navigation, and Control Conference*, no. AIAA 2011-6408, 2011.

[15] Barlow, J. S., Stepanyan, V., and Krishnakumar, K., "Predicting loss-of-control boundaries toward a piloting aid," *Infotech@Aerospace*, no. AIAA 2012-2579, 2012.

[16] Belcastro, C. M., "Aircraft loss of control: Analysis and requirements for future safety-critical systems and their validation," in *Proceedings of 2011 8th Asian Control Conference*, 2011.

[17] Belcastro, C. M. and Foster, J. V., "Aircraft loss-of-control accident analysis," in *AIAA Guidance, Navigation, and Control Conference*, 2010.

[18] Belcastro, C. M., Foster, J. V., Newman, R. L., Groff, L., Crider, D. A., and Klyde, D. H., "Aircraft loss of control: problem analysis for the development and validation of technology solutions," in *AIAA Guidance, Navigation, and Control Conference*, p. 0092, 2016.

[19] Belcastro, C. M., Foster, J. V., Shah, G. H., Gregory, I. M., Cox, D. E., Crider, D. A., Groff, L., Newman, R. L., and Klyde, D. H., "Aircraft loss of control problem analysis and research toward a holistic solution," *Journal of Guidance, Control, and Dynamics*, vol. 40, 4 2017.

[20] Belcastro, C. M., Groff, L., Newman, R. L., Foster, J. V., Crider, D. A., and Klyde, D. H., "Preliminary analysis of aircraft loss of control accidents: Worst case precursor combinations and temporal sequencing," in *AIAA Guidance, Navigation, and Control Conference*, 2014.

[21] Belcastro, C. M. and Jacobson, S. R., "Future integrated systems concept for preventing aircraft loss-of-control accidents," in *AIAA Guidance, Navigation, and Control Conference*, 2010.

[22] Bergqvist, P., "Piper archer through the years." `https://www.flyingmag.com/aircraft/pistons/piper-archer-through-years`, 2011.

[23] Betz, A., "Schraubenpropeller mit geringstem energieverlust," *Gottinger Nachrichten*, pp. 193–213, 1919.

[24] Bihrle, W., Barnhart, B., and Pantason, P., "Static aerodynamic characteristics of a typical single-engine low-wing general aviation design for an angle-of-attack range of -8 ° to 90 °," Tech. Rep. NASA-CR-2971, National Aeronautics and Space Administration, 1978.

[25] Bihrle, W. and Bowman, J. S., "Influence of wing, fuselage, and tail design on rotational flow aerodynamics beyond maximum lift," *Journal of Aircraft*, vol. 18, no. 11, pp. 920–925, 1981.

[26] Bihrle, W., Hultberg, R. S., and Mulcay, W., "Rotary balance data for a typical single-engine low-wing general aviation design for an angle-of-attack range of 30 to 90," Tech. Rep. NASA-CR-2972, National Aeronautics and Space Administration, 1978.

[27] Blanke, M., Staroswiecki, M., and Wu, N. E., "Concepts and methods in fault-tolerant control," in *Proceedings of the American Control Conference*, 2001.

[28] Boeing, "Statistical summary of commercial jet airplane accidents: Worldwide operations 1959-2016," tech. rep., 2017.

[29] Boyd, J. R., Christie, T. P., and Gibson, J. E., "Energy maneuverability," *Air Proving Ground Center Report APGC-TR-66-4*, vol. 1, 1966.

[30] Bunge, R. A., Alkurdi, A. E., Alfaris, E., and Kroo, I. M., "In-flight measurement of wing surface pressures on a small-scale uav during stall/spin maneuvers," in *AIAA Aviation*, 2016.

[31] Carroll, J. V. and Mehra, R. K., "Bifurcation analysis of nonlinear aircraft dynamics," *Journal of Guidance*, vol. 5, 9 1982.

[32] CAST/ICAO Common Taxonomy Team, "Aviation Occurrence Categories: Definitions and Usage Notes," 2013.

[33] Castrup, H., "Distributions for uncertainty analysis," in *Proc. Int. Dimensional Workshop (IDW)*, vol. 1, pp. 1–12, 2001.

[34] Chang, B.-C., , Kwatny, H. G., Belcastro, C., and Belcastro, C., "Aircraft loss-of-control accident prevention: Switching control of the gtm aircraft with elevator jam failures," in *AIAA Guidance, Navigation and Control Conference and Exhibit*, 2008.

[35] Chapman, C., Bushnell, M., Miron, D., Duncan, G., and Lund', J., "Sensory perception during movement in man," *Experimental Brain Research*, vol. 68, pp. 516–524, 1987.

[36] Cordero, M., Alarcon, F., Jimenez, A., Viguria, A., and Ollero, A., "Survey on attitude and heading reference systems for remotely piloted aircraft systems," in *2014 International Conference on Unmanned Aircraft Systems (ICUAS)*, 2014.

[37] Cummings, P. A., "Continuation methods for qualitative analysis of aircraft dynamics," Tech. Rep. NASA/CR-2004-213035 NIA Report No. 2004-06, National Aeronautics and Space Administration, 2004.

[38] DeMarco, A., Duke, E. L., and Berndt, J. S., "A general solution to the aircraft trim problem," in *AIAA Modeling and Simulation Technologies Conference and Exhibit*, 2007.

[39] Donato, P. F. D., Balachandran, S., McDonough, K., Atkins, E., and Kolmanovsky, I., "Envelope-aware flight management for loss of control prevention given rudder jam," *Journal of Guidance, Control, and Dynamics*, vol. 40, no. 4, 2017.

[40] Dongmo, J.-E. T., *Aircraft Loss-of-Control Prevention and Recovery: A Hybrid Control Strategy.* PhD thesis, Drexel University, 2010.

[41] Dongmo, J.-E. T., "Aircraft loss-of-control recovery using nonlinear smooth feedback regulators," in *Infotech@Aerospace*, 2011.

[42] Dongmo, J.-E. T., "Aircraft loss-of-control recovery using feedback linearization and high order sliding mode control," in *AIAA Guidance, Navigation, and Control Conference*, 2012.

[43] Dongmo, J.-E. T., "Nonlinear smooth trackers with control rates constraints for aeronautical vehicles loss-of-control autonomous recovery," in *AIAA SciTech*, 2015.

[44] Dongmo, J.-E. T., "Post loss-of-control autonomous recovery flight regimes using nonlinear smooth feedback regulators and neural network with nonlinear observers," in *AIAA SciTech*, 2016.

[45] Dongmo, J.-E. T., "Compact nonlinear smooth trackers with exponential observers using hybrid control rates design for flight vehicles loss-of-control autonomous recovery," in *AIAA SciTech*, 2017.

[46] Drela, M., *XFOIL: An analysis and design system for low Reynolds number airfoils*, 1989.

[47] Dual, "Dual gps solutions xgps170d," 2018. Accessed 10/18.

[48] Etkin, B., *Dynamics of Atmospheric Flight*. Dover Publications, 2000.

[49] Falkena, W., Borst, C., Chu, Q. P., and Mulder, J. A., "Investigation of practical flight envelope protection systems for small aircraft," *Journal of Guidance, Control, and Dynamics*, vol. 34, 7 2011.

[50] Federal Aviation Administration, "Airport characteristics database."

[51] Federal Aviation Administration, "Introduction to TCAS II Version 7.1," 2011.

[52] Federal Aviation Administration, "General Aviation and Part 135 Activity Surveys - CY 2015." https://www.faa.gov/data_research/aviation_data_statistics/general_aviation/CY2015/, November 2016.

[53] Federal Aviation Administration, "Advanced Avionics Handbook." https://www.faa.gov/regulations_policies/handbooks_manuals/aviation/advanced_avionics_handbook/, 2017.

[54] Federal Aviation Administration, "Airplane Flying Handbook." https://www.faa.gov/regulations_policies/handbooks_manuals/aviation/airplane_handbook/, 2017.

[55] Federal Aviation Administration, "Airworthiness standards: Normal, utility, acrobatic, and commuter catergory airplanes," *CFR Title 14, Pt. 23*, 2017.

[56] Federal Aviation Administration, "Airworthiness standards: Transport category airplanes," *CFR Title 14, Pt. 25*, 2017.

[57] Federal Aviation Administration, "Fact Sheet - General Aviation Safety." https://www.faa.gov/news/fact_sheets/news_story.cfm?newsId=21274, 10 2017.

[58] Federal Aviation Administration, "Fly Safe: Prevent Loss of Control Accidents." https://www.faa.gov/news/updates/?newsId=87169, 1 2017.

[59] Ferguson, C., *Internal Combustion Engines: Applied Thermodynamics*. John Wiley & Sons, 1986.

[60] Foreflight, "Stratus portable receivers." https://www.foreflight.com/products/stratus/. Accessed 10/18.

[61] Foster, J. V., Cunningham, K., Fremaux, C. M., Shah, G. H., and Stewart, E. C., "Dynamics modeling and simulation of large transport airplanes in upset conditions," in *AIAA Guidance, Navigation, and Control Conference and Exhibit*, 2005.

[62] Fravolini, M. L., Pastorelli, M., Pagnotelli, S., Valigi, P., Gururajan, S., Chao, H., and Napolitano, M. R., "Model-based approaches for the airspeed estimation and fault monitoring of an unmanned aerial vehicle," in *Environmental Energy and Structural Monitoring Systems (EESMS), 2012 IEEE Workshop on*, 2012.

[63] Fravolini, M. L., Rhudy, M., Gururajan, S., Cascianelli, S., and Napolitano, M., "Experimental evaluation of two pitot free analytical redundancy techniques for the estimation of the airspeed of an uav," *SAE International Journal of Aerospace*, vol. 7, 2014.

[64] Garcia, G., Keshmiri, S., and Huang, W., "Recovery of an aircraft from the loss of control using open final time dynamic optimization and receding horizon control," in *AIAA SciTech*, 2015.

[65] Gebre-Egziabher, D., Hayward, R. C., and Powell, J. D., "A low-cost gps/inertial attitude heading reference system (ahrs) for general aviation applications," in *Position Location and Navigation Symposium, IEEE 1998*, pp. 518–525, IEEE, 1998.

[66] General Aviation Manufacturers Association, "2016 General Aviation Statistical Databook & 2017 Industry Outlook." `https://gama.aero/wp-content/uploads/2016-GAMA-Databook_forWeb.pdf`, 2016.

[67] Ghahramani, Z. and Hinton, G. E., "Parameter estimation for linear dynamical systems," tech. rep., Technical Report CRG-TR-96-2, University of Totronto, Dept. of Computer Science, 1996.

[68] Gilbert, E. G. and Tan, K. T., "Linear systems with state and control constraints: The theory and application of maximal output admissible sets," *IEEE Transactions on Automatic Control*, vol. 36, no. 9, 1991.

[69] Gill, S. J., Lowenberg, M. H., Neild, S. A., Krauskopf, B., Puyou, G., and Coetzee, E., "Upset dynamics of an airliner model: A nonlinear bifurcation analysis," *Journal of Aircraft*, vol. 50, no. 6, 2013.

[70] Glaab, L. J. and Takallu, M. A., "Preliminary effect of synthetic vision systems displays to reduce low-visibility loss of control and controlled flight into terrain accidents," in *General Aviation Technology Conference and Exhibition*, 2002.

[71] Goldstein, S., "On the vortex theory of screw propellers," *Proceedings of the Royal Society of London*, 1929.

[72] Goman, M. G. and Khramtsovsky, A. V., "Global stability analysis of nonlinear aircraft dynamics," in *22nd Atmospheric Flight Mechanics Conference*, 1997.

[73] Goman, M. G. and Khramtsovsky, A. V., "Application of continuation and bifurcation methods to the design of control systems," *Philosophical Transactions of the Royal Society of London A: Mathematical, Physical and Engineering Sciences*, vol. 356, no. 1745, pp. 2277–2295, 1998.

[74] Goman, M. G. and Khramtsovsky, A. V., "Computational framework for investigation of aircraft nonlinear dynamics," *Advances in Engineering Software*, vol. 39, no. 3, pp. 167 – 177, 2008.

[75] Goman, M., Zagainov, G., and Khramtsovsky, A., "Application of bifurcation methods to nonlinear flight dynamics problems," *Progress in Aerospace Sciences*, vol. 33, no. 9, pp. 539 – 586, 1997.

[76] Gudmundsson, S., *General Aviation Aircraft Design: Applied Methods and Procedures*. Elsevier, 2014.

[77] Haddad, W. M. and Chellaboina, V., *Nonlinear Dynamical Systems and Control: A Lyapunov-based approach*. Princeton University Press, 2008.

[78] Harrison, E., Jimenez, H., and Mavris, D., "Investigation and flight dynamic analysis of general aviation safety," in *AIAA Atmospheric Flight Mechanics Conference*, 2016.

[79] Harrison, E., Min, S., Jimenez, H., and Mavris, D., "Implementation and validation of an internal combustion engine and propeller model for general aviation performance studies," *AIAA Aviation*, 2015.

[80] Haynes, G. W. and Hermes, H., "Nonlinear controllability vs lie theory," *Journal of Aircraft*, vol. 8, 11 1970.

[81] Hepner, S. A. R. and Geering, H. P., "Observability analysis for target maneuver estimation via bearing-only and bearing-rate-only measurements," *Journal of Guidance*, vol. 13, 11 1990.

[82] Hwang, I., Kim, S., Kim, Y., and Seah, C. E., "A survey of fault detection, isolation, and reconfiguration methods," *IEEE Transactions on Control Systems Technology*, vol. 18, pp. 636–653, 5 2010.

[83] Iliff, K. W., "Parameter estimation for flight vehicles," *Journal of Guidance, Control, and Dynamics*, vol. 12, no. 5, pp. 609–622, 1989.

[84] Inertial Labs, "Attitude and heading reference systems key performance," 2018. Accessed 10/18.

[85] ISO, "Iso/iec guide 98-3: 2008, guide to the expression of uncertainty in measurement," *International Organization for Standardization, Geneva, Switzerland*, 2008.

[86] ISO, "Iso/iec guide 98-3/suppl.1: 2008, propagation of distributions using a monte carlo method," *International Organization for Standardization, Geneva, Switzerland*, 2008.

[87] Jackson, P., Peacock, L. T., Bushnell, S., Willis, D., and Winchester, J., *Jane's All the World's Aircraft 2017-2018: Development & Production*. IHS Global, 2017.

[88] Jacobson, S. R., "Aircraft loss of control causal factors and mitigation challenges," in *AIAA Guidance, Navigation, and Control Conference*, 2010.

[89] Jeram, G. J., "Open platform for limit protection with carefree maneuver applications," 12 2004.

[90] Jorgensen, L. H., "Effects of reynolds number and body corner radius on aerodynamic characteristics of a space shuttle-type vehicle at subsonic mach numbers," Tech. Rep. NASA-TN-D-6615, National Aeronautics and Space Administration, 1972.

[91] Jorgensen, L. H., "A method for estimating static aerodynamic characteristics for slender bodies of circular and noncircular cross sections alone and with lifting surfaces at angles of attack from 0 to 90," Tech. Rep. NASA-TN-D-7228, National Aeronautics and Space Administration, 1973.

[92] Jorgensen, L. H., "Prediction of static aerodynamic characteristics for space-shuttle-like and other bodies at angles of attack from 0 to 180," Tech. Rep. NASA-TN-D-6996, National Aeronautics and Space Administration, 1973.

[93] Keller, J. D., Robert M. McKillip, J., and Kim, S., "Aircraft flight envelope determination using upset detection and physical modeling methods," *AIAA Guidance, Navigation, and Control Conference*, 2009.

[94] Kolmanovsky, I. and Gilbert, E. G., "Theory and computation of disturbance invariant sets for discrete-time linear systems," *Mathematical Problems in Engineering*, vol. 4, pp. 317–367, 1998.

[95] Kwatny, H. G., Bennett, W. H., and Berg, J., "Regulation of relaxed static stability aircraft," *IEEE Transactions on Automatic Control*, vol. 36, 11 1991.

[96] Kwatny, H. G., Chang, B.-C., and Wang, S.-P., *Static Bifurcation in Mechanical Control Systems*, pp. 67–81. Berlin, Heidelberg: Springer Berlin Heidelberg, 2003.

[97] Kwatny, H. G., Dongmo, J.-E. T., Allen, R. C., and Chang, B.-C., "Loss-of-control: Perspectives on flight dynamics and control of impaired aircraft," in *AIAA Guidance, Navigation, and Control Conference*, 2010.

[98] Kwatny, H. G., Dongmo, J.-E. T., Chang, B.-C., Bajpai, G., Yasar, M., and Belcastro, C., "Aircraft accident prevention: Loss-of-control analysis," *AIAA Guidance, Navigation, and Control Conference*, 2009.

[99] Kwatny, H. G., Dongmo, J.-E. T., Chang, B.-C., Bajpai, G., Yasar, M., and Belcastro, C., "Nonlinear analysis of aircraft loss of control," *Journal of Guidance, Control, and Dynamics*, vol. 36, no. 1, 2013.

[100] Laghrouche, S., Plestan, F., and Glumineau, A., "Multivariable practical higher order sliding mode control," in *Decision and Control, 2005 and 2005 European Control Conference. CDC-ECC'05. 44th IEEE Conference on*, pp. 1252–1257, IEEE, 2005.

[101] Lambregts, A. A., Nesemeier, G., Wilborn, J. E., and Newman, R. L., "Airplane upset: Old problem, new issues," in *AIAA Modeling and Simulation Technologies Conference and Exhibit*, 2008.

[102] Lee, D.-C. and Nagati, M., "Optimal control strategy for spin recovery," 1997.

[103] Levil Aviation, "ilevil 3 sw," 2018. Accessed 10/18.

[104] Levil Aviation, "ilevil sport - warranty standard (2 year)," 2018. Accessed 10/18.

[105] Lombaerts, T. J. J., Schuet, S. R., Wheeler, K. R., Acosta, D. M., and Kaneshige, J. T., "Safe maneuvering envelope estimation based on a physical approach," in *AIAA Guidance, Navigation, and Control (GNC) Conference*, 2013.

[106] Lygeros, J., "On reachability and minimum cost optimal control," *Automatica*, vol. 40, no. 6, pp. 917 – 927, 2004.

[107] Martin, C. and Hill, S., "Prediction of aircraft spin recovery," in *16th Atmospheric Flight Mechanics Conference*, 1989.

[108] Mattingley, J., Wang, Y., and Boyd, S., "Receding horizon control," *IEEE Control Systems*, vol. 31, no. 3, pp. 52–65, 2011.

[109] McCormick, B. W., *Aerodynamics, Aeronautics and Flight Mechanics*. John Wiley, New York, second edition ed., 1995.

[110] McDonald, R., "Openvsp," *URL: www. openvsp. org [cited 27 September 2018]*, 2018.

[111] McDonough, K. and Kolmanovsky, I., "Fast computable recoverable sets and their use for aircraft loss-of-control handling read more: https://arc.aiaa.org/doi/10.2514/1.g001747," *Journal of Guidance, Control, and Dynamics*, vol. 40, no. 4, pp. 934–947, 2017.

[112] McDonough, K., Kolmanovsky, I., and Atkins, E., "Recoverable sets of initial condition and their use for aircraft flight planning after a loss of control event," in *AIAA Guidance, Navigation, and Control Conference*, 2014.

[113] McLaren, S. A., "Velocity estimate following air data system failure," Master's thesis, Air Force Institute of Technology, 2008.

[114] Mehra, R. K. and Carroll, J. V., "Global stability and control analysis of aircraft at high angles of attack," tech. rep., Office of Naval Research, 1979.

[115] Merkt, J. R., "Flight energy management training: Promoting safety and efficiency," *Journal of Aviation Technology and Engineering*, vol. 3, no. 1, pp. 24–36, 2013.

[116] Min, S., Harrison, E., Jimenez, H., and Mavris, D., "Development of aerodynamic model and calibration method for general aviation aircraft performance analysis - a survey and comparison of models," *AIAA Aviation*, 2015.

[117] Mitchell, I. and Tomlin, C. J., "Level set methods for computation in hybrid systems," in *International Workshop on Hybrid Systems: Computation and Control*, pp. 310–323, Springer, 2000.

[118] MITRE, "General Aviation Pilots Get Their GAARD Up with New App," 2015. Accessed 12/17.

[119] Montgomerie, B., "Methods for root effects, tip effects and extending the angle of attack range to±180, with application to aerodynamics for blades on wind turbines and propellers," *FOI, Swedish Defense Research Agency, Stockholm, Sweden, Report No. FOI*, 2004.

[120] Munk, M. M., "The aerodynamic forces on airship hulls," Tech. Rep. NACA-184, National Advisory Committee for Aeronautics, 1924.

[121] Murch, A. M. and Foster, J. V., "Recent nasa research on aerodynamic modeling of post-stall and spin dynamics of large transport airplanes," in *45th AIAA Aerospace Sciences Meeting and Exhibit*, 2007.

[122] Murphy, K., "The paperless aircraft." `http://www.nytimes.com/2011/07/05/business/05pilots.html`, Jul 2011. Accessed 12/17.

[123] National Transportation Safety Board, "2015 NTSB US Civil Aviation Accident Statistics." `https://www.ntsb.gov/investigations/data/Pages/AviationDataStats2015.aspx#`, November 2017.

[124] Nguyen, L. T., Ogburn, M. E., Gilbert, W. P., Kibler, K. S., Brown, P. W., and Deal, P. L., "Simulator study of stall/post-stall characteristics of a fighter airplane with relaxed longitudinal static stability," tech. rep., National Aeronautics and Space Administration, 1979.

[125] Omran, A. and Newman, B., "Nonlinearity index theory for aircraft dynamic assessment," *Journal of Guidance, Control, and Dynamics*, vol. 36, 1 2013.

[126] Open Flight Solutions, "Flight box," 2018. Accessed 10/18.

[127] Padfield, G. D. and Lawrence, B., "The birth of flight control: An engineering analysis of the wright brothers' 1902 glider," *The Aeronautical Journal*, 12 2003.

[128] Pamadi, B. N. and Taylor, L. W., "Semi empirical method for prediction of aerodynamic forces and moments on a steadily spinning light airplane," Tech. Rep. NASA-TM-4009, National Aeronautics and Space Administration, 1987.

[129] Pamadi, B. N. and Taylor, L., "Estimation of aerodynamic forces and moments on a steadily spinning airplane," *Journal of Aircraft*, vol. 21, no. 12, pp. 943–954, 1984.

[130] Pandita, R., Chakraborty, A., and Seiler, P., "Reachability and region of attraction analysis applied to gtm dynamic flight envelope assessment," in *AIAA Guidance, Navigation, and Control Conference*, 2009.

[131] Paranjape, A. and Ananthkirshnan, N., "Analytical criterion for aircraft spin susceptibility," in *AIAA Atmospheric Flight Mechanics Conference*, 2010.

[132] Paranjape, A., Sinha, N. K., and Ananthkrishnan, N. in *45th AIAA Aerospace Sciences Meeting and Exhibit*, 2007.

[133] Pauck, S. J. and Engelbrecht, J. A. A., "Bifurcation analysis of the generic transport model with a view to upset recovery," in *AIAA Atmospheric Flight Mechanics Conference*, 2012.

[134] Petovello, M., "How does a gnss receiver estimate velocity?," *Inside GNSS*, 2015.

[135] Phillips, W. F. and Snyder, D. O., "Modern adaptation of prandtl's classic lifting-line theory," *Journal of Aircraft*, vol. 37, no. 4, pp. 662–670, 2000.

[136] Phillips, W. and Anderson, E. A., "Predicting the contribution of running propellers to aircraft stability derivatives," *40th Aerospace Sciences Meeting & Exhibit*, no. AIAA 2002-0390, 2002.

[137] Piper Aircraft, I., *Piper Cherokee 180 E PA-28-180 Owner's Handbook*, 1974.

[138] Piper Aircraft, I., *PA-28-181 Airplane Maintenance Manual*, 1994.

[139] Piper Aircraft, I., *Piper Archer III PA-28-181 Pilot's Operating Handbook and FAA Approved Airplane Flight Manual*, 1995.

[140] Piper Aircraft, I., *Piper Cherokee Service Manual*, 1995.

[141] Polhamus, E. C., "Effect of flow incidence and reynolds number on low-speed aerodynamic characteristics of several noncircular cylinders with applications to directional stability and spinning," Tech. Rep. NACA-TN-4176, National Advisory Committee for Aeronautics, 1958.

[142] Polhamus, E. C., Geller, E. W., and Grunwald, K. J., "Pressure and force characteristics of noncircular cylinders as affected by reynolds number with a method included for determining the potential flow about arbitrary shapes," Tech. Rep. NASA-TR-R-46, National Aeronautics and Space Administration, 1959.

[143] Prandtl, L., "Tragflügeltheorie. i. mitteilung," *Nachrichten von der Gesellschaft der Wissenschaften zu Göttingen, Mathematisch-Physikalische Klasse*, vol. 1918, pp. 451–477, 1918.

[144] Prandtl, L. and Betz, A., *Vier Abhandlungen zur Hydrodynamik und Aerodynamik*. Universitätsverlag Göttingen, 1927.

[145] Puranik, T., Harrison, E., Min, S., Jimenez, H., and Mavris, D., "Energy-based metrics for general aviation flight data record analysis," *AIAA AVIATION Forum*, 2016.

[146] Raghavendra, P. K., Sahai, T., Kumar, P. A., Chauhan, M., and Ananthkrishnan, N., "Aircraft spin recovery, with and without thrust vectoring, using nonlinear dynamic inversion," *Journal of Aircraft*, vol. 42, no. 6, 2005.

[147] Ragheb, A. M., "Modeling and validation of a subscale aerobatic aircraft configuration in spin," 2016.

[148] Rao, D. M. K. K. V. and Sinha, N. K., "Aircraft spin recovery using a sliding-mode controller," *Journal of Guidance, Control, and Dynamics*, vol. 33, no. 5, 2010.

[149] Raymer, D. P., *Aircraft Design: A Conceptual Approach*. American Institute of Aeronautics and Astronautics, Inc., 2006.

[150] Rhudy, M. B., Fravolini, M. L., Gu, Y., Napolitano, M. R., Gururajan, S., and Chao, H., "Aircraft model-independent airspeed estimation without pitot tube measurements," *IEEE Transactions on Aerospace and Electronic Systems*, vol. 51, no. 3, 2015.

[151] Richards, N. D., Gandhi, N., Bateman, A. J., Klyde, D. H., and Lampton, A. K., "Vehicle upset detection and recovery for onboard guidance and control," *Journal of Guidance, Control, and Dynamics*, vol. 40, no. 4, 2017.

[152] Schuet, S., Lombaerts, T., Kaneshige, J., Shish, K., and Stepanyan, V., "Stall recovery guidance using fast model predictive control," in *AIAA Guidance, Navigation, and Control Conference*, 2017.

[153] Selig, M. S., "Modeling full-envelope aerodynamics of small uavs in real-time," in *AIAA Atmospheric Flight Mechanics Conference*, 2010.

[154] Selig, M. S., "Real-time flight simulation of highly maneuverable unmanned aerial vehicles," *Journal of Aircraft*, vol. 51, no. 6, 2014.

[155] Sethian, J. A., *Level set methods and fast marching methods: evolving interfaces in computational geometry, fluid mechanics, computer vision, and materials science*, vol. 3. Cambridge university press, 1999.

[156] Sheidahl, R. E. and Klimas, P. C., "Aerodynamic characteristics of seven symmetrical airfoil sections through 180-degree angle of attack for use in aerodynamic analysis of vertical axis wind turbines," Tech. Rep. SAND80-2114, Sandia National Laboratories, 1981.

[157] Shtessel, Y. B. and Shkolnikov, I. A., "Aeronautical and space vehicle control in dynamic sliding manifolds," *International Journal of Control*, vol. 76, no. 9-10, pp. 1000–1017, 2003.

[158] Simon, D., *Optimal State Estimation: Kalman, H_∞, and Nonlinear Approaches*. John Wiley & Sons, 2006.

[159] Sklar, A. E. and Sarter, N. B., "Good vibrations: Tactile feedback in support of attention allocation and human-automation coordination in event-driven domains," *Human Factors*, vol. 41, no. 4, pp. 543–552, 1999.

[160] Snyder, M. H., Wentz, W. H., and Ahmed, A., "Two-dimensional tests of four airfoils at angles of attack from 0 to 360 degrees," Tech. Rep. WER-16, Center for Energy Studies, Wichita State University, 1984.

[161] Spera, D. A., "Models of lift and drag coefficients of stalled and unstalled airfoils in wind turbines and wind tunnels," Tech. Rep. CR 2008-215434, National Aeronautics and Space Administration, 2008.

[162] Staal, M. A., "Stress, cognition, and human performance: A literature review and conceptual framework," Tech. Rep. NASA/TM-2004-212824, National Aeronautics and Space Administration, 2004.

[163] Stepanyan, V., Krishnakumar, K., Dorais, G., Reardon, S., Barlow, J. S., Lampton, A. K., and Hardy, G., "Loss-of-control mitigation via predictive cuing," *Journal of Guidance, Control, and Dynamics*, vol. 40, no. 4, 2017.

[164] Stratux, "Stratux ads-b diy/low-cost portable ads-b," 2018. Accessed 10/18.

[165] Sussmann, H. J. and Jurdjevic, V., "Controllability of nonlinear systems," *Journal of Differential Equations*, vol. 12, 1972.

[166] Tang, L., Roemer, M., Ge, J., Crassidis, A., Prasad, J. V. R., and Belcastro, C., "Methodologies for adaptive flight envelope estimation and protection," in *AIAA Guidance, Navigation, and Control Conference*, 2009.

[167] Team, C. A. S., "Jsat loss of control: Cast approved final report," 2000.

[168] Theodorou, D., Meligotsidou, L., Karavoltsos, S., Burnetas, A., Dassenakis, M., and Scoullos, M., "Comparison of iso-gum and monte carlo methods for the evaluation of measurement uncertainty: Application to direct cadmium measurement in water by gfaas," *Talanta*, vol. 83, no. 5, pp. 1568–1574, 2011.

[169] Thomas, S., Bajpai, G., Kwatny, H. G., and Chang, B.-C., "Nonlinear dynamics, stability & bifurcation in aircraft: Simulation and analysis tools," in *AIAA Guidance, Navigation, and Control Conference and Exhibit*, 2005.

[170] United States Department of Defense, "Global positioning system standard positioning service performance standard," tech. rep., 2008.

[171] van Oort, E. R., Chu, Q. P., and Mulder, J. A., *Maneuver Envelope Determination through Reachability Analysis*, pp. 91–102. Berlin, Heidelberg: Springer Berlin Heidelberg, 2011.

[172] Viterna, L. A. and Janetzke, D. C., "Theoretical and experimental power from large horizontal-axis wind turbines," tech. rep., National Aeronautics and Space Administration, 1982.

[173] Vora, A. S. and Sinha, N. K., "Direct methodology for constrained system analysis with applications to aircraft dynamics," *Journal of Aircraft*, 2017.

[174] Wilborn, J. E. and Foster, J. V., "Defining commercial transport loss-of-control: A quantitative approach," *AIAA Atmospheric Flight Mechanics Conference and Exhibit*, no. AIAA 2004-4811, 2004.

[175] Worobel, R., "Advanced general aviation propeller study," 1971.

[176] Worobel, R. and Mayo, M. G., "Advanced general aviation propeller study," 1971.

[177] Wu, N. E., Zhang, Y., and Zhou, K., "Detection, estimation, and accommodation of loss of control effectiveness," *International Journal of Adaptive Control and Signal Processing*, vol. 14, 2000.

[178] Zhang, W. and Chen, H., "Aircraft loss-of-control recovery strategy using high order sliding mode control based on optimal trim condition," in *AIAA Aviation Technology, Integration, and Operations Conference*, 2016.

[179] Zhang, Y., Suresh, V. S., Jiang, B., and Theilliol, D., "Reconfigurable control allocation against aircraft control effector failures," in *16th IEEE International Conference on Control Applications*, 2007.

[180] Zhao, Y., *Automatic Prevention and Recovery of Aircraft Loss-of-Control by a Hybrid Control Approach*. PhD thesis, Russ College of Engineering and Technology of Ohio University, 2016.

[181] Zhao, Y. and Zhu, J. J., "Aircraft loss-of-control autonomous recovery: Mission trajectory tracking restoration," in *International Conference on Unmanned Aircraft Systems*, 2016.